



11/26/04

AF/2814/28

Express Mail No. ED 003 998 912 US

IN THE UNITED STATES PATENT AND TRADEMARK OFFICE
BEFORE THE BOARD OF PATENT APPEALS AND INTERFERENCES

Application of: Alexandre M. Zagoskin Confirmation No.: 1798
Serial No.: 09/452,749 Art Unit: 2814
Filed: December 1, 1999 Examiner: Douglas A. Wille
For: PERMANENT READOUT Attorney Docket No: 706700-999101
SUPERCONDUCTING QUBIT

BRIEF ON APPEAL FEE TRANSMITTAL

Commissioner for Patents
P.O. Box 1450
Alexandria, VA 22313-1450

Sir:

An original and two copies of the applicant's Brief on Appeal in the above-entitled application are submitted herewith. The item(s) checked below apply:

- ☐ The Brief filing fee is \$340.00
☒ Applicant has qualified for the 50% reduction in fee for an independent inventor, nonprofit organization or small business concern and the Brief filing fee is \$170.00

The brief filing fee is:

- ☒ Required.
☐ Not required. (Fee paid in prior appeal.)

Please charge the required Brief filing fee to Jones Day Deposit Account No. 50-3013. A copy of this sheet is enclosed.

Respectfully submitted,

Date: November 23, 2004

Brett Lovejoy
Brett Lovejoy
JONES DAY

222 East 41st Street
New York, New York 10017
(415) 875-5744

42,813
(Reg. No.)

Enclosure



Express Mail No.: ED 003 998 912 US

IN THE UNITED STATES PATENT AND TRADEMARK OFFICE
BEFORE THE BOARD OF PATENT APPEALS AND INTERFERENCES

In re application of:)	Art Unit: 2814
)	
Alexandre M. Zagoskin)	Confirmation Number: 1708
)	
Serial No. 09/452,749)	Examiner: Douglas A. Wille
)	
Filed: December 1, 1999)	Attorney Docket No: 706700-999101
)	(Formerly 11090-003-999)
For: PERMANENT READOUT)	
SUPERCONDUCTING QUBIT)	
_____)

APPEAL BRIEF TABLE OF CONTENTS

1. REAL PARTY IN INTEREST	2
2. RELATED APPEALS AND INTERFERENCES	2
3. STATUS OF CLAIMS	2
4. STATUS OF AMENDMENTS	2
5. SUMMARY OF THE INVENTION	3
5.1 Use of a d-wave superconductor for at least one of a bank and mesoscopic island	4
5.2 Mesoscopic island	4
5.3 Clean Josephson junction between a bank and a mesoscopic island	5
6. ISSUES	6
7. GROUPING OF CLAIMS	7
8. ARGUMENTS	7
8.1 Group I: Claims 1, 8, 28, 39, 60, and 64 and each of the claims that depend from these independent claims	7
8.1.1 Char does not teach or suggest a clean Josephson junction	8
8.1.1.1 Josephson junction current-phase relationships	9
8.1.1.2 Clean Josephson junctions	10
8.1.1.3 Char	11
8.1.2 Tinkham does not teach or suggest a clean Josephson junction	12
8.1.3 There is no motivation in the art to modify Char so that it would have a clean Josephson junction	12
8.1.3.1 Neither Char nor the best quality crystal structures available for biepitaxial Josephson junction technology at the time of filing of the application were sufficiently advanced to make a clean Josephson junction.	12
8.1.3.2 Unpredictability of the second harmonic in clean Josephson junctions	15
8.1.4 The prior art provides no motivation to combine Tinkham and Char	16
8.1.5 Conclusion	16
8.2 Group II: Claims 60-63	17



Express Mail No.: ED 003 998 912 US

IN THE UNITED STATES PATENT AND TRADEMARK OFFICE
BEFORE THE BOARD OF PATENT APPEALS AND INTERFERENCES

In re application of:)	Art Unit: 2814
)	
Alexandre M. Zagoskin)	Confirmation Number: 1708
)	
Serial No. 09/452,749)	Examiner: Douglas A. Wille
)	
Filed: December 1, 1999)	Attorney Docket No: 706700-999101
)	(Formerly 11090-003-999)
)	
For: PERMANENT READOUT)	
SUPERCONDUCTING QUBIT)	
)	

APPEAL BRIEF

Mail Stop Appeal Brief - Patents
Honorable Commissioner for Patents
US Patent and Trademark Office
P.O. Box 1450
Alexandria, Virginia 22313-1450

Sir:

This is an appeal pursuant to the provisions of 37 C.F.R. § 1.192 from the Examiner's final rejection of claims 1-8, 11-18 and 28, 30-39, and 42-65 of October 20, 2004. Claims 1, 3-5, 28, 33, 34, 39, 54, 56, 58, and 60-63 were rejected under 35 U.S.C. §103(a) as being unpatentable over Tinkham, *Introduction to Superconductivity*, Second Edition, McGraw-Hill, 1996 (hereinafter "Tinkham"), in view of United States Patent 5,157,466 to Char *et al.* (hereinafter "Char"). Further, claims 2, 30, 31, 32, and 52 were rejected under 35 U.S.C. §103(a) as being unpatentable over Tinkham in view of Char and further in view of Shnirman *et al.*, Physical Review B 57, p. 15400, 1998 (hereinafter "Shnirman"). Further claims 6, 8, 35, 53, 55, 57, 59, 64, and 65 were rejected under 35 U.S.C. §103(a) as being unpatentable over Tinkham in view of Char and further in view of United States Patent 3,953,749 to Baechtold *et al.* (hereinafter "Baechtold"). Claims 7, 11-18, 36, 37, 42, 43, 45, 46, and 48-50 were rejected under 35 U.S.C. § 103(a) as being unpatentable over Tinkham in view of Char,

11/30/2004 AWONDAF1 00000010 503013 09452749

01 FC:2402

170.00 DA

Baechtold and further in view of Shnirman. Claims 38, 44, 47, and 51 were also rejected under 35 U.S.C. § 103(a) as being unpatentable over Tinkham, in view of Char, Baechtold and further in view of Shnirman.

The Notice of Appeal was filed by facsimile transmission to the United States Patent and Trademark Office on November 23, 2004. This brief is being filed with the time permitted by 37 CFR § 1.192(a) which permits the brief to be filed "within the time allowed for reply to the action from which the appeal was taken, if such time is later."

A "Brief on Appeal Fee Transmittal" accompanies this brief.

1. REAL PARTY IN INTEREST

The real party in interest is D-Wave Systems, Inc. D-Wave Systems, Inc. is a Canadian corporation having headquarters at 320-1985 West Broadway, Vancouver, British Columbia, Canada, V6J 4Y3, by whom the Applicant is employed. An assignment of the invention was recorded on January 24, 2000.

2. RELATED APPEALS AND INTERFERENCES

There are no interferences or other appeals related to the present application.

3. STATUS OF CLAIMS

On October 20, 2004, Examiner Wille issued a final rejection of claims 1-8, 11-18 and 28, 30-39, and 42-65.

4. STATUS OF AMENDMENTS

All amendments filed by the Applicant have been duly entered by the Examiner.

5. SUMMARY OF THE INVENTION

The present invention is directed to structures used to perform quantum computing. As outlined on page 3, first paragraph, of DiVincenzo in *Scalable Quantum Computers*, Braunstein and Lo, *eds.*, Wiley-VCH, 2001, Berlin, (attached hereto as Exhibit A), a quantum computing device requires qubits. A qubit is a quantum two-level system (DiVincenzo, page 3, first paragraph). The feature that distinguishes a qubit from a bit is that the permitted states of a single qubit fill up a two-dimensional complex vector space $a|0\rangle + b|1\rangle$, where a and b are complex numbers and $|0\rangle$ and $|1\rangle$ are two distinct basis states. A qubit has a nonzero probability of occupying the states $|0\rangle$ and $|1\rangle$ at the same time. See page 2, lines 11-13, as well as page 2, line 20, through page 3, line 6, of the specification. By comparison, a conventional bit can only occupy the states “0” or “1”.

For physical intuition of the dynamics of a qubit, one can consider a particle with mass, termed a “phase particle,” as moving along, under the effect of gravity, in a landscape that defines potential energy barriers. Since the phase particle is governed by quantum mechanics rather than classical mechanics, it is possible for the phase particle to coherently tunnel through the energy barrier separating two ground states ($|0\rangle$ and $|1\rangle$). Tunneling permits the qubit to have a nonzero probability of occupying the two ground states $|0\rangle$ and $|1\rangle$ at the same time. If the tunneling is coherent, the qubit’s probability of occupying the states $|0\rangle$ and $|1\rangle$ includes phase information. This is in contrast to classical dynamics where a particle cannot tunnel under a barrier and where, to transition from one state to another, it must possess sufficient energy to be able to transition over the potential energy barrier.

The invention is directed to new types of quantum computing devices (*e.g.*, quantum computing structures, quantum registers, qubits) that exploit currents spontaneously arising in a superconductor in the vicinity of a grain boundary Josephson junction. See specification, page 6, lines 18-28. As described on page 3, lines 11-21, as well as Fig. 1A of the specification, these new types of quantum computing devices comprise a superconducting mesoscopic island 120 and a superconducting bank 110 formed on an insulating substrate 140. The mesoscopic island 120 and superconducting bank 110 are separated by a clean Josephson junction 130. At least one of the superconducting bank 110 and superconducting island 120 is a d-wave superconductor, which is a special form of superconductor.

Upon entry of the attached amendment under 37 C.F.R. § 1.116, the structures recited in each of the independent pending claims combines three features to form a quantum computing device: (i) the use of a d-wave superconductor to form at least one of the

superconducting bank 110 and island 120, (ii) a mesoscopic-sized island 120 and (iii) a clean Josephson junction 130 between the superconducting bank 110 and mesoscopic island 120. The purpose of each of these recited features in forming a quantum computing device will be discussed in turn.

5.1 Use of a d-wave superconductor for at least one of a bank and mesoscopic island

As explained on page 9, lines 6-17, of the specification, the use of a d-wave superconductor to form at least one of the superconducting bank 110 and mesoscopic island 120 causes persistent supercurrents to arise in the vicinity of clean Josephson junction 130. These persistent supercurrents are illustrated in Fig. 1A of the specification. This is a known phenomenon. For example, the second paragraph in column 1 of Lindström et al., 2003, Physical Review Letters 90, 117002, attached hereto as Exhibit D (hereinafter “Lindström”), notes that “[t]ime-reversal symmetry can ... be spontaneously violated and thus spontaneous currents generated.”

5.2 Mesoscopic island

A mesoscopic island 120 is used in the claimed devices so that the phase of the persistent supercurrents discussed in Section 5.1 adopts quantum mechanical behavior rather than classical mechanical behavior. A mesoscopic system is any system that is small enough to be governed by quantum mechanical principles rather than classical mechanical principles. Here, a mesoscopic island 120 is a block of superconducting material that is sufficiently small to be governed by quantum mechanical principles. Generally, in order for island 120 to be mesoscopic, it must have dimensions that are in the low micrometer range or smaller. As noted on page 7, line 30, through page 8, line 2, of the specification, an exemplary mesoscopic island has a width that is 0.2 microns or less, a length of 0.5 micron or less, and a thickness that is 0.2 microns or less. The determination of whether an island 120 is mesoscopic is realized by coherent tunneling of the phase of the persistent supercurrents. Coherent tunneling is a uniquely quantum phenomenon. Coherent tunneling is not the same as incoherent tunneling. Incoherent tunneling is also a quantum effect but it does not support quantum computing. Incoherent tunneling occurs in many devices including SQUID containing macroscopic Josephson junctions. Note that, if island 120 is mesoscopic, the phase of the persistent supercurrents has a nonzero probability of being in one of two degenerate states. If island 120 is too large to be mesoscopic, the phase of the persistent

supercurrents adopts a constant value, does not have two degenerate ground states, and cannot support quantum computing.

5.3 Clean Josephson junction between a bank and a mesoscopic island

One of the requirements of quantum computing is the establishment of two basis states (*e.g.*, two degenerate states). See specification page 2, lines 11-13. In the novel structures of the present invention, Applicant takes advantage of the properties of a clean Josephson junction in which at least one side of the junction is d-wave superconductor. As noted on page 7, lines 12-14, of the specification, and as illustrated in Fig. 1A, a clean junction 130 separates a bank 110 and island 120. Then, on page 9, lines 6-28, of the specification it is stated that junction 130 causes a non-zero supercurrent in the ground state that is represented by two different states each of which has the same potential energy. In other words, the two different states are degenerate. Page 9 of the specification further states that the two degenerate states correspond to minimal supercurrents circulating through Josephson junction 130 in clockwise and counterclockwise senses. Page 9, lines 15-17, indicate that the two degenerate states associated with the supercurrent on island 120 (*i.e.*, the clockwise and counterclockwise currents respectively) permit quantum computing. The clockwise and counterclockwise supercurrents described on page 9 of the specification serve as the basis states needed for quantum computing. As noted on page 9, lines 27-28, quantum tunneling between these basis states (the two degenerate states) causes the state of island 120 to evolve. This means that the phase of the persistent supercurrents can tunnel through the energy barrier that separates the degenerate state represented by the clockwise persistent supercurrent and the degenerate state represented by the counterclockwise persistent supercurrent through a phenomenon that is known as quantum mechanical tunneling. Furthermore, because the two states are degenerate, this quantum tunneling can occur in both directions (*i.e.*, from $|0\rangle$ to $|1\rangle$ and vice versa) without the application of an external force on the qubit. Due to the quantum mechanical tunneling between the two degenerate states, there is a nonzero probability that states $|0\rangle$ and $|1\rangle$ (where $|0\rangle$ is arbitrarily assigned to either the clockwise or counterclockwise supercurrent and $|1\rangle$ is assigned to the other supercurrent) are occupied at the same time, hence satisfying a central requirement for forming a qubit capable of quantum computation. As noted on page 9 of the specification, the coexistence of the two degenerate ground states results in the coexistence in persistent supercurrents that are traveling in opposite directions (clockwise and counterclockwise as viewed using the

framework of Fig. 1A). Because the claimed devices are superconducting, these clockwise and counterclockwise currents do not interact with each other. Thus, no energy is lost and the persistent supercurrents can coexist for long periods of time. This phenomenon is also described in Lindström et al., 2003, page 117002-1, (Exhibit D) bridging paragraph between columns 1 and 2.

Table 1 summarizes the three novel features of the present invention, how they contribute to the formation of a quantum computing device, and where they are described in the specification.

Table 1. Features that are recited in each pending independent claim.

FEATURE	CONTRIBUTION	SUPPORT IN SPECIFICATION
Use of a d-wave superconductor to form at least one of the bank 110 and mesoscopic island 120 across a Josephson junction.	Causes persistent supercurrents to arise in the vicinity of the Josephson junction.	Page 7, lines 6-11
Mesoscopic island 120.	Causes the persistent supercurrents to adopt quantum mechanical behavior, including the ability for the phase of the persistent supercurrents to spontaneously tunnel through a potential energy barrier between degenerate phase states (basis states).	Page 7, line 27, through page 8, line 2
Clean Josephson junction between bank 110 and mesoscopic island 120.	Causes the persistent supercurrents to have two degenerate phase states (basis states).	Page 7, lines 12-16; page 9, line 29, through page 10, line 7

6. ISSUES

Upon entry of all amendments filed for this application, the issues presented are:

(1) whether claims 1, 3-5, 28, 33, 34, 39, 54, 56, 58, and 60-63 are patentable under 35 U.S.C. § 103(a) over Tinkham in view of Char;

(2) whether claims 2, 30, 31, 32, and 52 are patentable under 35 U.S.C. § 103(a) over Tinkham in view of Char and further in view of Shnirman;

(3) whether claims 6, 8, 35, 53, 55, 57, 59, 64, and 65 are patentable under 35 U.S.C. § 103(a) over Tinkham in view of Char and further in view of Baechtold;

(4) whether claims 7, 11-18, 36, 37, 42, 43, 45, 46, and 48-50 are patentable under 35 U.S.C. § 103(a) over Tinkham in view of Char, Baechtold and further in view of Shnirman;
and

(5) whether claims 38, 44, 47, 51 are patentable under 35 U.S.C. § 103(a) over Tinkham in view of Char, Baechtold and further in view of Shnirman.

7. GROUPING OF CLAIMS

Claims 1-8, 11-18, 28, 30-39, and 42-65 are pending in this case. Many of the pending claims are believed to be separately patentable for the reasons set forth in Section 8 below and do not stand or fall together. In particular, at least the two following groups are believed to be separately patentable:

Group I: claims 1-8, 11-18, 28, 30-39, 42-59, and 64-65; and

Group II: claims 60-63

8. ARGUMENTS

8.1 Group I: Claims 1, 8, 28, 39, 60, and 64 and each of the claims that depend from these independent claims

In the final office action mailed October 20, 2004, the Examiner rejected claim 1 under 35 U.S.C. § 103(a) as being unpatentable over Tinkham in view of Char. Claim 1 recites (i) a first bank of a superconducting material, (ii) a mesoscopic island of a superconducting material, where at least one of the island and the bank comprises a d-wave superconducting material, and (iii) a clean Josephson junction between the island and the bank. Each of the independent claims (claims 1, 8, 28, 39, 60, and 64) recite at least these

three elements in a quantum computing device (*e.g.* a quantum computing structure, a quantum register, or a qubit).

The Examiner asserts that page 248, top paragraph, of Tinkham shows a small superconducting island connected to charge reservoirs and further, page 256, last full paragraph, shows a small superconducting island connected to two macroscopic superconducting leads. Next, the Examiner points out that column 2, line 3 et seq. and Fig. 14 of Char show the formation of a grain boundary Josephson junction 314 of high temperature superconductor material where an island 310 is connected to a body 312. The Examiner states that it would have been obvious to use the Char structure for the Tinkham device “since it is known to be functional.” Although neither Char nor Tinkham teach or suggest a clean Josephson junction, the Examiner states that it would be obvious to provide the best quality crystal structures since this is standard in semiconductor processing.

When rejecting claims under 35 U.S.C. § 103, the PTO bears the burden of establishing a *prima facie* case of obviousness. *In re Bell*, 26 USPQ2d 1529 (Fed. Cir. 1993). To establish a *prima facie* case, the prior art reference, or references when combined, must teach or suggest each and every limitation of the claimed invention. MPEP § 706.02(j). The teaching or suggestion to make the claimed invention and the reasonable expectation of success must both be found in the prior art, not in the Applicant’s disclosure. *In re Vaeck*, 20 USPQ2d 1438 (Fed. Cir. 1991). There must be some motivation, suggestion, or teaching of the desirability of making the specific combination that was made by the Applicant. *In re Fine*, 837 F.2d 1071, 1075 (Fed. Cir. 1988).

In the present instance, one relevant inquiry is whether the cited art, either alone or in combination, teaches each and every limitation of the rejected claims. To this end, Applicant submits that the Examiner’s rejection of the claims is unfounded because Char and Tinkham, either alone or in combination, do not teach or suggest the clean Josephson junction(s) that are recited in each of the independent claims. Another relevant inquiry is whether the prior art provides one of ordinary skill in the art with a suggestion or motivation to modify or combine the teachings of the references relied upon by the Examiner to arrive at the claimed invention. As discussed in detail below, the cited art fails to satisfy either of these requirements.

8.1.1 Char does not teach or suggest a clean Josephson junction

Each of the independent claims recites at least one clean Josephson junction. In the October 20, 2004 Office Action, the Examiner stated that the clean Josephson junction

limitation in claim 1 does not render the claim patentable over the combination of Char and Tinkham. The Examiner reasoned that it would have been obvious to provide the best quality crystal structures since this is standard in semiconductor processing. The Applicant will discuss the current-phase relationship of Josephson junctions made from conventional superconducting materials and unconventional superconducting materials in Section 8.1.1.1. Then, the current-phase relationship of clean Josephson junctions will be discussed in Section 8.1.1.2. Then, in subsequent sections, the Applicant will discuss why Char and Tinkham do not teach or suggest clean Josephson junctions and why there is no motivation to modify Char to incorporate clean Josephson junctions into Char devices.

8.1.1.1 Josephson junction current-phase relationships

In general, the current-phase relation of a Josephson junction is described by an odd periodic function commonly represented by the Fourier expansion:

$$I(\varphi) = I_1 \cdot \sin(\varphi) + I_2 \cdot \sin(2\varphi) + \dots, \quad (1)$$

where I_1 and I_2 represent the critical current of the first and second harmonics respectively. In Josephson junctions formed out of conventional superconducting materials, the second harmonic term and higher terms are negligible. See Il'ichev *et al.*, 1999, Physical Review B 60, p. 3096, (hereinafter "Il'ichev 1999"), second column ("The I_2 term is also present in weak links based on conventional *s*-wave superconductors but for all known types of weak links $|I_2 / I_1| < 1$. For instance, for a tunnel junction $|I_2 / I_1| \ll 1$ ").

The order parameter of a superconducting material determines the properties and characteristics of the superconducting material, and hence the current-phase relationship of weak links formed in the material. Conventional superconducting materials have isotropic order parameters. In contrast, unconventional superconducting materials have anisotropic order parameters. A common unconventional superconducting material is the d-wave superconductor $\text{YBa}_2\text{Cu}_3\text{O}_{7-x}$ (YBCO), which is used in both Char and Il'ichev 1999. The term "d-wave" indicates the type of symmetry of the anisotropic order parameter.

Due to the anisotropy of the d-wave order parameter, the current-phase relationship for a Josephson junction in a d-wave superconductor has the potential of having a temperature dependent second harmonic term. The current-phase relationship of the Josephson junctions described in Il'ichev 1999 is:

$$I_p = I_c^I \cdot \sin(\varphi) + I_c^{II} \cdot \sin(2\varphi), \quad (2)$$

where I_c^I and I_c^{II} are the critical currents of the first and second harmonics respectively.

Il'ichev 1999 established that the realized non-sinusoidal behavior in the current-phase relationship of this clean Josephson junction is explained by the presence, and in some cases dominance, of the second harmonic term. See, for example, Fig. 4 of Il'ichev 1999, where the second order harmonic I_2 dominates over the first order harmonic I_1 at lower temperatures.

8.1.1.2 Clean Josephson junctions

The greater the influence of the second harmonic in the current-phase relationship of a Josephson junction, the greater the deviation from conventional 2π periodic sinusoidal behavior. A clean Josephson junction is defined by a current-phase relationship in which the second harmonic makes a distinct contribution to the characteristics of the junction. (See point 5 of the declaration of Dr. Alexander Tzalenchuk under 37 C.F.R. § 1.132 submitted in response to the February 19, 2003 Office Action on April 18, 2003, attached hereto as Exhibit H). In terms of Eqn. 2, this is the regime where $I_c^{II} > I_c^I / 2$, which causes the equilibrium state to shift from $\varphi=0$, in the sinusoidal case, to about $\pm\pi/2$, creating a double degenerate ground state phase difference across the junction. In other words, the phase differences of about $+\pi/2$ and $-\pi/2$ have equal energy across the unconventional superconductor clean Josephson junction.

The double degenerate ground state associated with a clean Josephson junction is used in the present invention in order to cause persistent supercurrents that spontaneously arise in the claimed devices to have two degenerate ground states. See page 9, lines 6-28, of Applicant's specification. As discussed in Section 5.1, such persistent supercurrents arise spontaneously in the vicinity of the clean Josephson junction when at least one of bank 110 and island 120 (Applicant's Fig. 1A) is made of a d-wave superconducting material. As discussed in Il'ichev 1999, page 3098, first column, and as depicted in Fig. 4 of Il'ichev 1999 (Exhibit B), the size of the second harmonic is dependent on temperature. It can be

suppressed by raising the temperature of the junction. When the second harmonic is suppressed, the junction behaves as a conventional Josephson junction.

8.1.1.3 Char

Char does not teach or suggest clean Josephson junctions. The current-phase relationship of a Josephson junction comprised of a conventional superconducting material has a sinusoidal dependence. See Il'ichev, 1998, Physical Review Letters 81, p. 894, first column, "[t]his sinusoidal dependence has been confirmed experimentally numerous times for standard tunnel junctions between conventional superconductors"). Il'ichev 1998 is attached hereto as Exhibit C. Il'ichev 1998 describes the fabrication of clean Josephson junctions in unconventional superconductors and measurement of their current-phase relationship. Il'ichev 1998 predicted and found significant deviations from the sinusoidal dependence that is typical of conventional Josephson junctions (See Il'ichev 1998, p. 896, first column, "strong deviations from the standard sinusoidal dependence have been predicted for the current-phase relations of various configurations of Josephson junctions employing such unconventional superconductors"). Il'ichev 1999 (Exhibit B) found that the deviations from the sinusoidal dependence were temperature dependent (Il'ichev, page 3098, column 1, "the amplitude of the π -periodic component of the CPR decreases drastically with increasing temperature").

A review of Fig. 15 of Char is instructive. As illustrated in Fig. 15 of Char, the voltage phase properties of the Char devices illustrate temperature independent conventional sinusoidal behavior, indicating that the second harmonic is suppressed at *all* temperatures in complete contrast to the teachings of Il'ichev 1999 (Exhibit B, p. 3098 column 1, first full paragraph). In other words, Fig. 15 of Char shows that the Char devices "operate properly" (*i.e.*, exhibits 2π periodic sinusoidal behavior) at temperatures ranging from 4.2K to 77K (see Char, column 15, lines 35-40). This indicates that the Josephson junctions of Char are not in the clean regime. If the Char devices were in the clean regime, then the voltage phase relationship of a Char device would adopt a sinusoidal waveform at high temperatures (68K) and a non-sinusoidal waveform at low temperatures (4.2K). Fig. 3 of Il'ichev 1999 (p. 3098) shows such a temperature dependence. In Fig. 3 of Il'ichev 1999 (Exhibit B), the non-sinusoidal behavior of a Josephson junction capable of exhibiting second harmonic effects is lost as the temperature of the junction is shifted from 4.2K to 40K. Thus, Char describes

Josephson junctions for which the second harmonic is suppressed between 4.2K and 77K. This means that Char does not teach or suggest clean Josephson junctions.

8.1.2 Tinkham does not teach or suggest a clean Josephson junction

Tinkham does not remedy the deficiencies of Char. In particular, Tinkham does not teach or suggest a clean Josephson junction. As noted by the Examiner on page 2 of the October 20, 2004 office action, Tinkham does not detail the materials of the island, leads to the island or Josephson junctions.

8.1.3 There is no motivation in the art to modify Char so that it would have a clean Josephson junction

In the October 20, 2004 Office Action, the Examiner stated that it would have been obvious to provide the best quality crystal structures since this is the standard in semiconductor processing. Applicant respectfully submits that the practice of providing the best quality crystal structures would not have resulted in the modification of Char or Tinkham to include clean Josephson junctions at the time the present application was filed for two reasons. First, the Char devices were constructed using biepitaxial technology. Even the best biepitaxial technology available at the time the present application was filed could not have achieved the unconventional superconductor clean Josephson junctions recited in the pending claims. Second, even if it were possible to modify Char to make the claimed junctions, such junctions would have electrical characteristics that are undesirable for the conventional devices proposed by Char. Because of these undesirable electrical characteristics, their use in the conventional electronic devices described in Char would result in unsatisfactory device performance. This reasoning is outlined in the following subsections.

8.1.3.1 Neither Char nor the best quality crystal structures available for biepitaxial Josephson junction technology at the time of filing of the application were sufficiently advanced to make a clean Josephson junction.

In order to produce a Josephson junction in a d-wave superconducting material such as $\text{YBa}_2\text{Cu}_3\text{O}_{7-x}$ (YBCO), the two sides of the junction must have different crystallographic orientation. There are three general approaches to fabricating such junctions, bicrystal, biepitaxial, and step-edge. See page 1, middle of column 2, of Tafuri *et al.*, cond-mat/0010128, Oct. 9, 2000, attached hereto as Exhibit E “YBCO GB junctions are usually classified as bicrystals, biepitaxials, and step-edges, depending on the fabrication

procedure.” While not intending to be limited to any particular fabrication technique, Applicant discloses a bicrystal fabrication technique on page 8, lines 3-18, of the specification. In Applicant’s bicrystal fabrication technique, the substrate itself is a bicrystal substrate, such as a strontium-titanate bicrystal. When a d-wave superconductor such as YBCO is grown or deposited on the bicrystal substrate, it produces two banks having different orientations. On page 8 of the specification, Applicant cites and incorporates by reference Il’ichev *et al.*, 1998 cond-mat/9811017, which is attached hereto as Exhibit F. Page 2, bridging paragraph between columns 1 and 2 of Il’ichev 1998, disclose more details of the bicrystal fabrication technique. Further, the reference demonstrates the successful use of the fabrication technique to make clean Josephson junctions in YBCO. As noted by Tafuri *et al.*, bicrystal techniques typically offer junctions with better performances than biepitaxials (Tafuri, Exhibit E, page 1, second column, “[t]he bicrystal technique typically offers junctions with better performances”).

Char uses a biepitaxial technique to form Josephson junctions. In the Char biepitaxial approach, a seed layer is introduced onto a portion of the substrate. See, for example, element 42 in Figs. 3-10 of Char. When YBCO is grown or deposited on a substrate that includes the seed layer, the YBCO overlying the seed layer adopts a different orientation than the portion of the substrate that does not overlay the seed layer. The boundary, therefore, between the YBCO overlying the seed layer and the YBCO overlying the native substrate forms a Josephson junction. See, for example, Fig. 3 of Char, including the Josephson junction (element 30).

Biepitaxial grain boundary Josephson junction technology was not sufficiently advanced at the time of filing of the instant Application to form clean Josephson junctions. This is evidenced by Tafuri (Exhibit E), and Koelle (Exhibit I). Tafuri provides new experimental procedures to produce biepitaxial YBCO Josephson junctions. Koelle provides a technical and historical review of a class of devices, SQUIDs, formed by YBCO Josephson junctions. SQUIDs is one embodiment of an electrical device proposed by Char.

Tafuri post dates the instant application. Tafuri states that known biepitaxial technology (such as that of Char) does not produce clean Josephson junctions. On page 1 of Tafuri, it is noted that the new experimental techniques disclosed in Tafuri could *possibly* be used to obtain a Josephson junction that has a double degenerate state [*i.e.*, a clean Josephson junction, “[i]n this paper we discuss how $\text{YBa}_2\text{Cu}_3\text{O}_{7-x}$ (YBCO) structures made by the biepitaxial technique can be successfully employed to produce arbitrary circuit geometries in which both “0” and π -loops are present, and possibly to obtain a doubly degenerate state”].

Further, Tafuri notes that the biepitaxial techniques of Tafuri represent significant improvements over the biepitaxial techniques of Char (Tafuri, page 1, second column, referencing Char *et al.*, 1991, Applied Physics Letters 59, p. 733, attached hereto as Exhibit G, “we intend to show that significant improvements with respect to the original technique developed by Char *et al.* are possible for biepitaxial junctions, and that the resulting devices have potential for applications”). The Char *et al.* reference cited by Tafuri is the same biepitaxial technology that is disclosed in United States Patent 5,157,466 to Char. Compare, for example, the text beginning on the second full paragraph on p. 733, column 2 of Char, Applied Physics Letters 59, to column 9, lines 49-64 of United States Patent 5,157, 466. Also, compare Figs. 2, 3, and 4 of Char, Applied Physics Letters 59 to Figs. 13, 14, and 15 of United States Patent 5,157, 466. Clearly, when Tafuri was published, more than ten months after the time of filing Applicant’s application, biepitaxial techniques that *might* produce double degenerate (clean) Josephson junctions in YBCO were only first being proposed.

As Tafuri indicates, the Char devices do not work well. Koelle *et al.*, Rev. Mod. Phys. 71, pp. 631–686, further supports this contention. Koelle *et al.* write at p. 634 “[t]he requirements for a successful junction technology include a nonhysteretic I-V characteristic, with properties close to the predictions of the RSJ model, a high $I_0 R$ product, controllable and reproducible parameters (I_0 , R , C), high yield, high stability under room-temperature storage and thermal cycling, and low $1/f$ noise.” Later on the same page Koelle *et al.* continues, “[t]hus the superconducting electrodes need to have perfect crystallinity, and a well-defined interface has to be achieved within a single unit cell.” Finally, “[a]lthough important historically, biepitaxial GBJ’s (Char *et al.*, 1991) are no longer used for SQUIDS, because of their small $I_0 R$ products.” Here Char *et al.*, 1991, refers to Applied Physics Letters 59, p. 733 (Exhibit G), which is the same biepitaxial technology disclosed in United States Patent 5,157,466 to Char, see above.

Given the difficulties with biepitaxial technology at the time the present application was filed, one of ordinary skill in the art would not have been able to modify Char to produce the devices claimed in the instant application. As such, the combination of Char and Tinkham does not provide a motivation to modify such references in order to make the claimed devices.

8.1.3.2 Unpredictability of the second harmonic in clean Josephson junctions

Even if biepitaxial technology could be used to make a clean Josephson junction, the prior art does not provide a fair motivation to make such junctions. As discussed above, the current-phase relationship of a clean Josephson junction is nonsinusoidal, due to contributions from the second harmonic term, whereas a conventional Josephson junction is sinusoidal, due to the dominance of a first harmonic term and the suppression of a second harmonic term. Further, at least in the case of a YBCO thin film with asymmetric 45 degree [001]-tilt grain boundaries, the contribution from the second harmonic term in clean Josephson junctions is temperature dependent. Thus, the use of clean Josephson junctions in the devices of Char would introduce an unpredictable temperature dependence on the current-phase dependence in such devices. Since the devices of Char are typically used in applications such as the precise measurement of magnetic fields (Char, column 2, lines 15-17, “[w]eak-link junctions make it possible to create extremely sensitive instruments to measure magnetic field, voltage, and current”), this unpredictable current-phase dependence is undesirable.

The unpredictability in the current-phase relationship of clean Josephson junctions, comes from at least two sources. First, as discussed above and as illustrated in Il’ichev 1999 (Exhibit B, e.g., Figs. 3 and 4), the second harmonic contribution associated with a clean Josephson junction is temperature dependent. Second, as detailed in Il’ichev 1999 and in Lindström, state of the art methods for manufacturing clean Josephson junctions still have not developed to the point where the strength of the second harmonic can be precisely engineered. In Il’ichev 1999, six bicrystal YBCO Josephson junctions were fabricated and studied. Of the six samples, only four produced clean Josephson junctions (Il’ichev 1999, page 3097, column 2, “[w]e have studied six samples, out of which for four samples the π -periodic component $I(\phi)$ was experimentally observed”). Furthermore the second harmonic contribution of each of the six samples was different (See Il’ichev 1999, column 2, page 3097). Lindström fabricated a number of devices that include Josephson junctions in YBCO using bicrystal techniques. Lindström reported that the critical current varied from sample to sample (Lindström, Exhibit D, page 117002-2, column 2, third full paragraph). Further, Lindström found that the first order and second order harmonics varied by as much as ten times between the two junctions in each of the manufactured devices. (Lindström, page 117002-4, column 1, first paragraph “[t]he ratios of I_c' and I_c'' can vary as much as 10 times

between two junctions in the same SQUID”). Thus, even the state of the art methods for manufacturing clean Josephson junctions such as Il’ichev 1999 and Lindström have failed to make clean Josephson junctions with consistent second order harmonics.

The results of Il’ichev 1999 and Lindström show that each clean Josephson junction would have to be characterized to determine the magnitude of the first and second harmonics. Such a step is not presently needed in Char and there is simply no motivation to alter Char to introduce such a step since Char does not teach or suggest the use of devices that make use of the second order harmonics of clean Josephson junctions. In contrast, characterization of each clean Josephson junction for use in the quantum devices claimed by Applicant provides no drawback.

8.1.4 The prior art provides no motivation to combine Tinkham and Char

If it is not shown that the prior art gives a reason or motivation to make the claimed invention, then there is no *prima facie* case and the Applicant should prevail. *In re Grabiak*, 769 F.2d 729 (Fed Cir 1985). It is improper to use hindsight reconstruction based upon the disclosure of the Applicant’s own specification. These type of hindsight rejections are specifically prohibited. See *In re Vaeck*, 947 F.2d 488, 493, 20 U.S.P.Q.2d 1438, 1442 (Fed. Cir. 1991); and *In re Fine*, 837 F.2d 1071, 1075, 5 U.S.P.Q.2d 1596 (Fed. Cir. 1988).

Even if Char were combined with Tinkham, the present invention would not be obvious since neither of them teaches the specific claimed structures as explained above. In addition, there is nothing in the references to motivate one of ordinary skill in the art to modify the structures disclosed in the cited references to arrive at the claimed invention. The Applicant’s own disclosure cannot be used to fill the gap between the cited references and the claimed invention.

8.1.5 Conclusion

For the above-identified reasons, claims 1, 8, 28, 39, 60, and 64 are patentable over any combination of Tinkham and Char. Furthermore, all other pending claims depend from one of these claims and are therefore patentable over the combination of Tinkham and Char for at least the same reasons. Certain claims are rejected as being unpatentable over Tinkham, in view of Char and further in view of Baechtold. However, Baechtold merely teaches a binary circuit consisting of a series/parallel arrangement of Josephson junctions. As such, Baechtold does not remedy the above-identified deficiencies in the combination of Tinkham and Char. Certain of the claims are rejected as being unpatentable over Tinkham, in

view of Char, in view of Shnirman. However, Shnirman merely teaches a single-electron transistor capacitively coupled to a Josephson junction qubit. As such, Shnirman does not remedy the above-identified deficiencies in the combination of Tinkham and Char. Certain of the claims are rejected as being unpatentable over Tinkham, in view of Char, Baechtold, and further in view of Shnirman. None of these references, either alone or in combination, remedy the above-identified deficiencies. For these reasons, all the claims are patentable over any combination of Tinkham, Char, Baechtold, and Shnirman. Additional reasons for patentability of some of the pending claims are provided in the following subsection.

8.2 Group II: Claims 60-63

Claims 60-63 are directed to a qubit with circuitry to allow selective interruption of quantum tunneling between a first ground state and a second ground state. In the October 20, 2004, Office Action, the Examiner stated that claims 60-63 are unpatentable over Tinkham in view of Char because Char shows a superconducting quantum interference device (SQUID) and the Examiner argued that tunneling occurs in such devices. While tunneling may in fact occur in such devices, it is not quantum tunneling as claimed in claims 60-63. Quantum tunneling can only arise in a mesoscopic system. Char does not teach or suggest a SQUID that is mesoscopic. Tinkham teaches a mesoscopic island but does not teach or suggest a SQUID. Furthermore, there is no suggestion in either reference nor any motivation in the art to combine the two references to make a mesoscopic SQUID.

9. CONCLUSION

For all of the foregoing reasons, reversal of the rejections of claims 1-8, 11-18, 28, 30-39, and 42-65 is respectfully requested.

Respectfully submitted,

Date: November 23, 2004


Brett Lovejoy 42,813
JONES DAY (Reg. No.)
222 East 41st Street
New York, New York 10017-6702
Telephone: (415) 875-5744



APPENDIX A

APPEALED CLAIMS

1. (previously presented) A quantum computing structure comprising:
a first bank of a superconducting material having a first crystal orientation;
a mesoscopic island of a superconducting material having a second crystal orientation,
wherein at least one of the island and the bank comprises a d-wave superconducting material;
and
a clean Josephson junction between the island and the bank.
2. (original) The structure of claim 1, further comprising a single electron transistor connected between the island and ground.
3. (previously presented) The structure of claim 1, wherein the clean Josephson junction comprises a grain boundary between the bank and the island.
4. (original) The structure of claim 1, wherein the island comprises a d-wave superconducting material.
5. (original) The structure of claim 4, wherein the bank comprises a d-wave superconducting material.
6. (original) The structure of claim 1, further comprising:
a second bank of superconducting material having a third crystal orientation; and
a Josephson junction between the first and second banks.
7. (original) The structure of claim 6, further comprising a single electron transistor coupled between the second bank and the island.
8. (previously presented) A quantum register comprising:
a bank of a superconducting material;
a plurality of mesoscopic islands of superconducting material; and

a plurality of clean Josephson junctions, each clean Josephson junction being between the bank and a corresponding one of the islands, wherein at least one of the plurality of mesoscopic islands and the bank comprises a d-wave superconducting material.

9-10. (cancelled)

11. (original) The quantum register of claim 8, further comprising a plurality of single electron transistors, each electron transistor being between ground and a corresponding one of the islands.

12. (original) The quantum register of claim 8, further comprising a first plurality of single electron transistors, each single electron transistor in the first plurality being between islands in a corresponding pair of the islands.

13. (previously presented) The quantum register of claim 12, further comprising a second plurality of single electron transistors, each single electron transistor in the second plurality being between ground and a corresponding one of the plurality of mesoscopic islands.

14. (original) The quantum register of claim 8, further comprising:
a second bank of superconducting material; and
a Josephson junction between the first and second banks.

15. (original) The quantum register of claim 14, further comprising a first plurality of single electron transistors, each single electron transistor being coupled between the second bank and a corresponding one of the islands.

16. (original) The quantum register of claim 15, further comprising a second plurality of single electron transistors, each single electron transistor in the second plurality being between ground and a corresponding one of the islands.

17. (original) The quantum register of claim 15, further comprising a second plurality of a single electron transistors, each single electron transistor in the second plurality being between islands in a corresponding pair of the islands.

18. (previously presented) The quantum register of claim 17, further comprising a third plurality of single electron transistors, each single electron transistor in the third plurality being between ground and a corresponding one of the plurality of mesoscopic islands.

28. (previously presented) A qubit, comprising:
a first bank of a superconducting material having a first crystal orientation;
a mesoscopic island having a second crystal orientation formed adjacent to the first bank; and
a clean Josephson junction formed between the first bank and the mesoscopic island, wherein the first crystal orientation and the second crystal orientation are different wherein at least one of the mesoscopic island and the first bank comprises a d-wave superconducting material.

29. (cancelled)

30. (previously presented) The qubit of Claim 28, further including a grounding mechanism coupled between the mesoscopic island and a ground.

31. (previously presented) The qubit of Claim 30, wherein the grounding mechanism is a single electron transistor.

32. (previously presented) The qubit of Claim 30, wherein the grounding mechanism is a parity key.

33. (previously presented) The qubit of Claim 28, wherein the clean Josephson junction includes a grain boundary between the island and the first bank.

34. (previously presented) The qubit of Claim 28, wherein the clean Josephson junction includes a normal metal.

35. (previously presented) The qubit of Claim 28, further comprising:
a second bank of superconducting material having a third crystal orientation; and

a Josephson junction formed between the first bank and the second bank.

36. (previously presented) The qubit of Claim 35, further comprising:
a coupling mechanism coupled between the mesoscopic island and the second bank.

37. (previously presented) The qubit of Claim 36, wherein the coupling mechanism includes a single electron transistor.

38. (previously presented) The qubit of Claim 36, wherein the coupling mechanism includes a parity key.

39. (previously presented) A quantum register, comprising:
a first bank of superconducting material;
at least one mesoscopic island of a superconducting material; and
at least one clean Josephson junction, each clean Josephson junction in said at least one clean Josephson junction formed between a mesoscopic island in the at least one mesoscopic island and the first bank, wherein at least one of the at least one mesoscopic island and the first bank comprises a d-wave superconducting material.

40-41. (cancelled)

42. (previously presented) The quantum register of Claim 39, further including at least one first coupling mechanism, each of the at least one first coupling mechanisms coupling a corresponding one of the at least one mesoscopic islands to ground.

43. (previously presented) The quantum register of Claim 42, wherein said at least one first coupling mechanism includes a single electron transistor.

44. (previously presented) The quantum register of Claim 42, wherein said at least one first coupling mechanism includes a parity key.

45. (previously presented) The quantum register of Claim 39, wherein said at least one mesoscopic island includes a pair of mesoscopic islands that are coupled to each other by a second coupling mechanism.

46. (previously presented) The quantum register of Claim 45, wherein the second coupling mechanism includes a single electron transistor.

47. (previously presented) The quantum register of Claim 45, wherein the second coupling mechanism includes a parity key.

48. (previously presented) The quantum register of Claim 39, further including:
a second bank of superconducting material; and
a Josephson junction formed between the second bank and the first bank.

49. (previously presented) The quantum register of Claim 48, further including a third coupling mechanism coupled between a mesoscopic island in said at least one mesoscopic island and the second bank.

50. (previously presented) The quantum register of Claim 49, wherein the third coupling mechanism includes a single electron transistor.

51. (previously presented) The quantum register of Claim 49, wherein the third coupling mechanism includes a parity key.

52. (previously presented) The structure of claim 1, wherein a qubit is formed by the first bank, the mesoscopic island and the clean Josephson junction, and wherein each quantum state on the qubit is characterized by a clockwise or a counterclockwise supercurrent that circulates in a plane in the vicinity of the clean Josephson junction.

53. (previously presented) The quantum register of claim 8, wherein a plurality of qubits is formed by the plurality of mesoscopic islands, the bank, and the plurality of clean Josephson junctions, and wherein each quantum state on each respective qubit in said plurality of qubits is characterized by a clockwise or a counterclockwise supercurrent that circulates in a plane in the vicinity of the Josephson junction in said respective qubit.

54. (previously presented) The qubit of claim 28, wherein each quantum state on the qubit is characterized by a clockwise or a counterclockwise supercurrent that circulates in a plane in the vicinity of the clean Josephson junction.

55. (previously presented) The quantum register of claim 39, wherein a qubit is formed by each mesoscopic island in the at least one mesoscopic island together with the first bank and a Josephson junction in the at least one Josephson junction, and wherein each quantum state of each said qubit is characterized by a clockwise or a counterclockwise supercurrent that circulates in a plane in the vicinity of the Josephson junction in said qubit.

56. (previously presented) The structure of claim 1, wherein a qubit is formed by the first bank, the mesoscopic island and the clean Josephson junction, and wherein the qubit has a quantum state that is twice degenerate in the absence of an external electromagnetic field.

57. (previously presented) The quantum register of claim 8, wherein a plurality of qubits is formed by the plurality of mesoscopic islands, the bank, and the plurality of clean Josephson junctions, and wherein each qubit in said plurality of qubits has a quantum state that is twice degenerate in the absence of an external electromagnetic field.

58. (previously presented) The qubit of claim 28, wherein the qubit has a quantum state that is twice degenerate in the absence of an external electromagnetic field.

59. (previously presented) The quantum register of claim 39, wherein a qubit is formed by each mesoscopic island in the at least one mesoscopic island together with the first bank and a Josephson junction in the at least one Josephson junction, and wherein each said qubit has a quantum state that is twice degenerate in the absence of an external electromagnetic field.

60. (previously presented) A qubit comprising:
a first bank of a superconducting material having a first crystal orientation;
a mesoscopic island of a superconducting material having a second crystal orientation,
wherein at least one of the mesoscopic island and the bank comprises a d-wave superconducting material;

a clean Josephson junction between the island and the bank, wherein the Josephson junction is configured so that a supercurrent proximate to the Josephson junction alternates between a first ground state having a first magnetic moment and a second ground state having a second magnetic moment by means of quantum tunneling; and

circuitry to allow selective interruption of quantum tunneling between the first ground state and the second ground state.

61. (previously presented) The qubit of claim 60, wherein the circuitry comprises a parity key that connects the island to ground.

62. (previously presented) The qubit of claim 60, wherein the circuitry comprises a single electron transistor that connects the island to ground.

63. (previously presented) A quantum computer comprising the qubit of claim 60 and a readout device for detecting whether the supercurrent has the first magnetic moment or the second magnetic moment.

64. (previously presented) A quantum register comprising:
a bank of a superconducting material;
a plurality of mesoscopic islands of superconducting material;
a plurality of clean Josephson junctions, wherein each respective Josephson junction:
is between the bank and a corresponding one of the islands; and
is configured so that a supercurrent proximate to the respective Josephson junction alternates between a first ground state having a first magnetic moment and a second ground state having a second magnetic moment; and
circuitry to allow selective interruption of the alternating between the first ground state and the second ground state of the supercurrent associated with each Josephson junction, and wherein at least one of the plurality of mesoscopic islands and the bank comprises a d-wave superconducting material.

65. (previously presented) A quantum computer comprising the quantum register of claim 64 and a readout device for detecting whether the supercurrent of each clean Josephson junction has the first magnetic moment or the second magnetic moment.

Exhibit A

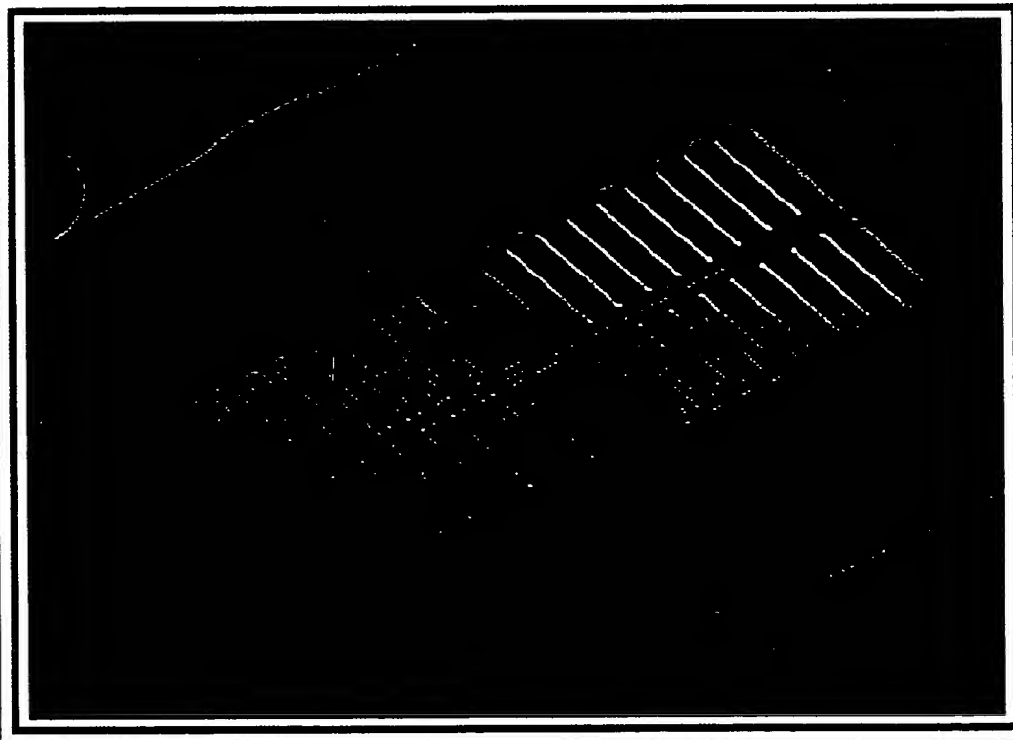
DiVincenzo in *Scalable Quantum Computers*, Braunstein and Lo, eds.,
Wiley-VCH, 2001, Berlin

BEST AVAILABLE COPY

S. L. BRAUNSTEIN and H.-K. LO (eds.)

SCALABLE QUANTUM COMPUTERS

PAVING THE WAY TO REALIZATION



 WILEY-VCH

Editors:

Prof. Dr. Samuel L. Braunstein, University of Wales, Bangor, UK

e-mail: schmuel@sees.bangor.ac.uk

Dr. Hoi-Kwong Lo, MagiQ Technologies, Inc., New York

e-mail: hoi_kwong@magiqtech.com

Assistant Editor:

Pieter Kok, University of Wales, Bangor, UK

e-mail: pieter@sees.bangor.ac.uk

This book was carefully produced. Nevertheless, editors, authors and publisher do not warrant the information contained therein to be free of errors. Readers are advised to keep in mind that statements, data, illustrations, procedural details or other items may inadvertently be inaccurate.

1st edition, 2001

Cover Picture:

Photograph of a structured electronic device, showing an array of inter-connected microchannels. 1.6 μm deep and 16 μm wide. Surface-state electrons on superfluid helium in these channels is one of the novel systems under investigation for quantum computing.

(The device was fabricated on GaAs at the Niels Bohr Institute, Copenhagen. Image by Philip Glasson.)

Library of Congress Card No.: applied for

A catalogue record for this book is available from the British Library.

Die Deutsche Bibliothek - CIP Cataloguing-in-Publication-Data

A catalogue record for this publication is available from Die Deutsche Bibliothek

ISBN 3-527-40321-3

© WILEY-VCH Verlag Berlin GmbH, Berlin (Federal Republic of Germany), 2001

Printed on acid-free paper.

All rights reserved (including those of translation in other languages). No part of this book may be reproduced in any form - by photoprinting, microfilm, or any other means - nor transmitted or translated into machine language without written permission from the publishers. Registered names, trademarks, etc. used in this book, even when not specifically marked as such, are not to be considered unprotected by law.

Composition: Druckhaus „Thomas Müntzer“ GmbH, D-99947 Bad Langensalza. Printing: Strauss Offsetdruck GmbH, D-69509 Mörlenbach. Bookbinding: Wilhelm Osswald & Co., D-67433 Neustadt.

Printed in the Federal Republic of Germany.

WILEY-VCH Verlag Berlin GmbH

Böhringstraße 10

D-13086 Berlin

Federal Republic of Germany

..... 229

The Physical Implementation of Quantum Computation

..... 235

DAVID P. DiVINCENZO

IBM T. J. Watson Research Center, Yorktown Heights, NY 10598 USA

..... 253

Abstract

..... 273

After a brief introduction to the principles and promise of quantum information processing, the requirements for the physical implementation of quantum computation are discussed. These five requirements, plus two relating to the communication of quantum information, are extensively explored and related to the many schemes in atomic physics, quantum optics, nuclear and electron magnetic resonance spectroscopy, superconducting electronics, and quantum-dot physics, for achieving quantum computing.

..... 287

..... 305

1. Introduction

..... 325

The advent of quantum information processing, as an abstract concept, has given birth to a great deal of new thinking, of a very concrete form, about how to create physical computing devices that operate in the hitherto unexplored quantum mechanical regime. The efforts now underway to produce working laboratory devices that perform this profoundly new form of information processing are the subject of this book.

..... 339

In this chapter I provide an overview of the common objectives of the investigations reported in the remainder of this special issue. The scope of the approaches, proposed and underway, to the implementation of quantum hardware is remarkable, emerging from specialties in atomic physics [1], in quantum optics [2], in nuclear [3] and electron [4] magnetic resonance spectroscopy, in superconducting device physics [5], in electron physics [6], and in mesoscopic and quantum dot research [7]. This amazing variety of approaches has arisen because, as we will see, the principles of quantum computing are posed using the most fundamental ideas of quantum mechanics, ones whose embodiment can be contemplated in virtually every branch of quantum physics.

..... 355

..... 363

The interdisciplinary spirit which has been fostered as a result is one of the most pleasant and remarkable features of this field. The excitement and freshness that has been produced bodes well for the prospect for discovery, invention, and innovation in this endeavor.

2. Why *Quantum* Information Processing?

The shortest of answers to this question would be, why not? The manipulation and transmission of information is today carried out by physical machines (computers, routers, scanners, etc.), in which the embodiment and transformations of this information can be described using the language of classical mechanics. But the final physical theory of the world is not Newtonian mechanics, and there is no reason to suppose that machines following the laws of quantum mechanics should have the same computational power as classical machines; indeed, since Newtonian mechanics emerges as a special limit of quantum mechanics, quantum machines can only have greater computational power than classical ones. The great pioneers and visionaries who pointed the way towards quantum computers, DEUTSCH [8], FEYNMAN [9], and others, were stimulated by such thoughts. Of course, by a

similar line of reasoning, it may well be asked whether machines embodying the principles of other refined descriptions of nature (perhaps general relativity or string theory) may have even more information processing capabilities; speculations exist about these more exotic possibilities, but they are beyond the scope of the present discussion.

But computing with quantum mechanics really deserves a lot more attention than worm-hole computing or quantum-gravity computing; quantum computing, while far in the future from the perspective of CMOS roadmaps and projections of chip fab advances, can certainly be seen as a real prospect from the perspective of research studies in quantum physics. It does not require science fiction to envision a quantum computer: the proposals discussed later in this issue paint a rather definite picture of what a real quantum computer will look like.

So, how much is gained by computing with quantum physics over computing with classical physics? We do not seem to be near to a final answer to this question, which is natural since even the ultimate computing power of classical machines remains unknown. But the answer as we know it today has an unexpected structure; it is not that quantum tools simply speed up all information processing tasks by a uniform amount. By a standard complexity measure (i.e., the way in which the number of computational steps required to complete a task grows with the "size" n of the task), some tasks are not sped up at all [10] by using quantum tools (e.g., obtaining the n th iterate of a function $f(f(\dots f(x)\dots))$ [11]), some are sped up moderately (locating an entry in a database of n entries [12]), and some are apparently sped up exponentially (Shor's algorithm for factoring an n -digit number [13]).

In other types of information processing tasks, particularly those involving communication [14], both quantitative and qualitative improvements are seen [15]: for certain tasks (choosing a free day for an appointment between two parties from out of n days) there is a quadratic reduction of the amount of communicated data required, if quantum states rather than classical states are transmitted [16]. For some tasks (the "set disjointness problem", related to allocating non-overlapping segments of a shared memory in a distributed computation) the reduction of required communication is exponential [17]. Finally, there are tasks that are doable in the quantum world that have no counterpart classically: quantum cryptography provides an absolute secrecy of communication between parties that is impossible classically [18]. And for some games, winning strategies become possible with the use of quantum resources that are not available otherwise [19, 20].

This issue, and this chapter, are primarily concerned with the "hows" of quantum computing rather than the "whys," so we will leave behind the computer science after this extremely brief mention. There is no shortage of other places to obtain more information about these things; I recommend the recent articles by Aharonov [21] and by Cleve [22]; other general introductions [23] will give the reader pointers to the already vast specialized literature on this subject.

3. Realizing Quantum Computation

Let me proceed with the main topic: the physical realization of quantum information processing. As a guide to the remainder of the special issue, and as a means of reviewing the basic steps required to make quantum computation work, I can think of no better plan than to review a set of basic criteria that my coworkers and I have been discussing over the last few years [24] for the realization of quantum computation (and communication), and to discuss the application of these criteria to the multitude of physical implementations that are found below.

So, without further ado, here are the

Five (plus two) requirements for the implementation of quantum computation

1. A scalable physical system with well characterized qubits

For a start, a physical system containing a collection of qubits is needed. A qubit (or, more precisely, the embodiment of a qubit) is [25] simply a quantum two-level system like the two spin states of a spin 1/2 particle, like the ground and excited states of an atom, or like the vertical and horizontal polarization of a single photon. The generic notation for a qubit state denotes one state as $|0\rangle$ and the other as $|1\rangle$. The essential feature that distinguishes a qubit from a bit is that, according to the laws of quantum mechanics, the permitted states of a single qubit fills up a two-dimensional complex vector space; the general state is written $a|0\rangle + b|1\rangle$, where a and b are complex numbers, and a normalization convention $|a|^2 + |b|^2 = 1$ is normally adopted. The general state of two qubits, $a|00\rangle + b|01\rangle + c|10\rangle + d|11\rangle$, is a four-dimensional vector, one dimension for each distinguishable state of the two systems. These states are generically *entangled*, meaning that they cannot be written as a product of the states of two individual qubits. The general state of n qubits is specified by a 2^n -dimensional complex vector.

A qubit being "well characterized" means several different things. Its physical parameters should be accurately known, including the internal Hamiltonian of the qubit (which determines the energy eigenstates of the qubit, which are often, although not always, taken as the $|0\rangle$ and $|1\rangle$ states), the presence of and couplings to other states of the qubit, the interactions with other qubits, and the couplings to external fields that might be used to manipulate the state of the qubit. If the qubit has third, fourth, etc., levels, the computer's control apparatus should be designed so that the probability of the system ever going into these states is small. The smallness of this and other parameters will be determined by the capabilities of quantum error correction, which will be discussed under requirement 3.

Recognizing a qubit can be trickier than one might think. For example, we might consider a pair of one-electron quantum dots that share a single electron between them as a two-qubit system. It is certainly true that we can denote the presence or absence of an electron on each dot by $|0\rangle$ and $|1\rangle$, and it is well known experimentally how to put this system into the "entangled" state $1/\sqrt{2}(|01\rangle + |10\rangle)$ in which the electron is in a superposition of being on the left dot and the right dot. But it is fallacious to consider this as a two-qubit system; while the states $|00\rangle$ and $|11\rangle$ are other allowed physical states of the dots, superselection principles forbid the creation of entangled states involving different particle numbers such as $1/\sqrt{2}(|00\rangle + |11\rangle)$.

It is therefore false to consider this as a two-qubit system, and, since there are not two qubits, it is nonsense to say that there is entanglement in this system. It is correct to say that the electron is in a superposition of different quantum states living on the two different dots. It is also perfectly correct to consider this system to be the embodiment of a *single* qubit, spanned by the states (in the misleading notation above) $|01\rangle$ ("electron on the right dot") and $|10\rangle$ ("electron on the left dot"). Indeed, several of the viable proposals, including the ones by Schön, Averin, and Tanamoto in this special issue, use exactly this system as a qubit. However, false lines of reasoning like the one outlined here have sunk various proposals before they were properly launched (no such abortive proposals are represented in this book, but they can be found occasionally in the literature).

An amazing variety of realizations of the qubit are represented in this volume. There is a very well developed line of work that began with the proposal of CIRAC and ZOLLER [1] for an ion-trap quantum computer, in which, in its quiescent state, the computer holds the qubits in pairs of energy levels of ions held in a linear electromagnetic trap. Various pairs of energy levels (e.g., Zeeman-degenerate ground states, as are also used in the NMR approach [3] discussed by Cory) have been proposed and investigated experimentally. The many neutral-atom proposals (see chapters by KIMBLE [2], DEUTSCH [26], and BRIEGEL [27]) use similar atomic energy levels of neutral species. These atomic-physics based propos-

als use other auxiliary qubits such as the position of atoms in a trap or lattice, the presence or absence of a photon in an optical cavity, or the vibrational quanta of trapped electrons, ions or atoms (in the Platzman proposal below [6] this is the primary qubit). Many of the solid-state proposals exploit the fact that impurities or quantum dots have well characterized discrete energy level spectra; these include the spin states of quantum dots (see chapters by LOSS [7] and IMAMOGLU [2]), the spin states of donor impurities (see KANE [4]), and the orbital or charge states of quantum dots (see TANAMOTO [7]). Finally, there are a variety of interesting proposals which use the quantized states of superconducting devices, either ones involving the (Cooper-pair) charge (see SCHÖN, AVERIN), or the flux (see MOOIJ) [5].

2. The ability to initialize the state of the qubits to a simple fiducial state, such as $|000\dots\rangle$

This arises first from the straightforward computing requirement that registers should be initialized to a known value before the start of computation. There is a second reason for this initialization requirement: quantum error correction (see requirement 3 below) requires a continuous, fresh supply of qubits in a low-entropy state (like the $|0\rangle$ state). The need for a continuous supply of 0s, rather than just an initial supply, is a real headache for many proposed implementations. But since it is likely that a demonstration of a substantial degree of quantum error correction is still quite some time off, the problem of continuous initialization does not have to be solved very soon; still, experimentalists should be aware that the speed with which a qubit can be zeroed will eventually be a very important issue. If the time it takes to do this initialization is relatively long compared with gate-operation times (see requirement 4), then the quantum computer will have to be equipped with some kind of "qubit conveyor belt", on which qubits in need of initialization are carried away from the region in which active computation is taking place, initialized while on the "belt", then brought back to the active place after the initialization is finished. (A similar parade of qubits will be envisioned in requirement 5 for the case of low quantum-efficiency measurements [28].)

There are two main approaches to setting qubits to a standard state: the system can either be "naturally" cooled when the ground state of its Hamiltonian is the state of interest, or the standard state can be achieved by a measurement which projects the system either into the state desired or another state which can be rotated into it. These approaches are not fundamentally different from one another, since the projection procedure is a form of cooling; for instance, the laser cooling techniques used routinely now for the cooling of ion states to near their ground state in a trap [1] are closely connected to the fluorescence techniques used to measure the state of these ions. A more "natural" kind of cooling is advocated in many of the electron spin resonance based techniques (using quantum dots or impurities) [7, 4] in which the spins are placed in a strong magnetic field and allowed to align with it via interaction with their heat bath. In this kind of approach the time scale will be a problem. Since the natural thermalization times are never shorter than the decoherence time of the system, this procedure will be too slow for the needs of error correction and a "conveyor belt" scheme would be required. Cooling by projection, in which the Hamiltonian of the system and its environment are necessarily perturbed strongly, will have a time scale dependent on the details of the setup, but potentially much shorter than the natural relaxation times. One cannot say too much more at this point, as the schemes for measurement have in many cases not been fully implemented (see requirement 5). In the NMR quantum computer implementations to date (see Cory below), cooling of the initial state has been foregone altogether; it is acknowledged [3] that until some of the proposed cooling schemes are implemented (a nontrivial thing to do), NMR can never be a scalable scheme for quantum computing.

3. Long relevant decoherence times, much longer than the gate operation time

Decoherence times characterize the dynamics of a qubit (or any quantum system) in contact with its environment. The (somewhat overly) simplified definition of this time is that it is

the characteristic time for a generic qubit state $|\psi\rangle = a|0\rangle + b|1\rangle$ to be transformed into the mixture $\rho = |a|^2|0\rangle\langle 0| + |b|^2|1\rangle\langle 1|$. A more proper characterization of decoherence, in which the decay can depend on the form of the initial state, in which the state amplitudes may change as well, and in which other quantum states of the qubit can play a role (in a special form of state decay called "leakage" in quantum computing [29, 30]), is rather more technical than I want to get here; but see Refs. [31] and [32] for a good general discussion of all these. Even the simplest discussion of decoherence that I have given here should also be extended to include the possibility that the decoherence of neighboring qubits is correlated. It seems safest to assume that they will be neither completely correlated nor completely uncorrelated, and the thinking about error correction has taken this into account.

Decoherence is very important for the fundamentals of quantum physics, as it is identified as the principal mechanism for the emergence of classical behavior. For the same reason, decoherence is very dangerous for quantum computing, since if it acts for very long, the capability of the quantum computer will not be so different from that of a classical machine. The decoherence time must be long enough that the uniquely quantum features of this style of computation have a chance to come into play. How long is "long enough" is also indicated by the results of quantum error correction, which I will summarize shortly.

I have indicated that the "relevant" decoherence times should be long enough. This emphasizes that a quantum particle can have many decoherence times pertaining to different degrees of freedom of that particle. But many of these can be irrelevant to the functioning of this particle as a qubit. For example, the rapid decoherence of an electron's position state in a solid state environment does not preclude its having a very long spin coherence time, and it can be arranged that this is the only time relevant for quantum computation. Which time is relevant is determined by the choice of the qubit basis states $|0\rangle$ and $|1\rangle$; for example, if these two states correspond to different spin states but identical orbital states, then orbital decoherence will be irrelevant.

One might worry that the decoherence time necessary to do a successful quantum computation will scale with the duration of the computation. This would place incredibly stringent requirements on the physical system implementing the computation. Fortunately, in one of the great discoveries of quantum information theory (in 1995–1996), it was found that error correction of quantum states is possible [33] and that this correction procedure can be successfully applied in quantum computation [34], putting much more reasonable (although still daunting) requirements on the needed decoherence times.

In brief, quantum error correction starts with coding; as in binary error correction codes, in which only a subset of all boolean strings are "legal" states, quantum error correction codes consist of legal states confined to a subspace of the vector space of a collection of qubits. Departure from this subspace is caused by decoherence. Codes can be chosen such that, with a suitable sequence of quantum computations and measurements of some ancillary qubits, the error caused by decoherence can be detected and corrected. As noted above, these ancillary qubits have to be continuously refreshed for use. I will not go much farther into the subject here, see [31] for more. It is known that quantum error correction can be made fully fault tolerant, meaning that error correction operations can be successfully intermingled with quantum computation operations, that errors occurring during the act of error correction, if they occur at a sufficiently small rate, do no harm, and that the act of quantum computation does not itself cause an unreasonable proliferation of errors.

These detailed analyses have indicated the magnitude of decoherence time scales that are acceptable for fault-tolerant quantum computation. The result is that, if the decoherence time is 10^4 – 10^5 times the "clock time" of the quantum computer, that is, the time for the execution of an individual quantum gate (see requirement 4), then error correction can be successful. This is, to tell the truth, a rather stringent condition, quantum systems frequently do not have such long decoherence times. But sometimes they do, and our search for a successful physical implementation must turn towards these. At least this result says that

the required decoherence rate does not become ever smaller as the size and duration of the quantum computation grows. So, once the desired threshold is attainable, decoherence will not be an obstacle to scalable quantum computation.

Having said this, it must be admitted that it will be some time before it is even possible to subject quantum error correction to a reasonable test. Nearly all parts of requirements 1–5 must be in place before such a test is possible. And even the most limited application of quantum error correction has quite a large overhead: roughly 10 ancillary qubits must be added for each individual qubit of the computation. Fortunately, this overhead ratio grows only logarithmically as the size of the quantum computation is increased.

In the short run, it is at least possible to design and perform experiments which measure the decoherence times and other relevant properties (such as the correlation of decoherence of neighboring qubits) of candidate implementations of qubits. With such initial test experiments, caution must be exercised in interpreting the results, because decoherence is a very system-specific phenomenon, depending on the details of all the qubits' couplings to various environmental degrees of freedom. For example, the decoherence time of the spin of an impurity in the bulk of a perfect semiconductor may not be the same as its decoherence time when it is near the surface of the solid, in the immediate neighborhood of device structures designed to manipulate its quantum state. Test experiments should probe decoherence in as realistic a structure as is possible.

4. A "universal" set of quantum gates

This requirement is of course at the heart of quantum computing. A quantum algorithm is typically specified [8] as a sequence of unitary transformations U_1, U_2, U_3, \dots , each acting on a small number of qubits, typically no more than three. The most straightforward transcription of this into a physical specification is to identify Hamiltonians which generate these unitary transformations, viz., $U_1 = e^{iH_1 t/\hbar}$, $U_2 = e^{iH_2 t/\hbar}$, $U_3 = e^{iH_3 t/\hbar}$, etc.; then, the physical apparatus should be designed so that H_1 can be turned on from time 0 to time t , then turned off and H_2 turned on from time t to time $2t$, etc.

Would that life were so simple! In reality what can be done is much less, but much less can be sufficient. Understanding exactly how much less is still enough, is the main complication of this requirement. In all the physical implementations discussed in this volume, only particular sorts of Hamiltonians can be turned on and off; in most cases, for example, only two-body (two-qubit) interactions are considered. This immediately poses a problem for a quantum computation specified with three-qubit unitary transformations; fortunately, of course, these can always be re-expressed in terms of sequences of one- and two-body interactions [35], and the two-body interactions can be of just one type [36], the "quantum XOR" or "cNOT". There are some implementations in which multi-qubit gates can be implemented directly [37].

However, this still leaves a lot of work to do. In some systems, notably in NMR (see Cory), there are two-body interactions present which cannot be turned off, as well as others which are switchable. This would in general be fatal for quantum computation, but the particular form of the fixed interactions permit their effects to be annulled by particular "refocusing" sequences of the controllable interactions, and it has recently been discovered [38] that these refocusing sequences can be designed and implemented efficiently.

For many other systems, the two-body Hamiltonian needed to generate directly the cNOT unitary transformation is not available. For example, in the quantum-dot proposal described by Loss below [7], the only two-body interaction which should be easily achievable is the exchange interaction between neighboring spins, $H \propto \vec{S}_i \cdot \vec{S}_{i+1}$; in the Imamoglu chapter [2], the attainable interaction is of the XY type, i.e., $H \propto S_{ix}S_{jx} + S_{iy}S_{jy}$. An important observation is that with the appropriate sequence of exchange or XY interactions, in conjunction with particular one-body interactions (which are assumed to be more easily doable), the cNOT transformation can be synthesized [39]. It is incumbent on each implementation pro-

duration of the
ecoherence will

is even possible
of requirements
ited application
qubits must be
ead ratio grows

which measure
of decoherence
initial test experi-
ence is a very
couplings to var-
e of the spin of
its decoherence
hood of device
probe decoher-

um algorithm is
..., each acting
ghtforward tran-
which generate
, etc.; then, the
ime 0 to time t ,

s, but much less
ne main compli-
in this volume,
es, for example,
oses a problem
ons; fortunately,
- and two-body
, the "quantum
it gates can be

ty in NMR (see
is well as others
utation, but the
ed by particular
been discovered
iently.

rectly the cNOT
oposal described
chievable is the
oglu chapter [2],
portant observa-
, in conjunction
sily doable), the
lementation pro-

posal to exhibit such a sequence for producing the cNOT using the interactions that are naturally realizable.

Often there is also some sophisticated thinking required about the time profile of the two-qubit interaction. The naive description above uses a "square pulse" time profile, but often this is completely inappropriate; for instance, if the Hamiltonian can also couple the qubit to other, higher-lying levels of the quantum system, often the only way to get the desired transformation is to turn on and off the interaction smoothly and slowly enough that an adiabatic approximation is accurate [29, 30] (in a solid-state context, see also [40]). The actual duration of the pulse will have to be sufficiently long that any such adiabatic requirement is satisfied; then typically only the time integral $\int dt H(t)$ is relevant for the quantum gate action. The overall time scale of the interaction pulse is also controlled by the attainable maximum size of the matrix elements of $H(t)$, which will be determined by various fundamental considerations, like the requirement that the system remains in the regime of validity of a linear approximation, and practical considerations, like the laser power that can be concentrated on a particular ion. Given these various constraints, the "clock time" of the quantum computer will be determined by the time interval needed such that two consecutive pulses have negligible overlap.

Another consideration, which does not seem to present a problem with any current implementation schemes, but which may be an issue in the future, is the classicality of the control apparatus. We say that the interaction Hamiltonian $H(t)$ has a time profile which is controlled externally by some "classical" means, that is, by the intensity of a laser beam, the value of a gate voltage, or the current level in a wire. But each of these control devices is made up themselves of quantum mechanical parts. When we require that these behave classically, it means that their action should proceed without any entanglement developing between these control devices and the quantum computer. Estimates indicate that this entanglement can indeed be negligible, but this effect needs to be assessed for each individual case.

In many cases it is impossible to turn on the desired interaction between a pair of qubits; for instance, in the ion-trap scheme, no direct interaction is available between the ion-level qubits [1]. In this and in other cases, a special quantum subsystem (sometimes referred to as a "bus qubit") is used which can interact with each of the qubits in turn and mediate the desired interaction: for the ion trap, this is envisioned to be the vibrational state of the ion chain in the trap; in other cases it is a cavity photon whose wavefunction overlaps all the qubits. Unfortunately, this auxiliary quantum system introduces new channels for the environment to couple to the system and cause decoherence, and indeed the decoherence occurring during gate operation is of concern in the ion-trap and cavity-quantum electrodynamics schemes.

Some points about requirement 4 are important to note in relation to the implementation of error correction. Successful error correction requires fully parallel operation, meaning that gate operations involving a finite fraction of all the qubits must be doable simultaneously. This can present a problem with some of the proposals in which the single "bus qubit" is needed to mediate each interaction. On the other hand, the constraint that interactions are only among nearest neighbors in a lattice, as in many of the solid-state proposals, does allow for sufficient parallelism [41].

Quantum gates cannot be implemented perfectly; we must expect both systematic and random errors in the implementation of the necessary Hamiltonians. Both types of errors can be viewed as another source of decoherence and thus error correction techniques are effective for producing reliable computations from unreliable gates, if the unreliability is small enough. The tolerable unreliability due to random errors is in the same vicinity as the decoherence threshold, that is, the magnitude of random errors should be 10^{-4} – 10^{-5} per gate operation or so. It might be hoped that systematic errors could be virtually eliminated by careful calibration; but this will surely not always be the case. It seems harder to give a

good rule for how much systematic error is tolerable, the conservative estimates give a very, very small number (the square of the above) [31], but on the other hand there seems to be some evidence that certain important quantum computations (e.g., the quantum Fourier transform) can tolerate a very high level of systematic error (over- or under-rotation). Some types of very large errors may be tolerable if their presence can be detected and accounted for on the fly (we are thinking, for example, about charge switching in semiconductors or superconductors).

Error correction requires that gate operations be done on coded qubits, and one might worry that such operations would require a new repertoire of elementary gate operations for the base-level qubits which make up the code. For the most important error correction techniques, using the so called "stabilizer" codes, this is not the case. The base-level toolkit is exactly the same as for the unencoded case: one-bit gates and cNOTs, or any gate repertoire that can produce these, are adequate. Sometimes the use of coding can actually *reduce* the gate repertoire required: in the work on decoherence free subspaces and subsystems, codes are introduced using blocks of three and four qubits for which two-qubit exchange interactions alone are enough to implement general quantum computation [42, 43]. This simplification could be very useful in the quantum-dot [7] or semiconductor-impurity [4] implementations.

5. A qubit-specific measurement capability

Finally, the result of a computation must be read out, and this requires the ability to measure specific qubits. In an ideal measurement, if a qubit's density matrix is $\rho = p|0\rangle\langle 0| + (1-p)|1\rangle\langle 1| + \alpha|0\rangle\langle 1| + \alpha^*|1\rangle\langle 0|$, the measurement should give outcome "0" with probability p and "1" with probability $1-p$ independent of α and of any other parameters of the system, including the state of nearby qubits, and without changing the state of the rest of the quantum computer. If the measurement is "non-demolition", that is, if in addition to reporting outcome "0" the measurement leaves the qubit in state $|0\rangle\langle 0|$, then it can also be used for the state preparation of requirement 2; but requirement 2 can be fulfilled in other ways.

Such an ideal measurement as I have described is said to have 100% quantum efficiency: real measurements always have less. While the fidelity of a quantum measurement is not captured by a single number, the single quantum-efficiency parameter is often a very useful way to summarize it, just as the decoherence time is a useful if incomplete summary of the damage caused to a quantum state by the environment.

While quantum efficiency of 100% is desirable, much less is needed for quantum computation; there is, in fact, a tradeoff possible between quantum efficiency and other resources which results in reliable computation. As a simple example, if the quantum efficiency is 90%, then, in the absence of any other imperfections, a computation with a single-bit output (a so-called "decision problem", common in computer science) will have 90% reliability. If 97% reliability is needed, this can just be achieved by rerunning the calculation three times. Much better, actually, is to "copy" the single output qubit to three, by applying two cNOT gates involving the output qubit and two other qubits set to $|0\rangle$, and measuring those three. (Of course, qubits cannot be "copied", but their value in a particular basis can.) In general, if quantum efficiency q is available, then copying to somewhat more than $1/q$ qubits and measuring all of these will result in a reliable outcome. So, a quantum efficiency of 1% would be usable for quantum computation, at the expense of hundreds of copies/re-measures of the same output qubit. (This assumes that the measurement does not otherwise disturb the quantum computer. If it does, the possibilities are much more limited.)

Even quantum efficiencies much, much lower than 1% can be and are used for successful quantum computation: this is the "bulk" model of NMR (see Cory and [3]), where macroscopic numbers of copies of the same quantum computer (different molecules in solu-

estimates give a and there seems e quantum Four- under-rotation). be detected and hing in semicon-

tion) run simultaneously, with the final measurement done as an ensemble average over the whole sample. These kinds of weak measurements, in which each individual qubit is hardly disturbed, are quite common and well understood in condensed-matter physics.

If a measurement can be completed quickly, on the timescale of 10^{-4} of the decoherence time, say, then its repeated application during the course of quantum computation is valuable for simplifying the process of quantum error correction. On the other hand, if this fast measurement capability is not available, quantum error correction is still possible, but it then requires a greater number of quantum gates to implement.

Other tradeoffs between the complexity and reliability of quantum measurement vs. those of quantum computation have recently been explored. It has been shown that if qubits can be initialized into pairs of maximally entangled states, and two-qubit measurements in the so-called Bell basis ($\Psi^\pm = |01\rangle \pm |10\rangle$, $\Phi^\pm = |00\rangle \pm |11\rangle$) are possible, then no two-qubit quantum gates are needed, one-bit gates alone suffice [44]. Now, often this tradeoff will not be useful, as in many schemes a Bell measurement would require two-bit quantum gates.

But the overall message, seen in many of our requirements, is that more and more, the theoretical study of quantum computation has offered a great variety of tradeoffs for the potential implementations: if X is very hard, it can be substituted with more of Y. Of course, in many cases both X and Y are beyond the present experimental state of the art; but a thorough knowledge of these tradeoffs should be very useful for devising a rational plan for the pursuit of future experiments.

4. Desiderata for Quantum Communication

For computation alone, the five requirements above suffice. But the advantages of quantum information processing are not manifest solely, or perhaps even principally, for straightforward computation only. There are many kinds of information-processing tasks, reviewed briefly at the beginning, that involve more than just computation, and for which quantum tools provide a unique advantage.

The tasks we have in mind here all involve not only computation but also communication. The list of these tasks that have been considered in the light of quantum capabilities, and for which some advantage has been found in using quantum tools, is fairly long and diverse: it includes secret key distribution, multiparty function evaluation as in appointment scheduling, secret sharing, and game playing [14].

When we say communication we mean quantum communication: the transmission of intact qubits from place to place. This obviously adds more features that the physical apparatus must have to carry out this information processing. We formalize these by adding two more items to the list of requirements:

6. The ability to interconvert stationary and flying qubits

7. The ability to faithfully transmit flying qubits between specified locations

These two requirements are obviously closely related, but it is worthwhile to consider them separately, because some tasks need one but not the other. For instance, quantum cryptography [18] involves only requirement 7; it is sufficient to create and detect flying qubits directly.

I have used the jargon "flying qubits" [2], which has become current in the discussions of quantum communication. Using this term emphasizes that the optimal embodiment of qubits that are readily transmitted from place to place is likely to be very different from the optimal qubits for reliable local computation. Indeed, almost all proposals assume that photon states, with the qubit encoded either in the polarization or in the spatial wavefunction of the photon, will be the flying qubit of choice, and indeed, the well developed tech-

nology of light transmission through optical fibers provides a very promising system for the transmission of qubits. I would note, though, that my colleagues and I have raised the possibility that electrons traveling through solids could provide another realization of the flying qubit [14, 45].

Only a few completely developed proposals exist which incorporate requirements 6 and 7. Of course, there are a number of quite detailed studies of 7, in the sense that experiments on quantum cryptography have been very concerned with the preservation of the photon quantum state during transmission through optical fibers or through the atmosphere. However, these studies are rather disconnected from the other concerns of quantum computing. Requirement 6 is the really hard one; to date the only theoretical proposal sufficiently concrete that experiments addressing it have been planned is the scheme produced by Kimble and coworkers [46] for unloading a cavity photon into a traveling mode via atomic spectroscopy, and loading it by the time-reversed process. Other promising concepts, like the launching of electrons from quantum dots into quantum wires such that the spin coherence of the electrons is preserved, need to be worked out more fully.

5. Summary

So, what is the "winning" technology going to be? I don't think that any living mortal has an answer to this question, and at this point it may be counterproductive even to ask it. Even though we have lived with quantum mechanics for a century, our study of quantum effects in complex artificial systems like those we have in mind for quantum computing is in its infancy. No one can see how or whether all the requirements above can be fulfilled, or whether there are new tradeoffs, not envisioned in our present theoretical discussions but suggested by further experiments, that might take our investigations in an entirely new path.

Indeed, the above discussion, and the other chapters of this special issue, really do not cover all the foreseeable approaches. I will mention two of which I am aware: first, another computational paradigm, that of the cellular automaton, is potentially available for exploitation. This is distinguished from the above "general purpose" approach in that it assumes that every bit pattern throughout the computer will be subjected to the same evolution rule. It is known that general-purpose computation is performable, although with considerable overhead, by a cellular automaton. This is true as well for the quantum version of the cellular automaton, as LLOYD [47] indicated in his original work. New theoretical work by BENJAMIN [48] shows very explicitly how relatively simple local rules would permit the implementation of some quantum computations. This could point us perhaps towards some sort of polymer with a string of qubits on its backbone that can be addressed globally in a spectroscopic fashion. Experiments are not oriented towards this at the moment, but the tradeoffs are very different, and I don't believe it should be excluded in the future.

Second, even more speculative, but very elegant, is the proposal of KITAEV [49] to use quantum systems with particular kinds of topological excitations, for example nonabelian anyons, for quantum computing. It is hard to see at the moment how to turn this exciting proposal into an experimental program, as no known physical system is agreed to have the appropriate topological excitations. But further research in, for example, the quantum Hall effect might reveal such a system; more likely, perhaps, is that further understanding of this approach, and that of Freedman and his colleagues [50], will shed more light on doing quantum computing using the "standard" approach being considered in this book.

I am convinced of one thing: the ideas of quantum information theory will continue to exert a decisive influence on the further investigation of the fundamental quantum properties of complex quantum systems, and will stimulate many creative and exciting developments for many years to come.

Acknowledgments

I gratefully acknowledge support from the Army Research Office under contract number DAAG55-98-C-0041. I thank Alec Maassen van den Brink for a careful reading of this manuscript.

References

- [1] J. I. CIRAC and P. ZOLLER, Phys. Rev. Lett. **74**, 4091 (1995); T. PELLIZZARI, S. A. GARDINER, J. I. CIRAC, and P. ZOLLER, Phys. Rev. Lett. **75**, 3788 (1995); C. MONROE, D. M. MEEKHOF, B. E. KING, W. M. ITANO, and D. J. WINELAND, *Demonstration of a fundamental quantum logic gate*, Phys. Rev. Lett. **75**, 4714 (1995); A. SORENSEN and K. MOLMER, Phys. Rev. Lett. **82**, 1971 (1999); S. SCHNEIDER, D. F. V. JAMES, and G. J. MILBURN, *Method of quantum computation with 'hot' trapped ions*, quant-ph/9808012.
- [2] Q. A. TURCHETTE, C. J. HOOD, W. LANGE, H. MABUCHI, and H. J. KIMBLE, *Measurement of conditional phase shifts for quantum logic*, Phys. Rev. Lett. **75**, 4710 (1995); A. IMAMOGLU, D. D. AWSCHALOM, G. BURKARD, D. P. DiVINCENZO, D. LOSS, M. SHERWIN, and A. SMALL, Phys. Rev. Lett. **83**, 4204 (1999) (quant-ph/9904096).
- [3] N. GERSHENFELD and I. CHUANG, SCIENCE **275**, 350 (1997); D. CORY, A. FAHMY, and T. HAVEL, Proc. Nat. Acad. Sci. **94** (5), 1634 (1997).
- [4] B. KANE, NATURE **393**, 133 (1998); R. VRIJEN et al., *Electron spin resonance transistors for quantum computing in silicon-germanium heterostructures*, Phys. Rev. A, in press (quant-ph/9905096).
- [5] D. AVERIN, Solid State Commun. **105**, 659 (1998); A. SHNIRMAN, G. SCHÖN, and Z. HERMIN, Phys. Rev. Lett. **79**, 2371 (1997); J. E. MOOIJ, T. P. ORLANDO, L. LEVITOV, L. TIAN, C. H. VAN DER WAL, and S. LLOYD, Science **285**, 1036 (1999).
- [6] P. M. PLATZMAN and M. I. DYKMAN, SCIENCE **284**, 1967 (1999).
- [7] D. LOSS and D. P. DiVINCENZO, Phys. Rev. A **57**, 120 (1998) (cond-mat/9701055); M. SHERWIN, A. IMAMOGLU, and T. MONTROY, *Quantum computation with quantum dots and terahertz cavity quantum electrodynamics*, Phys. Rev. A **60**, 3508 (1999) (quant-ph/9903065); T. TANAMOTO, Phys. Rev. A **61**, 022305 (2000) (quant-ph/9902031).
- [8] D. DEUTSCH, Proc. R. Soc. London A **400**, 97 (1985); **425**, 73 (1989).
- [9] R. P. FEYNMAN, Int. J. Theor. Phys. **21**, 467 (1982); Found. Phys. **16**, 507 (1986). See also *Feynman Lectures on Computation*, eds. A. J. G. Hey and R. Allen (Perseus Press, 1996).
- [10] R. BEALS, H. BUHRMAN, R. CLEVE, M. MOSCA, and R. DE WOLF, *Quantum lower bounds by polynomials*, Proc. of the 39th Annual Symposium on the Foundations of Computer Science (IEEE Press, Los Alamitos, 1998), p. 352; quant-ph/9802049.
- [11] Y. OZHIGOV, *Quantum computer cannot speed up iterated applications of a black box*, quant-ph/9712051; B. Terhal, PhD Thesis, University of Amsterdam, 1999.
- [12] L. K. GROVER, *Quantum mechanics helps in searching for a needle in a haystack*, Phys. Rev. Lett. **79**, 325 (1997).
- [13] P. W. SHOR, *Polynomial time algorithms for prime factorization and discrete logarithms on a quantum computer*, SIAM J. Comput. **26**, 1484 (1997), and references therein.
- [14] D. P. DiVINCENZO and D. LOSS, *Quantum Computers and Quantum Coherence*, J. Magnetism Magn. Matl. **200**, 202–218 (1999).
- [15] R. CLEVE and H. BUHRMAN, Phys. Rev. A **56**, 1201 (1997).
- [16] H. BUHRMAN, R. CLEVE, and A. WIGDERSON, *Quantum vs. Classical Communication and Computation*, in Proc. of the 30th Ann. ACM Symp. on the Theory of Computing (ACM Press, 1998), p. 63; eprint quant-ph/9802040.
- [17] A. AMBAINIS, L. SCHULMAN, A. TA-SHMA, U. VAZIRANI, and A. WIGDERSON, *The quantum communication complexity of sampling*, in Proc. of the 39th Annual Symposium on the Foundations of Computer Science (IEEE Press, Los Alamitos, 1998); see <http://www.icsi.berkeley.edu/~amnon/Papers/qcc.ps>.
- [18] C. H. BENNETT and G. BRASSARD, *Quantum Cryptography: Public Key Distribution and Coin Tossing*, in Proceedings of the IEEE International Conference on Computers, Systems and Signal Processing, Bangalore, India (IEEE, New York, 1984), p. 175.

- [19] D. A. MEYER, *Quantum strategies*, Phys. Rev. Lett. **82**, 1052 (1999) (quant-ph/9804010); J. EISERT, M. WILKENS, and M. LEWENSTEIN, *Quantum games and quantum strategies*, Phys. Rev. Lett. **83**, 3077 (1999) (quant-ph/9806088); L. GOLDENBERG, L. VAIDMAN, and S. WIESNER, *Quantum gambling*, Phys. Rev. Lett. **82**, 3356 (1999) (quant-ph/9808001).
- [20] A. M. STEANE and W. VAN DAM, *Physicists Triumph at 'Guess my Number'*, Physics Today **53** (2), 35–39 (2000).
- [21] D. AHARONOV, *Quantum Computation in Annual Reviews of Computational Physics*, vol. VI (ed. Dietrich Stauffer, World Scientific, Singapore, 1998) (quant-ph/9812037).
- [22] R. CLEVE, *An Introduction to Quantum Complexity Theory*, to appear in *Collected Papers on Quantum Computation and Quantum Information Theory* (eds. C. Macchiavello, G. M. Palma, and A. Zeilinger, World Scientific, 2000) (quant-ph/9906111).
- [23] C. H. BENNETT, Physics Today **48** (10), 24 (1995); D. P. DiVINCENZO, Science **270**, 255 (1995); D. P. DiVINCENZO, Proc. R. Soc. London A **454**, 261 (1998) (and quant-ph/9705009); A. BARENCO, Contemp. Phys. **37**, 375 (1996); A. STEANE, Rep. Prog. Phys. **61**, 117 (1998); C. H. BENNETT and P. W. SHOR, IEEE Trans. Info. Theory **44**, 2724 (1998).
- [24] D. P. DiVINCENZO, in *Mesoscopic Electron Transport*, eds. L. Sohn, L. Kouwenhoven, and G. Schön (Vol. 345, NATO ASI Series E, Kluwer, 1997), p. 657 (cond-mat/9612126); D. P. DiVINCENZO and D. LOSS, *Superlattices and Microstructures* **23**, 419 (1998) (cond-mat/9710259); D. P. DiVINCENZO and D. LOSS, J. Magn. Mag. Matl. **200**, 202 (1999) (cond-mat/9901137).
- [25] B. SCHUMACHER, Phys. Rev. A **54**, 2614 (1996).
- [26] G. K. BRENNEN, C. M. CAVES, P. S. JESSEN, and I. H. DEUTSCH, Phys. Rev. Lett. **82**, 1060 (1999).
- [27] D. JAKSCH, H. J. BRIEGEL, I. J. CIRAC, C. GARDINER, and P. ZOLLER, Phys. Rev. Lett. **82**, 1975 (1999).
- [28] I am grateful to R. SCHOELKOPF and M. DEVORET for clarifying discussion on these points.
- [29] M. B. PLENIO and P. L. KNIGHT, Phys. Rev. A **53**, 2986 (1996).
- [30] M. B. PLENIO and P. L. KNIGHT, Proc. Roy. Soc. Lond. A **453**, 2017–2041 (1997).
- [31] J. PRESKILL, Proc. R. Soc. Lond. A **454**, 385 (1998) (quant-ph/9705031).
- [32] M. A. NIELSEN and I. L. CHUANG, *Quantum Computation and Quantum Information* (Cambridge University Press, 2000); see also M. A. NIELSEN, C. M. CAVES, B. SCHUMACHER, and H. BARNUM, Proc. R. Soc. Lond. A **454**, 277–304 (1998) (quant-ph/9706064).
- [33] P. SHOR, Phys. Rev. A **52**, 2493 (1995); A. M. STEANE, Phys. Rev. Lett. **77**, 793–797 (1996).
- [34] P. SHOR, in *Proceedings of the 37th Symposium on the Foundations of Computer Science* (IEEE Press, Los Alamitos, CA, 1996) (quant-ph/9605011); D. AHARONOV and M. BEN-OR, in *Proceedings of the 29th Annual ACM Symposium on the Theory of Computing* (ACM Press, New York, 1997) (quant-ph/9611025); E. KNILL, R. LAFLAMME, and W. ZUREK, Science **279**, 342 (1998). These results are reviewed in [31].
- [35] D. P. DiVINCENZO, *Two-bit gates are universal for quantum computation*, Phys. Rev. A **51**, 1015 (1995), cond-mat/9407022.
- [36] A. BARENCO, C. H. BENNETT, R. CLEVE, D. P. DiVINCENZO, N. MARGOLUS, P. SHOR, T. SLEATOR, J. A. SMOLIN, and H. WEINFURTER, *Elementary gates for quantum computation*, Phys. Rev. A **52**, 3457 (1995), quant-ph/9503016.
- [37] K. MOLMER and A. SORENSEN, Phys. Rev. Lett. **82**, 1835 (1999).
- [38] D. W. LEUNG, I. L. CHUANG, F. YAMAGUCHI, and Y. YAMAMOTO, *Efficient implementation of selective recoupling in heteronuclear spin systems using Hadamard matrices*, quant-ph/9904100.
- [39] G. BURKARD, D. LOSS, D. P. DiVINCENZO, and J. A. SMOLIN, Phys. Rev. B **60**, 11404 (1999); cond-mat/9905230.
- [40] G. BURKARD, D. LOSS, D. P. DiVINCENZO, Phys. Rev. B **59**, 2070 (1999); cond-mat/9808026.
- [41] D. GOTTESMAN, *Fault-Tolerant Quantum Computation with Local Gates*, J. Mod. Optics **47**, 333 (2000); quant-ph/9903099.
- [42] D. BACON, J. KEMPE, D. A. LIDAR, and K. B. WHALEY, *Universal fault-tolerant computation on decoherence-free subspaces*, quant-ph/9909058.
- [43] D. P. DiVINCENZO, G. BURKARD, D. LOSS, and E. V. SUKHORUKOV, *Quantum computation and spin electronics in Quantum Mesoscopic Phenomena and Mesoscopic Devices in Microelectronics*, eds. I. O. Kulik and R. Ellialtioglu (NATO Advanced Study Institute, Turkey, June 13–25, 1999), to be published; cond-mat/9911245.
- [44] D. GOTTESMAN and I. L. CHUANG, Nature **402**, 390 (1999).
- [45] D. LOSS and E. V. SUKHORUKOV, Phys. Rev. Lett. **84**, 1035 (2000).

[40] J. Eisner, Phys. Rev. Lett. **78**, 3221 (1997) (quant-ph/9611017).

[41] S. Lloyd, Science **261**, 1569 (1993); **263**, 695 (1994).

[42] S. Benjamin, Phys. Rev. A **61**, 020301(R) (2000) (quant-ph/9909007).

[43] A. Yu. Kitaev, *Fault-tolerant quantum computation with anyons*, quant-ph/9707021; see also J. Preskill, in *Introduction to Quantum Computation and Information* (eds. H.-K. Lo, S. Popescu, and T. Spiller, World Scientific, Singapore, 1998) pp. 213–269 (quant-ph/9712048).

[44] M. H. Freedman, M. Larsen, and Z. Wang, *A modular functor which is universal for quantum computation*, quant-ph/0001108; M. H. Freedman, *Poly-locality in quantum computing*, quant-ph/0001077; M. H. Freedman, A. Yu. Kitaev, and Z. Wang, *Simulation of topological field theories by quantum computers*, quant-ph/0001071.

[45] J. I. Cirac, P. Zoller, H. J. Kimble, and H. Mabuchi, Phys. Rev. Lett. **78**, 3221 (1997) (quant-ph/9611017).

[46] S. Lloyd, Science **261**, 1569 (1993); **263**, 695 (1994).

[47] S. Benjamin, Phys. Rev. A **61**, 020301(R) (2000) (quant-ph/9909007).

[48] A. Yu. Kitaev, *Fault-tolerant quantum computation with anyons*, quant-ph/9707021; see also J. Preskill, in *Introduction to Quantum Computation and Information* (eds. H.-K. Lo, S. Popescu, and T. Spiller, World Scientific, Singapore, 1998) pp. 213–269 (quant-ph/9712048).

[49] M. H. Freedman, M. Larsen, and Z. Wang, *A modular functor which is universal for quantum computation*, quant-ph/0001108; M. H. Freedman, *Poly-locality in quantum computing*, quant-ph/0001077; M. H. Freedman, A. Yu. Kitaev, and Z. Wang, *Simulation of topological field theories by quantum computers*, quant-ph/0001071.

[50] J. I. Cirac, P. Zoller, H. J. Kimble, and H. Mabuchi, Phys. Rev. Lett. **78**, 3221 (1997) (quant-ph/9611017).

[51] S. Lloyd, Science **261**, 1569 (1993); **263**, 695 (1994).

[52] S. Benjamin, Phys. Rev. A **61**, 020301(R) (2000) (quant-ph/9909007).

[53] A. Yu. Kitaev, *Fault-tolerant quantum computation with anyons*, quant-ph/9707021; see also J. Preskill, in *Introduction to Quantum Computation and Information* (eds. H.-K. Lo, S. Popescu, and T. Spiller, World Scientific, Singapore, 1998) pp. 213–269 (quant-ph/9712048).

[54] M. H. Freedman, M. Larsen, and Z. Wang, *A modular functor which is universal for quantum computation*, quant-ph/0001108; M. H. Freedman, *Poly-locality in quantum computing*, quant-ph/0001077; M. H. Freedman, A. Yu. Kitaev, and Z. Wang, *Simulation of topological field theories by quantum computers*, quant-ph/0001071.

[55] J. I. Cirac, P. Zoller, H. J. Kimble, and H. Mabuchi, Phys. Rev. Lett. **78**, 3221 (1997) (quant-ph/9611017).

Exhibit B

Il'ichev et al., 1999, Physical Review B 60, p. 3096

Anomalous periodicity of the current-phase relationship of grain-boundary Josephson junctions in high- T_c superconductors

E. Il'ichev, V. Zakosarenko, R. P. J. IJsselsteijn, H. E. Hoenig, V. Schultze, and H.-G. Meyer
Department of Cryoelectronics, Institute for Physical High Technology, P.O. Box 100239, D-07702 Jena, Germany

M. Grajcar and R. Hlubina
Department of Solid State Physics, Comenius University, Mlynská Dolina F2, 842 15 Bratislava, Slovakia
 (Received 28 January 1999)

The current-phase relation (CPR) for asymmetric 45° Josephson junctions between two d -wave superconductors has been predicted to exhibit an anomalous periodicity. We have used the single-junction interferometer to investigate the CPR for these kinds of junctions in $\text{YBa}_2\text{Cu}_3\text{O}_{7-x}$ thin films. A remarkable amplitude of the π -periodical component of the CPR has been experimentally found, providing an additional source of evidence for the d -wave symmetry of the pairing state of the cuprates. [S0163-1829(99)05629-5]

A number of experimental results confirm $d_{x^2-y^2}$ -wave symmetry of the pairing state of high-temperature superconductors.¹ An unconventional pairing state requires the existence of zeros of the order parameter in certain directions in momentum space. Thermodynamic and spectroscopic measurements do indeed suggest their existence, but by themselves they do not exclude conventional s -wave pairing with nodes.¹ Direct evidence for the d -wave pairing state is provided by phase-sensitive experiments, which are based on the Josephson effect.² Quite generally, the current-phase relationship (CPR) of a Josephson junction, $I(\varphi)$ is an odd periodic function of φ with a period 2π .³ Therefore $I(\varphi)$ can be expanded in a Fourier series

$$I(\varphi) = I_1 \sin \varphi + I_2 \sin 2\varphi + \dots \quad (1)$$

In the tunnel limit we can restrict ourselves to the first two terms in Eq. (1). Since the order parameter is bound to the crystal lattice, $I(\varphi)$ of a weak link depends on the orientation of the d -wave electrodes with respect to their boundary. The existing phase-sensitive experiments exploit possible sign changes of I_1 between different geometries.² In this work we present a phase-sensitive experimental test of the pairing state symmetry of cuprates. Namely, in certain geometries, the I_1 term should vanish by symmetry. In such cases, the CPR should exhibit an anomalous periodicity.

Let us analyze the angular dependence of $I_{1,2}$ in a junction between two macroscopically tetragonal d -wave superconductors. As emphasized in Ref. 4, also heavily twinned orthorhombic materials such as $\text{YBa}_2\text{Cu}_3\text{O}_{7-x}$ belong to this class, if the twin boundaries have odd symmetry. We consider an ideally flat interface between two superconducting electrodes. Let θ_1 (θ_2) denote the angle between the normal to the grain boundary and the a axis in electrode 1 (2), see Fig. 1. If we only keep the lowest-order angular harmonics, the symmetry of the problem dictates that⁴

$$I_1 = I_c \cos 2\theta_1 \cos 2\theta_2 + I_s \sin 2\theta_1 \sin 2\theta_2. \quad (2)$$

The coefficients I_c, I_s are functions of the barrier strength, temperature T , etc. The I_2 term results from higher-order tunneling processes and we neglect its weak angular depen-

dence. It is seen from Eq. (2) that the criterion for the observation of an anomalous period of the CPR, $I_1 = 0$, is realized for an asymmetric 45° junction, i.e., a junction with $\theta_1 = 45^\circ$ and $\theta_2 = 0$.

The I_2 term is also present in weak links based on conventional s -wave superconductors but for all known types of weak links $|I_2/I_1| < 1$. For instance, for a tunnel junction $|I_2/I_1| \ll 1$. For a superconductor-normal-metal-superconductor (SNS) junction, $I \propto \sin \varphi/2$ at $T = 0$,⁵ and the Fourier expansion of Eq. (1) leads to $I_2/I_1 = -2/5$. Therefore a possible experimental observation of $|I_2/I_1| \gg 1$ in an asymmetric 45° junction provides direct evidence of d -wave symmetry of the pairing state in the cuprates.

We have investigated the CPR of $\text{YBa}_2\text{Cu}_3\text{O}_{7-x}$ thin-film bicrystals with asymmetric 45° [001]-tilt grain boundaries as sketched in Fig. 1, using a single-junction interferometer configuration in which the Josephson junction is inserted into a superconducting loop with a small inductance L . In a stationary state without fluctuations, the phase difference φ across the junction is controlled by applying an external magnetic flux Φ_e penetrating the loop: $\varphi = \varphi_e - \beta f(\varphi)$. Here $\varphi_e = 2\pi\Phi_e/\Phi_0$; $\Phi_0 = 2.07 \times 10^{-15} \text{ Tm}^2$ is the flux quantum; $f(\varphi) = I(\varphi)/I_0$ is the CPR normalized to the maximal Josephson current I_0 , and $\beta = 2\pi LI_0/\Phi_0$ is the normalized

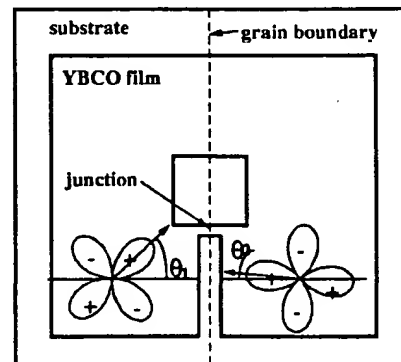


FIG. 1. Washer-shaped interferometer with one short Josephson junction (not in scale). Dimensions are given in the text.

critical current. In order to obtain the CPR for the complete phase range $-\pi \leq \varphi \leq \pi$ the condition $\beta < 1$ has to be fulfilled, because for $\beta > 1$ the curve $\varphi(\varphi_e)$ becomes multivalued. Following Ref. 3, we express the effective inductance of the interferometer using the derivative f' with respect to φ as $L_{int} = L[1 + 1/\beta f'(\varphi)]$. The inductance can be probed by coupling the interferometer to a tank circuit with inductance L_T , quality factor Q , and resonance frequency ω_0 through the mutual inductance M .⁸ External flux in the interferometer is produced by a current $I_{dc} + I_{rf}$ in the tank coil and can be expressed as $\varphi_e = 2\pi(I_{dc} + I_{rf})M/\Phi_0 = \varphi_{dc} + \varphi_{rf}$, where $M^2 = k^2 L L_T$ with k a coupling coefficient. Taking into account the quasiparticle current in the presence of a voltage V across the junction the phase difference is given by the relation $\varphi = \varphi_{dc} + \varphi_{rf} - \beta f(\varphi) - 2\pi\tau(\varphi)V/\Phi_0$, where $\tau(\varphi) = L/R_J(\varphi)$ with $R_J(\varphi)$ the resistance of the junction. In the small-signal limit $\varphi_{rf} \ll 1$ and in the adiabatic case $\omega\tau \ll 1$, keeping only the first-order terms, the effective inductance L_{eff} of the tank circuit-interferometer system is

$$L_{eff} = L_T \left(1 - k^2 \frac{L}{L_{int}} \right) = L_T \left(1 - \frac{k^2 \beta f'(\varphi)}{1 + \beta f'(\varphi)} \right).$$

Thus the phase angle α between the driving current and the tank voltage U at the resonance frequency of the tank circuit ω_0 is

$$\tan \alpha(\varphi) = \frac{k^2 Q \beta f'(\varphi)}{1 + \beta f'(\varphi)}. \quad (3)$$

Using the relation $[1 + \beta f'(\varphi)]d\varphi = d\varphi_{dc}$ which is valid for $\varphi_{rf} \ll 1$ and $\omega\tau \ll 1$, one can find the CPR from Eq. (3) by numerical integration.

The advantage of the CPR measurement of an asymmetric 45° junction with respect to the by-now standard phase-sensitive tests of pairing symmetry based on the angular dependence of I_1 is twofold. First, it avoids the complications of the analysis of experiments caused by the presence of the term I_s .⁴ Second, flux trapped in the interferometer washer (see Fig. 1) does not invalidate the conclusions about the ratio $|I_2/I_1|$ and hence about the pairing symmetry, which is not the case in standard phase-sensitive tests of the d -wave symmetry of the pairing state.⁹

The films of 100-nm thickness were fabricated using standard pulsed laser deposition on (001) oriented SrTiO₃ bicrystalline substrates with asymmetric [001] tilt misorientation angles of $45^\circ \pm 1^\circ$. The films were subsequently patterned by Ar ion-beam etching into 4×4 -mm² square washer single-junction interferometer structures (Fig. 1). The widths of the junctions were 1–2 μm . The square washer holes had a side length of 50 μm . This geometry of the interferometer gives $L \approx 80$ pH. The resistance of a similar single junction (without interferometer loop) was measured directly and $R_J > 1$ Ω was found. Therefore the condition for the adiabatic limit $\omega\tau \ll 1$ is satisfied. For measurements of $\alpha(\varphi_{dc})$, several tank circuits with inductances 0.2–0.8 μH and resonance frequencies 16–35 MHz have been used. The unloaded quality factor of the tank circuits $70 < Q < 150$ has been measured at various temperatures. The coupling factor k was determined from the period ΔI_{dc} of $\alpha(I_{dc})$ using $M\Delta I_{dc} = \Phi_0$. Its value varied between 0.03 and 0.09. The

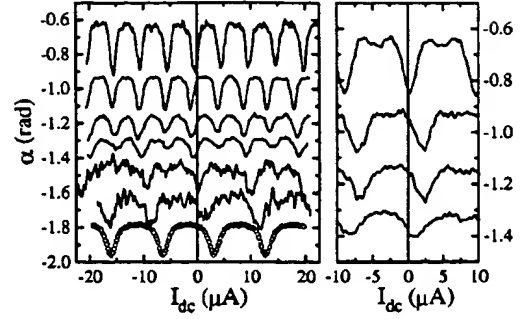


FIG. 2. Left panel: Phase angle between the driving current and the output voltage measured for sample No. 1 at different temperatures as a function of the dc current I_{dc} . The curves are shifted along the y axis and the data for $T = 30$ and 40 K are multiplied by factor 4 for clarity. From top to bottom, the data correspond to $T = 4.2, 10, 15, 20, 30$, and 40 K. The data measured for 36° bicrystals ($\theta_1 \approx 36^\circ, \theta_2 \approx 0$) at $T = 40$ K in the same washer geometry are shown for comparison (open circles). Right panel: The same for sample No. 3. From top to bottom, the data correspond to $T = 4.2, 10, 15$, and 20 K.

amplitude of I_{rf} was set to produce a flux in the interferometer smaller than $0.1 \Phi_0$ to ensure the small-signal limit.

The measurements have been performed in a gas-flow cryostat with a five-layer magnetic shielding in the temperature range $4.2 \leq T < 90$ K. The experimental setup was calibrated by measuring interferometers of the same size with 24° and 36° grain boundaries. We have studied six samples, out of which for four samples the π -periodic component of $I(\varphi)$ was experimentally observed. At low temperatures for two samples (Nos. 1 and 2) the value of I_2 is larger than I_1 . For sample Nos. 3 and 4 I_2 is approximately 10–20% of I_1 and for sample Nos. 5 and 6 I_2 is negligible. As an example we plot the phase angle α as a function of the dc current I_{dc} for sample Nos. 1 and 3 (Fig. 2). The behavior of sample No. 1 at low temperatures is defined by the π periodic component of $I(\varphi)$. The curves for sample No. 3 are 2π -periodic, nevertheless for the curve at $T = 4.2$ K the local minima clearly show the presence of a π -periodic component.

In order to determine the CPR we assume that the period of $\alpha(I_{dc})$ at $T = 40$ K and $\Delta I_{dc} = 9.6$ μA , corresponds to $\Delta\varphi_{dc} = 2\pi$. We take $\varphi_{dc} = 0$ at a maximum or minimum of α . This is necessary in order to satisfy $I(\varphi = 0) = 0$, as required by general principles.³ The experimentally observed shift of the first extreme of $\alpha(I_{dc})$ from $I_{dc} = 0$ (Fig. 2) can be due to flux trapped in the interferometer washer. Most probably, this flux resides in the long junction originated by the grain boundary crossing the washer of the interferometer. This long junction does not play an active role because the Josephson penetration depth is much smaller than the junction length, and external fields produced by I_{dc} are smaller than the first critical field. Nevertheless, the long junction sets the phase difference for $I_{dc} = 0$ at the small junction.

In Fig. 3, we show the CPR determined from the data in Fig. 2. For all curves we have performed a minimal necessary shift consistent with $I(\varphi = 0) = 0$. Thus we have assumed that at $\varphi_{dc} = 0$ a minimum of $\alpha(\varphi_{dc})$ is realized. For an interferometer with a conventional s -wave weak link (and also for the 36° junction), at $\varphi_{dc} = 0$ one gets a maximum of

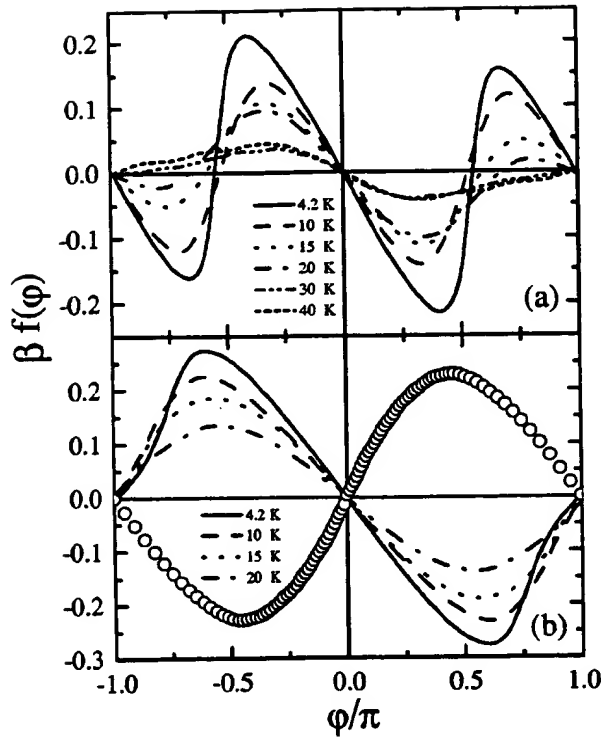


FIG. 3. (a) Josephson current through the junction for sample No. 1 as a function of the phase difference φ , determined from the data in Fig. 2. The scattering of $\alpha(\varphi)$ values was reduced by folding the data back to the interval $(0, \pi)$ and taking the average. Here, the symmetry $\alpha(\varphi) = \alpha(-\varphi)$ was assumed. (b) The same for sample No. 3. The data for the asymmetric 36° bicrystal at $T = 40$ K (open circles) are also shown.

$\alpha(\varphi_{dc})$. Note that the minimum of $\alpha(\varphi_{dc})$ at $\varphi_{dc} = 0$ implies a paramagnetic response of the interferometer in the limit of small applied fields.

The amplitude of the π -periodic component of the CPR decreases drastically with increasing temperature, and at $T = 40$ K its contribution is negligible for all samples. The temperature dependence of I_1 and I_2 could be determined with acceptable accuracy for sample No. 1 only. With decreasing T , $|I_2|$ grows monotonically down to $T = 4.2$ K, while the I_1 component exhibits only a weak temperature dependence (Fig. 4).

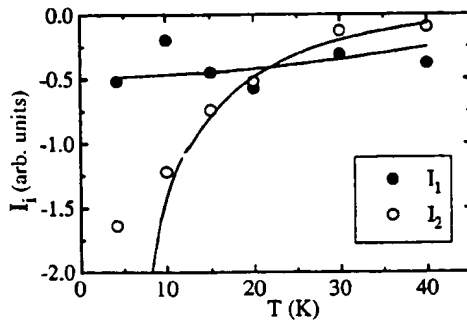


FIG. 4. Temperature dependence of the Fourier expansion coefficients $I_{1,2}$ determined from the experimental data in Fig. 3(a). Solid lines are the Fourier expansion coefficients for the numerical data in Fig. 5.

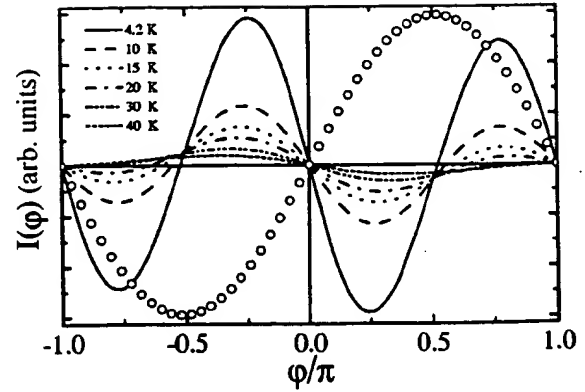


FIG. 5. $I(\varphi)$ calculated according to Eq. (64) of Ref. 11 for a junction with $\theta_1 = 45.5^\circ$, $\theta_2 = 0$, $\lambda d = 1.5$, $\kappa = 0.5$, and $T_c = 60$ K. $I(\varphi)$ at $T = 40$ K for the 36° bicrystal (open circles) was calculated with the same parameters except for $\theta_1 = 36^\circ$.

Our experimental results can be understood as follows. It is well known that the microstructural properties of the grain boundaries, especially 45° boundaries, are defined by their faceted nature. Faceting is an intrinsic property of the grain boundaries,^{6,7} and, due to d -wave symmetry of the order parameter, the properties of the junctions strongly depend on the particular distribution of the facets. Small deviations from the ideal geometry of the asymmetric 45° junction lead to a finite value of I_1 . Thus for nearly ideal junctions $|I_2/I_1| \gg 1$ at $T \rightarrow 0$. The region $T \sim T_c$ can be analyzed quite generally within the Ginzburg-Landau theory. Let the electrodes be described by the (macroscopic) order parameters $\Delta_{1,2} = |\Delta|e^{i\varphi_{1,2}}$. Then the phase-dependent part of the energy of the junction is $E = a[\Delta_1\Delta_2^* + \text{H.c.}] + b[(\Delta_1\Delta_2^*)^2 + \text{H.c.}] + \dots$ where a, b, \dots depend weakly on T .¹⁰ Thus for T close to T_c we estimate $I_1 \propto |\Delta|^2 \propto (T_c - T)$ and $I_2 \propto |\Delta|^4 \propto (T_c - T)^2$, leading to $|I_2/I_1| \ll 1$. With increasing deviations from ideal geometry $|I_2/I_1|$ decreases. For large enough deviations, negligible values of $|I_2|$ are expected. These expectations are qualitatively consistent with the experimental data (see also Fig. 4).

So far, our discussion was based solely on symmetry arguments. Let us attempt a more quantitative analysis of our data now. Two different microscopic pictures of asymmetric 45° Josephson junctions between d -wave superconductors have been considered in the literature. The first picture assumes a microscopically tetragonal material and an ideally flat interface.¹⁰⁻¹² Within this picture, only sample No. 1 can be analyzed. Sample No. 2 had $I_0(T = 1.5 \text{ K}) \cong 10^{-2} \mu\text{A}$. At this temperature only the π -periodic component of $I(\varphi)$ was observed. At higher temperatures I_0 was not measurable. $I(\varphi)$ for sample No. 1 calculated according to the model of Ref. 11 is shown in Fig. 5. The experimental data can be fitted within a relatively broad range of barrier heights. However, if we require the $I(\varphi)$ relation of the 36° junction to be fitted by the same (or smaller) barrier height as for the 45° junction, we conclude the barrier of the 45° junction to be rather low.¹⁴ The dependence of $I(\varphi)$ on T requires a choice of $T_c \approx 60$ K in the non-self-consistent theory of Ref. 11. The reduction from the bulk $T_c = 90$ K is probably due to a combined effect of surface degradation and order-parameter suppression at the sample surface. The temperature dependence

of the ratio of the π and 2π periodic components in $I(\varphi)$ is seen to be in qualitative agreement with experimental data in Fig. 3(a). This is explicitly demonstrated in Fig. 4 where we compare the experimentally obtained $I_{1,2}$ with the results of the Fourier analysis of the curves in Fig. 5. The divergence of I_2 as $T \rightarrow 0$ is an artifact of the ideal junction geometry assumed in Ref. 11. If a finite roughness of the interface is taken into account, this divergence is cut off and the experimental data in Fig. 4 do indeed resemble theoretical predictions for a rough interface.¹² However, the non-self-consistent theory of Ref. 11 is unable to explain the experimentally observed steep CPR close to the minima of the junction energy [see Fig. 3(a)].

In a different approach a heavily meandering interface with $\theta_i = \theta_i(x)$ is assumed. Now, the critical current density $j_c(x)$ is a random function with a typical amplitude $\langle |j_c(x)| \rangle \sim j_c$. If the average critical current along the junction $\langle j_c \rangle < j_c$, a remarkable π -periodic component is present in the CPR. The relation $|I_2/I_1|$ depends on the distribution of $j_c(x)$ and can be much larger than one for $\langle j_c \rangle \ll j_c$.^{15,16} This model qualitatively explains the obtained results for all samples, however for a quantitative comparison the actual microscopic distribution $j_c(x)$ should be known. Note that

also within the picture of Refs. 15 and 16 the d -wave symmetry of the pairing state is crucial, otherwise the condition $\langle j_c \rangle \ll j_c$ is difficult to satisfy.

Our present understanding of $I(\varphi)$ in the asymmetric 45° junction is only qualitative. We cannot say whether the remarkable amplitude of the π -periodic component of $I(\varphi)$ is dominated by the microscopically flat regions,¹³ or due to the spatial inhomogeneity of the junction. This issue requires further study.

In conclusion, we have measured the magnetic-field response of a single-junction interferometer based on asymmetric 45° grain-boundary junctions in $\text{YBa}_2\text{Cu}_3\text{O}_{7-x}$ thin films. A large π -periodic component of $I(\varphi)$ has been experimentally found, which is in agreement with theoretical predictions for $d_{x^2-y^2}$ -wave superconductors. Hence our results provide an additional source of evidence for the d -wave symmetry of the pairing state in the cuprates.

Financial support by the DFG (Ho 461/3-1) and partial support by INTAS (N 11459) are gratefully acknowledged. M. G. and R. H. were supported by the Slovak Grant Agency (Grant No. 1/4300/97) and the Comenius University (Grant No. UK/3927/98).

¹For a review, see J. Annett, N. Goldenfeld, and A. J. Leggett, in *Physical Properties of High Temperature Superconductors*, edited by D. M. Ginsberg (World Scientific, New Jersey, 1996), Vol. V.

²See C. C. Tsuei *et al.*, *Science* **271**, 329 (1996), and references therein.

³A. Barone and G. Paterno, *Physics and Applications of the Josephson Effect* (Wiley, New York, 1982).

⁴M. B. Walker and J. Luettmann-Strathmann, *Phys. Rev. B* **54**, 588 (1996).

⁵I. O. Kulik and A. N. Omel'yanchuk, *Fiz. Nizk. Temp.* **4**, 296 (1978) [*Sov. J. Low Temp. Phys.* **4**, 142 (1978)].

⁶H. Hilgenkamp, J. Mannhart, and B. Mayer, *Phys. Rev. B* **53**, 14 586 (1996).

⁷J. Mannhart *et al.*, *Phys. Rev. Lett.* **77**, 2782 (1996).

⁸E. V. Il'ichev *et al.*, *J. Low Temp. Phys.* **106**, 503 (1997).

⁹R. A. Klemm, *Phys. Rev. Lett.* **73**, 1871 (1994).

¹⁰A. Huck, A. van Otterlo, and M. Sigrist, *Phys. Rev. B* **56**, 14 163 (1997).

¹¹Y. Tanaka and S. Kashiwaya, *Phys. Rev. B* **56**, 892 (1997).

¹²Y. S. Barash, H. Burkhardt, and D. Rainer, *Phys. Rev. Lett.* **77**, 4070 (1996).

¹³C. R. Hu, *Phys. Rev. Lett.* **72**, 1526 (1994).

¹⁴This is consistent with the Fourier analysis of the data in Fig. 3 which results in a non-negligible I_n also for $n \geq 3$.

¹⁵A. J. Millis, *Phys. Rev. B* **49**, 15 408 (1994).

¹⁶R. G. Mints, *Phys. Rev. B* **57**, R3221 (1998).

Exhibit C

Il'ichev, 1998, Physical Review Letters 81, p. 894

Nonsinusoidal Current-Phase Relationship of Grain Boundary Josephson Junctions in High- T_c Superconductors

E. Il'ichev, V. Zakosarenko, R. P. J. IJsselsteijn, V. Schultze, H.-G. Meyer, and H. E. Hoenig

Department of Cryoelectronics, Institute for Physical High Technology, P.O. Box 100239, D-07702 Jena, Germany

H. Hilgenkamp and J. Mannhart

Experimental Physics VI, Center for Electronic Correlations and Magnetism, Institute of Physics, Augsburg University, D-86135 Augsburg, Germany

(Received 13 January 1998)

For various configurations of Josephson junctions incorporating superconductors with unconventional order parameter symmetry, such as most high- T_c cuprates, deviations from the standard sinusoidal current-phase dependence have been predicted. To this point, these deviations have never been observed experimentally. We have measured the current-phase relation of high- T_c Josephson junctions, namely, $\text{YBa}_2\text{Cu}_3\text{O}_{7-x}$ thin film bicrystals, comprising symmetric 45° [001] tilt grain boundaries. The current-phase relations of all junctions investigated were found to be extremely nonharmonic, in agreement with a $d_{x^2-y^2}$ -wave dominated symmetry of the order parameter. [S0031-9007(98)06674-5]

PACS numbers: 74.50.+r

The current-phase relation (CPR) $f(\varphi)$ is a characteristic property of any weak link connecting two superconductors. It describes the dependence of the Cooper-pair current I_p on the phase difference φ of the order parameters of both superconducting electrodes. In a general form it is expressed as

$$I_p = I_c f(\varphi), \quad -1 \leq f(\varphi) \leq 1, \quad (1)$$

I_c being the critical current of the weak link. It was shown by Josephson [1] that for ideal tunnel junctions between conventional superconductors the CPR is sinusoidal, i.e., $f(\varphi) = \sin(\varphi)$. This sinusoidal dependence has been confirmed experimentally numerous times for standard tunnel junctions between conventional superconductors [2].

Recently, it has been revealed that the order parameter of most high- T_c cuprates is unconventional, dominated by a $d_{x^2-y^2}$ symmetry component [3–5]. Because of the sign change of the order parameter associated with this symmetry, strong deviations from the standard sinusoidal dependence have been predicted for the current-phase relations of various configurations of Josephson junctions employing such unconventional superconductors [6–9]. In particular, nonharmonic and double-periodic current-phase relations are expected for junctions oriented nominally perpendicular to the $\langle 110 \rangle$ direction of one or of both electrodes, as well as for junctions for which the $\langle 110 \rangle$ direction of one of the electrodes is aligned with the $\langle 100 \rangle$ direction of the other, such as for 45° [001] tilt grain boundaries.

These predictions are highly unusual. Therefore, an experimental clarification of the CPR for high- T_c junctions for which deviations from a standard harmonic behavior are expected is desirable. Such experiments will further

enhance the understanding of the influence of the order parameter symmetry on the properties of grain boundaries and high- T_c Josephson junctions. In addition, they will provide valuable information for the design and use of Josephson junction-based circuits, of which many characteristics directly depend on the CPR. However, to our knowledge, such experiments have not been carried out. All available data refer to Josephson junctions for which nominally sinusoidal current-phase relations are expected. The CPR was measured for weak links prepared by ion irradiation [10], for step-edge junctions [11,12], and also for 24° bicrystal grain boundaries [12]. In nearly all of these cases sinusoidal current-phase relations were found. Deviations from a sinusoidal dependence have been observed only for one step-edge junction, measured at 77 K [12]. These deviations can be explained by the influence of thermal noise [13].

For these reasons we have investigated the CPR of $\text{YBa}_2\text{Cu}_3\text{O}_{7-x}$ thin film bicrystals with symmetric 45° [001]-tilt grain boundaries, as sketched in Fig. 1(a). For these junctions, strong deviations from a sinusoidal CPR are anticipated.

Following a standard approach [14], the CPR was measured using a single-junction interferometer configuration in which the Josephson junction is part of a superconducting loop with a small inductance L . The phase difference φ across the junction is controlled by applying an external magnetic flux Φ_e penetrating the loop:

$$\varphi = \varphi_e - \beta f(\varphi) + \varphi_n + 2\pi m. \quad (2)$$

Here, $\varphi_e = 2\pi\Phi_e/\Phi_0$ is the external flux normalized to the flux quantum Φ_0 ($= 2.07 \times 10^{-15} \text{ Tm}^2$). The constant $\beta = 2\pi LI_c/\Phi_0$ is the normalized critical current, φ_n is a term accounting for the effective noise, and m is

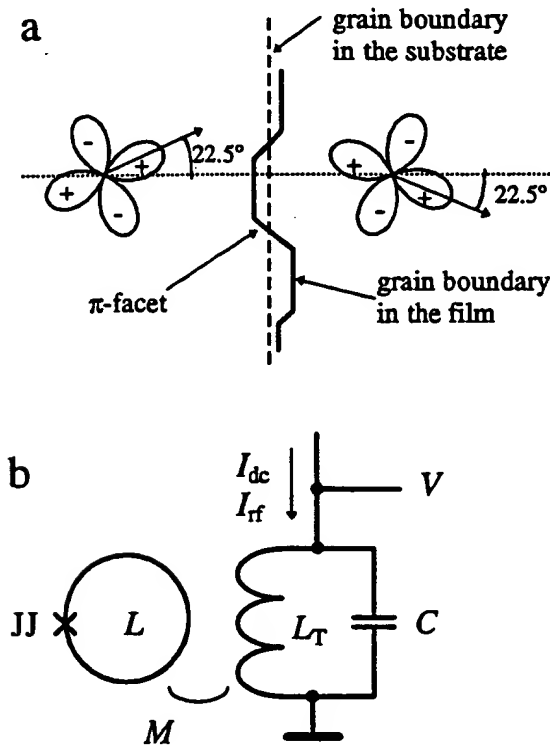


FIG. 1. (a) Schematic representation of a symmetric 45° [001]-tilt grain boundary junction in a $d_{x^2-y^2}$ superconductor. The boundary in the superconducting thin film is meandering, leading to the occurrence of π facets. (b) Schematic of the measurement setup. The Josephson junction is denoted by JJ, and C indicates the capacitance of the tank circuit. The other denotations are explained in the text.

an integer. As capacitive contributions to the loop current are insignificant at the measurement frequencies, the junction capacitance has been neglected. The quasiparticle current is also negligible, for reasons discussed below.

The superconducting loop is inductively coupled to a tank circuit with inductance L_T [see Fig. 1(b)]. This tank circuit is driven with a current I_{rf} at a frequency ω and a dc current I_{dc} . Thus, φ_e can be expressed as a sum of a dc and an rf component $\varphi_e = \varphi_{dc} + \varphi_{rf}$. In this arrangement, the effective impedance $Z_{eff}(\omega)$ of the loop-tank circuit combination is a function of φ_e . As shown by Rifkin and Deaver [14], the CPR can be obtained from this dependence, provided that $\varphi_{rf} \ll 1$. To obtain the CPR for the complete phase range $0 \leq \varphi \leq 2\pi$, the condition $\beta < 1$ has to be fulfilled in addition.

To enhance the accuracy of the measurement, we have adapted this common approach and retrieved the CPR from a measurement of the φ_{dc} dependence of the phase angle α between the drive current I_{rf} and the tank voltage V at the resonant frequency of the tank circuit ω_0 . As described in Ref. [12], at ω_0 , the $\alpha(\varphi_{dc})$ dependence is related to the derivative of the CPR $f'(\varphi) \equiv df(\varphi)/d\varphi$ in the following way:

$$\tan \alpha(\varphi_{dc}) = \frac{k^2 Q \beta f'(\varphi(\varphi_{dc}))}{1 + \beta f'(\varphi(\varphi_{dc}))}. \quad (3)$$

Here k is the coupling factor between the tank inductance and the interferometer, $k^2 = M^2/(LL_T)$, where M is the mutual inductance [Fig. 1(b)]. Using Eq. (3), from the measured $\alpha(\varphi_{dc})$ dependence $f'(\varphi(\varphi_{dc}))$ is obtained. The CPR is restored by integrating $f'(\varphi(\varphi_{dc}))$ numerically, using the $d\varphi(\varphi_{dc})/d\varphi_{dc}$ dependence obtained from differentiating Eq. (2) with respect to φ_{dc} .

The samples investigated consisted of three bicrystalline $\text{YBa}_2\text{Cu}_3\text{O}_{7-x}$ films with a T_c ($R = 0$) of 88 K. The films, with thickness $t = 100$ nm, were deposited by standard pulsed laser deposition on (001)-oriented SrTiO_3 bicrystalline substrates [15] with symmetric [001]-tilt misorientation angles of $45^\circ \pm 2^\circ$ and were subsequently patterned by Ar ion-beam etching into 8×8 mm² or 5×5 mm² square washer single-junction interferometer structures. The widths of the junctions were $b \approx 2-3$ μm . The washer holes had a side length of 50 μm , leading to $L \approx 80$ pH.

To minimize the influence of external noise, the samples were measured in superconducting and double magnetic shielding at a temperature of 4.2 K. The condition $\beta < 1$ for the investigated interferometers was confirmed experimentally from the character of its response versus φ_{dc} [12].

$\text{YBa}_2\text{Cu}_3\text{O}_{7-x}$ grain boundaries with a symmetric [001] tilt angle of 45° typically have a normal-state interface-resistivity $\rho_n > 1 \times 10^{-8} \Omega \text{ cm}^2$, which we also measured for boundaries fabricated under identical conditions as the junctions used in the present experiments. In the configuration used, this ρ_n corresponds to normal-state resistances $R_n > 1 \Omega$. Accordingly, the relaxation time of the interferometer $\tau = L/R$ is short ($\tau \ll 1/\omega_0$), and hence the quasiparticle current is negligible [12].

For the measurements of $\alpha(\varphi_{dc})$, two tank circuits with quality factor $Q = 120$ and inductance $L_T = 0.4$ μH , $\omega_0 = 30$ MHz, and $L_T = 0.73$ μH , $\omega_0 = 23$ MHz, respectively, were employed. The phase angle was recorded as a function of I_{dc} after amplification of the tank voltage by a high-impedance amplifier. The coupling coefficient k was determined from the period of the $\alpha(I_{dc})$ dependence. Values of $k = 0.072$ and $k = 0.054$ for the respective tank circuits are obtained. To ensure the validity of the small-signal limit, the measurements were carried out with $\varphi_{rf} < 0.15$.

A typical $\alpha(I_{dc})$ dependence is shown in Fig. 2. The corresponding CPR, depicted in Fig. 3, is clearly deviating from the standard sinusoidal behavior. Samples fabricated on different substrates and measured with both tank coils followed closely the same behavior. It is emphasized that the experimental setup employed and the procedure followed are identical to those used to measure the current-phase relations of step-edge junctions and thin-film bicrystals with a symmetric [001] tilt of 24° . For

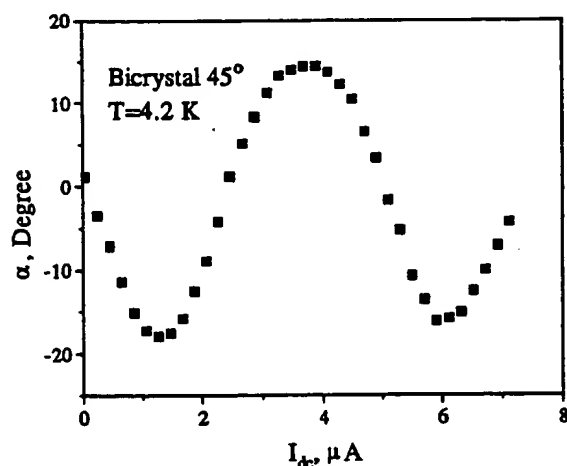


FIG. 2. Phase angle α between the driving current and the output voltage measured at 4.2 K as a function of the dc current I_{dc} , for an $\text{YBa}_2\text{Cu}_3\text{O}_{7-x}$ single junction interferometer circuit containing a symmetric 45° [001]-tilt grain boundary.

all of those samples nominally sinusoidal current-phase relations were observed, and all deviations of the apparent CPR from a sinusoidal one can be attributed to thermal noise [12,13].

The measured deviations from a sinusoidal dependence for the current-phase relations of these 45° bicrystals are startling. It is important to note that the effective Josephson penetration depth $\Lambda_J = [\Phi_0 / (4\pi\mu_0\langle j_c \rangle \lambda)]^{1/2} \approx 5 \mu\text{m}$ is larger than the width of the junction b (narrow-junction limit). Here λ is the London penetration depth. Although several mechanisms are known to cause nonsinusoidal current-phase relations for narrow junctions fabricated from conventional superconductors, all of these mechanisms fail to account for the anomalous dependencies presented.

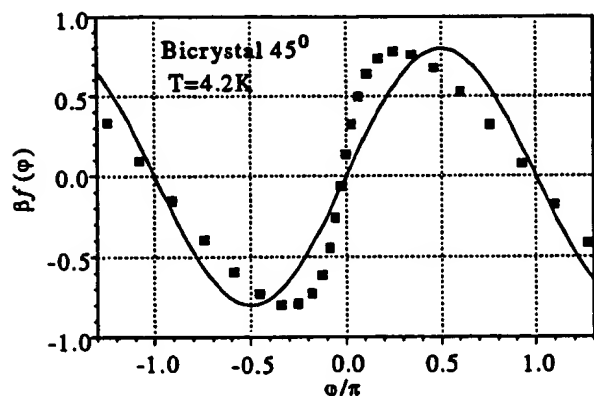


FIG. 3. The normalized current through the junction $\beta f(\varphi)$ as a function of the phase difference φ restored from the measured $\alpha(I_{dc})$ as shown in Fig. 2. For comparison, the function $\beta \sin(\varphi)$ with $\beta = 0.8$ is plotted as a solid line.

First, one potential source of such deviations is thermal noise. To evaluate its influence we consider a sinusoidal CPR and calculate with Eq. (3) the $\alpha(\varphi_{dc})$ dependence, assuming a thermally induced Gaussian spread $\rho(\varphi_n)$. With this, the value of $\tan \alpha(\varphi_{dc})$ is given by [12]

$$\tan \alpha(\varphi_{dc}) = k^2 Q \beta \times \int_{-\infty}^{\infty} \frac{\cos \varphi(\varphi_c, \varphi_n)}{1 + \beta \cos \varphi(\varphi_c, \varphi_n)} \rho(\varphi_n) d\varphi_n. \quad (4)$$

Using Eq. (4), minor deviations of the CPR from a standard sinusoidal behavior are well described quantitatively for 24° boundaries measured at 77 K [12]. However, no realistic set of β and φ_n exists to account for the large deviations of the CPR observed for the 45° boundaries.

Second, for weak links with a high current density, current-induced suppression of the order parameter in the electrodes close to the weak link can give rise to nonharmonic current-phase relations [16]. It is unrealistic that this effect is the cause for the deviations presented here, as the intragrain critical current density exceeds 10^7 A/cm^2 at 4.2 K and is therefore much larger than the grain boundary $\langle j_c \rangle < 4000 \text{ A/cm}^2$ at the same temperature.

Third, several additional mechanisms, described in [2], lead to deviations from a harmonic CPR. In all these cases, the slope of $f(\varphi)$ at $\varphi = 0$ is smaller than at $\varphi = \pi$, which is in contrast to our results. Therefore, these mechanisms cannot explain the current-phase relations observed either.

On the other hand, as will be pointed out in the following, the measured CPR can be accounted for by the unconventional order parameter symmetry of $\text{YBa}_2\text{Cu}_3\text{O}_{7-x}$ and by the microstructural properties of the grain boundaries, in particular by their faceted nature [17,18]. Interestingly, due to the $d_{x^2-y^2}$ -wave character of the order parameter, the faceting has a more significant influence on the electronic properties of boundaries with a misorientation close to 45° than on boundaries with considerably smaller misorientation angles [18]. This also concerns the CPR, as the 45° boundaries contain a higher density of facets that themselves show anomalous behavior. Two kinds of such anomalies, to be considered here, are described in the literature.

First, due to the sign difference of the adjacent lobes of the $d_{x^2-y^2}$ -wave order parameter, many facets are biased with an additional π phase shift (π facets) [17–19]. These phase shifts give rise to unconventional junction properties, such as a spontaneous generation of magnetic flux in the grain boundary junction [19–21]. As described in Ref. [21], the local phase difference $\varphi(x)$ along the grain boundary ($0 < x < b$) can be written as

$$\varphi(x) = \xi(x) + \psi(x), \quad (5)$$

where $\xi(x)$ is a rapidly alternating function accounting for the π phase shifts and for the spontaneously generated

magnetic flux in the junction, and $\psi(x)$ is the remaining slowly varying phase difference reflecting the magnetic flux in the interferometer loop. For a narrow junction ($b < \Lambda_J$), ψ is independent of x . With Eq. (5), the time-independent sine-Gordon equation, describing the spatial dependence of the local phase difference over the junction, becomes

$$\Lambda_J^2 \frac{\partial^2 \xi(x)}{\partial x^2} = \frac{j_c(x)}{\langle j_c \rangle} \sin[\psi + \xi(x)]. \quad (6)$$

The solution $\xi(x)$ of this equation, and thus the pattern of self-generated flux, depends on ψ . The redistribution of this flux by a change of ψ is expected to lead to remarkable deviations from a harmonic dependence for the CPR measured for the entire junction, also if the local CPR is nominally sinusoidal.

Second, it has been proposed [7,8] that the CPR of facets formed by the (110) and by the (100) planes of the adjacent grains is periodic with π and thus has a double periodicity as compared to the standard case. Transmission electron microscopy has revealed that 45° [001] tilt grain boundaries in $\text{YBa}_2\text{Cu}_3\text{O}_{7-x}$ tend to be composed for a considerable part of such facets [22]. For the whole junction, this leads to an anomalous CPR:

$$I = I_{c1} \sin \psi + I_{c2} \sin 2\psi, \quad (7)$$

by which the observed CPR can be described.

In summary, the current-phase relations of grain boundary junctions with a misorientation of 45° were measured with a modified Rifkin-Deaver method. The CPRs were deduced from measurements of the phase angle between the rf drive current and the rf tank voltage. The current-phase relations of the Josephson junctions showed pronounced deviations from a harmonic behavior, which cannot be accounted for by thermal noise or by other standard mechanisms, but are attributed to the $d_{x^2-y^2}$ -wave symmetry of the order parameter and the faceting of the grain boundaries.

We are grateful to A. Golubov and M. Kupriyanov for fruitful discussions. Part of this work has been performed at the IBM Zürich Research Laboratory. Financial support by the DFG (Ho 461/1-1) and the BMBF (13N6519 and 13N6918/1) is gratefully acknowledged. One of us

(H. H.) thanks the Royal Dutch Academy of Sciences and the University of Twente for their support.

- [1] B. D. Josephson, Phys. Lett. 1, 251 (1962); Rev. Mod. Phys. 36, 216 (1964).
- [2] K. K. Likharev, Rev. Mod. Phys. 51, 101 (1979).
- [3] C. C. Tsuei, J. R. Kirtley, C. C. Chi, Lock See Yu-Jahnes, A. Gupta, T. Shaw, J. Z. Sun, and M. B. Ketchen, Phys. Rev. Lett. 73, 593 (1994).
- [4] D. J. Van Harlingen, Rev. Mod. Phys. 67, 515 (1995).
- [5] D. J. Scalapino, Phys. Rep. 250, 329 (1995).
- [6] Yu. S. Barash, A. V. Galaktionov, and A. D. Zaikin, Phys. Rev. B 52, 665 (1995).
- [7] W. Zhang, Phys. Rev. B 52, 3772 (1995).
- [8] Y. Tanaka and S. Kashiwaya, Phys. Rev. B 53, R11957 (1996).
- [9] H. Burkhardt (to be published).
- [10] S. S. Tinchev, Physica (Amsterdam) 222C, 173 (1994).
- [11] V. Polushkin, S. Uchaikin, S. Knappe, H. Koch, B. David, and D. Grundler, IEEE Trans. Appl. Supercond. 5, 2790 (1995).
- [12] V. Zakosarenko, E. V. Il'ichev, R. P. J. IJsselsteijn, and V. Schultze, IEEE Trans. Appl. Supercond. 7, 1057 (1997).
- [13] E. V. Il'ichev, V. Zakosarenko, V. Schultze, H.-G. Meyer, H. E. Hoenig, V. N. Glyantsev, and A. Golubov, Appl. Phys. Lett. 72, 731 (1998).
- [14] R. Rifkin and B. S. Deaver, Phys. Rev. B 13, 3894 (1976).
- [15] D. Dimos, P. Chaudhari, J. Mannhart, and F. K. LeGoues, Phys. Rev. Lett. 61, 219 (1988).
- [16] M. Yu. Kupriyanov, Pis'ma Zh. Eksp. Teor. Fiz. 56, 414 (1992) [JETP Lett. 56, 399 (1992)].
- [17] C. A. Copetti, F. Rüders, B. Oelze, Ch. Buchal, B. Kabius, and J. W. Seo, Physica (Amsterdam) 253C, 63 (1995).
- [18] H. Hilgenkamp, J. Mannhart, and B. Mayer, Phys. Rev. B 53, 14586 (1996).
- [19] J. Mannhart, H. Hilgenkamp, B. Mayer, Ch. Gerber, J. R. Kirtley, K. A. Moler, and M. Sigrist, Phys. Rev. Lett. 77, 2782 (1996).
- [20] R. G. Mints and V. G. Kogan, Phys. Rev. B 55, R8681 (1997).
- [21] R. G. Mints (to be published).
- [22] J. A. Alarco, E. Olsson, Z. G. Ivanov, P. A. Nilsson, D. Winkler, E. A. Stepanov, and A. Ya. Tzalenchuk, Ultramicroscopy 51, 239 (1993).

Exhibit D

Lindström et al., 2003, Physical Review Letters 90, 117002

Dynamical Effects of an Unconventional Current-Phase Relation in YBCO dc SQUIDS

T. Lindström,^{1,*} S. A. Charlebois,¹ A. Ya. Tzalenchuk,² Z. Ivanov,¹ M. H. S. Amin,³ and A. M. Zagorskin^{3,4}

¹Department of Microelectronics and Nanoscience, Chalmers University of Technology and Göteborg University, SE-412 96 Göteborg, Sweden

²National Physical Laboratory, Teddington, Middlesex TW11 0LW, United Kingdom

³D-Wave Systems Inc., 320-1985 Broadway, Vancouver, British Columbia, Canada V6J 4Y3

⁴Physics and Astronomy Department, The University of British Columbia, 6224 Agricultural Road, Vancouver, Canada V6T 1Z1
(Received 20 December 2002; published 17 March 2003)

The predominant *d*-wave pairing symmetry in high-temperature superconductors allows for a variety of current-phase relations in Josephson junctions, which is to a certain degree fabrication controlled. In this Letter, we report on direct experimental observations of the effects of a non-sinusoidal current-phase dependence in YBCO dc SQUIDS, which agree with the theoretical description of the system.

DOI: 10.1103/PhysRevLett.90.117002

PACS numbers: 74.50.+r, 85.25.Dq

It is well established [1] that the wave function of a Cooper pair in most cuprate high-temperature superconductors (HTS) has a *d*-wave symmetry. Its qualitative distinction from, e.g., the anisotropic *s*-wave case is that the order parameter changes sign in certain directions, which can be interpreted as an *intrinsic* difference in the superconducting phase between the lobes equal to π .

The latter leads to a plethora of effects, such as formation of Andreev bound states at surfaces and interfaces in certain crystallographic orientations [2–4]. The current-phase dependence $I_s(\phi)$ in Josephson junctions formed by *dd* junctions, as well as by *sd* junctions comprised of a cuprate and a conventional superconductor, depends both on the spatial orientation of the *d*-wave order parameter with respect to the interface, and on the quality of the latter [5–9]. Time-reversal symmetry can also be spontaneously violated and thus spontaneous currents generated [10–12]. Another effect can be doubling of the Josephson frequency [6,13,14].

In this Letter, we report on experimental observations of strong effects of an unconventional current-phase relation on the dynamics of two *dd* junctions integrated into a superconducting interference device (SQUID) configuration.

Since $I_s(\phi)$ must be a 2π -periodic odd function, it can be expanded in a Fourier series. In most cases, only the first two harmonics give a significant contribution to the current:

$$I_s(\phi) = I_c^I \sin \phi - I_c^{II} \sin 2\phi. \quad (1)$$

In Josephson systems of conventional superconductors, the second harmonic will usually be negligible [15] but in *dd* junctions the second harmonic may dominate. If $I_c^{II} > I_c^I/2$, the equilibrium state is no longer $\phi = 0$ but becomes double degenerate at $\phi = \pm \arccos(I_c^I/2I_c^{II}) \rightarrow \pm \pi/2$. The system can then spontaneously break time-reversal symmetry by choosing either state. Spontaneous currents as well as fluxes can be generated in this state. The potential will have the shape of a double

well, and there are reasons to believe that it will be possible to observe quantum coherence in this system. The presence of a second harmonic in the current-phase relation (CPR) of a *dd* junction was confirmed by Il'ichev *et al.* [8].

A nonsinusoidal CPR of the junctions will change the dynamics of a dc SQUID [16]. Regarding the junctions as magnetically small, the supercurrent through the SQUID in the presence of an external flux $\Phi_x \equiv \Phi_0 \cdot (\phi_x/2\pi)$ can be written as

$$I_s(\phi, \phi_x) = I_{c1}^I \sin \phi - I_{c1}^{II} \sin(2\phi) + I_{c2}^I \sin(\phi + \phi_x) - I_{c2}^{II} \sin 2(\phi + \phi_x). \quad (2)$$

The critical current through the SQUID is given by the usual expression $I_c(\phi_x) = \max_{\phi} I_s(\phi, \phi_x)$. The time-averaged voltage over the SQUID in the resistive regime is readily obtained in the resistively shunted junction approximation. By introducing $\delta[\phi, \phi_x] = \phi_2 - \phi_1$ and applying the same method as in [17] with the necessary generalizations, we obtain the following for the average voltage over the SQUID:

$$\bar{V}^{-1} = \frac{G_1 + G_2}{2\pi} \int_{-\pi}^{\pi} d\phi \left[1 - (G_1 - G_2) \frac{\hbar}{2e} \frac{d\delta}{dt} - I_1 \left(\phi + \frac{\delta}{2} \right) - I_2 \left(\phi - \frac{\delta}{2} \right) \right]^{-1}. \quad (3)$$

Here $G_{1,2}$ are the normal conductances of the junctions, and

$$\delta + \phi_x + \frac{\pi L}{\Phi_0} [I_2(\phi - \delta/2) - I_1(\phi + \delta/2)] = 0 \quad (4)$$

gives the difference, δ , in phase drops across each junction. In deriving (3) and (4), we have assumed that the inductance L is equally divided between the SQUID arms. We have also neglected the spontaneous magnetic fluxes in the *dd* junctions, due to their small amplitude [11,18]. Though (4) is only explicitly solvable in the limit

$L \rightarrow 0$, it always yields $\delta[-\phi, -\phi_x] = -\delta[\phi, \phi_x]$. This means that the usual inversion symmetry is retained.

The results of numerical calculations based on (2) and (3) are shown in Fig. 1. The cusps in the critical current correspond to the points at which the global maximum in (1) switches from one local maximum to another [16]. Note the quasi- $\Phi_0/2$ periodicity of the current isolines in the $\bar{V} - \phi_x$ picture, reflecting the current-phase dependence (1), and their shift along the Φ_x axis, which depends on the sign of the bias current (as it must to maintain the central symmetry with respect to the origin). The shift does not depend on the magnitude of the current since we neglect the self-inductance. For large biases, the Φ_0 periodicity is restored. Indeed, as the bias grows, one set of minima of the washboard potential, $U = (h/2e)[-I^I \cos \phi + (I^{II}/2) \cos 2\phi - I\phi]$, disappears first unless the first harmonic I^I is *exactly* zero.

We have fabricated and studied a large number of dc SQUIDs. The samples were fabricated from 250 nm thick YBCO films deposited on SrTiO₃ bicrystals. The grain-boundary junctions (GBJs) are of the asymmetric [001]-tilt type with the misorientation angle of 45° (0°–45° GBJ). For more information on GBJs see, for example, Ref. [19].

The pattern was defined using *E*-beam lithography and then transferred to a carbon mask employing a multistep process. Finally, the YBCO is etched through the mask using ion milling. This scheme allows us to fabricate

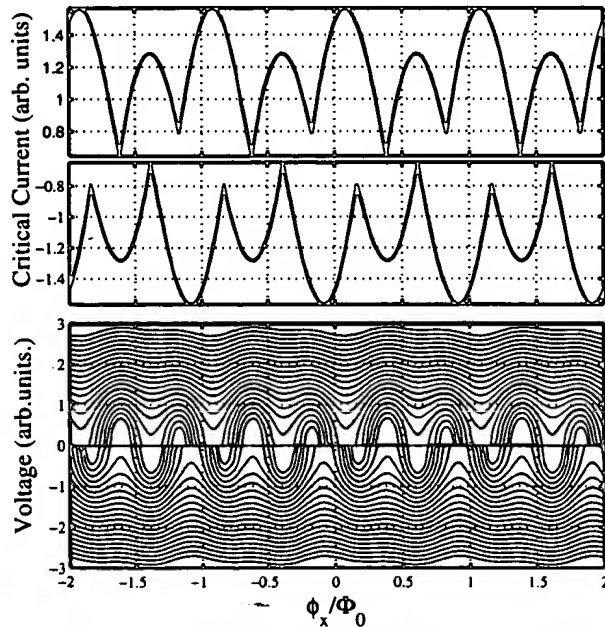


FIG. 1. The results of simulations of the $I_c - \phi_x$ and $\bar{V} - \phi_x$ dependence for a dc SQUID with $I_{c1}^I = 1$, $I_{c2}^I = 0.1$, $I_{c1}^{II} = 0.2$ and $I_{c2}^{II} = 0.4$ (arbitrary units). The different curves correspond to bias currents in the range $I = I_{c1}^I$ to $I = 5I_{c1}^I$. We assume $L = 0$ and $G_1 = G_2$.

high-quality bicrystal junctions as narrow as 0.2 μm , as has been reported elsewhere [20]. In the SQUIDs under investigation, the junctions are nominally 2 μm wide; hence, the fabrication-induced damage of the junctions is small.

The measurements were done in an EMC-protected environment using a magnetically shielded LHe cryostat. However, the magnetic shielding is imperfect, as is evident from the fact that the expected zero-field response of our SQUIDs is not exactly at zero. The measuring electronics is carefully filtered and battery powered whenever possible. In order to measure the dependence of the critical current on the applied field, we used a voltage discriminator combined with a sample-and-hold circuit. All measurements reported here were performed at 4.2 K.

The SQUID loops are $(15 \times 15) \mu\text{m}^2$. The numerically calculated inductance [21] is approximately 25 pH , yielding the factor $\beta = 2\pi LI_c/\Phi_0$ between 0.5–2.

The SQUIDs were largely nonhysteretic with a resistance of about 2 Ω . The measured critical current varies from sample to sample but is in the range of tens of microamperes giving a current density of the order of $J_c = 10^3 \text{ A/cm}^2$. The estimated Josephson penetration length $\lambda_J = \Phi_0/\sqrt{4\pi\mu_0 J_c \lambda_L}$ is approximately 2 μm in all junctions, which means that the junctions are magnetically short. This is supported by the quasiperiod of the pattern in Fig. 2 being close to the expected value $\Phi_0/2\lambda_L w$ [17]. The differential conductance curves do not show any trace of a zero bias anomaly (ZBA), as is expected for 0°–45° GBJs. ZBAs have been observed by other groups in GBJs with other orientations [2].

The critical current is plotted as a function of applied magnetic field for two SQUIDs in Fig. 3. The result is in qualitative agreement with theory if we assume that the SQUID junctions have different ratios of the first and second harmonics of the critical current. This assumption

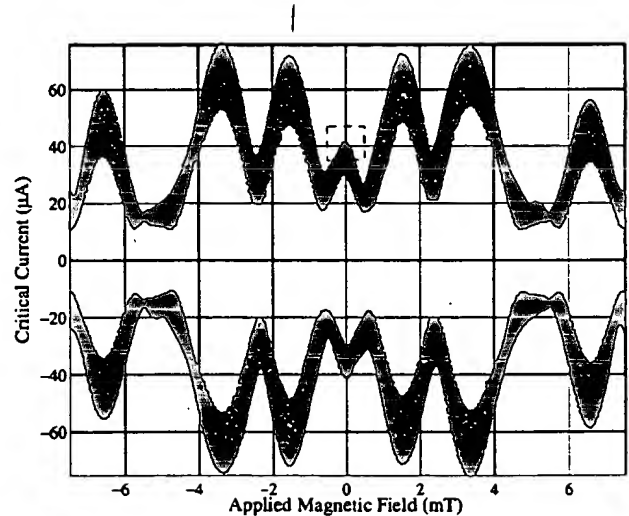


FIG. 2. Critical current as a function of magnetic field at 4.2 K. The dashed box indicates the area plotted in Fig. 3(a).

is supported by the fairly small modulation depth [it is easy to see from Eq. (2) that I_c would go exactly to zero in a SQUID with junctions of identical I_{c2}/I_{c1}].

We can fit the data to Eq. (2), if we compensate for the residual background magnetic field and assume that we have a small excess current (of the order of a few μA) in the junctions. The fitting parameters again confirm that there is a large asymmetry between the arms of the SQUIDs. Note that the model does not consider the flux penetration into the junctions,

The result for fields of the order of mT is presented in Fig. 2, which shows the I_c modulation of the SQUID enveloped by an anomalous Fraunhofer pattern quite similar to what has been reported by other groups [22,23] for 0° – 45° GBJs. Note the inversion symmetry

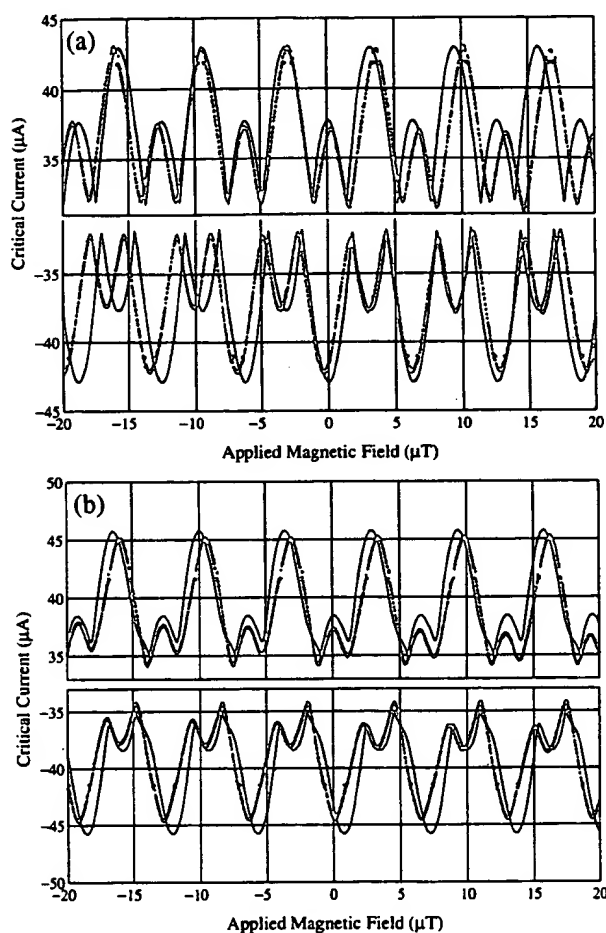


FIG. 3. Critical current as a function of applied magnetic field for two different SQUIDs that are nominally identical. The solid line represents the fitted expression. The fitting parameters are as follows: (a) $I_{c1}^I = 9 \mu\text{A}$, $I_{c2}^I = 0.3 \mu\text{A}$, $I_{c1}^{II} = 3.7 \mu\text{A}$, and $I_{c2}^{II} = 22.7 \mu\text{A}$; (b) $I_{c1}^I = 7.8 \mu\text{A}$, $I_{c2}^I = 3.0 \mu\text{A}$, $I_{c1}^{II} = 5.3 \mu\text{A}$, and $I_{c2}^{II} = 4.3 \mu\text{A}$. In both cases, the fit has been adjusted with respect to the residual background field and the excess current of the junctions.

of the pattern with respect to the origin. That the global maximum is not in the center can be explained in several ways; it has been shown, for example, that this could be due to the presence of so-called π loops in the junction interface [24].

Figure 4 shows the V - B dependence of one of the SQUIDs. The pattern is again field inversion symmetric. The overall structure is the same as in the model dependence of Fig. 1, but there is also an additional shift due to self-field effects, which depends on the magnitude of the bias current and corresponds (at maximum) to a flux $\sim 0.1\Phi_0$. In a beautiful experiment, a similar dependence was recently observed by Baselmans *et al.* in a Nb-Ag-Nb SNS junction where current injectors were used to change the occupation of current-carrying states in the normal region [25]. A deviation from the model occurs at $\bar{V} = 100 \mu\text{V}$ where the minima and maxima switch. This is probably due to an LC resonance in the SQUID. Taking $L = 25 \text{ pH}$, this would require $C = 0.8 \text{ pF}$, which agrees with our measurements on single junctions

Remarkably, the observed offset of the V - B characteristics with respect to the *direction* of the bias current appears to be a much more robust manifestation of the presence of a second harmonic of the Josephson current than the shape of the $I_c - B$ curves itself. We observed the shift even in SQUIDs with the smallest junctions down to $0.5 \mu\text{m}$ wide, where the deviations from the usual sinusoidal CPR were not obvious from the $I_c - B$ dependence.

Generally, the nature of the transport through a GBJ will depend on its transmissivity D . Il'ichev *et al.* [8] have reported values of D as high as 0.3 in symmetric (22.5° – 22.5°) dd junctions as opposed to the usual estimate for a GBJ, $D \sim 10^{-5}$ – 10^{-2} . Since usually $I_{c1}^{II}/I_{c1}^I \propto D$, a high-transmissivity GBJ is required in order

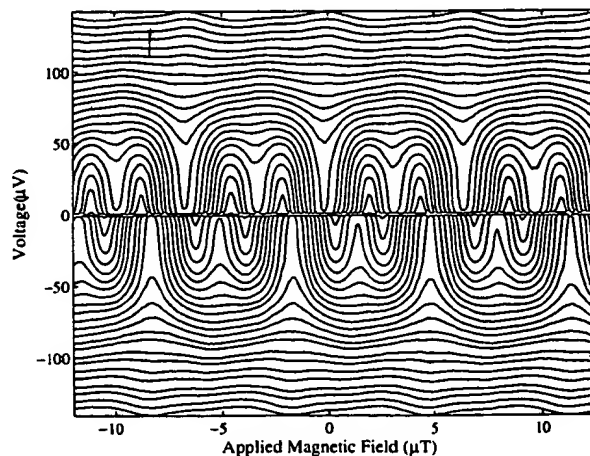


FIG. 4. Voltage modulation as a function of applied magnetic field for the SQUID whose $I_c - B$ is shown in Fig. 3(a). The pattern is again inversion symmetric. Note the sign change at $100 \mu\text{V}$, which we believe is due to a LC resonance in the SQUID loop.

to observe effects of the second harmonic. An estimate of the *average* transmissivity of our junctions would be $\rho_{ab}l/R_N A \sim 10^{-2}$ [26] assuming l , the mean-free path, to be equal to 10 nm and a resistivity in the a - b plane ρ_{ab} equal to $10^{-4} \Omega \text{ cm}$. This is still too low to explain the strong second harmonic we observe. However, it is known from, e.g., TEM studies [19], that the grain-boundary is far from uniform; the properties can significantly vary depending on the local properties of the interface, effects such as oxygen diffusion out of the GB, etc., which are difficult to control. It is therefore reasonable to assume that there are many parallel transport channels through the GB [27,28]. Channels with high-transmissivity dominate the transport and might have $D \sim 0.1$ even though the *average* transmissivity is much lower. This is also consistent with the fact that most of our SQUIDs seem to be highly asymmetrical which is to be expected if the distribution of channels is random. The ratios of I_c^I and I_c^{II} can vary as much as 10 times between two junctions in the same SQUID, even though the fluctuations of the *total* I_c from sample to sample are much smaller. It is also clear from general considerations that a high value of I_c^{II} *excludes* a high value of I_c^I , since the second harmonic usually dominates if the odd harmonics of the supercurrent are canceled by symmetry [29].

Recent studies of 0° – 45° GBJs have demonstrated that the SQUID dynamics can be altered by the d -wave order parameter in YBCO [30]. It is, however, important to point out that our results *do not* directly relate to, e.g., tetracystal π -SQUID experiments; the latter crucially depend on having one π junction with negative critical current, but still only the first harmonic present in $I_c(\phi)$. Our SQUIDs have a conventional geometry, but unconventional current-phase relations.

One explanation for the pronounced effects of the second harmonic could be that relatively large sections of the interface are highly transparent and have a low degree of disorder. This in turn could be related to our fabrication scheme which seems to preserve the integrity of the barrier. This makes feasible their applicability in the quantum regime and supports our expectations that quantum coherence can be observed in this kind of structures.

In summary, we have observed a very pronounced second harmonic in the current-phase relation of a “conventional” YBCO dc SQUID with 0° – 45° grain-boundary junctions. It has strongly influenced the SQUID dynamics. All details of the SQUID behavior were explained within a simple model of a dd junction with relatively high transparency. We believe that these effects are important for better understanding of HTS Josephson junction and SQUIDs.

Discussions with Evgeni Il'ichev, Alexander Golubov, Tord Claeson, and John Gallop are gratefully acknowledged. The work is in part supported by The Board for Strategic Research (SSF) via the “OXIDE” program, the Science Research Council, and the “Fonds québécois de la

recherche sur la nature et les technologies.” The processing work is done at the MC2 process laboratory at Chalmers University of Technology.

*Electronic address: tobiasl@fy.chalmers.se

- [1] C. Tsuei and J. Kirtley, *Rev. Mod. Phys.* **72**, 969 (2000).
- [2] L. Alff *et al.*, *Phys. Rev. B* **58**, 11 197 (1998).
- [3] T. Löfwander, V. Shumeiko, and G. Wendin, *Supercond. Sci. Technol.* **14**, R53 (2001).
- [4] C.-R. Hu, *Phys. Rev. Lett.* **72**, 1526 (1994).
- [5] S. Yip, *Phys. Rev. B* **52**, 3087 (1994).
- [6] A. Zagorskin, *J. Phys. Condens. Matter* **9**, L419 (1997).
- [7] E. Il'ichev *et al.*, *Phys. Rev. B* **60**, 3096 (1999).
- [8] E. Il'ichev *et al.*, *Phys. Rev. Lett.* **86**, 5369 (2001).
- [9] P. Komissinski *et al.*, *Europhys. Lett.* **57**, 585 (2002).
- [10] A. Huck, A. van Otterlo, and M. Sigrist, *Phys. Rev. B* **56**, 14163 (1997).
- [11] M. H. S. Amin, A. N. Omelyanchouk, and A. M. Zagorskin, *Phys. Rev. B* **63**, 212502 (2001).
- [12] S. Östlund, *Phys. Rev. B* **58**, R14 757 (1998).
- [13] T. Löfwander, G. Johansson, M. Hurd, and G. Wendin, *Phys. Rev. B* **57**, R3225 (1998).
- [14] H. Arie *et al.*, *Phys. Rev. B* **62**, 11864 (2000).
- [15] M. Keene, C. Gough, and A. Rae, *J. Phys. Condens. Matter* **3**, 6079 (1991).
- [16] M. H. S. Amin, M. Coury, and R. Rose, *IEEE Trans. Appl. Supercond.* **12**, 1877 (2002).
- [17] A. Barone and G. Paterno, *Physics and Applications of the Josephson Effect* (Wiley, New York, 1982).
- [18] M. H. S. Amin, S. N. Rashkeev, M. Coury, A. N. Omelyanchouk, and A. M. Zagorskin, *Phys. Rev. B* **66**, 174515 (2002).
- [19] H. Hilgenkamp and J. Mannhart, *Rev. Mod. Phys.* **74**, 297 (2002).
- [20] A. Tzalenchuk *et al.*, *Appl. Phys. Lett.* (to be published).
- [21] M. Khapaev, A. Kidiyarova-Shevchenko, P. Magnelind, and M. Kupriyanov, *IEEE Trans. Appl. Supercond.* **11**, 1090 (2001).
- [22] J. Mannhart, B. Mayer, and H. Hilgenkamp, *Z. Phys. B* **101**, 175 (1996).
- [23] W. Neils and D. van Harlingen, *Physica (Amsterdam)* **284B–288B**, 587 (2000).
- [24] H. Smilde *et al.*, *Phys. Rev. Lett.* **88**, 057004 (2002).
- [25] J. Baselmans, T. Heikkilä, B. van Wees, and T. Klapwijk, *Phys. Rev. Lett.* **89**, 207002 (2002); the pronounced second harmonic in this experiment appears due to nonequilibrium effects, see, e.g., J. C. Clarke, in *Nonequilibrium Superconductivity, Phonons and Kapitza Boundaries*, edited by K. E. Gray, NATO ASI Series (Plenum, New York, 1981), p. 353.
- [26] G. Blonder, M. Tinkham, and T. Klapwijk, *Phys. Rev. B* **25**, 4515 (1982).
- [27] Y. Naveh, D. Averin, and K. Likharev, *Phys. Rev. Lett.* **79**, 3482 (1997).
- [28] E. Sarnelli, G. Testa, and E. Esposito, *J. Supercond.* **7**, 387 (1994).
- [29] Y. Barash, *Phys. Rev. B* **61**, 678 (2000).
- [30] B. Chesca *et al.*, *Phys. Rev. Lett.* **88**, 177003 (2002).

Exhibit E

Tafari et al., cond-mat/0010128, Oct. 9, 2000

Feasibility of biepitaxial $\text{YBa}_2\text{Cu}_3\text{O}_{7-x}$ Josephson junctions for fundamental studies and potential circuit implementation

F. Tafuri

*Dipartimento di Ingegneria dell'Informazione, Seconda Università di Napoli, 81031 Aversa (CE) and
INFN-Dipartimento Scienze Fisiche dell'Università di Napoli "Federico II", 80125 Napoli (ITALY)*

F. Carillo, F. Lombardi, F. Miletto Granozio, F. Ricci, U. Scotti di Uccio and A. Barone
INFN-Dipartimento Scienze Fisiche dell'Università di Napoli "Federico II", 80125 Napoli (ITALY)

G. Testa and E. Sarnelli

*Istituto di Cibernetica del CNR, Via Toiano 6, Arco Felice (NA) (ITALY) also
INFN*

J.R. Kirtley

*IBM T.J. Watson Research Center, P.O. Box 218, Yorktown Heights, NY 10598,
USA*

(July 4, 2003)

We present various concepts and experimental procedures to produce biepitaxial $\text{YBa}_2\text{Cu}_3\text{O}_{7-x}$ grain boundary Josephson junctions. The device properties have an interesting phenomenology, related in part to the possible influence of " π -loops". The performance of our junctions and Superconducting Quantum Interference Devices indicates significant improvement in the biepitaxial technique. Further, we propose methods for fabricating circuits in which "0-" and " π -loops" are controllably located on the same chip.

I. INTRODUCTION

The possibility of realizing electronic circuits in which the phase differences of selected Josephson junctions are biased by π in equilibrium is quite stimulating.¹ The concept of such π -phase shifts was originally developed in the "extrinsic" case for junctions with ferromagnetic barriers² and in the "intrinsic" case for junctions exploiting superconductors with unconventional order parameter symmetries.³ As a result of the possible $d_{x^2-y^2}$ order parameter symmetry of high critical temperature superconductors (HTS),⁴ the presence of intrinsic π loops has also been considered for HTS systems.⁵ This has been discussed recently in view of novel device concepts, and in particular for the implementation of a solid state qubit^{1,6-8} and for Complementary Josephson junction electronics.⁹ In this paper we discuss how $\text{YBa}_2\text{Cu}_3\text{O}_{7-x}$ (YBCO) structures made by the biepitaxial technique^{10,11} can be successfully employed to produce arbitrary circuit geometries in which both "0" and π -loops are present, and possibly to obtain a doubly degenerate state.^{1,6} Of course, great caution should be used because of stringent requirements on junction parameters for practical applications of such devices.

Josephson junctions based on artificially controlled grain boundaries have been widely employed for fundamental studies on the nature of HTS.^{4,7,8} The lack of a

reliable technology based on the traditional trilayer configuration (i.e. a sandwich type junction with an insulator between the two superconducting electrodes) also enhanced interest in GB Josephson junctions for applications. Although the mechanism of high- T_C superconductivity and the influence of grain boundaries on the transport properties are not completely determined, reproducible and good quality devices are routinely fabricated. YBCO GB junctions are usually classified as bicrystals,¹² biepitaxials,¹¹ and step-edges,¹³ depending on the fabrication procedure. The bicrystal technique typically offers junctions with better performances and allows in principle the realization of all different types of GBs ranging from [001] and [100] tilt to [100] twist boundaries. GB junctions based on the step-edge and biepitaxial techniques offer the advantage, with respect to the bicrystal technology, of placing the junctions on the substrate without imposing any restrictions on the geometry. A comparison between the different GB techniques is far beyond the aim of this paper. Nevertheless we intend to show that significant improvements with respect to the original technique developed by Char et al.¹¹ are possible for biepitaxial junctions, and that the resulting devices have potential for applications. As a matter of fact, in traditional biepitaxial junctions, the seed layer used to modify the YBCO crystal orientation on part of the substrate produces an artificial 45° [001] tilt (c-axis

tilt) GB. The nature of such a GB seems to be an intrinsic limit for some real applications. A convincing explanation has been given in terms of the d-wave nature of the order parameter and more specifically by the presence of π -loops.¹⁴ As demonstrated by studies on bicrystals, based on the same type of 45° [001] tilt GB, the presence of π -loops reduces the $I_C R_N$ values (where I_C and R_N are the critical current and the high normal state resistance respectively), produces a dependence of the critical current I_C on the magnetic field H quite different from the Fraunhofer-like pattern, and generates unquantized flux noise at the grain boundary.¹⁴

We will show that the implementation of the biepitaxial technique¹⁰ we developed to obtain 45° [100] tilt and twist (a-axis tilt and twist) GBs junctions makes such a technique interesting for both applications and fundamental studies. The phenomenology observed for the junctions based on these GBs and Scanning SQUID Microscopy investigations demonstrate the absence of π -loops, as we expect from their microstructure. As a consequence higher values of the $I_C R_N$ values, a Fraunhofer like dependence of I_C on the magnetic field and lower values of the low frequency flux noise, when compared with 45° c-axis tilt GBs, have been measured. These features are important tests to employ junctions for applications. Scanning SQUID Microscopy investigations also gave evidence of "fractional" vortices in the presence of impurities. Finally, we extended the biepitaxial process to other types of GB by using different seed layers to obtain junction configurations where π loops can be controllably produced. We shall not dwell on conceptual principles and actual feasibility of qubit devices. Instead we discuss the importance of the biepitaxial technique in having "0" and " π " loops on the same chip. This makes the biepitaxial technique more versatile and promising for circuit design.

II. DEVICES: CONCEPTS AND FABRICATION PROCEDURE

As mentioned above, the biepitaxial technique allows the fabrication of various GBs by growing different seed layers and using substrates with different orientations. We have used MgO, CeO₂ and SrTiO₃ as seed layers. The MgO and CeO₂ layers are deposited on (110) SrTiO₃ substrates, while SrTiO₃ layers are deposited on (110) MgO substrates; in all these cases the seed layers grow along the [110] direction. Ion milling is used to define the required geometry of the seed layer and of the YBCO thin film respectively, by means of photoresist masks. YBCO films, typically 120nm in thickness, are deposited by inverted cylindrical magnetron sputtering at a temperature of 780° C. YBCO grows along the [001] direction on MgO (substrates or seed layers) and on the CeO₂ (seed layers), while it grows along the [103]/[013] direction on SrTiO₃ (substrates or seed layers). In order to select the [103] or [013] growth and to ensure a better structural uniformity

of the GB interface, we have also successfully employed vicinal substrates. However, most of the transport properties presented in this paper refer to samples not using vicinal substrates. Detailed structural investigations on these GBs, including Transmission Electron Microscopy (TEM) analyses, have been performed and the results have been presented elsewhere.^{10,16}

Depending on the patterning of the seed layer and the YBCO thin film, different types of GBs ranging from the two ideal limiting cases of 45° a-axis tilt and 45° a-axis twist have been obtained (see Fig.1). The intermediate situation occurs when the junction interface is tilted at an angle α different from 0 or $\pi/2$ with respect to the a- or b-axis of the [001] YBCO thin film. In all cases, the order parameter orientations do not produce an additional π phase shift along our junction, in contrast with the 45° asymmetric [001] tilt junctions. As a consequence, no π loops should occur independently of the details of the interface orientation. In Fig. 1 we consider ideal interfaces and neglect meandering of the GBs or interface anomalies that will be considered below. The CeO₂ seed layer may produce a more complicated GB structure, in which a 45° c-axis tilt accompanies the 45° a-axis tilt or twist (see Fig.2a).¹⁵ In this case, as shown in Fig.2b, π loops should occur in analogy with the traditional biepitaxial junctions based on 45° c-axis tilt GBs. In both Figs. 1 and 2 we display the possible $d_{x^2-y^2}$ -wave order parameter symmetry in the junction configuration. Junctions were typically 4 microns wide. We also performed systematic measurements on SQUIDs based on the structure employing MgO as a seed layer and SrTiO₃ as a substrate. DC SQUIDs in different configurations and with loop inductance typically ranging from 10 to 100 pH have been investigated. The typical loop size leading to the 10(100) pH inductance is approximately $10^2 \mu\text{m}^2$ ($10^4 \mu\text{m}^2$).

III. EXPERIMENTAL RESULTS

A. Biepitaxial junctions employing MgO seed layers

In this section we attempt to cover most of the phenomenology of the transport properties of 45° a-axis tilt and twist biepitaxial junctions. In Fig. 3, current vs voltage (I-V) characteristics of a typical biepitaxial junction are given for various temperatures close to the critical temperature. In the inset the corresponding I-V characteristic at $T = 4.2$ K is reported. They are closely described by the resistively-shunted-junction (RSJ) model and no excess current is observed. Nominal critical current densities J_C of $5 \times 10^2 \text{ A/cm}^2$ at $T = 77$ K, and of $9 \times 10^3 \text{ A/cm}^2$ at $T = 4.2$ K have been measured respectively. The R_N value (3.2Ω) is roughly independent of the temperature for $T < T_C$, providing a normal state specific conductance $\sigma_N = 70 (\mu\Omega\text{cm}^2)^{-1}$. The maximum working temperature T_C of this device was 82 K. In this case

$I_C R_N$ is 1.3 mV at $T = 4.2$ K. These values typically ranged from 1 mV to 2 mV at $T = 4.2$ K. They are larger for the corresponding J_C values than those provided by conventional biepitaxials, and are of the same order of magnitude as in GB bicrystal and step edge junctions.¹⁰ While the values of critical current density and normal state specific conductance in the tilt case are quite different from the twist case, the $I_C R_N$ values are approximately the same for both. Moreover $I_C R_N$ does not scale with the critical current density.¹⁰ In the tilt cases $J_C \approx 0.5\text{--}10 \times 10^3$ A/cm² and $\sigma_N \approx 1\text{--}10$ ($\mu\Omega\text{cm}^2$)⁻¹ are measured at $T = 4.2$ K respectively. Twist GBs junctions are typically characterized by higher values of J_C in the range $0.1\text{--}4.0 \times 10^5$ A/cm² and of σ_N in the range $20\text{--}120$ ($\mu\Omega\text{cm}^2$)⁻¹ (at $T = 4.2$ K). For the twist case deviations from the RSJ model are more marked as a result of higher critical current densities. For high values of J_C GB junctions do not present any clear modulation of the critical current as a function of the magnetic field.

A demonstration of the possibility of tailoring the critical current density and of the different transport regimes occurring in the tilt and twist cases has been given by measuring the properties of junctions with different orientations of the GB barrier on the same chip. By patterning the seed layer as shown in Fig. 4a, we could measure the properties of a tilt junction and of junctions whose interface is tilted in plane by an angle $\alpha = 30^\circ, 45^\circ$ and 60° with respect to the *a*- or *b*-axis of the [001] YBCO thin film respectively. In all cases the order parameter orientations do not produce an additional π phase shift along our junction, in contrast with the 45° [001] tilt junctions, and no π loops should occur. We measured the expected increase of the critical current density with increasing angle, which corresponds on average to an increase of the twist current component. The values measured at $T = 4.2$ K are reported in Fig. 4a and range from the minimum value $J_C = 3 \times 10^2$ A/cm² in the tilt case to the maximum $J_C = 10^4$ A/cm² corresponding to an angle of 60° , for which the twist component is higher. The consistency of this result has been confirmed by the values of normal state resistances, which are higher in the tilt case and decrease with increasing α . The $I_C R_N$ values are about the same for all the junctions independently of the angle α . In Fig. 4b the I-V characteristics measured at $T = 4.2$ K, corresponding to the junctions of Fig. 4a, are shown for approximately the same voltage range. Deviations from RSJ behavior appear for higher values of the critical current density ($\alpha = 60^\circ$). These results demonstrate that the grain boundary acts as a tunable barrier. This possibility of modifying the GB macroscopic interface plane by controlling the orientation of the seed layer's edge is somehow equivalent to the degree of freedom offered by bicrystal technology to create symmetric or asymmetric GBs, with the advantage of placing all the junctions on the same substrate. The 45° *a*-axis tilt and twist GBs and the intermediate situations can represent ideal structures to investigate the junction physics in a wide range of configurations. The anisotropy of the (103)

films and the possibility to select the orientation of the junction interface by suitably patterning the seed layer, and eventually the use of other seed layers which produce different YBCO in plane orientations, allow the fabrication of different types of junctions and the investigation of different aspects of HTS junction phenomenology. In particular we refer to the possibility of changing the tunneling matrix elements (by selecting the angle α) and to use the anisotropy of the layered structure of YBCO properties and of the order parameter symmetry.

The study of the junction properties in the presence of an external magnetic field H is a fundamental tool for the investigation of the Josephson effect in the various junctions, as well as a test of junction quality.¹⁷ We observe modulations of the critical current I_C following the usual Fraunhofer-like dependence. The $I_C(H)$ patterns are mostly symmetric around zero magnetic field, and in all samples the absolute maximum of I_C occurs at $H=0$. The presence of the current maximum at zero magnetic field is consistent with the fact that in our junction configuration the order parameter orientations do not produce an additional π phase shift, in contrast with the 45° [001] tilt GB junctions.^{14,10} Some examples are given in Fig. 5, where the magnetic pattern relative to a SQUID and a single junction at $T = 4.2$ K are shown respectively. In the former case we can also distinguish a smaller field modulation (with a period of 8 mG) which corresponds to the SQUID modulation (inset a). In the latter case the I-V characteristics are reported for different magnetic fields (inset b). Despite the Fraunhofer-like dependence, some deviations are evident, in agreement with most of the data available in literature.

For sake of completeness we also acknowledge some work we carried out by investigating Fiske steps as a function of H in other junctions, giving some evidence of a dielectric-like behavior¹⁸ of some of the layers at the junction interface. We already reported about this work elsewhere.¹⁹ The Fiske steps do not depend on the use of a particular substrate, since they have been observed in junctions based both on SrTiO₃ and MgO substrates. Typical values of the ratio between the barrier thickness t and the relative dielectric constant ϵ_r range from 0.2 nm to 0.7 nm. Considerations on the dependence of I_C on the temperature (T) can be also found in Ref.¹⁹. In junctions characterized by lower critical current densities, I_C tends to saturate at low temperatures, in contrast to those characterized by higher critical currents, for which there is a linear increase.^{10,20}

B. Scanning SQUID microscopy on biepitaxial junctions with MgO seed layer

Figure 6 is a scanning SQUID microscope²¹ image of a $200 \times 200 \mu\text{m}^2$ area along a grain boundary separating a (100) region from a (103) region (as labelled in the figure) of a thin YBCO biepitaxial film grown as described

above. The position of the grain boundary is indicated by the dashed line. The image was taken at 4.2 K in liquid helium with an octagonal SQUID pickup loop 4 microns in diameter after cooling the sample in a few tenths of a μ T externally applied magnetic field normal to the plane of the sample. The grey-scaling in the image corresponds to a total variation of $0.13\Phi_0$ of flux through the SQUID pickup loop. Visible in this image are elongated interlayer Josephson vortices in the (103) area to the right, and "fractional" vortices in the (100) area to the left, of the grain boundary. Fits to the interlayer vortices give a value for the *c*-axis penetration depth of about $4\mu\text{m}$. The "fractional" vortices are spontaneously generated in the (100) film, regardless of the value of external field applied.²² Temperature dependent scanning SQUID microscope imaging shows that this spontaneous magnetization, which appears to be associated with defects in the film, arises when the film becomes superconducting.^{4,23} Although it is difficult to assign precise values of total flux to the "fractional" vortices, since they are not well separated from each other, fits imply that they have less than Φ_0 of total flux in them, an indication of broken time-reversal symmetry. Although there is apparently some flux generated in the grain boundary region, the fact that these SQUIDs have relatively low noise seems to indicate that this flux is well pinned at the temperatures at which the noise measurements were made. These results are consistent with the absence of π loops along the grain boundary.

C. Biepitaxial junctions employing CeO_2 seed layers

The CeO_2 seed layer, as anticipated in section II, may produce an artificial GB that can be seen as a result of two rotations: a 45° [100] tilt or twist followed by a 45° [001] tilt around the *c*-axis of the (001) film. For this junction configuration a *d*-wave order parameter symmetry would produce π -loops, as shown in Fig. 2. We notice that such π -loops are structurally different from those usually obtained by the 45° [001] tilt GB junctions based on the traditional biepitaxial and bicrystal techniques. Due to the microstructure we expect especially in the [100] tilt case low critical current densities and high normal state resistances. We found that the deposition conditions to select the uniform growth of YBCO 45° tilted around the *c*-axis of the (001) film are critical. Preliminary measurements realized on tilt-type junctions with a CeO_2 seed layer gave evidence of Josephson coupling in these GBs. The measured $I_C R_N$ values are from $200\mu\text{V}$ to $750\mu\text{V}$ and are in the typical range of the GBs Josephson junctions.

D. Biepitaxial SQUIDs employing MgO seed layers

In this section we report on the characterization of dc-SQUIDs which are to our knowledge the first employing the GBs discussed above.²⁴ These SQUIDs exhibit very good properties, and noise levels which are among the lowest ever reported for biepitaxial junctions.²⁴ Apart from implications for applications, these performances are important for the study of the transport properties of HTS Josephson junctions. In Fig. 7 we show the magnetic field dependence of the voltage at 77 K for different values of the bias current for a dc-SQUID with an inductance of 13 pH. At this temperature $I_C R_N$ is about $20\mu\text{V}$. The corresponding value of the screening parameter $\beta = 2LI_C/\Phi_0$ is 0.03. In general low β values are mandatory to avoid the influence of asymmetric inductances in SQUID properties, and this has been crucial for experiments designed to study the order parameter symmetry.⁷ The presented curves are quite typical. These SQUIDs usually work in a wide temperature range from low temperatures (4.2 K) up to temperatures above 77 K. The maximum working temperature was in this case 82 K. The achieved magnetic flux-to-voltage transfer functions $V_\Phi = \partial V/\partial \Phi$, where *V* and Φ are the voltage across the device and the applied magnetic flux in the SQUID loop respectively, are suitable for applications. For instance at $T = 77\text{ K}$ an experimental value of the SQUID amplitude voltage modulation ΔV of 10.4 mV was measured, corresponding to $V_\Phi = 36.9\mu\text{V}/\Phi_0$.²⁴ Steps of different nature have been recurrently observed in the *I*-*V* characteristics in the washer and hole configurations and characterized also in terms of the magnetic field dependence of the voltage at different values of the bias current.

The noise spectral densities of the same dc-SQUID have been measured at $T = 4.2\text{ K}$ and $T = 77\text{ K}$ using standard flux-locked-loop modulated electronics. The energy resolution $\epsilon = S_\Phi/2L$ (with S_Φ being the magnetic-flux-noise spectral density) at $T = 4.2\text{ K}$ and $T = 77\text{ K}$ is reported in Fig. 8. At $T = 4.2\text{ K}$ and 10 kHz, a value of $S_\Phi = 3\mu\Phi_0/\sqrt{\text{Hz}}$ has been measured, corresponding to an energy resolution $\epsilon = 1.6 \times 10^{-30}\text{ J/Hz}$. This value is the lowest reported in the literature for YBCO biepitaxial SQUIDs. Moreover, the low frequency $1/f$ flux noise spectral density at 1 Hz is more than one order of magnitude lower than the one reported for traditional biepitaxials, as is also evident from the comparison with data at $T = 4.2\text{ K}$ of Ref.²⁵. The lower values of low frequency noise are consistent with the absence of π -loops on the scale of the faceting for these types of GBs, as clearly shown by Scanning SQUID Microscopy results. The π -loops produce some types of spontaneous magnetic flux in the GB region, which among other effects tends to degrade the SQUID's noise levels.¹⁴

IV. BIEPITAXIAL JUNCTIONS FOR EXPERIMENTS ON THE SYMMETRY OF THE ORDER PARAMETER AND FOR A DEVELOPMENT OF CONCEPTS FOR QUBITS

The particular junction configurations investigated in this work allow some consideration of the possible impact of these types of junctions on the study of the Josephson effect and the order parameter symmetry in YBCO and on the development of concepts for devices.^{1,6,9,7} We first recall that the biepitaxial technique can provide circuits composed completely of junctions without any π -loops (see Fig. 9a). By varying the interface orientation with respect to the [103] electrode orientation, the junction properties can be adjusted. On the other hand the traditional biepitaxial technique,¹¹ producing 45° [001] tilt GBs (see Fig. 9b) or the types of junctions described in the previous section by using CeO₂ (see Fig. 9c), can controllably generate π -loops on macroscopic scales. In these schemes we use a corner geometry with a 90° angle. This angle α can be obviously tuned to enhance the effects related to the phase shift (see dashed line in Fig. 9b) and this change is particularly easy to realize by using the biepitaxial technique.

In this section we focus our attention mainly on the feasibility of the biepitaxial junctions to obtain the doubly degenerate state required for a qubit. In Ref.^{1a} the design is based on quenching the lowest order coupling by arranging a junction with its normal aligned with the node of the d-wave order parameter, thus producing a double periodic current-phase relation. It has been shown that the use of π phase shifts in a superconducting phase qubit provides a naturally bistable device and does not require external bias currents and magnetic fields.^{1b} The direct consequence is the quietness of the device over other designs. A π junction provides the required doubly degenerate fundamental state, which also manifests itself in a doubly periodic function of the critical current density as a function of the phase.⁸ The same principle has been used in small inductance five junction loop frustrated by a π -phase shift.^{1b} This design provides a perfectly degenerate two-level system and offers some advantages in terms of fabrication ease and performance. HTS may represent a natural solution for the realization of the required π -phase shift due to the pairing symmetry of the order parameter and, therefore, due to the possibility of producing π phase shifts. Experimental evidence of YBCO π -SQUIDS has been given by employing the bicrystal technique on special tetracrystal substrates.⁷ The biepitaxial technique, beyond providing junctions with opportune properties, would guarantee the versatility necessary for the implementation of a real device, as shown below. As a matter of fact, we notice that our technique allows the realization of circuits where π -loops can be controllably located in part of the substrate and separated from the rest of the circuit based on "0"-loops, i.e. junctions where no additional π phase

shifts arise. This can be easily made by depositing the MgO and CeO₂ seed layers on different parts of the substrate, which will be also partly not covered by any seed layer.

As a test to show how the biepitaxial junctions could be considered for preliminary tests and device implementation for quantum computing without the topological restriction imposed by the bicrystal technique, we refer to the structures proposed in Ref.¹ as exemplary circuits.

The former is composed by a s-wave (S)- d-wave (D)- s-wave (S') double junction connected with a capacitor and an ordinary "0" Josephson junction based on s-wave superconductors (the S-D'-S junction generates the doubly degenerate state). The latter consists of a five junction loop with a π junction. Our technique would combine the possibility of placing the ordinary "0" junctions corresponding to the MgO seed layer and to exploit the possible doubly degenerate state of asymmetric 45° GB junctions corresponding to the CeO₂ seed layer to replace the S-D-S' system or the π junction respectively. Our structure would be obviously composed only of HTS. In Figs. 10a and 10b we show how devices for instance such as those proposed in Ref.¹ could be obtained by employing the biepitaxial technique respectively. The application to the five junction loop is straightforward (Fig. 10b) and the advantages of this structure have been already discussed in Ref.^{1b}. The biepitaxial technique can offer possible alternatives for the realization of the structures above. In particular the double junctions of the original S-D-S' system can be also replaced by a D'-D-D' structure (Fig. 10c) by exploiting our technique, in contrast to the bicrystal technology which could not give this possibility. Such a configuration could offer some advantages, if we consider that asymmetric 45° bicrystal GB Josephson junctions did not give systematic evidence of the doubly degenerate state. The doubly degenerate state seems to occur only in high quality low transparency GB junctions^{8,26} and it is known that S-I-D junctions do not have double periodicity of the critical current as a function of the phase.²⁶ A consequence of a possible nodeless order parameter^{4,23} at the D-D' GB interface could be a closer similarity with a S-I-D junction with loss of the doubly degenerate state. If this is the case, we speculate that the double junctions structure for symmetry reasons would produce a leading term in the Josephson coupling energy of the form $E_d \cos 2\theta$ (double periodic) and that the possible dipolar component of the magnetic field would be almost completely compensated in this configuration.^{1b} This can be considered as an attempt to construct a "microscopic" 2θ -junction. We finally notice that the topological advantages offered by the biepitaxial junctions would therefore be crucial in both the cases considered for the realization of the structure in Fig. 10, and important to reduce de-coherence effects. Bicrystal substrates would in fact impose on the circuit additional junctions required by the circuit design and, as a consequence, generate additional noise and de-coherence in the device.

V. CONCLUSIONS

The performance of the presented junctions and SQUIDS demonstrates that significant improvements in the biepitaxial technique are possible, and the resulting devices have potential for applications. We have presented a phenomenology that is consistent with the expected absence of π -loops in 45° [100] tilt and twist grain boundaries junctions. The use of a CeO_2 rather than a MgO seed layer can produce π -loops in the same junction configurations. The versatility of the biepitaxial technique has been recently used to obtain different types of grain boundaries. The advantage of placing junctions in arbitrary locations on the substrate without imposing any restrictions on the geometry, and the ease of obtaining different device configurations by suitably patterning the seed layer, make the biepitaxial technique competitive for the testing of new concept devices, such as those based on π -loops. Some simple examples of situations in which π -loops can be suitably produced in specific locations of a more complicated circuit have also been discussed.

ACKNOWLEDGMENTS

This work has been partially supported by the projects PRA-INFM "HTS Devices" and SUD-INFM "Analisi non distruttive con correnti parassite tramite dispositivi superconduttori" and by a MURST COFIN98 program (Italy). The authors would like to thank Dr. E. Ilichev and A. Golubov for interesting discussions on the topic.

¹ L.B. Ioffe, V.B. Geshkenbein, M.V. Feigel'man, A.L. Fauchere and G. Blatter, *Nature* **398**, 679 (1999); G. Blatter, V. B. Geshkenbein and L. B. Ioffe, *Cond. Mat.* 9912163 (1999)

² L.N. Bulaevskii, V.V. Kuzii and A.A. Sobyenin, *JETP Lett.* **25**, 290 (1977)

³ V.B. Geshkenbein, A.I. Larkin and A. Barone, *Phys. Rev. B* **36**, 235 (1986)

⁴ C.C. Tsuei and J.R. Kirtley, to be published in *Review of Modern Physics* (1999); C.C. Tsuei, J.R. Kirtley, C.C. Chi, L.S. Yu-Jahnes, A. Gupta, T. Shaw, J.Z. Sun and M.B. Ketchen, *Phys. Rev. Lett.* **73**, 593 (1994); J.R. Kirtley, C.C. Tsuei, J.Z. Sun, C.C. Chi, L.S. Yu-Jahnes, A. Gupta, M. Rupp and M.B. Ketchen, *Nature* **373**, 225 (1995); D.A. Wollman, D.J. Van Harlingen, J. Giapintzakis, D.M. Ginsberg, *Phys. Rev. Lett.* **74**, 797 (1995); D.A. Wollman, D.J. Van Harlingen and A.J. Leggett, *Phys. Rev. Lett.* **73**, 1872 (1994)

⁵ M. Sigrist and T.M. Rice, *J. Phys. Soc. Jap.* **61**, 4283 (1992)

⁶ A.M. Zagorskin, *Cond. Mat.* 9903170 (1999)

⁷ R. Schulz, B. Chesca, B. Goetz, C.W. Schneider, A. Shmehl, H. Bielefeldt, H. Hilgenkamp and J. Mannhart, *Appl. Phys. Lett.* **76**, 912 (2000)

⁸ E. Il'ichev, V. Zakosarenko, R.P.J. Ijsselsteijn, H.E. Honig, V. Schultze, H.G. Meyer, M. Grajcar and R. Hlubina, *Phys. Rev. B* **60**, 3096 (1999)

⁹ E. Terzioglu and M.R. Beasley, *IEEE Trans. Appl. Supercond.* **8**, 48 (1998)

¹⁰ F. Tafuri, F. Miletto Granozio, F. Carillo, A. Di Chiara, K. Verbist and G. Van Tendeloo, *Phys. Rev. B* **59**, 11523 (1999)

¹¹ K. Char, M.S. Colclough, S.M. Garrison, N. Newman and G. Zaharchuk, *Appl. Phys. Lett.* **59**, 773 (1991)

¹² D. Dimos, P. Chaudari, J. Mannhart and F.K. LeGoues, *Phys. Rev. Lett.* **61**, 219 (1988)

¹³ R. W. Simon, J.F. Burch, K.P. Daly, W.D. Dozier, R. Hu, A.E. Lee, J.A. Luine, H.M. Manasevit, C.E. Platt, S.M. Schwarzbeck, D.St. John, M.S. Wire and M.J. Zani, in "Science and Technology of Thin Films Superconductors 2", R.D. McConnel and R. Noufi Eds. (Plenum, New York, 1990), p. 549

¹⁴ J. Mannhart, H. Hilgenkamp, B. Mayer, Ch. Gerber, J.R. Kirtley, K.A. Moler and M. Sigrist, *Phys. Rev. Lett.* **77**, 2782 (1996)

¹⁵ U. Scotti di Uccio, F. Lombardi, F. Ricci, E. Manzillo, F. Miletto Granozio, F. Carillo and F. Tafuri unpublished (2000)

¹⁶ K. Verbist, O. Lebedev, G. Van Tendeloo, F. Tafuri, F. Miletto Granozio and A. Di Chiara, *Appl. Phys. Lett.* **74**, 1024 (1999)

¹⁷ A. Barone and G. Paterno, *Physics and Applications of the Josephson Effect*, (J. Wiley, New York, 1982)

¹⁸ J. Mannhart, R. Gross, K. Hipler, R.P. Huebner, C.C. Tsuei, D. Dimos and P. Chaudari, *Science* **245**, 839 (1989)

¹⁹ F. Tafuri, B. Nadgorny, S. Shokhor, M. Gurvitch, F. Lombardi, F. Carillo, A. Di Chiara and E. Sarnelli, *Phys. Rev. B* **57**, R14076 (1998)

²⁰ F. Tafuri, S. Shokhor, B. Nadgorny, M. Gurvitch, F. Lombardi and A. Di Chiara, *Appl. Phys. Lett.* **71**, 125 (1997)

²¹ J.R. Kirtley *et al.*, *Appl. Phys. Lett.* **66**, 1138 (1995)

²² F. Tafuri and J.R. Kirtley, *cond-mat /0003106*

²³ D.B. Bailey, M. Sigrist and R.B. Laughlin, *Phys. Rev. B* **55**, 15239 (1997); M. Sigrist, *Progr. Theor. Physics* **99**, 899 (1998).

²⁴ G. Testa, E. Sarnelli, F. Carillo and F. Tafuri, *Appl. Phys. Lett.* **75**, 3542 (1999)

²⁵ A.H. Miklich, J. Clarke, M.S. Colclough, and K. Char, *Appl. Phys. Lett.* **60**, 1989 (1992)

²⁶ Y. Tanaka and S. Kashiwaya, *Phys. Rev. B* **56**, 893 (1997)

FIG. 1. A schematic representation of the artificial grain boundary structure. The boundary is obtained at the interface between the [001] oriented YBCO film grown on the [110] MgO seed layer and the [103] YBCO film grown on the bare [110] STO substrate. In contrast with the 45° [001] tilt bicrystal junctions, in this case the order parameter orientations do not produce an additional π phase shift.

FIG. 2. The CeO_2 seed layer produces an artificial GB that can be seen as a result of two rotations: a 45° [100] tilt or twist followed by a 45° tilt around the c-axis of the (001) film. For this junction configuration a d-wave order parameter symmetry would produce π -loops.

FIG. 3. Current vs voltage (I-V) characteristics of the biepitaxial junction for temperature close to the critical temperature. In the inset the I-V curve at $T = 4.2$ K is shown.

FIG. 4. a) Scheme of the seed layer patterning, which allows the measurement on the same chip of the properties of a tilt junction and of junctions whose interface is tilted in plane of an angle $\alpha = 30^\circ, 45^\circ$ and 60° with respect to the a- or b-axis of the (001) YBCO thin film respectively. b) The I-V characteristics (measured at $T = 4.2$ K) of the microbridges reported in Fig. 4a.

FIG. 5. Magnetic-field dependence of the critical current of a [100] tilt biepitaxial dc-SQUID. The absolute maximum is observed for zero field. A double-period modulation is observed. The longer period modulation is the diffraction pattern due to the magnetic field sensed by a single junction, while the shorter period SQUID modulation is shown more clearly in the inset (a). In the inset (b) I-V curves are shown as a function of an externally applied magnetic field at $T = 4.2$ K. A typical Fraunhofer-like dependence is evident.

FIG. 6. Scanning SQUID microscope image of a $200 \times 200 \mu\text{m}^2$ area along a grain boundary separating a (100) region from a (103) region of a thin YBCO biepitaxial film grown. The position of the grain boundary is indicated by the dashed line.

FIG. 7. Magnetic field dependence of the voltage of a [100] tilt biepitaxial dc-SQUID at 77 K for different values of the bias current.

FIG. 8. Magnetic flux noise spectral densities of a [100] tilt biepitaxial SQUID at $T = 77$ K and $T = 4.2$ K. The SQUID, with an inductance $L = 13$ pH, was modulated with a standard flux-locked-loop electronics. The right axis shows the energy resolution. Data at $T = 4.2$ K are compared with results on SQUIDs based on [001] tilt biepitaxial junctions from Ref. 25.

FIG. 9. a) 3-dimensional view of a SQUID based on 45° [100] tilt and twist GBs; no π -loops should occur. b) Top view of π -SQUID based on 45° [001] tilt GBs. c) 3-dimensional view of a π -SQUID based on GBs resulting from two rotations: a 45° [100] tilt or twist followed by a 45° [001] tilt

FIG. 10. Scheme of the qubit structure proposed in Ref. 1 designed using the biepitaxial grain boundaries proposed in the paper. The double junctions of the original S-D-S' system can be also replaced by D'-D-D''.

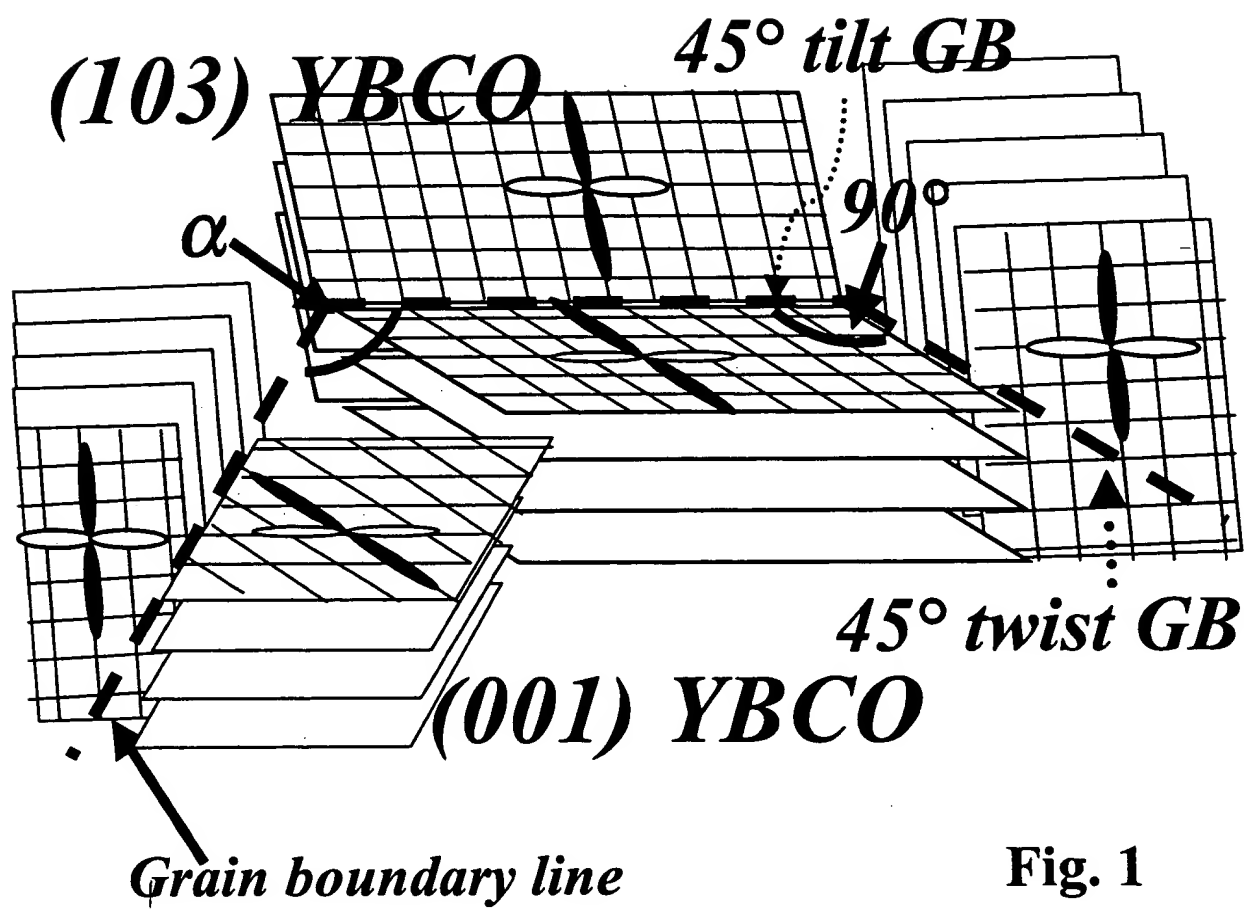


Fig. 1

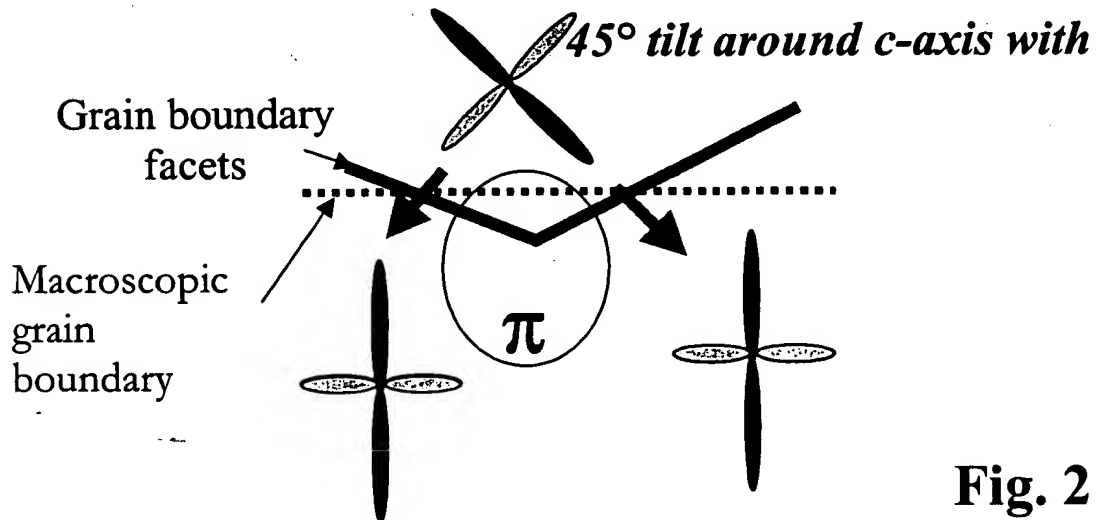
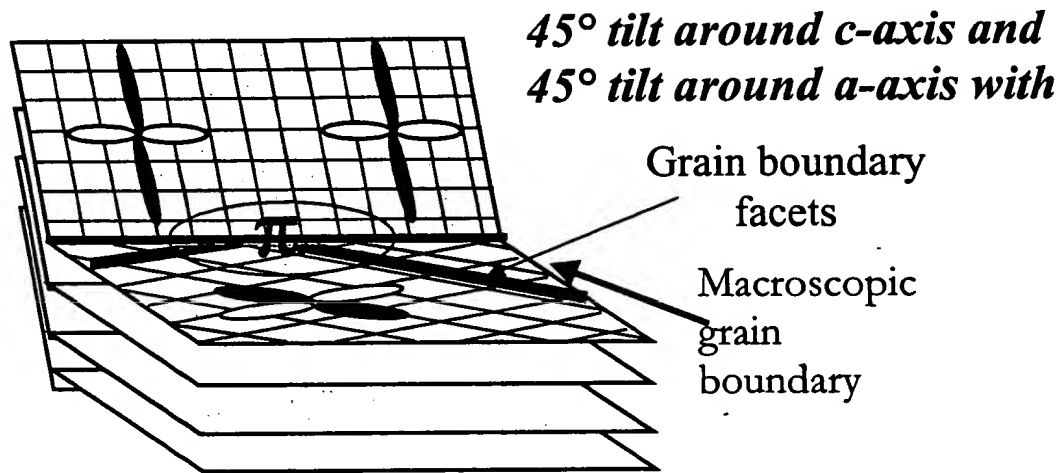
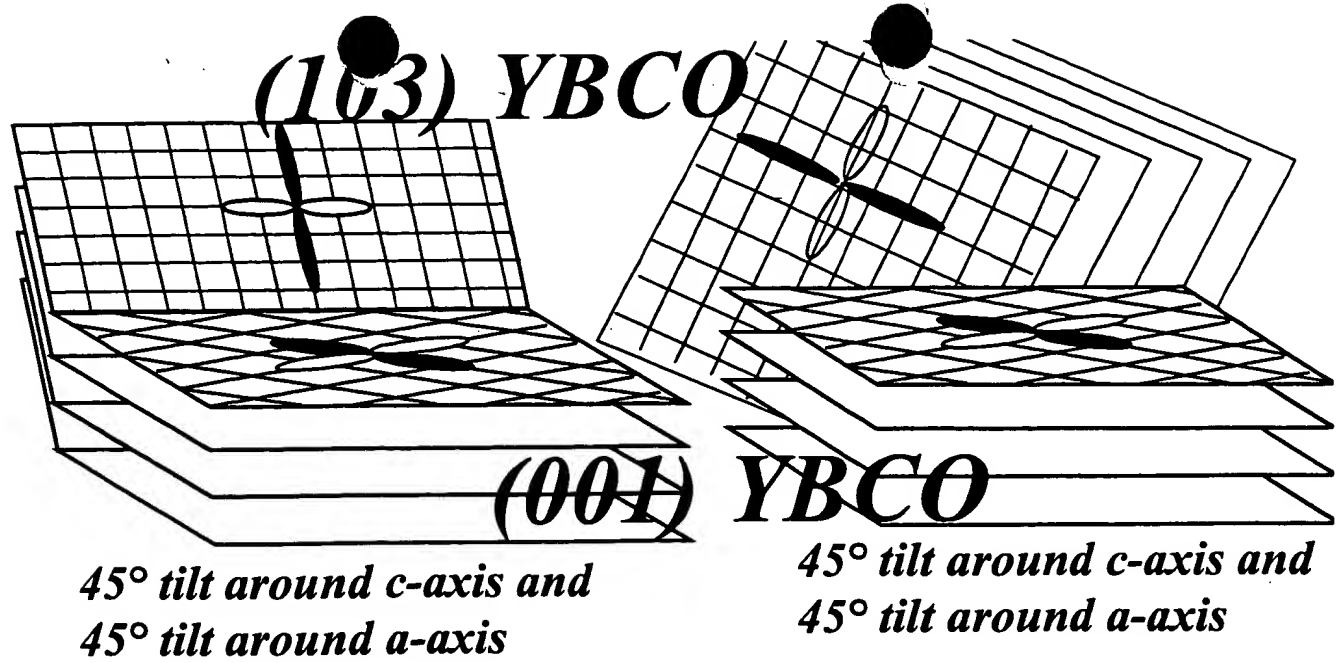


Fig. 2

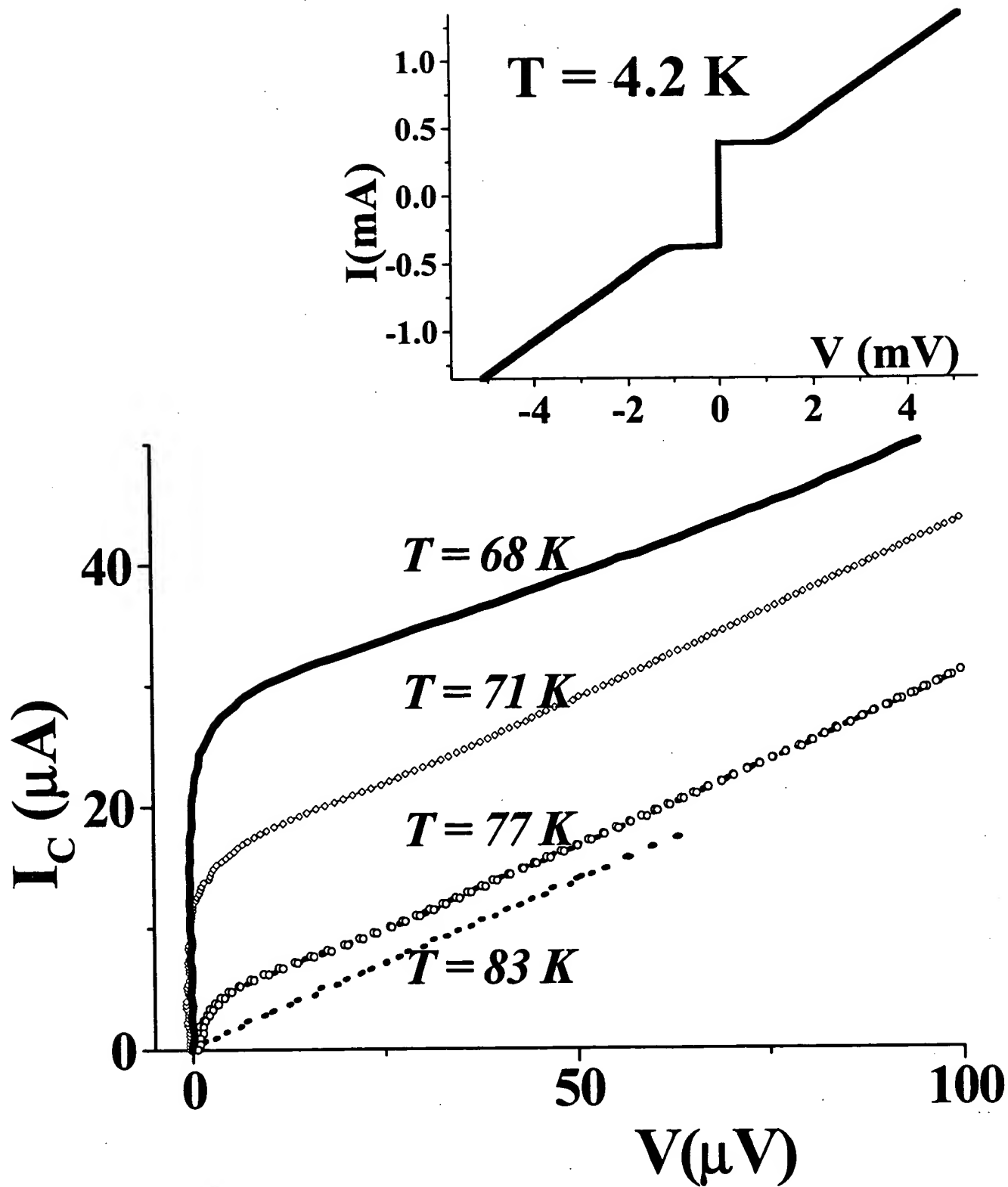


Fig. 3

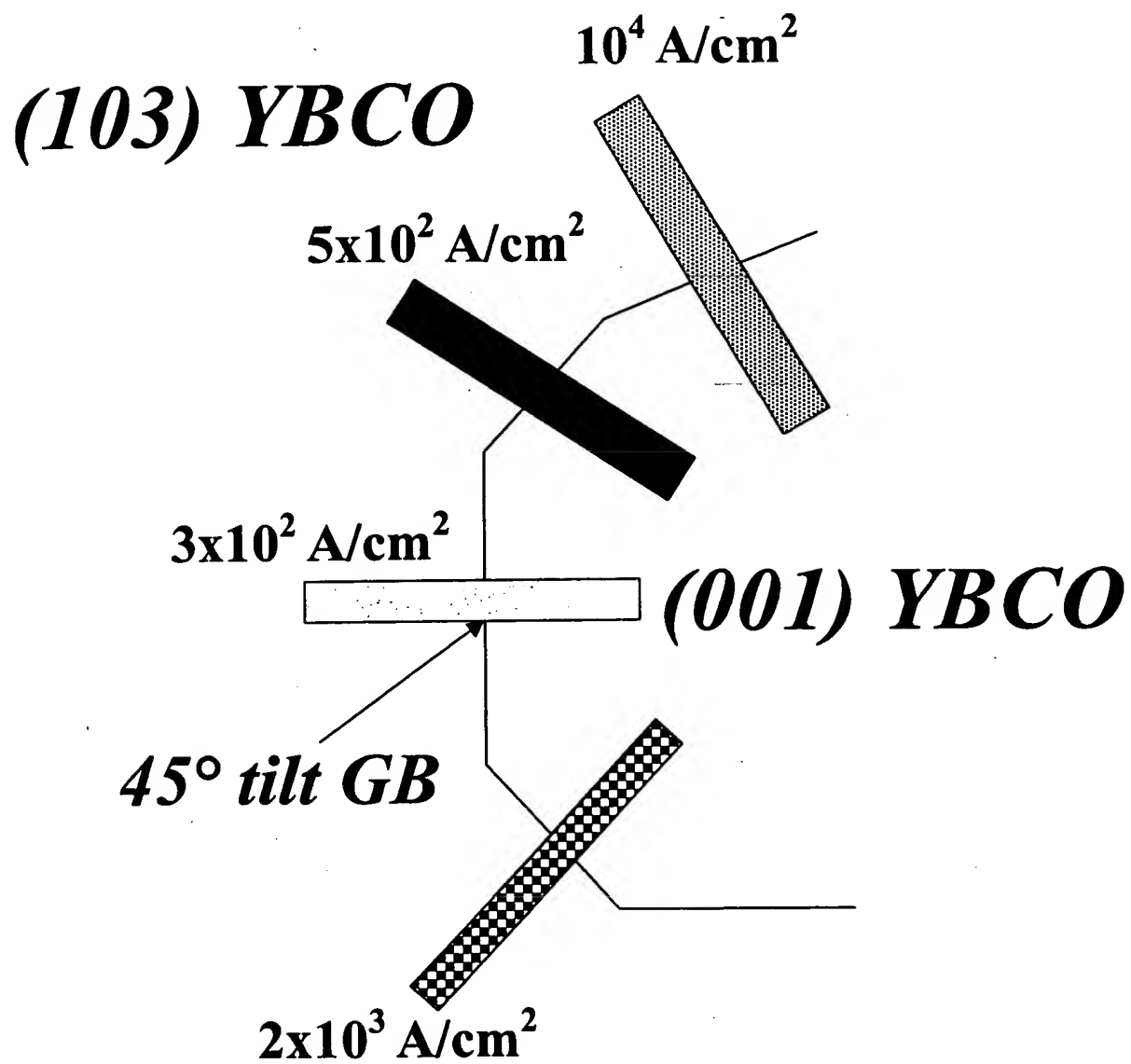


Fig. 4a

Fig. 4b

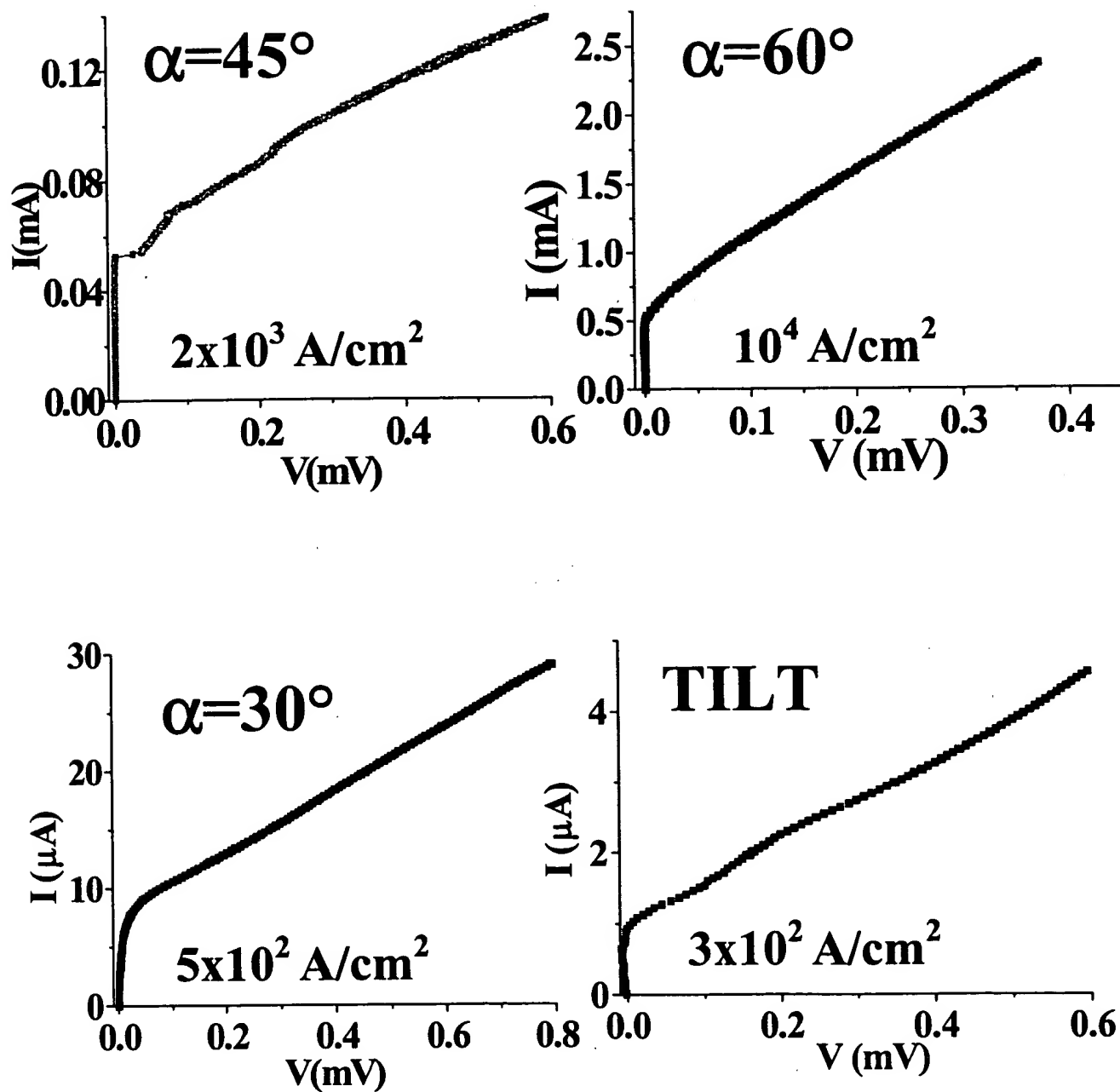
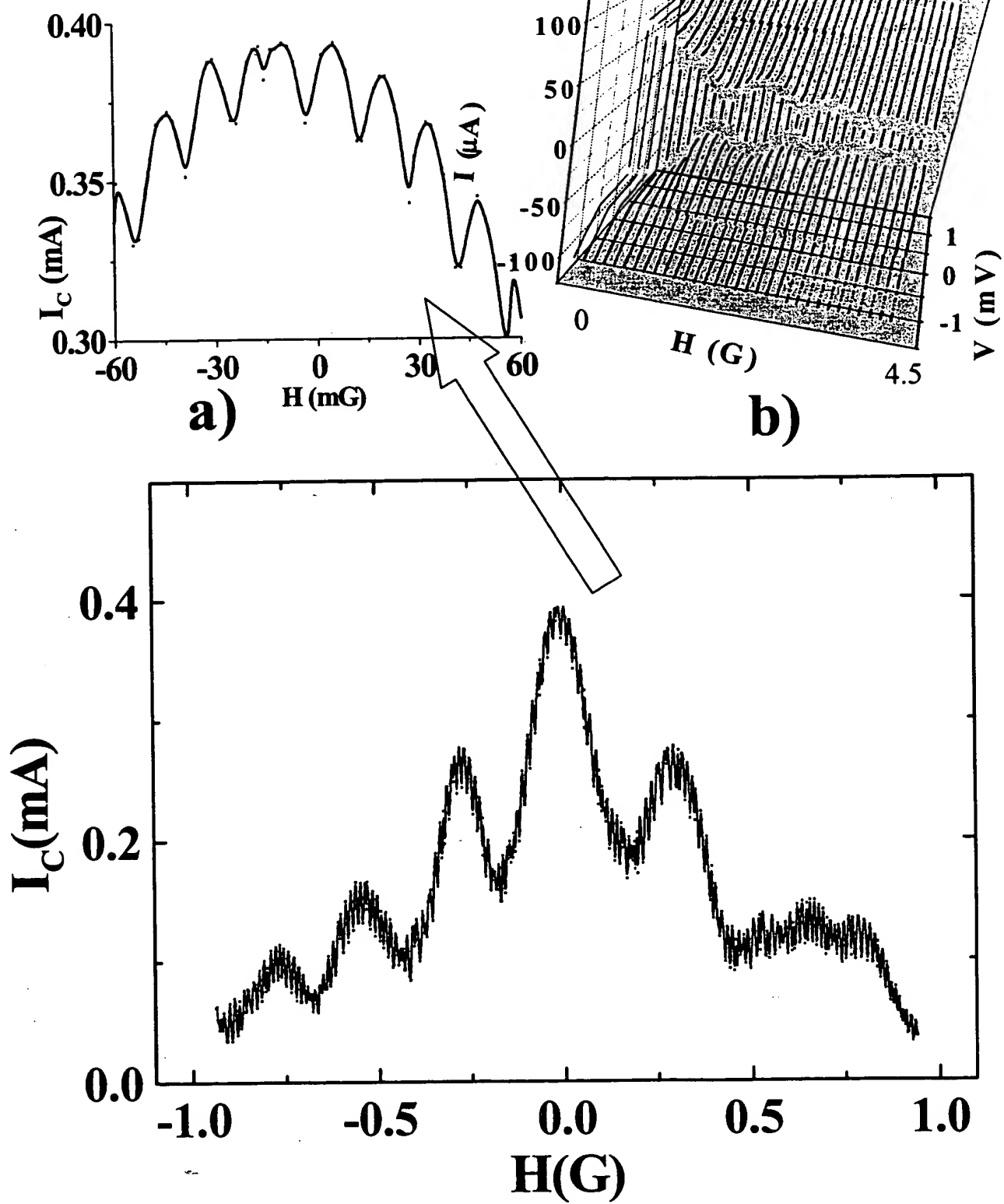


Fig. 5



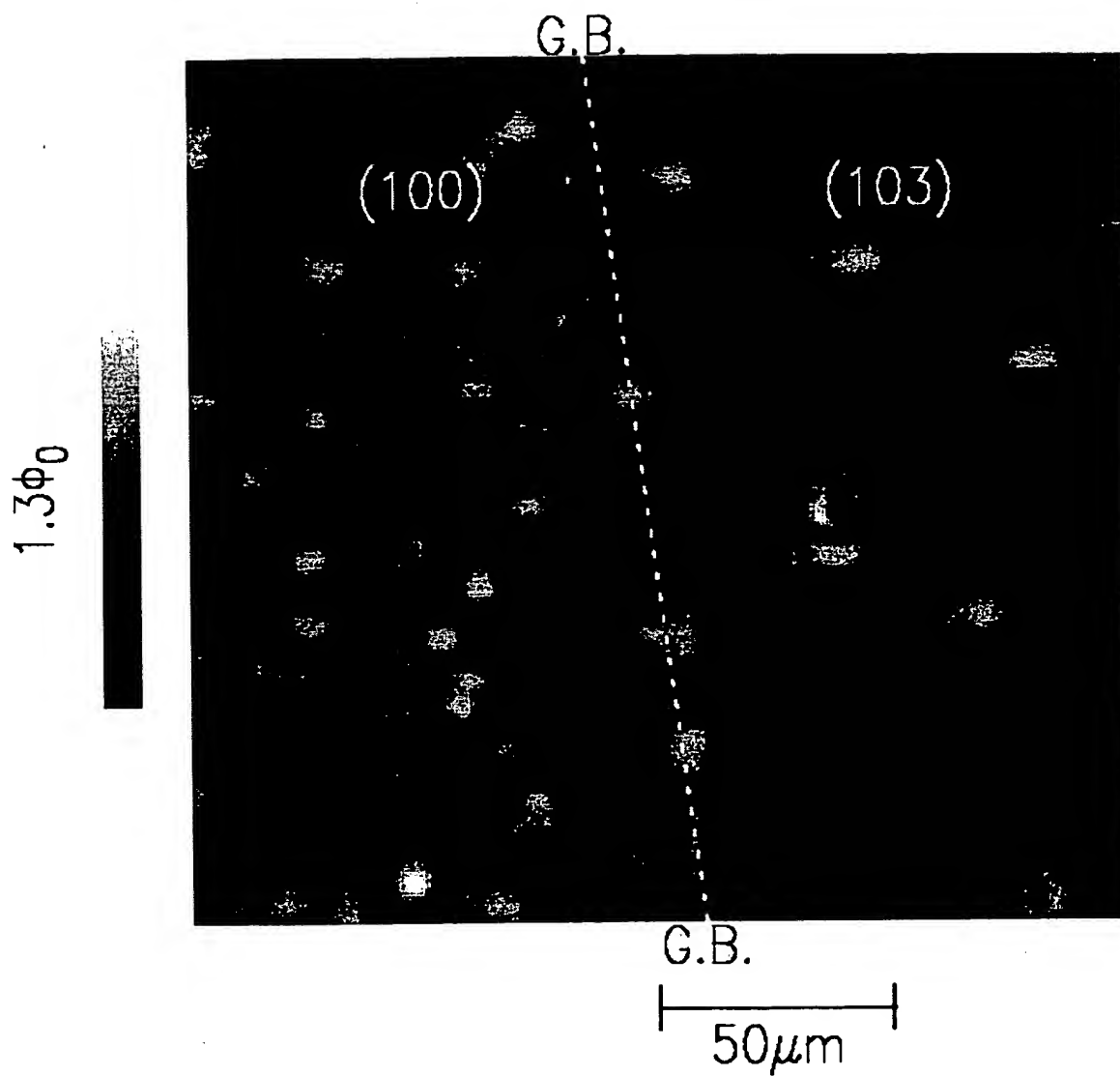


Fig. 6

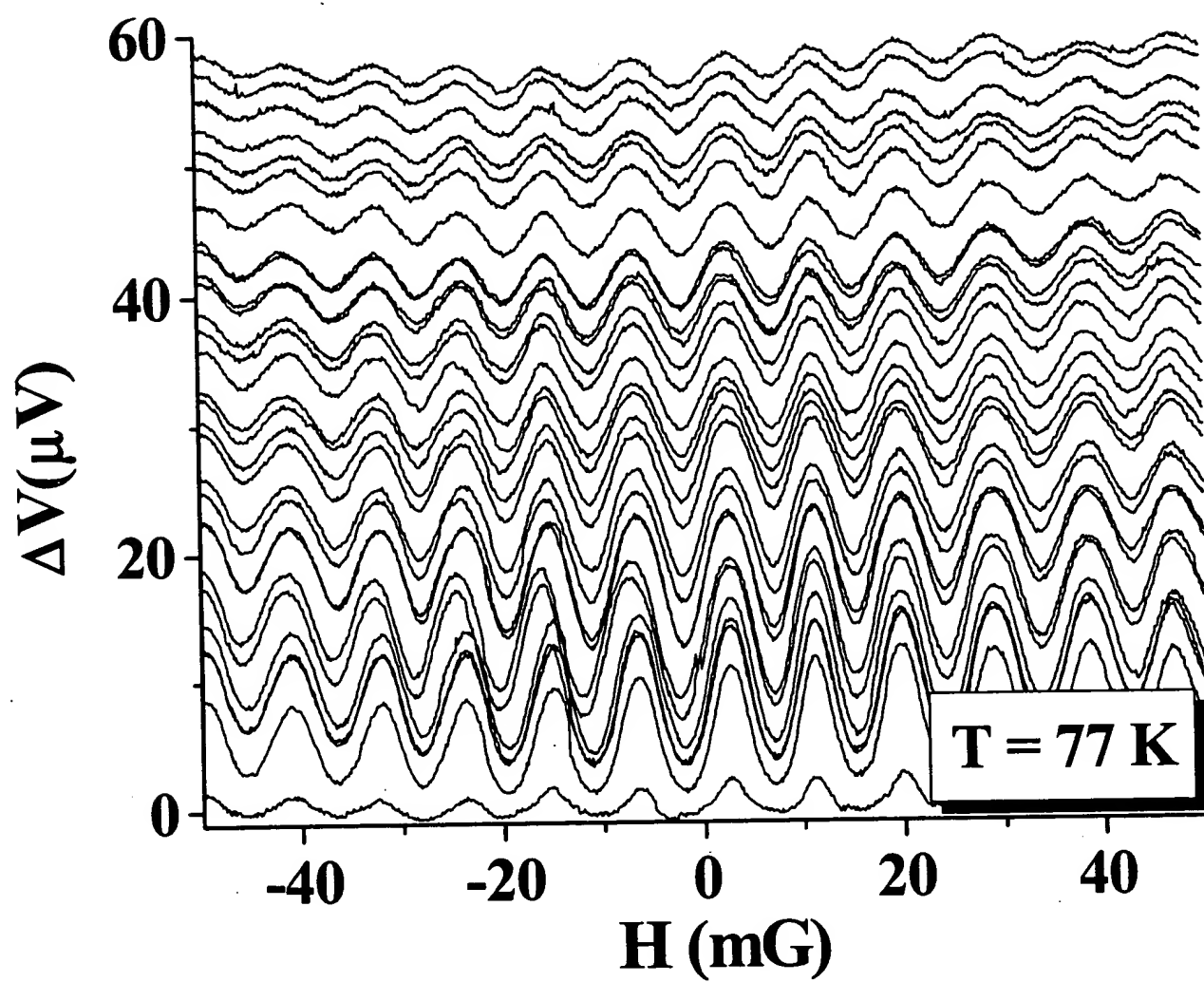
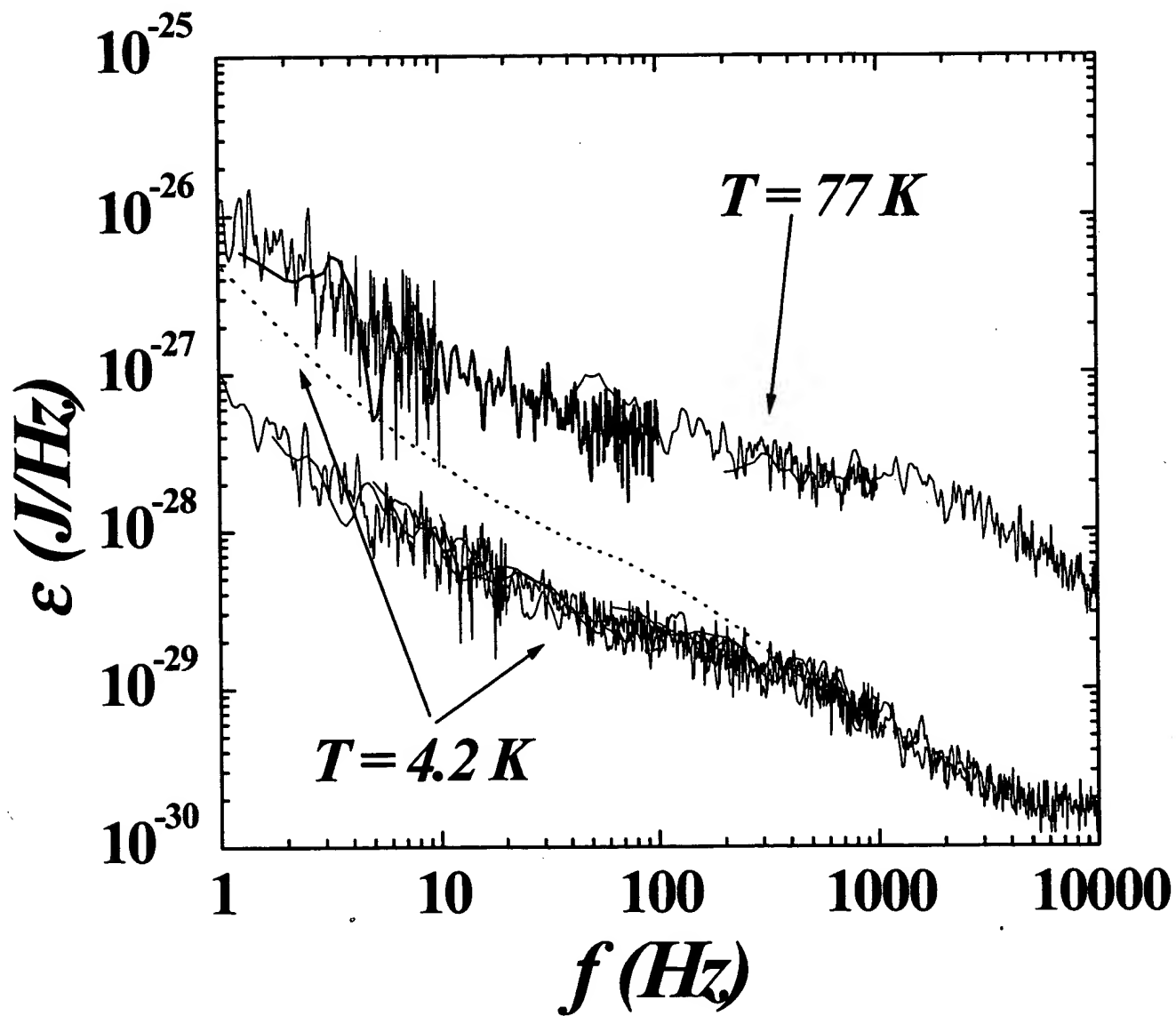


Fig. 7

Fig. 8



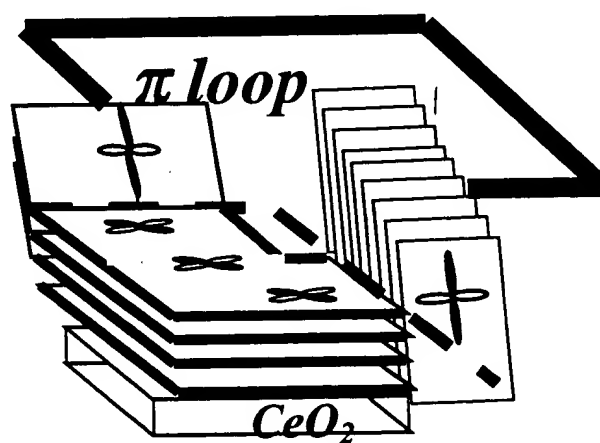
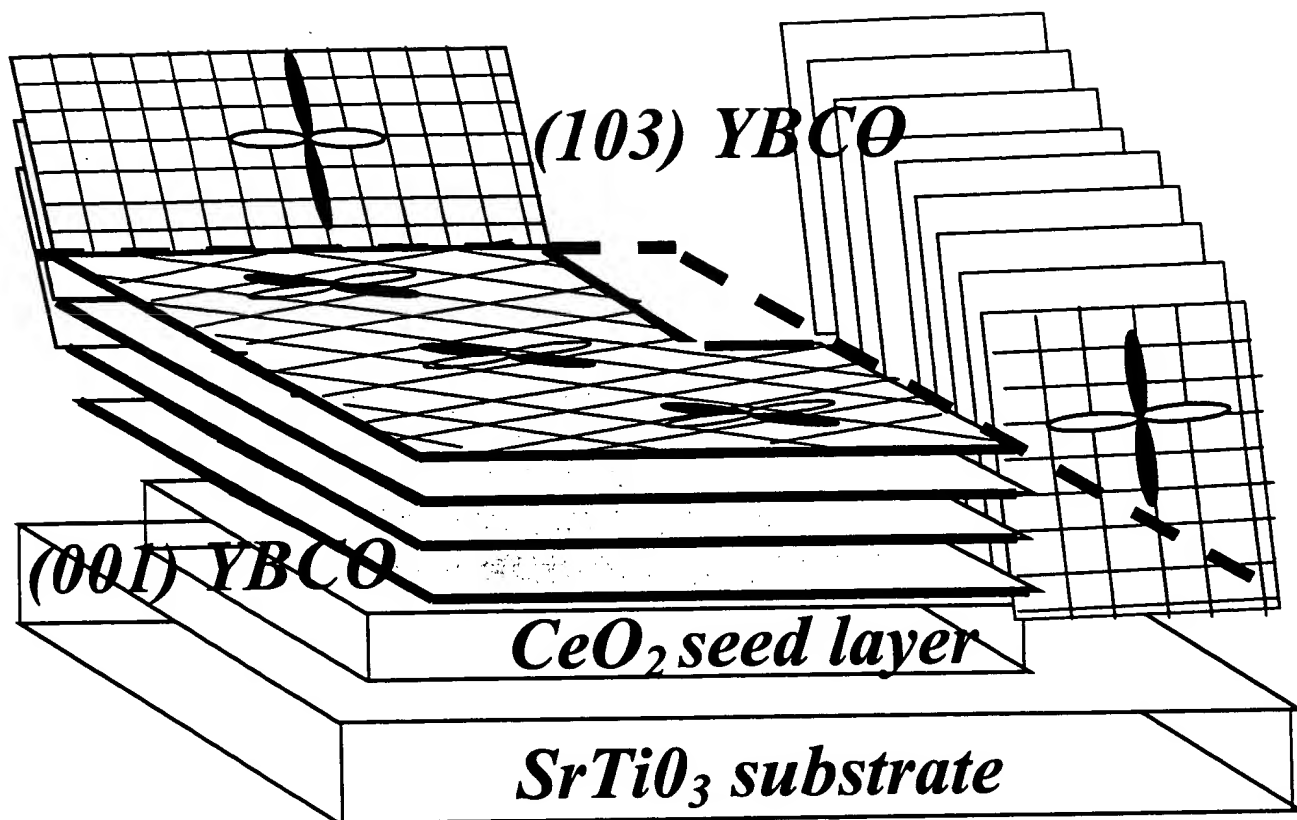


Fig. 9a

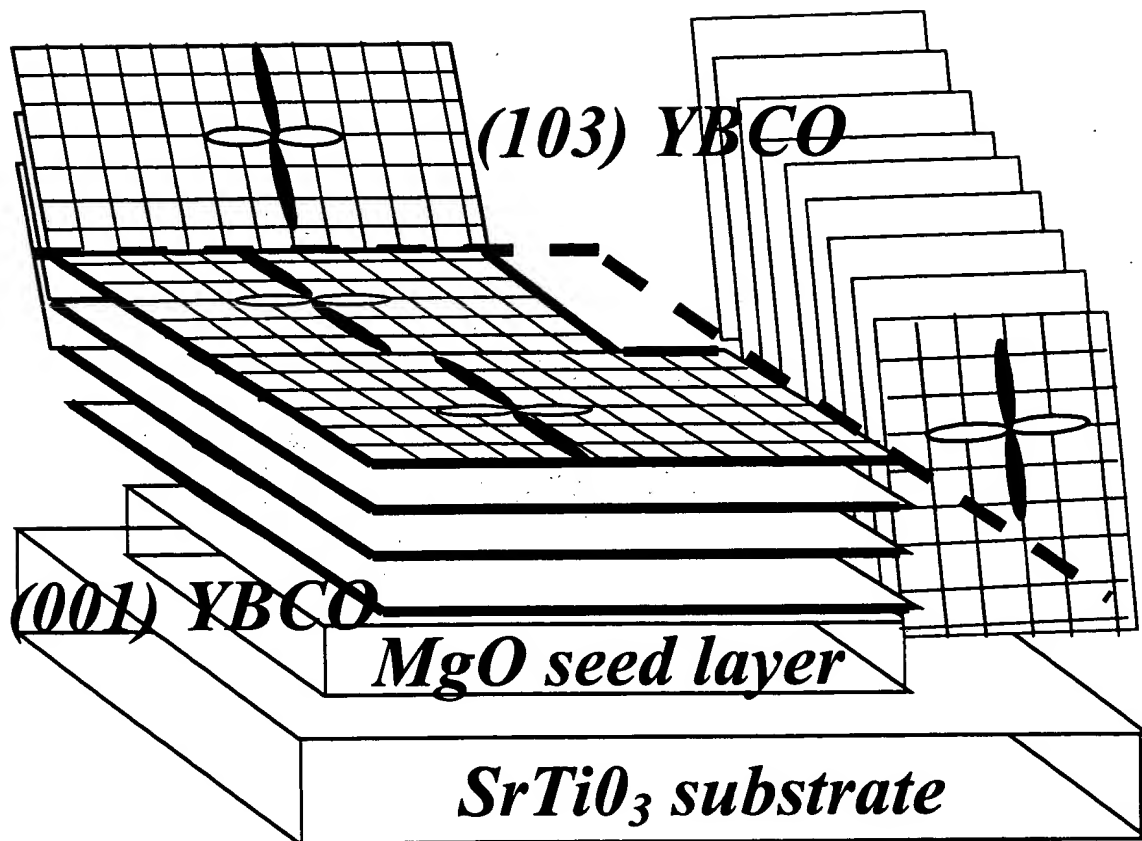
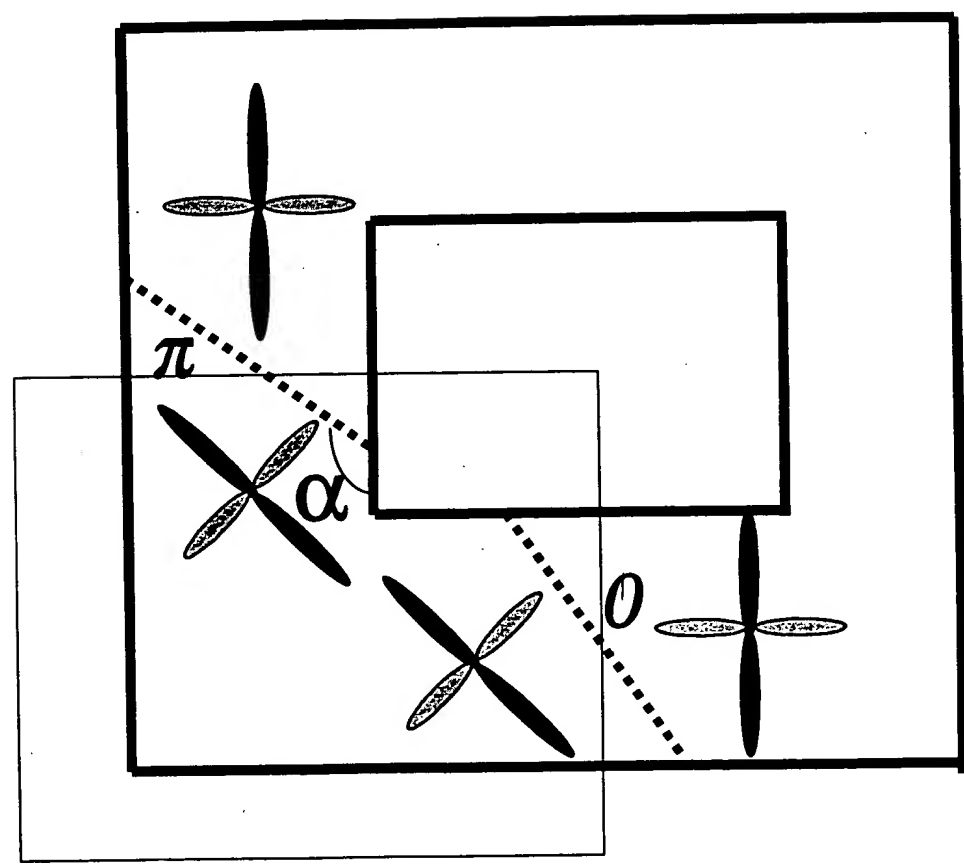
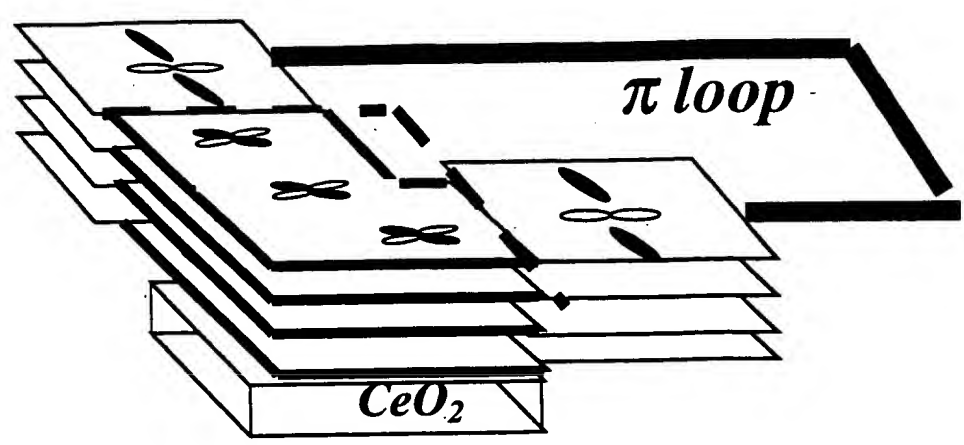
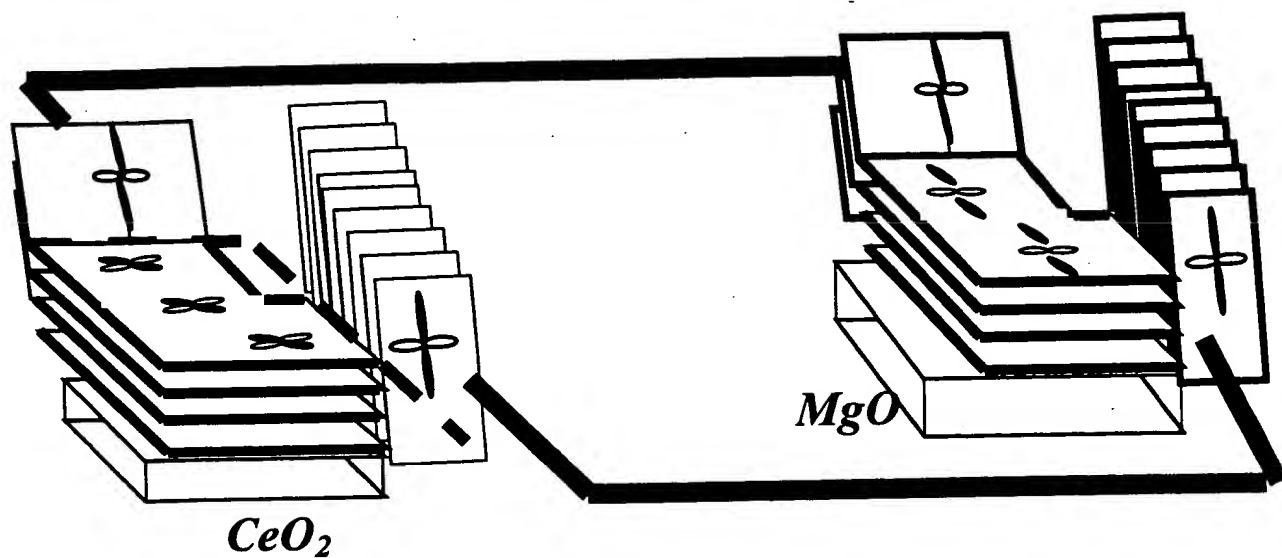


Fig. 9b

Fig. 9c



a)



b)

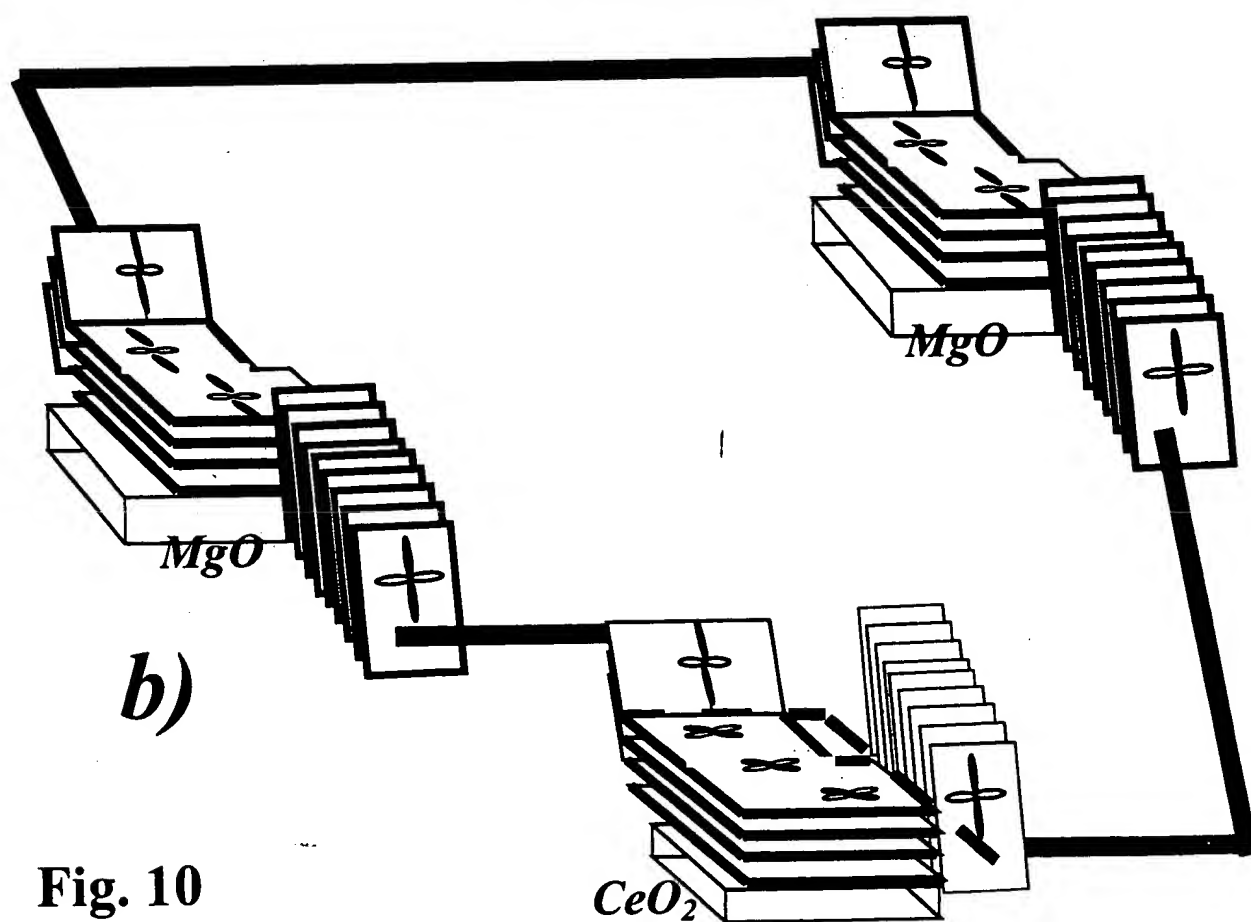


Fig. 10

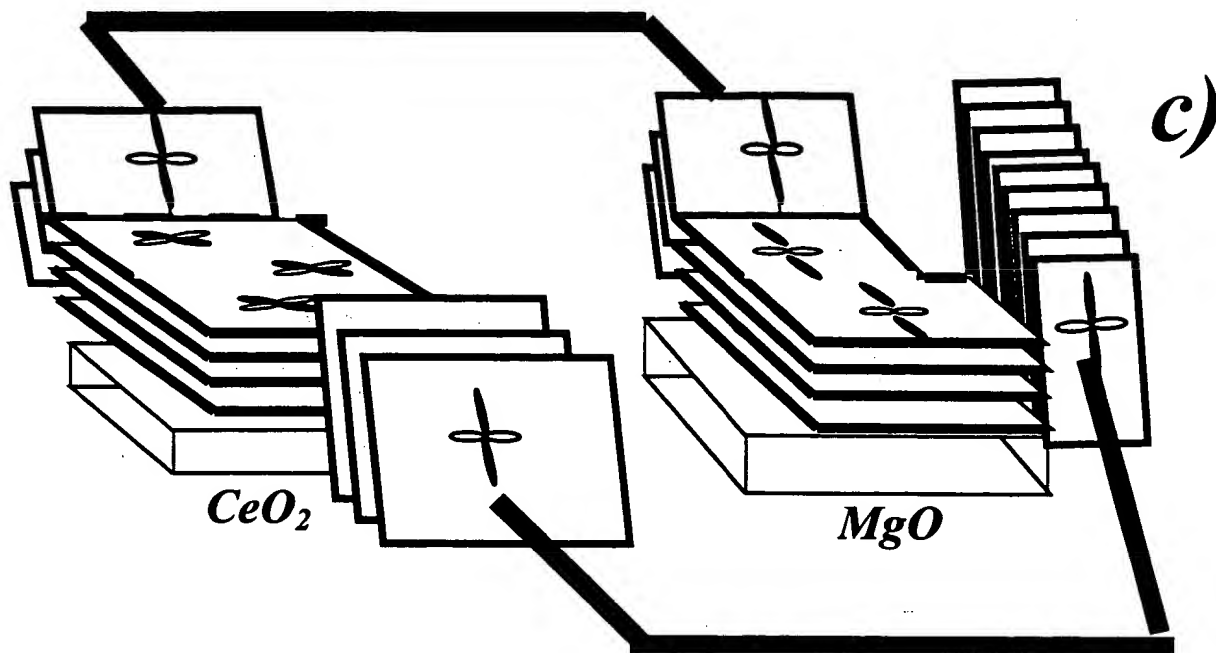


Fig. 10

Exhibit F

Il'ichev et al., 1991 cond-mat/9811017

Anomalous Periodicity of the Current-Phase Relationship of Grain-Boundary Josephson Junctions in High- T_c Superconductors

E. Il'ichev, V. Zakosarenko, R.P.J. IJsselsteijn, H. E. Hoenig, V. Schultze, H.-G. Meyer

Department of Cryoelectronics, Institute for Physical High Technology, P.O. Box 100239, D-07702 Jena, Germany

M. Grajcar and R. Hlubina

*Department of Solid State Physics, Comenius University, Mlynská Dolina F2, 842 15 Bratislava, Slovakia
(December 14, 2002)*

The current-phase relation (CPR) for asymmetric 45° Josephson junctions between two d -wave superconductors has been predicted to exhibit an anomalous periodicity. We have used the single-junction interferometer to investigate the CPR for this kind of junctions in $\text{YBa}_2\text{Cu}_3\text{O}_{7-x}$ thin films. Half-fluxon periodicity has been experimentally found, providing a novel source of evidence for the d -wave symmetry of the pairing state of the cuprates.

There is growing evidence in favor of the $d_{x^2-y^2}$ -wave symmetry of the pairing state of the high-temperature superconductors.¹ An unconventional pairing state requires the existence of zeros of the order parameter in certain directions in momentum space. Thermodynamic and spectroscopic measurements do indeed suggest their existence, but by themselves they do not exclude conventional s -wave pairing with nodes.¹ Direct evidence for the d -wave pairing state is provided by phase-sensitive experiments, which are based on the Josephson effect.² Quite generally, the current-phase relationship (CPR) of a Josephson junction, $I(\varphi)$, is an odd periodic function of φ with a period 2π .³ Therefore $I(\varphi)$ can be expanded in a Fourier series

$$I(\varphi) = I_1 \sin \varphi + I_2 \sin 2\varphi + \dots \quad (1)$$

In the tunnel limit we can restrict ourselves to the first two terms in Eq. (1). Since the order parameter is bound to the crystal lattice, $I(\varphi)$ of a weak link depends on the orientation of the d -wave electrodes with respect to their boundary. The existing phase-sensitive experiments exploit possible sign changes of I_1 between different geometries.² In this Letter we present a new phase-sensitive experimental test of the symmetry of the pairing state of the cuprates. Namely, in certain geometries, the I_1 term should vanish by symmetry. In such cases, the CPR should exhibit an anomalous periodicity.

Let us analyze the angular dependence of $I_{1,2}$ in a junction between two macroscopically tetragonal d -wave superconductors. As emphasized in Ref. 4, also heavily twinned orthorhombic materials such as $\text{YBa}_2\text{Cu}_3\text{O}_{7-x}$ belong to this class, if the twin boundaries have odd symmetry. We consider first an ideally flat interface between the superconducting electrodes. Let θ_1 (θ_2) denote the angle between the normal to the grain boundary and the a axis in the electrode 1 (2), see Fig. 1. If we keep only the lowest-order angular harmonics, the symmetry of the problem dictates that⁴

$$I_1 = I_c \cos 2\theta_1 \cos 2\theta_2 + I_s \sin 2\theta_1 \sin 2\theta_2. \quad (2)$$

The coefficients I_c, I_s are functions of the barrier strength, temperature T , etc. The I_2 term results from higher-order tunneling processes and we neglect its weak angular dependence. It is seen from Eq. (2) that the criterion for the observation of an anomalous CPR, $I_1 = 0$, is realized for an asymmetric 45° junction, i.e. a junction with $\theta_1 = 45^\circ$ and $\theta_2 = 0$. For an interface which is not ideally flat, $\theta_i = \theta_i(x)$ are functions of the coordinate x along the junction. $I_1 = 0$ remains valid even in this case, if the average values $\langle \theta_1(x) \rangle = 45^\circ$ and $\langle \theta_2(x) \rangle = 0$.

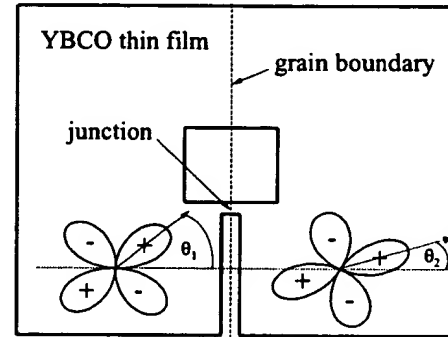


FIG. 1. Sketch of the interferometer (not in scale).

The I_2 term is present also in weak links based on conventional s -wave superconductors but for all known types of weak links $|I_2/I_1| < 1$. For instance, for a tunnel junction $|I_2/I_1| \ll 1$. For a SNS junction, $I \propto \sin \varphi/2$ at $T = 0$,⁵ and the Fourier expansion Eq. (1) leads to $I_2/I_1 = -2/5$. Therefore, a possible experimental observation of $|I_2/I_1| \gg 1$ in an asymmetric 45° junction provides direct evidence of d -wave symmetry of the pairing state in the cuprates.

We have investigated the CPR of $\text{YBa}_2\text{Cu}_3\text{O}_{7-x}$ thin film bicrystals with asymmetric 45° [001]-tilt grain boundaries⁶⁻⁸ as sketched in Fig. 1, using a single-junction interferometer configuration in which the

Josephson junction is inserted into a superconducting loop with a small inductance L . In a stationary state without fluctuations, the phase difference φ across the junction is controlled by applying external magnetic flux Φ_e penetrating the loop: $\varphi = \varphi_e - \beta f(\varphi)$. Here $\varphi_e = 2\pi\Phi_e/\Phi_0$ is the external flux normalized to the flux quantum $\Phi_0 = 2.07 \times 10^{-15} \text{ Tm}^2$. The CPR is written as $I(\varphi) = I_0 f(\varphi)$, where I_0 is the maximal Josephson current. $\beta = 2\pi L I_0 / \Phi_0$ is the normalized critical current. In order to obtain the CPR for the complete phase range $-\pi \leq \varphi \leq \pi$ the condition $\beta < 1$ has to be fulfilled, because for $\beta > 1$ the curve $\varphi(\varphi_e)$ becomes multivalued and there are jumps of φ and a hysteresis for a sweep of φ_e . Following Ref. 3, we express the effective inductance of the interferometer using the derivative f' with respect to φ as $L_{\text{int}} = L[1 + 1/f'(\varphi)]$. The inductance can be probed by coupling the interferometer to a tank circuit with inductance L_T , quality factor Q , and resonance frequency ω_0 .⁹ External flux in the interferometer is produced by a current $I_{dc} + I_{rf}$ in the tank coil and can be expressed as $\varphi_e = 2\pi(I_{dc} + I_{rf})M/\Phi_0 = \varphi_{dc} + \varphi_{rf}$, where $M^2 = k^2 L L_T$, and k is a coupling coefficient. Taking into account the quasiparticle current in the presence of voltage V across the junction the phase difference is given by the relation $\varphi = \varphi_{dc} + \varphi_{rf} - \beta f(\varphi) - 2\pi\tau(\varphi)V/\Phi_0$, where $\tau(\varphi) = L/R_J(\varphi)$ and $R_J(\varphi)$ is the resistance of the junction. In the small-signal limit $\varphi_{rf} \ll 1$ and in the adiabatic case $\omega\tau \ll 1$, keeping only the first-order terms, the effective inductance L_{eff} of the tank circuit-interferometer system reads

$$L_{\text{eff}} = L_T \left(1 - k^2 \frac{L}{L_{\text{int}}} \right) = L_T \left(1 - \frac{k^2 \beta f'(\varphi)}{1 + \beta f'(\varphi)} \right).$$

Thus the phase angle α between the driving current and the tank voltage U at the resonant frequency of the tank circuit ω_0 is

$$\tan \alpha(\varphi) = \frac{k^2 Q \beta f'(\varphi)}{1 + \beta f'(\varphi)}. \quad (3)$$

Using the relation $[1 + \beta f'(\varphi)]d\varphi = d\varphi_{dc}$ valid for $\varphi_{rf} \ll 1$ and $\omega\tau \ll 1$, one can find the CPR from Eq. (3) by numerical integration.

The advantage of the measurement of the CPR of an asymmetric 45° junction with respect to the by-now standard phase-sensitive tests of pairing symmetry based on the angular dependence of I_1 is twofold. First, it avoids the complications of the analysis of experiments caused by the presence of the term I_s .⁴ Second, a flux trapped in the SQUID does not invalidate the conclusions about the ratio $|I_2/I_1|$ and hence about the pairing symmetry, while this is not the case in standard phase-sensitive tests of the d -wave symmetry of the pairing state.¹⁰

The films of thickness 100 nm were fabricated using standard pulsed laser deposition on (001) oriented SrTiO_3 bicrystalline substrates with asymmetric $[001]$ tilt misorientation angles $45^\circ \pm 1^\circ$. They were subsequently patterned by Ar ion-beam etching into $4 \times 4 \text{ mm}^2$ square

washer single-junction interferometer structures (Fig. 1). The widths of the junctions were $1 \div 2 \text{ } \mu\text{m}$. The washer square holes had a side-length of $50 \text{ } \mu\text{m}$. This geometry of the interferometer gives $L \approx 80 \text{ pH}$. The resistance of the junction is higher than $1 \text{ } \Omega$ and the condition for the adiabatic limit $\omega\tau \ll 1$ is satisfied. For measurements of $\alpha(\varphi_{dc})$, several tank circuits with inductances $0.2 \div 0.8 \text{ } \mu\text{H}$ and resonance frequencies $16 \div 35 \text{ MHz}$ have been used. The unloaded quality factor of the tank circuits $70 < Q < 150$ has been measured at various temperatures. The coupling factor k was determined from the period ΔI_{dc} of $\alpha(I_{dc})$ using $M\Delta I_{dc} = \Phi_0$. Its value varied between 0.03 and 0.09. The amplitude of I_{rf} was set to produce the flux in the interferometer lower than $0.1\Phi_0$.

The measurements have been performed in a gas-flow cryostat with a five-layer magnetic shielding in the temperature range $4.2 \leq T < 90 \text{ K}$. The experimental setup was calibrated by measuring interferometers of the same size with 24° and 36° grain boundaries. We have studied 5 samples, out of which sample No. 1 exhibited the most anomalous behavior. Samples Nos. 2,3 were less anomalous and the remaining two samples had high critical currents and their $I(\varphi)$ was conventional. In Fig. 2 we plot the phase angle α as a function of the dc current I_{dc} for samples Nos. 1,2. The data for the 36° junction is shown for comparison. Note that at $T = 40 \text{ K}$ the periodicity of $\alpha(I_{dc})$ is the same for all samples.

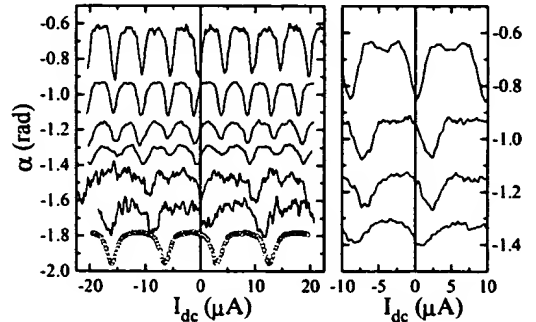


FIG. 2. Left panel: Phase angle between the driving current and the output voltage measured for the sample No. 1 at different temperatures as a function of the dc current I_{dc} . The curves are shifted along the y axis and the data for $T = 30$ and 40 K are multiplied by factor 4 for clarity. From top to bottom, the data correspond to $T = 4.2, 10, 15, 20, 30$ and 40 K . The data measured on 36° bicrystals ($\theta_1 \approx 36^\circ, \theta_2 \approx 0$) at $T = 40 \text{ K}$ in the same washer geometry are shown for comparison (open circles). Right panel: The same for the sample No. 2. From top to bottom, the data correspond to $T = 4.2, 10, 15$ and 20 K .

We assume that the period of $\alpha(I_{dc})$ at $T = 40 \text{ K}$, $\Delta I_{dc} = 9.6 \text{ } \mu\text{A}$, corresponds to $\Delta\varphi_{dc} = 2\pi$. In order to determine the CPR we take $\varphi_{dc} = 0$ at a maximum or minimum of α . This is necessary in order to satisfy

$I(\varphi = 0) = 0$, as required by general principles.³ The experimentally observed shift of the first local extreme of $\alpha(I_{dc})$ from $I_{dc} = 0$ (Fig. 2) can be due to flux trapped in the interferometer washer. Most probably, this flux resides in the long junction of the interferometer. The long junction does not play an active role because the Josephson penetration depth is much shorter than its length, and external fields producing I_{dc} are smaller than its critical field. Nevertheless the long junction sets the phase difference for $I_{dc} = 0$ at the small junction.

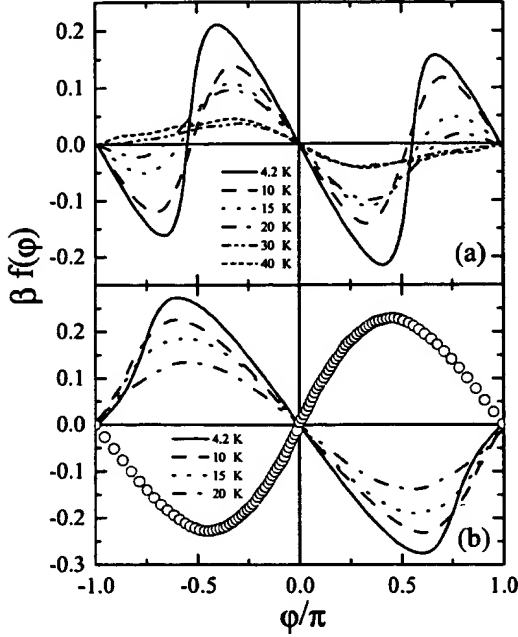


FIG. 3. a) Josephson current through the junction for the sample No. 1 as a function of the phase difference φ , determined from the data in Fig. 2. The statistics of $\alpha(\varphi)$ was improved by folding the data back to the interval $(0, \pi)$ and taking an average. The symmetry $\alpha(\varphi) = \alpha(-\varphi)$ was assumed. b) The same for the sample No. 2. The data for the asymmetric 36° bicrystal at $T = 40$ K (open circles) is also shown.

In Fig. 3, we show the CPR determined from the data in Fig. 2. For all curves we have performed a minimal necessary shift consistent with $I(\varphi = 0) = 0$. Thus, for the samples Nos. 1,2 we have assumed that at $\varphi_{dc} = 0$ a minimum of $\alpha(\varphi_{dc})$ is realized. For an interferometer with a conventional s -wave weak link (and also for the 36° junction), at $\varphi_{dc} = 0$ a maximum of $\alpha(\varphi_{dc})$ is realized. Note that the maximum (minimum) of $\alpha(\varphi_{dc})$ at $\varphi_{dc} = 0$ implies a diamagnetic (paramagnetic) response of the interferometer in the limit of small applied fields. In Fig. 4 we plot the coefficients I_1 and I_2 determined by Fourier analysis of the CPR for the sample No. 1 at various temperatures. With decreasing T , $|I_2|$ grows monotonically down to $T = 4.2$ K, while the I_1 component exhibits only a weak temperature dependence.

Our experimental results can be understood as follows. Deviations from ideal geometry of the asymmetric 45° junction, $\langle \theta_1 \rangle = 45^\circ + \alpha_1$ and $\langle \theta_2 \rangle = \alpha_2$, lead to a finite value of I_1 . Thus, imperfections of the junction increase its critical current. For this reason we believe that samples Nos. 2-5 contain imperfections and from now we concentrate on nearly ideal junctions (such as sample No. 1) with $|\alpha_1|, |\alpha_2| \ll 1$. For such junctions, the ratio I_2/I_1 exhibits the following temperature dependence. For $T \rightarrow 0$, $|I_2/I_1| \gg 1$. The region $T \sim T_c$ can be analyzed quite generally within Ginzburg-Landau theory. Let the electrodes be described by (macroscopic) order parameters $\Delta_{1,2} = |\Delta|e^{i\varphi_{1,2}}$. Then the phase-dependent part of the energy of the junction is $E = a[\Delta_1\Delta_2^* + \text{H.C.}] + b[(\Delta_1\Delta_2^*)^2 + \text{H.C.}] + \dots$ where a, b, \dots depend weakly on T .¹¹ Thus for T close to T_c we estimate $I_1 \propto |\Delta|^2 \propto (T_c - T)$ and $I_2 \propto |\Delta|^4 \propto (T_c - T)^2$, leading to $|I_2/I_1| \ll 1$. These expectations are qualitatively consistent with the experimental data shown in Fig. 4.

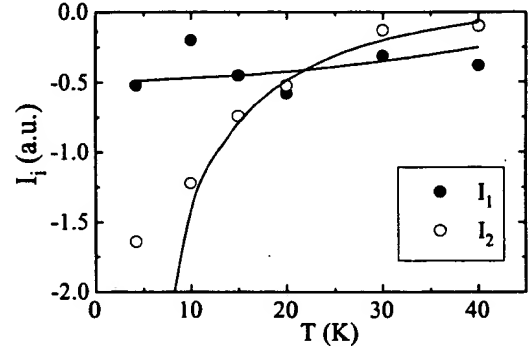


FIG. 4. Temperature dependence of the Fourier expansion coefficients $I_{1,2}$ determined from the experimental data in Fig. 3a. Solid lines are the Fourier expansion coefficients for the numerical data in Fig. 5.

So far, our discussion was based solely on symmetry arguments. Let us attempt a more quantitative analysis of our data now. Two different microscopic pictures of asymmetric 45° Josephson junctions between d -wave superconductors have been considered in the literature. The first picture assumes a microscopically tetragonal material and an ideally flat interface.¹¹⁻¹³ Within this picture, there are two contributions to the Josephson current. The first is due to bulk states and in the tunnel limit it is well described by the Sigrist-Rice term I_c in Eq. (2).¹⁴ The second is due to mid-gap states which develop close to the surfaces of unconventional superconductors.¹⁵ $I(\varphi)$ for the sample No. 1 calculated according to the model of Ref. 12 is shown in Fig. 5. The experimental data can be fitted by a relatively broad range of barrier heights. However, if we require the 36° junction to be fitted by the same (or smaller) barrier height as for the 45° junction, we conclude the barrier must be rather low.¹⁶ The T dependence of $I(\varphi)$ requires

a choice of $T_c \approx 60$ K in the non-selfconsistent theory of Ref. 12. The reduction from the bulk $T_c = 90$ K is probably due to a combined effect of surface degradation and order-parameter suppression at the sample surface. The temperature dependence of the ratio of the π and 2π periodic components in $I(\varphi)$ is seen to be in qualitative agreement with experimental data in Fig. 3a. This is explicitly demonstrated in Fig. 4 where we compare the experimentally obtained $I_{1,2}$ with the results of the Fourier analysis of the curves in Fig. 5. The divergence of I_2 as $T \rightarrow 0$ is an artifact of the ideal junction geometry assumed in Ref. 12. If the finite roughness of the interface is taken into account, this divergence is cut off and the experimental data in Fig. 4 do indeed resemble theoretical predictions for a rough interface.¹³ However, the nonselfconsistent theory of Ref. 12 is unable to explain the experimentally observed steep CPR close to the minima of the junction energy (see Fig. 3a). In the limit of vanishing barrier height, the theoretical CPR does have steep portions, but these are located close to the maxima of the junction energy (see also Ref. 11).

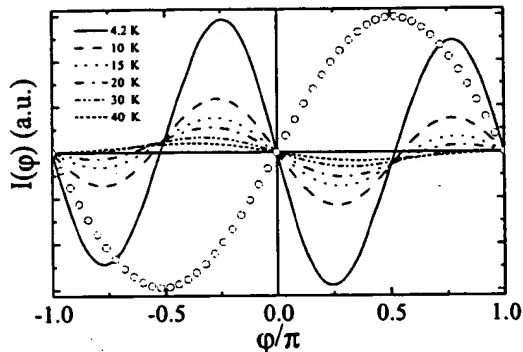


FIG. 5. $I(\varphi)$ calculated according to Eq. (64) of Ref. 12 for a junction with $\theta_1 = 45.5^\circ$, $\theta_2 = 0$, $\lambda d = 1.5$, $\kappa = 0.5$, and $T_c = 60$ K. $I(\varphi)$ at $T = 40$ K for the 36° bicrystal (open circles) was calculated for the same parameters except for $\theta_1 = 36^\circ$.

In a different approach to the asymmetric 45° junction, one assumes a heavily twinned orthorhombic material (which is macroscopically tetragonal, however) and/or a meandering interface with $\theta_i = \theta_i(x)$.^{17,18} Hence the critical current density $j_c(x)$ is a random function with a typical amplitude $\langle |j_c(x)| \rangle \sim j_c$. If the average critical current along the junction $\langle j_c \rangle \ll j_c$, a spontaneous flux is generated in the junction, and $|I_2/I_1| \gg 1$.^{17,18} In particular, for $\langle \theta_1 \rangle = 45^\circ$ and $\langle \theta_2 \rangle = 0$, there is an equal amount of parts having positive and negative j_c , leading to $\langle j_c \rangle = 0$ and $I_1 = 0$. Note that also within the picture of Refs. 17,18, the d -wave symmetry of the pairing state is crucial, otherwise the condition $\langle j_c \rangle \ll j_c$ is difficult to satisfy.

Our present understanding of $I(\varphi)$ in the asymmetric 45° junction is only qualitative. There is considerable experimental evidence⁶⁻⁸ that the grain boundary junctions are at most piecewise flat. However, we cannot say whether the shape of $I(\varphi)$ is dominated by the mid-gap states in the microscopically flat regions, or by spontaneous flux generation due to the spatial inhomogeneity of the junction. This issue requires further study.

In conclusion, we have measured the magnetic field response of a single-junction interferometer based on asymmetric 45° grain-boundary junctions in $\text{YBa}_2\text{Cu}_3\text{O}_{7-x}$ thin films. Half-fluxon periodicity has been experimentally found, in agreement with theoretical predictions for $d_{x^2-y^2}$ -wave superconductors. Hence, our results provide a novel source of evidence for the d -wave symmetry of the pairing state in the cuprates.

Financial support by the DFG (Ho 461/1-1) is gratefully acknowledged. M. G. and R. H. were supported by the Slovak Grant Agency Grant No. 1/4300/97 and the Comenius University Grant No. UK/3927/98.

- ¹ For a review, see J. Annett, N. Goldenfeld, and A. J. Leggett, in *Physical Properties of High Temperature Superconductors*, edited by D. M. Ginsberg (World Scientific, New Jersey, 1996), Vol. V.
- ² See C. C. Tsuei *et al.*, *Science* **271**, 329 (1996) and references therein.
- ³ A. Barone and G. Paterno, *Physics and Applications of the Josephson Effect*, (Wiley, New York, 1982).
- ⁴ M. B. Walker and J. Luettmmer-Strathmann, *Phys. Rev. B* **54**, 588 (1996).
- ⁵ I. O. Kulik and A. N. Omel'yanchuk, *Fiz. Nizk. Temp.* **4**, 296 (1978) [*Sov. J. Low Temp. Phys.* **4**, 142 (1978)].
- ⁶ J. R. Kirtley *et al.*, *Phys. Rev. B* **51**, 12 057 (1995).
- ⁷ H. Hilgenkamp, J. Mannhart, and B. Mayer, *Phys. Rev. B* **53**, 14586 (1996).
- ⁸ J. Mannhart *et al.*, *Phys. Rev. Lett.* **77**, 2782 (1996).
- ⁹ E. V. Il'ichev *et al.*, *J. Low Temp. Phys.* **106**, 503 (1997).
- ¹⁰ R. A. Klemm, *Phys. Rev. Lett.* **73**, 1871 (1994).
- ¹¹ A. Huck, A. van Otterlo, and M. Sigrist, *Phys. Rev. B* **56**, 14 163 (1997).
- ¹² Y. Tanaka and S. Kashiwaya, *Phys. Rev. B* **56**, 892 (1997).
- ¹³ Y. S. Barash, H. Burkhardt, and D. Rainer, *Phys. Rev. Lett.* **77**, 4070 (1996).
- ¹⁴ M. Sigrist and T. M. Rice, *J. Phys. Soc. Jpn.* **61**, 4293 (1992).
- ¹⁵ C. R. Hu, *Phys. Rev. Lett.* **72**, 1526 (1994).
- ¹⁶ This is consistent with the Fourier analysis of the data in Fig. 3 which finds non-negligible I_n also for $n \geq 3$.
- ¹⁷ A. J. Millis, *Phys. Rev. B* **49**, 15 408 (1994).
- ¹⁸ R. G. Mints, *Phys. Rev. B* **57**, R322 (1998).

Exhibit G

Char et al., 1991, Applied Physics Letters 59, p. 733

Bi-epitaxial grain boundary junctions in $\text{YBa}_2\text{Cu}_3\text{O}_7$

K. Char, M. S. Colclough, S. M. Garrison, N. Newman, and G. Zaharchuk
Conductus, Inc., Sunnyvale, California 94086

(Received 26 March 1991; accepted for publication 13 May 1991)

We have developed a new way of making grain boundary junctions in $\text{YBa}_2\text{Cu}_3\text{O}_7$ thin films by controlling the in-plane epitaxy of the deposited film using seed and buffer layers. We produce 45° grain boundaries along photolithographically defined lines. The typical value of the critical current density of the junctions is 10^3 – 10^4 A/cm² at 4.2 K and 10^2 – 10^3 A/cm² at 77 K, while the rest of the film has a critical current density of 1 – 3×10^6 A/cm² at 77 K. The current-voltage characteristics of the junctions show resistively shunted junction behavior and we have used them to fabricate dc superconducting quantum interference devices (SQUIDs) which show modulation at temperatures well above 77 K. This is the first planar high T_c Josephson junction technology that appears readily extendable to high T_c integrated circuits.

Most microelectronic applications of the high T_c superconductors will rely upon microbridges such as superconductor-normal metal-superconductor (S-N-S) junctions or other weak link geometries instead of superconductor-insulator-superconductor (S-I-S) tunnel junctions. A number of weak-link structures provide reliable critical current reduction in $\text{YBa}_2\text{Cu}_3\text{O}_7$ (YBCO) thin films; grain boundary junctions,^{1–3} traditional edge junctions,⁴ microbridges grown across a sharp substrate step,⁵ and S-N-S-type junctions with Au,⁶ $\text{PrBa}_2\text{Cu}_3\text{O}_7$,^{7,8} or $\text{SrTi}_{1-x}\text{Nb}_x\text{O}_3$ (Ref. 9) normal layers. Of these various weak-link geometries, grain boundary junctions work well at temperatures close to T_c , have reasonably high $I_c R_n$ products, and show behavior explained by a resistively shunted junction model with a relatively uniform current density. To date, the high angle grain boundary junctions that have been used were formed either by fusing differently oriented SrTiO_3 substrates¹ or by patterning the randomly occurring grain boundaries in granular films.^{2,3} Superconducting quantum interference devices (SQUIDs) made from the grain boundaries on SrTiO_3 bicrystals had reasonable signal and low noise¹⁰ up to temperatures very close to the T_c of the film. However, this SrTiO_3 bicrystal technique has a major drawback: it cannot be readily extended to integrated circuits. On the other hand, SQUIDs made from granular films are plagued by low yield and the presence of grain boundaries in the SQUID loop itself. These lead to excessive flux noise and hysteresis in the voltage-flux response of the SQUID.

In this letter, we report for the first time the successful fabrication of high T_c weak-link Josephson junctions operating at and above 77 K that are made from grain boundary junctions whose locations are determined by conventional photolithography. This result demonstrates the feasibility of an extendable technology for fabricating high T_c Josephson devices which avoids the problems associated with the devices made from granular thin films and on bicrystal substrates. We reproducibly fabricate 45° grain boundaries in YBCO films by controlling their in-plane epitaxy using seed and buffer layers deposited on r -plane sapphire substrates, a method we call "bi-epitaxy." The method is quite general, and can be used on a wide variety of substrates.

Recently, we reported¹¹ the existence of two in-plane epitaxial orientations of c -axis oriented epitaxial YBCO thin films on yttria-stabilized zirconia (YSZ), resulting from the poor lattice match between YBCO and YSZ. This observation led us to realize that it would be possible to make bi-epitaxial grain boundaries on such a substrate using seed and buffer layers, or, in an alternative geometry, on a well lattice-matched substrate using poorly lattice-matched seed layers. For example, we previously reported¹² the growth of YBCO thin films on r -plane sapphire using buffer layers such as SrTiO_3 , CaTiO_3 , YSZ, and MgO . We emphasized the importance of the in-plane epitaxy of YBCO, particularly because high-angle grain boundaries in YBCO films behave as weak links, leading to low critical current densities and high surface resistances.^{12,13} Our efforts towards minimizing the occurrence of these high-angle grain boundaries taught us how to control them and led us to design and demonstrate a variety of 45° weak-link junctions. One example takes advantage of the differing epitaxial directions of two different layers, MgO and SrTiO_3 , when they are deposited on an r -plane sapphire substrate. Using these two layers as a seed and a buffer layer, we have succeeded in fabricating bi-epitaxial 45° grain boundaries in YBCO on sapphire substrates by the following process.

Schematic views of our device structure are shown in Fig. 1. We first deposit 3–30 nm of epitaxial MgO as a seed layer on an r -plane sapphire substrate. MgO is produced by laser ablating a Mg metallic target in a 2–20 mTorr oxygen atmosphere with a substrate temperature of 300–700 °C. We then mask the MgO with conventional photoresist and remove it from, for example, half of the substrate by either Ar ion beam milling or chemical wet etching with dilute phosphoric acid. We then grow 10–100 nm of epitaxial SrTiO_3 buffer layer by laser ablation on both the exposed sapphire surface and on the patterned MgO seed layer. The deposition conditions are an oxygen pressure of 100–200 mTorr and a substrate temperature of 710–760 °C. The SrTiO_3 film grows in two different orientations separated by a 45° grain boundary. In the growth plane the epitaxial relations are $\text{SrTiO}_3[110]//\text{Al}_2\text{O}_3[11\bar{2}0]$ and $\text{SrTiO}_3[100]//\text{MgO}[100]//\text{Al}_2\text{O}_3[11\bar{2}0]$, as illustrated in

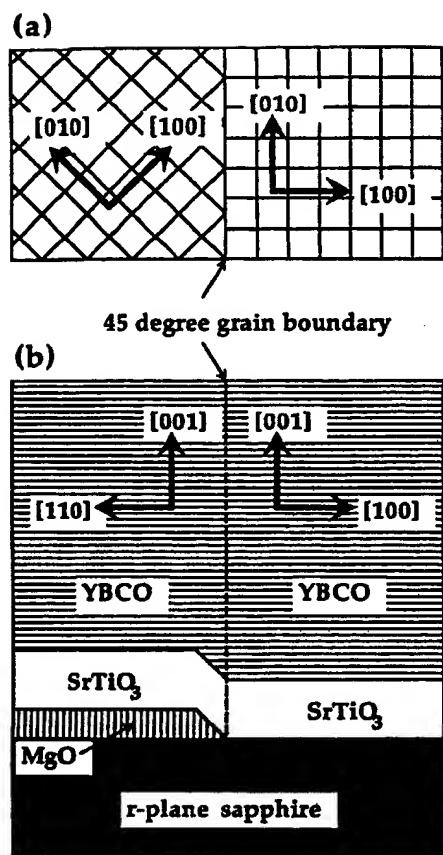


FIG. 1. Schematic view of the device structure with an MgO seed layer and a SrTiO₃ buffer layer on an *r*-plane sapphire substrate. (a) top view, (b) side view.

Fig. 1. We then immediately deposit YBCO, which grows epitaxially everywhere and thereby reproduces the grain boundary in the SrTiO₃ buffer layer. Finally the YBCO is patterned into an appropriate geometry.

The virtue of this structure is that, apart from the predefined 45° grain boundaries, there are no other high-angle grain boundaries in the YBCO film. It has been reported¹² that YBCO films grown on SrTiO₃ buffer layers on *r*-plane sapphire substrates have high critical current density and low surface resistance. In addition, the SrTiO₃ layer grown on the MgO buffer layer does not have any high-angle grain boundaries, as demonstrated in a ϕ scan of the SrTiO₃ (101), although it is found¹³ that YBCO deposited on MgO may have a number of high-angle grain boundaries. The probable explanation for this effect is that the energy needed to nucleate 45° misoriented SrTiO₃ grains on MgO is much higher than in the case of YBCO grown on MgO. Hence the YBCO film on SrTiO₃ on MgO also lacks any high-angle grain boundaries and has a high critical current density. Microbridges formed either side of the predetermined grain boundary have critical current densities of $1\text{--}3 \times 10^6 \text{ A/cm}^2$ at 77 K. In order to show that the critical current reduction is indeed due to the grain boundary rather than simply the step at the edge, we etched only part of the MgO, reducing its thickness on one side from 20 to 10 nm, such that YBCO/SrTiO₃/MgO

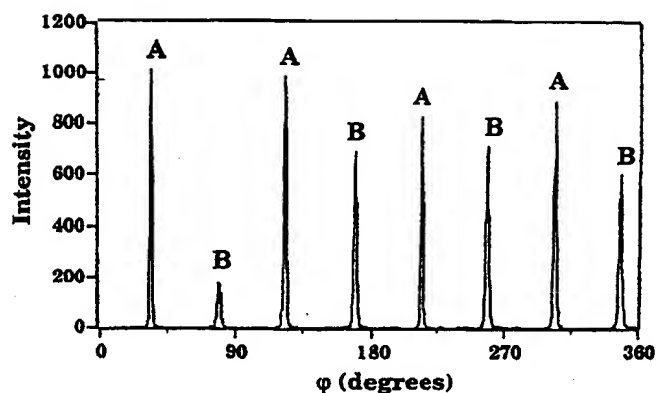


FIG. 2. X-ray ϕ scan of YBCO (103) of the unpatterned structure. The peaks labeled with "A" belong to YBCO/SrTiO₃/Al₂O₃ and the peaks labeled with "B" come from YBCO/SrTiO₃/MgO/Al₂O₃.

remained on the sapphire substrate on both sides of the step. The critical density across this step remained larger than 10^6 A/cm^2 at 77 K.

A ϕ scan of the YBCO (103) before the last patterning process is shown in Fig. 2. The peaks occurring 45° apart indicate that half of the YBCO is rotated 45° relative to the other half. Suitable etching experiments have shown that the peaks labeled with "A" belong to YBCO/SrTiO₃/Al₂O₃ and the peaks labeled with "B" come from YBCO/SrTiO₃/MgO/Al₂O₃. Cross-sectional transmission electron microscope images and microdiffraction patterns show that the 45° grain boundary begins at the end of the MgO seed layer.¹⁴

As the first example of a device using multiple junctions made with our process we fabricated a square washer SQUID¹⁵ as shown in the inset of Fig. 3. It was patterned across the grain boundary by photolithography and wet etched with dilute phosphoric acid. The current-voltage characteristic (*I-V*) of the SQUID at 4.2 K, which ex-

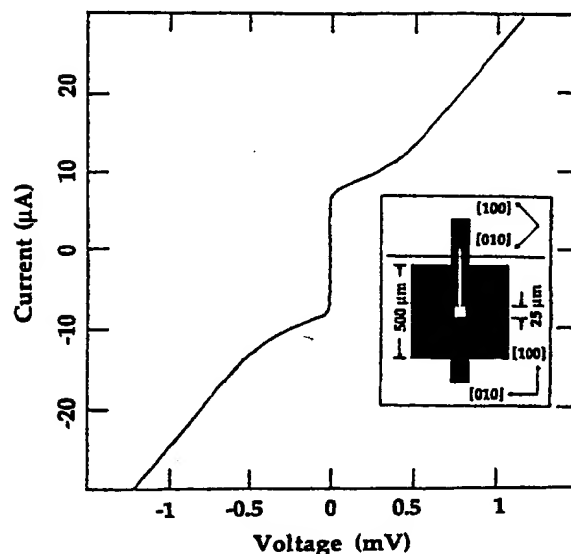


FIG. 3. Current (vertical)-voltage (horizontal) characteristics of a dc SQUID at 4.2 K. The inset shows the geometry of the SQUID.

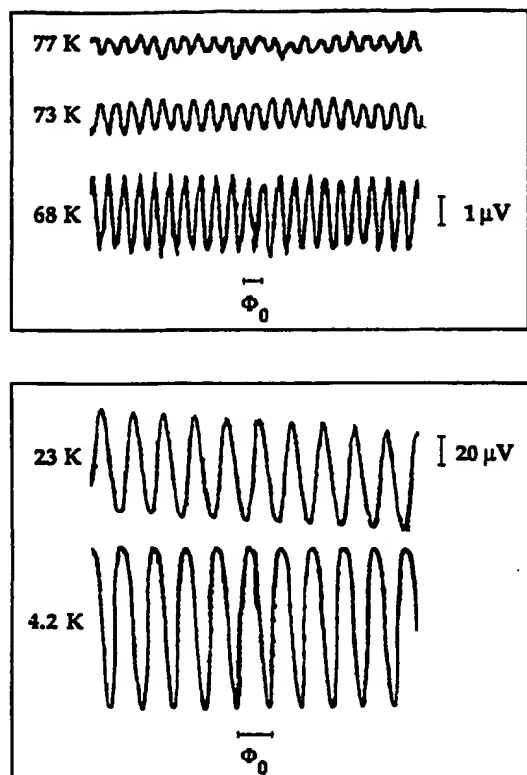


FIG. 4. Modulation voltage of the current-biased dc SQUID vs applied magnetic flux at various temperatures.

hibits resistively shunted Josephson junction behavior, is shown in Fig. 3. Each junction was $4\text{ }\mu\text{m}$ wide and $0.2\text{ }\mu\text{m}$ thick. The critical current of about $10\text{ }\mu\text{A}$ at 4.2 K translates to about 10^3 A/cm^2 critical current density across the junctions. The $I_c R_n$ product of the junctions is about $420\text{ }\mu\text{V}$ at 4.2 K . The I - V of the SQUID at 77 K shows no zero resistance part, although it is nonlinear. The small junction coupling energy $I_c \Phi_0 / 2\pi$ compared to the thermal energy $k_B T$ may lead to thermally activated phase slippage across the junctions, resulting in resistance at all currents.¹⁶ Detailed transport properties of the junctions including the magnetic field dependence of the critical current will be reported elsewhere.¹⁷

The voltage across the current-biased dc SQUID as a function of applied field is shown for various temperatures in Fig. 4. The data were taken in a bandwidth of 0 – 10 Hz without any signal averaging. The observed period corresponds to the expected value from the geometry of the SQUID. We believe that the reduction of the modulation voltage at high temperatures is due to the decreasing critical current and the large inductance of the SQUID. We have observed dc SQUID operation at temperatures as high as 88 K and have operated such a SQUID in a flux-locked loop up to 83 K . The noise of this SQUID is similar to that reported in dc SQUIDs made using bicrystal substrates.¹⁰ Detailed performance of the SQUID will be published elsewhere.¹⁸

A further example of small-scale integration using biepitaxial grain boundary junctions is provided by a flux

shuttle¹⁹ we have fabricated. It involves two dc SQUIDs as sensors and eleven more bi-epitaxial junctions as switching elements. Our work on such integrated circuits is continuing and will be reported later.

In summary, we have reported the development of biepitaxial grain boundary junctions in $\text{YBa}_2\text{Cu}_3\text{O}_7$ at multiple and predetermined locations by using only standard photolithographic techniques to control in-plane epitaxy with seed and buffer layers. The junctions have current-voltage characteristics that are well described by the resistively shunted junction model and dc SQUIDs fabricated using these junctions show modulation at temperatures as high as 88 K . By increasing the critical current density of the junctions and lowering the inductance of the SQUID, the performance of the SQUIDs should improve further, especially at 77 K . We believe that this technology, based on biepitaxial grain boundaries, can be extended to integrated circuits in the near future, and we are planning to demonstrate such circuits.

We would like to thank John Rowell, Mac Beasley, Ted Geballe, Bob Hammond, John Clarke, Aharon Kapitulnik, Randy Simon, and Roger Barton for helpful discussions on this work. We also would like to thank Jeff Rosner at Hewlett-Packard for the TEM studies.

¹D. Dimos, P. Chaudhari, J. Mannhart, and F. K. LeGoues, *Phys. Rev. Lett.* **60**, 1653 (1988).

²R. H. Koch, W. J. Gallagher, B. Bumble, and W. Y. Lee, *Appl. Phys. Lett.* **54**, 951 (1989).

³S. E. Russek, D. K. Lathrop, B. H. Moeckly, R. A. Buhrman, D. H. Shin, and J. Silcox, *Appl. Phys. Lett.* **57**, 1155 (1990).

⁴R. B. Laibowitz, R. H. Koch, A. Gupta, G. Koren, W. J. Gallagher, V. Foglietti, B. Oh, and J. M. Viggiano, *Appl. Phys. Lett.* **56**, 686 (1990).

⁵K. P. Daly, W. D. Dozier, J. F. Burch, S. B. Coons, R. Hu, C. E. Platt, and R. W. Simon, *Appl. Phys. Lett.* **58**, 543 (1991).

⁶D. B. Schwartz, P. M. Mankiewicz, R. E. Howard, L. D. Jackel, B. L. Straughn, E. G. Burkhardt, and A. H. Dayem, *IEEE Trans. Magn.* **25**, 1298 (1989).

⁷C. T. Rogers, M. S. Hedge, B. Dutta, X. D. Wu, and T. Venkatesan, *Appl. Phys. Lett.* **55**, 2032 (1989).

⁸J. Gao, W. A. M. Aarnink, G. J. Gerritsma, G. Veldhuis, and H. Rogalla, *IEEE Trans. Magn.* **27**, 3062 (1991).

⁹D. K. Chin and T. Van Duzer, *Appl. Phys. Lett.* **58**, 753 (1991).

¹⁰R. Gross, P. Chaudhari, M. Kawasaki, M. B. Ketchen, and A. Gupta, *Appl. Phys. Lett.* **57**, 727 (1990); *Physica C* **170**, 315 (1990).

¹¹S. M. Garrison, N. Newman, B. F. Cole, K. Char, and R. W. Barton, *Appl. Phys. Lett.* **58**, 2168 (1991).

¹²K. Char, N. Newman, S. M. Garrison, R. W. Barton, R. C. Taber, S. S. Laderman, and R. D. Jacowitz, *Appl. Phys. Lett.* **57**, 409 (1990); K. Char, N. Newman, S. M. Garrison, R. W. Barton, G. Zaharchuk, S. S. Laderman, R. C. Taber, and R. D. Jacowitz, presented at Applied Superconductivity Conference, Aspen, Colorado (1990).

¹³S. S. Laderman, R. C. Taber, R. D. Jacowitz, J. L. Moll, C. B. Eom, T. L. Hylton, A. F. Marshall, T. H. Geballe, and M. R. Beasley, *Phys. Rev. B* **43**, 2922 (1991).

¹⁴S. J. Rosner (private communication).

¹⁵M. B. Ketchen and J. M. Jaycox, *Appl. Phys. Lett.* **40**, 736 (1982).

¹⁶R. Gross, P. Chaudhari, D. Dimos, A. Gupta, and G. Koren, *Phys. Rev. Lett.* **64**, 228 (1990).

¹⁷P. Rosenthal, A. Barrera, M. R. Beasley, K. Char, M. S. Colclough, and G. Zaharchuk (unpublished).

¹⁸M. S. Colclough, K. Char, G. Zaharchuk, A. H. Miklich, and J. Clarke (unpublished).

¹⁹T. A. Fulton, R. C. Dynes, and P. W. Anderson, *Proc. IEEE* **61**, 28 (1973).

Exhibit H

**Declaration of Dr. Alexander Tzalenchuk under 37 C.F.R. § 1.132 submitted in response to
the February 19, 2003 Office Action on April 18, 2003**

IN THE UNITED STATES PATENT AND TRADEMARK OFFICE

In re application of:)	Art Unit: 2814
Zagoskin)	
)	Examiner:
)	Douglas A. Wille
Serial No. 09/452,749)	
Filed: December 1, 1999)	Attorney Docket:
)	11090-003-999
)	
For: Permanent Readout Superconducting Qubit)	
)	

DECLARATION OF DR. ALEXANDER TZALENCHUK UNDER 37 C.F.R. § 1.132

Assistant Commissioner for Patents
Washington, D.C. 20231

Sir:

I, ALEXANDER TZALENCHUK, declare and state as follows:

1. I am a citizen of Russia currently residing at 244 Ashburnham Road, Ham / Richmond, Surrey, United Kingdom TW10 7SA.
2. I am familiar with the specification and claims of the above-identified patent application ("Application"), the Office Action mailed February 19, 2003, United States Patent 5,157,466 to Char *et al.* (hereinafter "Char *et al.*") and Tinkham, *Introduction to Superconductivity*, Second Edition, (hereinafter "Tinkham").
3. I am an employee of the National Physics Laboratory of the United Kingdom of Great Britain and Northern Ireland and its affiliate NPL Management Limited (herein after "NPL"). NPL is located in Teddington, Middlesex, UK, TW11 0LW, where I am employed by it as a Senior Research Scientist in its Fundamental and Wavelength Standards Team. NPL has entered into a collaborative research agreement with D-Wave Systems Inc.

(hereinafter "D-Wave"), the assignee herein, dated March 27, 2002, whereby NPL carries out certain research and measurement work for D-Wave. One product of this research and measurement work is the creation of certain intellectual property, including patent applications, all rights, title and interest to which are held by D-Wave pursuant to the terms and conditions of the aforementioned collaborative research agreement.

4. I received a B.A. in Electronics Engineering from the Chair of Crystal Physics, Faculty of Electronic Materials and Devices, Moscow Steel and Alloys Institute and a Ph.D. in Physics and Mathematics from the A.V. Shubnikov Institute of Crystallography Russian Academy of Sciences, and have been actively performing research in the field of solid state and superconducting fabrication and characterization for the past nineteen years. During that time, I have published in excess of 35 articles in the fields of solid state physics, superconducting structure fabrication, and characterization of superconducting structures and have six allowed or issued patents. My research experience encompasses work in semiconductor structures formed on bi-crystal substrates, bi-crystal substrates for high-T_c superconductors, mesoscopic effects in high-T_c superconductors, Josephson phenomena in high-T_c bi-crystals and bi-epitaxial grain boundary Josephson junctions, and Josephson phenomena in high-T_c step edge Josephson junctions, and qubits using high-T_c Josephson junctions. I am a specialist in the fabrication of microstructures in high-T_c superconducting devices, these include three terminal devices, SQUIDs, and qubits. I have additional expertise in the characterization of superconducting devices including instrumentation for scanning SQUID/Hall microscopy, and investigation of local magnetization and superconductivity. I have received an individual George Soros Foundation grant, on the basis of high citation index, and the Swedish Foundation for International Cooperation in Research and Higher Education, through a program to bring eminent foreign scientists and scholars to Sweden.

5. I declare that a clean Josephson junction formed using a d-wave superconducting material is defined by a current-phase relationship in which the second

harmonic makes a distinct contribution to the current-phase relationship of the clean Josephson junction.

6. I declare that the second harmonic effect on the current-phase relationship of a clean Josephson junction formed using a d-wave superconducting material is temperature dependent.

7. I declare that, in the current state of the art, the second harmonic effect on the current-phase relationship of clean Josephson junctions formed using d-wave superconducting material cannot be precisely engineered.

8. I declare that, because of the temperature dependence of the second harmonic effect and the inability to precisely engineer the second harmonic effect, it would be undesirable to form a dc SQUID using clean Josephson junctions in a d-wave superconducting material, such as $\text{YBa}_2\text{Cu}_3\text{O}_{7-x}$ (YBCO), when the dc SQUID is intended for use in commercial SQUID magnetometers such as those described in Char *et al.*

9. I declare that Chapter 7 of Tinkham only considers conventional superconducting materials and devices made out of conventional superconducting materials.

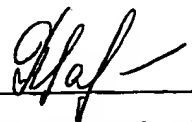
10. I declare that, based on my experience in the field of bi-epitaxial technology, neither the bi-epitaxial technology described in Char *et al.* nor the best quality crystal structures available for bi-epitaxial Josephson junction technology were sufficiently advanced at the time of filing of the Application to prepare a clean Josephson junction such as that

described in the Application.

11. I further declare, under penalty of perjury under the laws of the United States of America, that all statements made herein of my own knowledge are true and that these statements were made with the knowledge that willful false statements and the like are

punishable by fine or imprisonment, or both, under Section 1001 or Title 18 of the United States Code.

Date: 16/04/03
1



Dr. Alexander Tzalenchuk

Exhibit I

Koelle et al., Rev. Mod. Phys. 71, pp. 631–686

High-transition-temperature superconducting quantum interference devices

D. Koelle

*II. Physikalisches Institut, Lehrstuhl für Angewandte Physik, Universität zu Köln,
D-50937 Köln, Germany*

R. Kleiner

Physikalisches Institut III, Universität Erlangen-Nürnberg, D-91058 Erlangen, Germany

F. Ludwig

Physikalisch-Technische Bundesanstalt, Section Cryosensors, D-10587 Berlin, Germany

E. Dantsker* and John Clarke

*Physics Department, University of California, Berkeley, and Materials Sciences Division,
Lawrence Berkeley National Laboratory, Berkeley, California 94720*

The advent of high- T_c superconductors gave great impetus to the development of thin-film superconducting quantum interference devices (SQUIDs) for operation at temperatures up to the boiling point of liquid nitrogen, 77 K. The spectral density of the white flux noise can be calculated analytically for rf SQUIDs and by computer simulation for dc SQUIDs; however, observed noise spectral densities are typically an order of magnitude higher. Low-frequency $1/f$ noise from thermally activated vortex motion is a much bigger issue in high- T_c SQUIDs at 77 K than in low- T_c SQUIDs because of the low flux-pinning energies in high- T_c superconductors. The magnitude of the noise depends strongly on the quality of the thin films, and much effort has been expended to improve techniques for depositing $\text{YBa}_2\text{Cu}_3\text{O}_{7-x}$ (YBCO) on lattice-matched single-crystal substrates. Substantial effort has also been invested in the development of new types of Josephson junctions, of which grain-boundary junctions are the most widely used in SQUIDs. Appropriate electronic read-out schemes largely eliminate $1/f$ noise from fluctuations in the junction critical current in both rf and dc SQUIDs. Typical levels of white flux noise are a few $\mu\Phi_0 \text{ Hz}^{-1/2}$ (Φ_0 is the flux quantum). Magnetometers—consisting of a superconducting flux transformer coupled to a SQUID—achieve a white magnetic-field noise as low as $10 \text{ fT Hz}^{-1/2}$, increasing to typically $30 \text{ fT Hz}^{-1/2}$ at 1 Hz. When these devices are operated in an unshielded environment, it is important to minimize the motion of trapped vortices and induced supercurrents, which can greatly increase the $1/f$ noise. The ambient noise is far greater than the intrinsic noise of the devices, but can be substantially reduced by various gradiometer configurations. There is now considerable effort to apply high- T_c SQUIDs in magnetocardiography, nondestructive evaluation, microscopy, and geophysics. [S0034-6861(99)00403-1]

CONTENTS

I. Introduction	632	2. Step-edge grain-boundary junctions	644
II. Theory	634	B. Junctions with extrinsic interfaces	644
A. Resistively shunted junction model	634	1. Step-edge SNS junctions	645
B. dc SQUID: Overview	634	2. Ramp-edge Josephson junctions	645
C. dc SQUID: Transfer function and thermal noise	635	C. Discussion of high- T_c junctions	645
D. rf SQUID: Overview	637	V. dc SQUIDs	647
E. rf SQUID: Hysteretic mode	638	A. Practical devices	647
F. rf SQUID: Nonhysteretic mode	639	B. Readout schemes	647
III. Thin Films: Fabrication and $1/f$ Noise	640	1. Flux modulation	648
A. Materials	641	2. Direct readout	650
B. Thin-film deposition	641	C. White noise	650
C. Patterning	641	D. Flicker ($1/f$) noise	653
D. Multilayer processing	641	VI. dc SQUID Magnetometers	654
E. $1/f$ noise in YBCO films	642	A. Square-washer designs	654
IV. High- T_c Josephson Junctions	643	B. Directly coupled magnetometer	655
A. Junctions with intrinsic interfaces	643	C. Flux transformer with multiturn input coil	656
1. Bicrystal grain-boundary junctions	643	1. Flip-chip magnetometers	657
		2. Integrated magnetometers	658
		D. Multiloop magnetometer	658
		E. Comparison of magnetometers	659
		VII. rf SQUIDs	660
		A. rf SQUIDs with lumped resonant circuits	660
		B. rf SQUIDs with distributed element resonators	661
		C. $1/f$ noise	662

*Current address: TRW, Electronics & Technology Division, Redondo Beach, California 90278.



VIII. Gradiometers	663
A. Electronic subtraction gradiometers	664
B. Gradiometric flux transformers	665
IX. SQUIDs in Unshielded Environments	666
A. $1/f$ noise	667
B. Hysteresis	669
C. rf interference	670
D. Temperature fluctuations	670
X. Applications	670
A. Biomagnetism	671
B. Nondestructive evaluation	672
C. Scanning SQUID microscopy	674
D. Geophysics	675
XI. Concluding Remarks	676
Acknowledgments	678
References	678

I. INTRODUCTION

The discovery of superconductivity in ceramic oxides (Bednorz and Müller, 1986) such as $\text{YBa}_2\text{Cu}_3\text{O}_{7-x}$ (YBCO) (Wu *et al.*, 1987) with transition temperatures (T_c) above the boiling point of liquid nitrogen (77 K) generated a worldwide furor to develop new superconducting technologies for both large- and small-scale applications. This frenzy of activity was of course driven by the perception that superconductors cooled in liquid nitrogen at 77 K would quickly become much more widely applicable than superconductors cooled in liquid ^4He at 4.2 K. There were two broad reasons behind this perception: liquid nitrogen is much cheaper than liquid helium, and, for a given heat load, liquid nitrogen boils away much more slowly than liquid helium. It was immediately apparent that small-scale devices would require the development of thin-film techniques, and to provide a framework for this research many groups focused on the superconducting quantum interference device (SQUID). Thus at a very early stage of the field Koch *et al.* (1987) and subsequently Nakane *et al.* (1987) fabricated the first thin-film dc SQUIDs; the first rf SQUIDs appeared a little later (Colclough *et al.*, 1987; Zimmerman *et al.*, 1987), although they were actually formed from bulk YBCO. There were several good reasons for choosing the SQUID as a vehicle for the development of this new technology. Low- T_c SQUIDs are by far the most widely used superconducting thin-film devices at liquid ^4He temperatures, and it was a natural assumption that this trend would continue at liquid N_2 temperatures. Furthermore, the SQUID incorporates most of the components needed for a broader range of electronic devices. The first is a photolithographically patterned thin film with high crystalline quality and a transition temperature essentially equal to that of the bulk material. A second, essential component is the Josephson junction (Josephson, 1962), for which one would like a process that yields highly reproducible parameters. A third ingredient is an interconnect technology, that is, a multiple-level process that enables one to fabricate crossovers—two intersecting superconducting films separated by an insulating layer—and *vias*—superconducting contacts through the insulating layer.

Progress in high- T_c dc and rf SQUIDs over the last decade has been dramatic, and the purpose of this review is to give a perspective on the current state of the art.

The dc SQUID (Jaklevic *et al.*, 1964) consists of two Josephson junctions connected in parallel on a superconducting loop. When the magnetic flux Φ threading the loop is changed monotonically, the maximum supercurrent the SQUID can sustain (the critical current) is modulated with a period of one flux quantum, $\Phi_0 \equiv h/2e$. Provided the current-voltage (I - V) characteristic is nonhysteretic (Sec. II.A), this modulation results in a concomitant modulation of the voltage across the SQUID when it is biased with a constant current greater than the maximum critical current. In essence, the SQUID is a flux-to-voltage transducer, characterized by the transfer coefficient $|\partial V/\partial \Phi|_I$. The flux resolution of the SQUID is determined by its intrinsic noise, which has a spectral density that is white at frequencies above a certain threshold and that scales approximately as $1/f$ at frequencies f below the threshold. In low- T_c SQUIDs the threshold frequency can be 0.1 Hz or lower, while, as we shall see, in high- T_c SQUIDs it can be substantially higher. In Secs. II.B and C, we outline the theory of operation of the dc SQUID and solve its equations of motion numerically for both the transfer function and white noise. From the results of our simulations we discuss the optimum choice of parameters for operation at 77 K.

The rf SQUID (Zimmerman *et al.*, 1970; Mercereau, 1970; Nisenoff, 1970) involves a single Josephson junction that interrupts a superconducting loop. This loop is inductively coupled to the inductor of an LC -resonant circuit that is driven by an rf current at or near its resonant frequency, which ranges from 20 MHz to 10 GHz. The amplitude of the rf voltage across the tank circuit is periodic in the magnetic flux in the SQUID with period Φ_0 , so that, after demodulating this voltage, one obtains a quasistatic voltage that is periodic in Φ just as for the dc SQUID. For operation at 4.2 K the rf SQUID has been largely abandoned in favor of the dc SQUID, but the advantage in sensitivity of the latter device at 77 K is much narrower. In Secs. II.D–F, we outline the theory of operation and noise limitations of the rf SQUID.

Low- T_c SQUIDs have been used as sensors in a broad range of applications, including biomagnetism, nondestructive evaluation, geophysics, susceptometers, voltmeters, scanning SQUID microscopes, and nuclear magnetic and nuclear quadrupole resonance (Weinstock, 1996). Of these, the largest number of SQUIDs are deployed in multichannel systems for magnetoencephalography and, to a lesser extent, magnetocardiology. A major requirement for biomagnetic measurements is high magnetic-field sensitivity at frequencies down to 1 Hz. Although this requirement is readily met with niobium based SQUID magnetometers, which achieve a sensitivity of a few $\text{fT Hz}^{-1/2}$, the issue of $1/f$ noise in high- T_c SQUIDs has been a major challenge, and will emerge repeatedly throughout this review. There are two separate sources of $1/f$ noise (Koch *et al.*, 1983): fluctuations in the critical current of the junction(s) and the ther-



mally activated hopping of flux vortices among pinning sites in the thin-film loop. Fortunately, as will be described, $1/f$ noise due to critical-current fluctuations in both dc and rf SQUIDS can be largely eliminated electronically by means of appropriate schemes (Secs. V.B and VII.C). In the case of low- T_c SQUIDS, $1/f$ noise from vortex motion is rarely a problem, but for high- T_c SQUIDS it is a major issue. The reason is simple: flux-pinning energies are lower and thermal energies are higher. At an early stage, Ferrari *et al.* (1988, 1989) used a low- T_c dc SQUID to show that vortex motion in unpatterned high- T_c films indeed produced copious levels of $1/f$ flux noise and that the level diminished dramatically as the microstructural quality of the film was improved. This theme is first raised in Sec. III, in which we briefly review issues concerning the fabrication of thin films. We confine our discussion to YBCO, the only material that has been used for practical devices. Of the possible substrate materials only a handful are admissible. Pulsed laser deposition, sputtering, and recently, coevaporation have emerged as the deposition techniques of choice. Issues of patterning and multilayer processing as well as $1/f$ noise are also discussed in this section.

The other major challenge in the development of SQUIDS, and indeed for high- T_c electronics circuits in general, has been the need to develop an appropriate technology for Josephson junctions (Sec. IV). Many approaches have been tried, ranging from a single layer of YBCO in which grain-boundary junctions are formed along the misorientation boundary of a bicrystal substrate or at a step edge milled in a substrate, to multilayers in which insulating or metallic barriers are formed between two YBCO films. It seems fair to say that the ideal technology has not yet been invented. For virtually all applications, the figure of merit is the $I_0 R$ product, where I_0 is the critical current and R is the resistance for currents much greater than I_0 . Although one might hope to achieve values of several millivolts at 77 K, in practice the highest values achieved to date are more like 300 μV . For SQUIDS, the technique most widely used today is the grain-boundary junction formed on either a bicrystal or a step edge.

Section V reviews practical high- T_c dc SQUIDS. The two widely used readout schemes, flux modulation and direct readout, are briefly described, and the use of bias reversal to eliminate the $1/f$ noise due to critical-current fluctuations is outlined. Achieved levels of white noise and $1/f$ noise are summarized in a series of figures. For reasons that are not well understood, the levels of white noise are generally higher than the predictions of the computer model described in Sec. II.

Although dc SQUIDS are exquisitely sensitive to changes in magnetic flux—typical devices have a white noise of a few $\mu\Phi_0 \text{ Hz}^{-1/2}$ —their small area implies that they are relatively insensitive to changes in magnetic field. To increase this sensitivity, as described in Sec. VI, one almost invariably couples the SQUID to a flux transformer that increases its effective area. Broadly speaking, there are two classes of such magnetometers.

In the first, the so-called directly coupled magnetometer, a large pickup loop—perhaps 10 mm across—is patterned in the same layer as the SQUID so that the supercurrent produced by an applied magnetic field is injected directly into the body of the SQUID. This scheme has the advantage that it involves only a single superconducting layer but suffers from the disadvantage that the inductances of the pickup loop and SQUID are mismatched, thereby reducing the flux-coupling efficiency of the transformer. The mismatch is overcome in the second approach, mimicking that used for low- T_c magnetometers, in which a pickup loop is connected to a multiturn input coil that in turn is inductively coupled to the SQUID. The flux transformer can be either deposited directly onto the SQUID or deposited on a separate substrate and coupled to the SQUID in a flip-chip arrangement. This flux transformer matches the inductance of the pickup loop to the SQUID, but the multilayer structure required for the input coil complicates the fabrication. The best of these magnetometers have achieved a white noise below $10 \text{ fT Hz}^{-1/2}$. An alternative, multilayer magnetometer is the fractional-turn SQUID described in Sec. VI.D.

Section VII is concerned with practical rf SQUIDS, usually fabricated from single layers of YBCO. As discussed in Sec. II, the inductance of the rf SQUID can be somewhat larger than its dc counterpart, enabling one to obtain a higher effective area. Early devices consisted of square washers with step-edge, grain-boundary junctions, and were operated at typically 150 MHz. The sensitivity has been improved by increasing the frequency substantially; as shown in Sec. II, the spectral density of the flux noise is expected to scale inversely with the rf frequency. In the best device reported to date, the white noise was $16 \text{ fT Hz}^{-1/2}$. Section VII.C describes how the $1/f$ noise due to critical-current fluctuations is eliminated by the combination of rf biasing and flux modulation.

Sections VIII and IX are concerned with using SQUID magnetometers in real-world environments. Most notably in biomagnetism, one needs to measure a tiny magnetic signal against a magnetically noisy background. The standard approach to this problem is to use a spatial gradiometer, usually in conjunction with a magnetically shielded room. The gradiometer discriminates against distant noise sources in favor of a nearby signal source. Given the lack of a suitable high- T_c superconducting wire, two approaches have been adopted (Sec. VIII): electronic subtraction of the signals from two or more spatially separated magnetometers, usually to form axial gradiometers, and the use of planar, thin-film gradiometers that measure off-diagonal gradients. Section IX is largely concerned with the operation of magnetometers or gradiometers in the ambient magnetic field of the earth, which has two deleterious effects. The additional vortices created by the penetration of the earth's field into the thin films can greatly increase the level of $1/f$ noise. Fortunately, this problem can be largely alleviated by making the thin-film structures sufficiently narrow, if necessary, by patterning slots or holes

in them. A related problem is hysteresis produced by the entry of vortices when the device is rotated in the earth's field. Flux entry can be greatly reduced, fortunately, by patterning straight, near-vertical edges which provide high edge-pinning forces. Other issues discussed in Sec. IX include rf interference and temperature fluctuations.

In Sec. X we briefly review several applications of high- T_c SQUIDS, which are still in their infancy. Nonetheless, impressive progress has been made in biomagnetism, particularly magnetocardiography, and useful demonstrations have been made in both nondestructive evaluation and scanning SQUID microscopy. Prototype geophysical systems have been successfully deployed. Section XI contains our conclusions.

Writing this review brought home to us the enormous amount of effort that has been expended in developing the technology of high- T_c SQUIDS, and the vastness of the literature. Regrettably, it was out of the question to list more than a fraction of the publications in the space of this review. We have attempted to give a broad perspective on the field, but we are acutely aware that our choice of topics is subjective and far from exhaustive.

II. THEORY

A. Resistively shunted junction model

The Josephson junction (Josephson 1962, 1965; Barone and Paterno, 1982) consists of two weakly coupled superconducting electrodes separated—in the case of the low- T_c tunnel junction—by a thin insulating barrier. Cooper pairs tunneling through the barrier constitute a supercurrent $I = I_0 \sin \delta$, where I_0 is the critical current and δ is the difference between the phases of the order parameters in the two superconductors. For zero applied current, the two electrodes are coupled by an energy $I_0 \Phi_0 / 2\pi$. In the absence of thermal fluctuations, the voltage V across the barrier is zero for $I < I_0$; for $I > I_0$ a voltage is developed and δ evolves with time as $\dot{\delta} = 2eV/\hbar = 2\pi V/\Phi_0$. At least for low- T_c junctions, the current-voltage characteristics are well explained by the resistively and capacitively shunted junction (RCSJ) model (McCumber, 1968; Stewart, 1968). In this model, the Josephson element is in parallel with a resistance R (which may be an external shunt) and a capacitance C . For SQUIDS, one generally needs nonhysteretic I - V characteristics, a requirement that is met if $\beta_c \equiv 2\pi I_0 R^2 C / \Phi_0 \leq 1$. In the limit $\beta_c \ll 1$, which as we shall see is often the case for high- T_c junctions, the RCSJ model reduces to the RSJ model and the I - V characteristic in the absence of thermal noise is given by $V = R(I^2 - I_0^2)^{1/2}$ for $I \geq I_0$.

Particularly in the case of devices operating at 77 K, however, noise has an appreciable effect, and is added to the model by associating a Nyquist noise current I_N with spectral density $S_I(f) = 4k_B T/R$ with the shunt resistor. This noise term rounds the I - V characteristic at low voltages and reduces the apparent critical current (Ambegaokar and Halperin, 1969). To maintain a reasonable

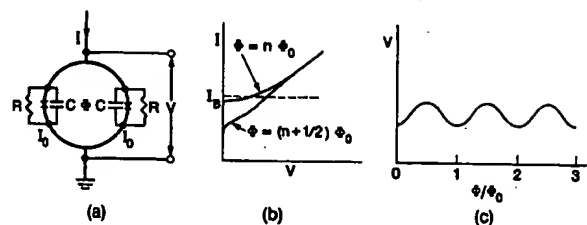


FIG. 1. The dc SQUID: (a) schematic, (b) I - V characteristic, (c) V vs Φ/Φ_0 at constant bias current I_B .

degree of Josephson coupling one requires the noise parameter $\Gamma \equiv 2\pi k_B T / I_0 \Phi_0 = I_{th} / I_0 \leq 1$; at 77 K, $I_{th} \approx 3.3 \mu A$.

B. dc SQUID: Overview

The dc SQUID (Jaklevic *et al.*, 1964) consists of two Josephson junctions connected in parallel on a superconducting loop of inductance L [Fig. 1(a)]. If one biases the SQUID with a constant current $I_B (> 2I_0)$ the voltage V across the SQUID oscillates with a period Φ_0 as one changes the external magnetic flux Φ [Figs. 1(b) and (c)]. To measure small changes in Φ ($\ll \Phi_0$) one generally chooses the bias current to maximize the amplitude of the voltage modulation and sets the external flux at $(2n+1)\Phi_0/4$ ($n=0,1,2,\dots$), so that the flux-to-voltage transfer coefficient $|\partial V/\partial \Phi|_I$ is a maximum, which we denote as V_Φ . Thus the SQUID produces a maximum output voltage signal $\delta V = V_\Phi \delta \Phi$ in response to a small flux signal $\delta \Phi$. For frequencies f well below the Josephson frequency $f_J = V/\Phi_0$, the two independent Nyquist noise currents in the shunt resistors produce a white voltage noise across the SQUID with a spectral density $S_V(f)$ (Teschke and Clarke, 1977) and a white current noise around the SQUID loop with a spectral density $S_I(f)$; in fact, these two noise terms are partially correlated (Teschke and Clarke, 1979). The intrinsic white flux noise of the SQUID is given by $S_\Phi(f) = S_V(f)/V_\Phi^2$; it is often convenient to introduce a noise energy per unit bandwidth $\varepsilon(f) = S_\Phi(f)/2L$. We note that noise imposes a second constraint on the parameters, namely that the magnetic energy per flux quantum $\Phi_0^2/2L$ must be substantially greater than $k_B T$. We can express this requirement as $\Gamma \beta_L = L/L_{th} \ll 1$, where we define $\beta_L = 2LI_0/\Phi_0$, and $L_{th} \equiv \Phi_0^2/4\pi k_B T = 321 \text{ pH}$ at 77 K. As we shall see, this restriction, which can also be written as $\Phi_0^2/2L \gg 2\pi k_B T$, will play a key role in our choice of parameters.

There have been extensive computer simulations of dc SQUIDS operated at 4.2 K (Teschke and Clarke, 1977, 1979; Bruines *et al.*, 1982; Voss, 1981; de Waal *et al.*, 1984; Ryhänen *et al.*, 1989). These simulations show that the minimum noise energy is obtained for $\beta_L \approx 1$ and that, for a representative value of the noise parameter $\Gamma = 0.05$, $V_\Phi \approx R/L$, $S_V(f) \approx 16k_B TR$ and $\varepsilon \approx 9k_B TL/R \approx 9k_B T \Phi_0/2I_0 R$. Thus ε inevitably increases with temperature and, for optimized parameters, scales as $1/I_0 R$. In addition to the white noise, there is usually low-

frequency $1/f$ noise generated by both $1/f$ noise in the critical current and by the motion of flux vortices trapped in the body of the SQUID. We defer the issue of $1/f$ noise to Sec. V.D, and turn our attention to optimizing the parameters of the SQUID at 77 K with regard to white noise.

C. dc SQUID: Transfer function and thermal noise

It is straightforward to show that the phase differences $\delta_1(t)$ and $\delta_2(t)$ across the two junctions obey the following equations (Teschke and Clarke, 1977):

$$\frac{\hbar C}{2e} \ddot{\delta}_1 + \frac{\hbar}{2eR} \dot{\delta}_1 + I_0 \sin \delta_1 + I_{N1} = \frac{I}{2} - J, \quad (2.1)$$

$$\frac{\hbar C}{2e} \ddot{\delta}_2 + \frac{\hbar}{2eR} \dot{\delta}_2 + I_0 \sin \delta_2 + I_{N2} = \frac{I}{2} + J, \quad (2.2)$$

$$\delta_1 - \delta_2 = \frac{2\pi}{\Phi_0} (\Phi + LJ), \quad (2.3)$$

and

$$\dot{\delta}_1 + \dot{\delta}_2 = \frac{4eV}{\hbar}. \quad (2.4)$$

The Langevin Eqs. (2.1) and (2.2) are coupled via the circulating current J , which is related to the external flux Φ in Eq. (2.3). Equation (2.4) expresses the voltage across the SQUID as the rate of the change of the phase differences. In all our simulations we set $\beta_c = 0.5$; the results change only slightly for the smaller values of β_c that we expect for many high- T_c junctions operated at 77 K. To find the transfer function we set $\Phi = \Phi_0/4$, integrate Eqs. (2.1)–(2.3) numerically over 10^4 to 10^6 time units ($\Phi_0/2\pi I_0 R$), and use Eq. (2.4) to obtain the average voltage across the SQUID (Kleiner, 1996). We compute $\partial V/\partial \Phi$ as a function of I to find the maximum value V_ϕ . To explore the dependence on the inductance L , it is convenient to plot V_ϕ vs $\Gamma\beta_L = L/L_{th} = (4\pi k_B T/\Phi_0^2)L$. The range of interest for $\Gamma\beta_L$ extends from well below 0.05 to unity. For convenience, we start from $\Gamma\beta_L = (0.05)2^{-2} = \frac{1}{80}$ and increase $\Gamma\beta_L$ in powers of $2^{1/2}$ up to $(0.05)2^{9/2} \approx 1.13$. For $T = 77$ K this corresponds to inductances between 4 and 362 pH, while for $T = 4.2$ K the corresponding range is 74 pH to 6.7 nH. For most high- T_c devices $\Gamma\beta_L \geq 0.1$, whereas for typical low- T_c devices $\Gamma\beta_L \leq 0.05$.

On calculating the dimensionless transfer function $v_\phi = V_\phi \Phi_0/I_0 R$ vs $\Gamma\beta_L$ for values of β_L ranging from 0.6 to 4 one finds that, although v_ϕ for a given value of $\Gamma\beta_L$ decreases with β_L , its functional dependence on $\Gamma\beta_L$ is essentially the same for all values of β_L . Thus, on normalizing curves of v_ϕ vs $\Gamma\beta_L$ to their value at, say, $\Gamma\beta_L = \frac{1}{80}$, one obtains a universal curve $g(\Gamma\beta_L) = v_\phi(\beta_L; \Gamma\beta_L)/v_\phi(\beta_L; \Gamma\beta_L = \frac{1}{80})$, which is independent of β_L . Note that the value of $\Gamma\beta_L = \frac{1}{80}$ is an arbitrary but convenient choice suggested by the smallest value of $\Gamma\beta_L$ used in the simulations. We denote the normalization factor $v_\phi(\beta_L; \Gamma\beta_L = \frac{1}{80})$ as $f(\beta_L)$. Figure 2 shows

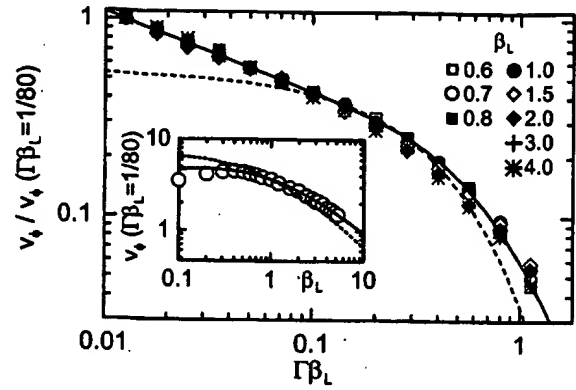


FIG. 2. Computed normalized transfer function $v_\phi/v_\phi(\beta_L; \Gamma\beta_L = \frac{1}{80})$ vs $\Gamma\beta_L$ for $\beta_c = 0.5$. Solid line corresponds to Eq. (2.5), dashed line to $(4/7.3)\exp(-2.75\Gamma\beta_L)$. Inset shows $v_\phi(\beta_L; \Gamma\beta_L = \frac{1}{80})$ vs β_L ; solid line corresponds to Eq. (2.6), dashed line to $7.3/(1+\beta_L)$.

the normalized curve $g(\Gamma\beta_L)$ vs $\Gamma\beta_L$ for eight values of β_L ranging from 0.6 to 4.0. As discussed, the results collapse onto a single curve. The solid line in Fig. 2 is an empirical fit to the computed values

$$g(\Gamma\beta_L) = v_\phi(\beta_L; \Gamma\beta_L)/v_\phi(\beta_L; \Gamma\beta_L = 1/80) = [(80\Gamma\beta_L)^{0.4} + 0.35(4\Gamma\beta_L)^{2.5}]^{-1}. \quad (2.5)$$

For $\Gamma\beta_L < 0.2$, Eq. (2.5) can be approximated as $g(\Gamma\beta_L) \approx (80\Gamma\beta_L)^{-0.4}$. The inset of Fig. 2 shows $f(\beta_L)$ vs β_L for the fixed value $\Gamma\beta_L = 1/80$ for $0.1 \leq \beta_L \leq 5.2$. For $\beta_L \geq 0.5$, the range of experimental interest, one can fit the transfer function with the expression

$$f(\beta_L) = v_\phi(\beta_L; \Gamma\beta_L = 1/80) = 7.3\beta_L^{0.15}/(1+\beta_L), \quad (2.6)$$

shown as a solid line in the inset. With the aid of the factorization $v_\phi = f(\beta_L)g(\Gamma\beta_L)$, these two curves, or Eqs. (2.5) and (2.6), enable one to calculate v_ϕ immediately for any value of β_L and $\Gamma\beta_L$ within the specified ranges. Note that v_ϕ , calculated numerically, decreases for $\beta_L \leq 0.4$. This decrease is not reproduced by Eq. (2.6). Furthermore, since the SQUID will no longer function when Γ becomes much greater than unity, the range of validity of Eqs. (2.5) and (2.6) is restricted to $\Gamma \leq 1$, that is $\Gamma\beta_L \leq \beta_L$. Note that in the range $\Gamma\beta_L < 0.2$, where $g(\Gamma\beta_L) \approx (80\Gamma\beta_L)^{-0.4}$, we can also factorize v_ϕ as $\hat{f}(\beta_L)\hat{g}(\Gamma)$, where $\hat{f}(\beta_L) = f(\beta_L)/\beta_L^{0.4}$ and $\hat{g}(\beta_L) = (80\Gamma)^{-0.4}$. Thus for $\Gamma\beta_L < 0.2$ the variables β_L and $\Gamma\beta_L$ are not the only possible choices for factorization. In order to confirm the validity of Eq. (2.6) for larger values of β_L , we also calculated v_ϕ for $\beta_L = 20$ and $\Gamma\beta_L = 1/80$. The numerical result is $v_\phi \approx 0.6$ whereas Eq. (2.6) yields 0.55.

It is of interest to compare our results with the expression of Enpuku, Doi *et al.* (1995) and Enpuku, Tokita *et al.* (1995),

$$v_\phi = \frac{4}{1+\beta_L} \exp\left(-\frac{3.5\pi^2(\delta\Phi_n)^2}{\Phi_0^2}\right) = \frac{4}{1+\beta_L} \exp(-2.75\Gamma\beta_L), \quad (2.7)$$

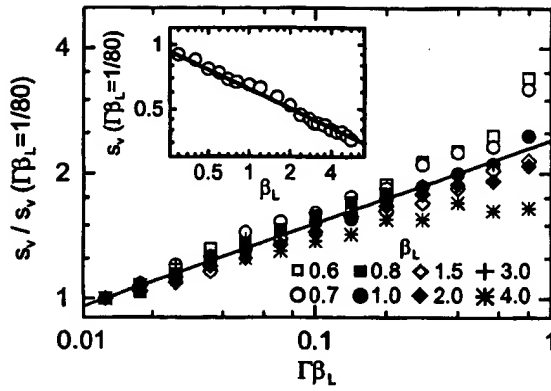


FIG. 3. Computed normalized voltage noise power $s_v/s_v(\beta_L; \Gamma\beta_L = \frac{1}{80})$, vs $\Gamma\beta_L$ for $\beta_c = 0.5$. Solid line shows $s_v(\beta_L; \Gamma\beta_L)/s_v(\beta_L; \Gamma\beta_L = \frac{1}{80}) = (80\Gamma\beta_L)^{0.2}$. Inset shows $s_v(\beta_L; \Gamma\beta_L = \frac{1}{80})$ vs β_L , solid line is $s_v(\beta_L; \Gamma\beta_L = \frac{1}{80}) = 0.62\beta_L^{-0.3}$.

where $(\delta\Phi_n)^2 = k_B T L$ is the mean square flux noise. This expression also factorizes into two terms, which depend on β_L and $\Gamma\beta_L$, respectively. Equation (2.7) agrees well with our results for intermediate values of β_L and $\Gamma\beta_L$, but underestimates v_ϕ outside this region. For example, for $\beta_L = 1$ the agreement is better than 5% for $0.09 < \Gamma\beta_L < 0.35$. The dashed line in Fig. 2 is given by $(4/7.3)\exp(-2.75\Gamma\beta_L)$, and the dashed line in the inset of Fig. 2 corresponds to $7.3/(1 + \beta_L)$. The prefactor $(\frac{7.3}{4})$ was chosen to obtain the best agreement with our simulations for $\beta_L = 1$. Similar results have been found by Koch (1994), Keene et al. (1995), and Foglietti et al. (1995).

We turn now to the voltage noise at frequencies well below the Josephson frequency, where its spectral density is white. Using Eqs. (2.1)–(2.4) we compute the Fourier transform of the time-varying voltage across the SQUID and hence the dimensionless power spectrum $s_V(f) = 2\pi S_V(f)/I_0 R \Phi_0$. We set $\Phi = \Phi_0/4$, vary the bias current so that V_ϕ takes its maximum value and calculate $S_V(f)$. In Fig. 3 we plot $s_v(\beta_L; \Gamma\beta_L)/s_v(\beta_L; \Gamma\beta_L = \frac{1}{80})$ vs $\Gamma\beta_L$ for eight values of β_L . For a given value of β_L , the noise power increases with $\Gamma\beta_L$. However, the overall variation in $s_v(\beta_L; \Gamma\beta_L)$ is weak: within a factor of 2, $s_v \approx 1$ or $S_V \approx I_0 R \Phi_0/2\pi$. In contrast to the transfer function (Fig. 2), there is no universal behavior for the noise power, although roughly speaking, s_v scales as $(80\Gamma\beta_L)^{0.2}$ (line in Fig. 3). The inset to Fig. 3 shows $s_v(\beta_L; \Gamma\beta_L = \frac{1}{80})$ vs β_L . For fixed $\Gamma\beta_L$, β_L is proportional to I_0/T ; the decrease in noise with increasing β_L thus reflects either the decrease in temperature if I_0 is fixed or the increase in I_0 if T is fixed. The line is a fit to $s_v(\beta_L; \Gamma\beta_L = \frac{1}{80}) = 0.62\beta_L^{-0.3}$; within the range $0.2 < \beta_L < 5.2$, we can approximate $s_v \approx 1.5\beta_L^{-0.3}(\Gamma\beta_L)^{0.2}$. For $\Gamma = 0.05$ and $\beta_L = 1$ we find $s_v = 0.82$, in excellent agreement with the result of Tesche and Clarke (1977), $S_V \approx 16k_B T R$. (To make the comparison, note that $s_v = (2\pi/I_0 R \Phi_0) 16k_B T R = 16\Gamma = 0.8$.)

We find the flux noise of the dc SQUID from the relation $S_\phi(f) = S_V(f)/\dot{V}_\phi^2$ or $s_\phi(f) = s_v/v_\phi^2 = (2\pi I_0 R/\Phi_0^3) S_\phi(f)$. Figure 4 shows $s_\phi(\beta_L; \Gamma\beta_L)/$

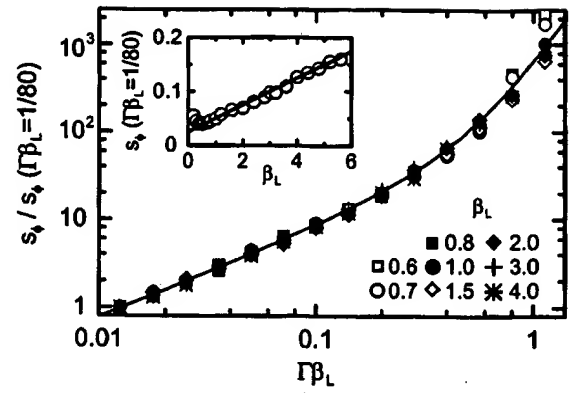


FIG. 4. Computed normalized flux noise power $s_\phi/s_\phi(\beta_L; \Gamma\beta_L = \frac{1}{80})$ vs $\Gamma\beta_L$ for $\beta_c = 0.5$. Solid line corresponds to Eq. (2.8). Inset shows $s_\phi(\beta_L; \Gamma\beta_L = \frac{1}{80})$ vs β_L . Solid line corresponds to Eq. (2.9).

$s_\phi(\beta_L; \Gamma\beta_L = \frac{1}{80})$ vs $\Gamma\beta_L$, obtained from the results in Figs. 2 and 3. The computed data very nearly follow a universal pattern, because of the universal, strong dependence of v_ϕ on $\Gamma\beta_L$ and the weak dependence of s_v . For $0.01 < \Gamma\beta_L < 1$ we can fit the curve reasonably well by the expression

$$s_\phi(\beta_L; \Gamma\beta_L)/s_\phi(\beta_L; \Gamma\beta_L = \frac{1}{80}) = 0.8[80\Gamma\beta_L + (1 + 4\Gamma\beta_L)^{4.1} - 1]. \quad (2.8)$$

For $\Gamma\beta_L < 0.1$, $s_\phi(\beta_L; \Gamma\beta_L)/s_\phi(\beta_L; \Gamma\beta_L = \frac{1}{80})$ reduces to approximately $80\Gamma\beta_L$, while for larger values of $\Gamma\beta_L$ it increases rapidly because of the rapid drop in v_ϕ . In the inset to Fig. 4 we plot $s_\phi(\beta_L; \Gamma\beta_L = \frac{1}{80})$ vs β_L , together with the fitted curve

$$s_\phi(\beta_L; \Gamma\beta_L = \frac{1}{80}) = (1 + \beta_L)/40. \quad (2.9)$$

Note that the increase of $s_\phi(\beta_L; \Gamma\beta_L = \frac{1}{80})$ for $\beta_L \leq 0.5$, which arises from the decrease of $v_\phi(\beta_L; \Gamma\beta_L = \frac{1}{80})$, is not reproduced by Eq. (2.9). Thus, for the range $\Gamma\beta_L < 0.1$ and $\beta_L \geq 0.5$, we find $s_\phi \approx 2(1 + \beta_L)\Gamma\beta_L$ or $S_\phi \approx 4(1 + \beta_L)\Phi_0 k_B T L/I_0 R$. For $\beta_L = 1$, this result becomes $16k_B T L^2/R$, in excellent agreement with the value of Tesche and Clarke (1977). As an example, from Fig. 4 for $\beta_L \Gamma = 0.1$ and $\beta_L = 1$ we find $s_\phi \approx 0.4$; with $I_0 R = 200 \mu\text{V}$, this value corresponds to $S_\phi \approx 0.6 \times 10^{-12} \Phi_0^2 \text{ Hz}^{-1}$.

Finally, we derive the noise energy $\varepsilon(f) = S_\phi(f)/2L$; in dimensionless units, $e = \varepsilon I_0 R/2\Phi_0 k_B T = s_\phi/2\Gamma\beta_L$. Figure 5 shows $e(\beta_L; \Gamma\beta_L)/e(\beta_L; \Gamma\beta_L = \frac{1}{80})$ vs $\Gamma\beta_L$, obtained from the results in Figs. 2 and 3. For $\Gamma\beta_L < 0.2$, the reduced noise energy is almost constant, while for higher values of $\Gamma\beta_L$ it increases rapidly. The rapid increase in noise energy arises from the rapid degradation of the transfer function over the same values of $\Gamma\beta_L$ (Fig. 2). In the inset of Fig. 5 we plot $e(\Gamma\beta_L = 1/80)$ as a function of β_L : the dependence is linear for $\beta_L \geq 0.5$, and to a good approximation $e(\beta_L; \Gamma\beta_L = 1/80) \approx (1 + \beta_L)$ for $\beta_L \geq 0.5$. For a SQUID with $\Gamma = 0.05$ and $\beta_L = 1$, Tesche and Clarke (1977) find $\varepsilon \approx 9k_B T L/R$, corresponding to $e = \varepsilon I_0 R/2\Phi_0 k_B T \approx 9L I_0/2\Phi_0 = 9\beta_L/4 = 2.25$. From Fig. 5, we predict $e \approx 2$, in good agreement,

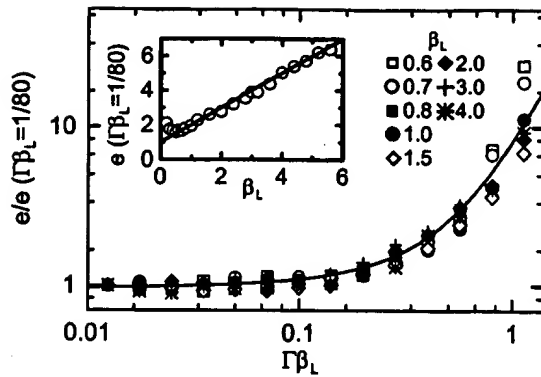


FIG. 5. Computed normalized energy resolution $e/e(\beta_L; \Gamma\beta_L = \frac{1}{80})$ vs $\Gamma\beta_L$ for $\beta_c = 0.5$. Solid line corresponds to Eq. (2.8) divided by $(80\Gamma\beta_L)$. Inset shows $e(\beta_L; \Gamma\beta_L = \frac{1}{80})$ vs β_L , solid line is the function $(1 + \beta_L)$.

and observe that this value remains valid for $\Gamma\beta_L < 0.2$. More generally, for $\Gamma\beta_L < 0.2$ and for an arbitrary value of β_L we find $e \approx (1 + \beta_L)$ or $e \approx 2(1 + \beta_L)\Phi_0 k_B T / I_0 R$.

This concludes our description of the signal and noise theory for the dc SQUID. The results dictate the range of parameters required to achieve near optimal performance. Low- T_c SQUIDS are usually optimized under the constraint $I_0 R^2 = \text{constant}$ (Tesche and Clarke, 1977), in order to keep β_c fixed. For a given value of L we then have $I_0 \propto \beta_L$ and $R \propto I_0^{-1/2}$, so that $I_0 R \propto \beta_L^{1/2}$. Since $e \propto (1 + \beta_L)$ we find $e \propto (1 + \beta_L)\beta_L^{1/2}$, which has a minimum at $\beta_L = 1$. The situation for high- T_c SQUIDS is more complicated. One way to optimize the SQUID is to vary the junction width on a given substrate. We then have $I_0 R = \text{constant}$, and the dependence of e on β_L can be scaled from the plots in Fig. 5; in this case, the minimum is at $\beta_L \approx 0.5$. However, we again emphasize that this value is at the lower end of the validity of our equations. A discussion of smaller values would be purely academic, since one generally couples the SQUID to a pickup loop with an inductance that is much higher than the SQUID inductance L (Sec. VI). Thus, to reduce the inductance mismatch, there is a strong incentive to make L as high as possible. As a result, values of $\beta_L \ll 1$ would require values of Γ that are outside the validity of our equations. An alternative philosophy is to fix the junction area and to vary the critical current, for example, by changing the barrier thickness. Since for many high- T_c junctions $I_0 R \propto j_c^{1/2}$ (Sec. IV), this approach leads to $I_0 R^2 = \text{constant}$ as for low- T_c SQUIDS, so that $\beta_L = 1$ is the optimum value.

Figure 5 shows clearly that the reduced noise energy increases rapidly once $\Gamma\beta_L = L/L_{th}$ is raised above about 0.15; for $T = 77$ K, this constraint implies $L \lesssim 50$ pH. However, one can use higher inductances either by adding a damping resistor across the SQUID loop (Enpuku, Sueoka *et al.*, 1985; Enpuku, Muta *et al.*, 1985; Enpuku, *et al.*, 1993; Enpuku, 1993) and/or a third Josephson junction (Enpuku, 1993; Enpuku *et al.*, 1994; Enpuku, Doi *et al.*, 1995). It is shown that with these additional circuit elements one may increase the SQUID inductance up to 500 pH. Recently, high- T_c SQUIDS

with integrated damping resistors have been studied by Kang *et al.* (1997), and three-junction SQUIDS have been investigated by Schultze, Ijsselstein *et al.* (1997). In both cases, an enhanced voltage modulation was observed. However, for the three-junction SQUID, large modulation was obtained only over a few periods and the authors concluded that this SQUID has no advantage over the conventional SQUID.

Finally, the fact that e scales as $1/I_0 R$ emphasizes the need to develop junction technologies with the largest possible value of $I_0 R$. In particular, one would like a type of junction in which I_0 and R can be varied independently. For example, for $L = 40$ pH, the requirement $\beta_L = 1$ leads to $I_0 = 25 \mu\text{A}$; increasing $I_0 R$ solely by increasing I_0 will not lead to significantly enhanced performance.

D. rf SQUID: Overview

The rf SQUID (Mercereau, 1970; Nisenoff, 1970; Zimmerman *et al.*, 1970) consists of a single Josephson junction integrated into a superconducting loop that is inductively coupled to the inductance L_T of an LC-resonant (tank) circuit [inset Fig. 6(b)]. The tank circuit is driven by an rf current, and the resultant rf voltage is periodic in the flux applied to the SQUID with period Φ_0 . Detailed reviews have been written by many authors (for example, Jackel and Buhrman, 1975; Ehnholm, 1977; Likharev and Ulrich, 1978; Likharev, 1986; Ryh nen *et al.*, 1989; Clarke, 1996).

The total flux Φ_T in the SQUID is related to the applied flux Φ by

$$\Phi_T = \Phi - LI_0 \sin(2\pi\Phi_T/\Phi_0). \quad (2.10)$$

We see immediately that Eq. (2.10) can exhibit two distinct kinds of behavior [Fig. 6(a)]. For $\beta'_L = 2\pi LI_0/\Phi_0 < 1$, the slope $d\Phi_T/d\Phi = [1 + \beta'_L \cos(2\pi\Phi_T/\Phi_0)]^{-1}$ is everywhere positive and the Φ_T vs Φ curve is nonhysteretic. On the other hand, for $\beta'_L > 1$, there are regions in which $d\Phi_T/d\Phi$ is positive, negative, or divergent so that the Φ_T vs Φ curve becomes hysteretic. Radio frequency superconducting quantum interference devices have been operated in both modes. In the hysteretic mode the SQUID makes transitions between quantum states and dissipates energy at a rate that is periodic in Φ . This periodic dissipation in turn modulates the quality factor Q of the tank circuit, so that when it is driven on resonance with a current of constant amplitude the rf voltage is periodic in Φ . In the case $\beta'_L < 1$, the nondissipative mode, the SQUID behaves as a parametric inductance, modulating the effective inductance and hence the resonant frequency of the tank circuit as the flux is varied. Thus when the tank circuit is driven at constant frequency, the variations in its resonant frequency cause the rf voltage to be periodic in Φ .

Historically, it appears that most low- T_c rf SQUIDS were operated in the hysteretic mode, although as we shall see, there are advantages to the nonhysteretic mode. However, the theory of noise in the nondissipa-

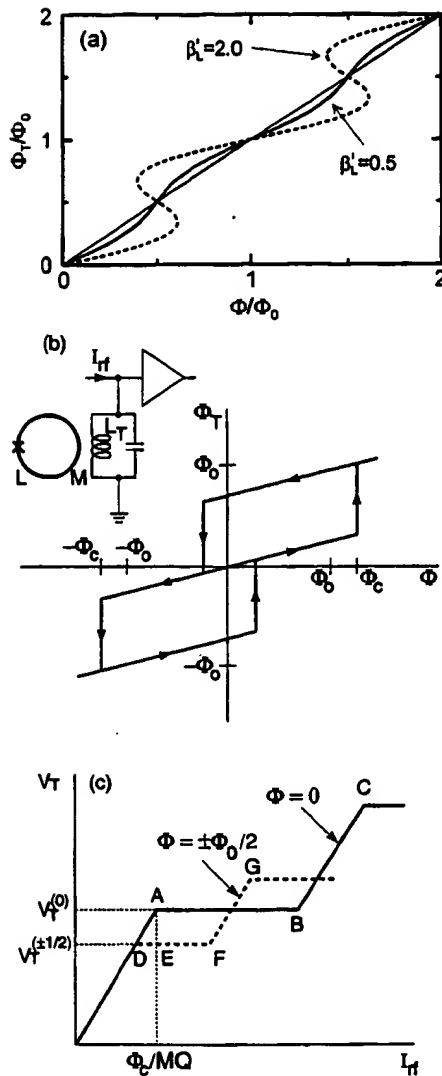


FIG. 6. The rf SQUID: (a) Normalized total flux Φ_T/Φ_0 vs normalized applied flux Φ/Φ_0 for $\beta_L' = 0.5, 2$. (b) Total flux Φ_T vs applied flux Φ for rf SQUID with $LI_0/\Phi_0 = \frac{1}{4}$, showing transitions between quantum states in absence of thermal noise as Φ is increased and subsequently decreased. Inset shows rf SQUID inductively coupled to the inductor of a resonant circuit. (c) Peak rf voltage V_T across tank circuit vs peak rf current I_{rf} in absence of thermal noise for $\Phi = 0$ (solid line) and $\Phi = \pm \Phi_0/2$ (dashed line).

tive regime was worked out in the late 1970s, just as dc SQUIDS began largely to replace rf SQUIDS. As a result, the importance of the nonhysteretic rf SQUID was not widely exploited experimentally. The advent of 77 K operation has changed this situation dramatically, largely due to the systematic experimental effort of the group at Jülich and the very recent theoretical work of Chesca (1998). In the following two sections we briefly outline the theory of the dissipative and nondissipative rf SQUIDS.

E. rf SQUID: Hysteretic mode

For the case $\beta_L' > 1$, the unstable nature of the Φ_T vs Φ curve in Fig. 6(a) causes the SQUID to make transi-

tions between stable quantum states as Φ is changed [Fig. 6(b)]. For example, when Φ is increased from 0, there is a transition from the $k=0$ flux state to the $k=1$ state at a critical flux (neglecting fluctuations) $\Phi_c = LI_0$. In rf operation, a current $I_{rf} \sin \omega_{rf} t$ is applied to the resonant circuit. The peak voltage V_T across the resonant circuit increases linearly with I_{rf} until, for $\Phi = 0$, $I_{rf} = \Phi_c/MQ$, at which value

$$V_T^{(0)} = \omega_{rf} L_T \Phi_c / M, \quad (2.11)$$

where $M = \kappa(LL_T)^{1/2}$. At this point [A in Fig. 6(c)] the SQUID makes a transition to the $k = +1$ or -1 state. As the SQUID traverses the hysteresis loop, energy ΔE is extracted from the tank circuit. Because of this loss, the peak flux on the next half cycle is less than Φ_c , and no transition occurs. The tank circuit takes many cycles to recover sufficient energy to induce a further transition, which may be into either the $k = +1$ or -1 states. If we now increase I_{rf} , transitions are induced at the same values of I_T and V_T but, because energy is supplied at a higher rate, the stored energy builds up more rapidly after each energy loss ΔE , and transitions occur more frequently. At B, a transition is induced on each positive and negative rf peak, and a further increase in I_{rf} produces the "riser" BC. At C, transitions from the $k = \pm 1$ states to the $k = \pm 2$ states occur, and a second step begins. A plot of the peak values $V_T^{(0)}$ vs I_{rf} produces the "steps and risers" shown in Fig. 6(c).

If we now apply an external flux $\Phi_0/2$, the hysteresis loops in Fig. 6(b) are shifted by this amount, and one finds

$$V_T^{(\pm 1/2)} = \omega_{rf} L_T (\Phi_c - \Phi_0/2) / M. \quad (2.12)$$

As I_{rf} is increased, this voltage remains constant until the point F, at which the SQUID traverses the hysteresis loop corresponding to the $k=0 \leftrightarrow k=+1$ transitions once per rf cycle. A further increase in I_{rf} produces the riser FG; at G, corresponding to a peak rf flux $-(\Phi_c + \Phi_0/2)$, transitions $k=0 \leftrightarrow k=-1$ begin. Thus an applied flux other than $n\Phi_0$ (n is an integer) causes the step AB to split as shown in Fig. 6(c).

The model outlined above enables us to calculate the transfer function at values of I_{rf} that maintain the SQUID biased on a step: the change in V_T as we increase Φ from 0 to $\Phi_0/2$ is $V_T^{(0)} - V_T^{(\pm 1/2)} = \omega_{rf} L_T \Phi_0 / 2M$, so that for small changes in flux in the range $0 < \Phi < \Phi_0/2$ we find $V_\Phi = \omega_{rf} L_T / M$. At first sight, this result seems to imply that V_Φ can be increased indefinitely by reducing κ . This is not the case, since one must ensure that the point F in Fig. 6(c) lies to the right of E, that is, DF must exceed DE. To calculate DF we note that the power dissipated in the SQUID is zero at D and approximately $I_0 \Phi_0 \omega_{rf} / 2\pi$ at F, since the energy dissipated per rf cycle is approximately $I_0 \Phi_0$ for a device with $LI_0 \approx \Phi_0$. Thus, taking account of the fact that the rf currents and voltages are peak values, we find $(I_{rf}^{(F)} - I_{rf}^{(D)}) = V_T^{(\pm 1/2)} / 2 \approx I_0 \Phi_0 \omega_{rf} / 2\pi$. Furthermore, we can easily see that $I_{rf}^{(E)} - I_{rf}^{(D)} = \Phi_0 / 2MQ$. Assuming LI_0

$\approx \Phi_0$ and using Eq. (2.12), we can write the requirement that DF exceeds DE in the form

$$\kappa^2 Q \geq \pi/4. \quad (2.13)$$

Taking $\kappa \approx 1/Q^{1/2}$, we find that the expression for V_Φ becomes

$$V_\Phi \approx \omega_{rf}(QL_T/L)^{1/2} \approx \omega_{rf}(L_T/L)^{1/2}/\kappa. \quad (2.14)$$

We note that V_Φ scales with ω_{rf} and as $L^{-1/2}$.

A detailed theory has been developed for noise in the hysteretic rf SQUID operating at liquid helium temperatures (Kurkijärvi, 1972, 1973; Jackel and Buhrman, 1975; Giffard et al., 1976; Ehnholm, 1977; Hollenhorst and Giffard, 1980; Ryhänen et al., 1989). Although in a noise-free model the steps are flat, thermal noise causes them to tilt to a slope η . In addition, thermal noise induces voltage noise on the step arising from fluctuations in the value of flux at which transitions between flux states occur. The corresponding intrinsic flux noise of the SQUID is (Kurkijärvi, 1973)

$$S_\Phi^i(f) \approx \frac{(LI_0)^2}{\omega_{rf}} \left(\frac{2\pi k_B T}{I_0 \Phi_0} \right)^{4/3}. \quad (2.15)$$

In the case of helium-cooled rf SQUIDS in which the tank circuit voltage is detected with a room-temperature amplifier, there is a second, extrinsic contribution to the flux noise. This arises in part because the noise temperature of the rf amplifier is above the bath temperature and in part because a fraction of the coaxial line connecting the tank circuit to the amplifier is at room temperature. We can represent these two contributions by an effective noise temperature T_a^{eff} , enabling us to write the noise energy due to intrinsic and extrinsic noise sources as (Jackel and Buhrman, 1975; Giffard et al., 1976)

$$\varepsilon \approx \frac{LI_0^2}{2\omega_{rf}} \left(\frac{2\pi k_B T}{I_0 \Phi_0} \right)^{4/3} + \frac{2\pi \eta k_B T_a^{\text{eff}}}{\omega_{rf}}. \quad (2.16)$$

Equation (2.16) makes two important points. First, ε scales as $1/\omega_{rf}$, up to a limiting value R/L . Second, for low- T_c SQUIDS, the extrinsic noise energy generally dominates the intrinsic noise: if we take the representative values $T=4$ K, $\Gamma=0.1$, $\eta=0.2$, $\beta'_L=2\pi$ and $T_a^{\text{eff}}=100$ K, we find that the extrinsic noise energy is about 20 times the intrinsic value. Thus, although we should be wary of extrapolating these results to 77 K where, to our knowledge, there are no simulations or calculations, the overall noise energy of the hysteretic rf SQUID should not increase very much as we raise the temperature from 4 K to 77 K. This result is in contrast to the dc SQUID, which for properly designed circuitry is limited largely by intrinsic noise at 4.2 K, so that the overall noise energy will increase significantly as the temperature is raised to 77 K.

F. rf SQUID: Nonhysteretic mode

To give an approximate account of the operation of the nonhysteretic rf SQUID we follow the description of

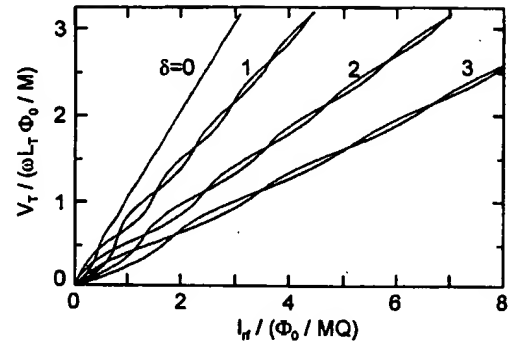


FIG. 7. Tank circuit voltage V_T vs rf drive current I_T for four values of the tuning parameter $\delta = [2(\omega_{rf} - \omega_0)/\omega_0]Q$ and for $\Phi = 0, \Phi_0/2$. Curves plotted for $\kappa^2 Q \beta'_L = \pi/2$ (Hansma, 1973).

Hansma (1973), which is valid in the limits $\beta'_L \ll 1$, where the total magnetic flux threading the SQUID is nearly equal to the applied flux, and $\omega_{rf} \ll I_0 R/\Phi_0$. More general treatments are given, for example, by Jackel and Buhrman (1975), Ern  et al. (1976), Danilov et al. (1980), Likharev (1986), and Ryh nen et al. (1989).

In the presence of a static flux Φ and rf flux $\Phi_{rf} \sin \omega_{rf} t$, the current in the SQUID loop is

$$I = I_0 \sin[(2\pi/\Phi_0)(\Phi + \Phi_{rf} \sin \omega_{rf} t)] \quad (2.17)$$

$(2\pi LI_0 \ll \Phi_0).$

The oscillating component of this current induces a current $I_i = -(M/Z)dI/dt$ into the tank circuit, where $Z = R_T + i[\omega_{rf}(L_T - M^2/L) - 1/\omega_{rf}C_T]$ is its impedance; the inductance of the tank circuit is modified by the contribution $-M^2/L$ from the SQUID. If we assume that the rf frequency is near resonance and that Q is reasonably large, we can neglect all frequency components other than the fundamental. Expanding the right-hand side of Eq. (2.17) in terms of the Bessel function J_1 , we find the induced current

$$I_i = \frac{2\kappa^2 Q LI_0}{M(1+\delta^2)^{1/2}} \cos\left(\frac{2\pi\Phi}{\Phi_0}\right) J_1\left(\frac{2\pi\Phi_{rf}}{\Phi_0}\right) \sin(\omega_{rf} t - \theta). \quad (2.18)$$

Here, $\delta = 2[(\omega_{rf} - \omega_0)/\omega_0]Q$ is the normalized difference between the rf frequency and the tank-circuit resonant frequency ω_0 , and $\theta = \tan^{-1} \delta + \pi/2$.

The rf flux applied to the SQUID is $MI_T \sin \omega_{rf} t$, where I_T is the amplitude of the total current in the inductor which, in addition to the induced current given by Eq. (2.18), also contains a component of amplitude $QI_{rf}/(1+\delta^2)^{1/2}$ produced by the external rf current. From Eq. (2.18) we see that the total current leads the induced current by a phase angle θ . The amplitudes of the total and external rf currents are related by

$$I_{rf} = \frac{(1+\delta^2)^{1/2}}{Q} \left\{ \left[\frac{2\kappa^2 Q LI_0}{(1+\delta^2)^{1/2} M} \cos\left(\frac{2\pi\Phi}{\Phi_0}\right) \times J_1\left(\frac{2\pi MI_T}{\Phi_0}\right) + I_T \cos \theta \right]^2 + I_T^2 \sin^2 \theta \right\}^{1/2}. \quad (2.19)$$

Figure 7 shows plots of V_T vs I_{rf} for $\Phi = 0$ and $\Phi_0/2$ for

four values of the tuning parameter δ . We see that the response is insensitive to the flux in the SQUID for $\delta = 0$; thus the tank circuit for the nonhysteretic SQUID is operated off resonance. For a given value of δ , the response shows a series of oscillations as I_{rf} is increased, arising from the oscillations of the Bessel function. The maximum peak-to-peak modulation of V_T at fixed I_{rf} is of the order of $2\kappa^2 Q L I_0 (\omega_{rf} L_T / M)$, so that

$$\begin{aligned} V_\Phi &\approx (2/\pi) \kappa^2 Q \beta'_L \omega_{rf} L_T / M \\ &\approx (2/\pi) (\kappa^2 Q \beta'_L) \omega_{rf} (L_T / L)^{1/2} / \kappa. \end{aligned} \quad (2.20)$$

This transfer function exceeds that of the hysteretic rf SQUID [Eq. (2.14)] by a factor of order $\kappa^2 Q \beta'_L$, which can be made larger than unity for the nonhysteretic case by choosing $\kappa^2 Q \gg 1$.

The intrinsic noise energy of low- T_c , nonhysteretic, rf SQUIDS has been calculated by several authors, and is approximately $3k_B T / (\beta'_L)^2 \omega_c$ (Likharev, 1986), where the drive frequency is set equal to $\omega_c = R/L$, the cutoff frequency of the SQUID. A noise energy as low as $20\hbar$ has been achieved by Kuzmin *et al.* (1985).

As a preamble to the discussion of nonhysteretic high- T_c SQUIDS, we note that Falco and Parker (1975) successfully observed flux modulation in an rf SQUID at 2 K with a supercurrent as low as 50 nA. The corresponding value of the noise parameter $\Gamma = 2\pi k_B T / I_0 \Phi_0$ was about 1.7; at this high value, they were unable to observe any trace of supercurrent in an isolated junction. Thus it is evident that one can expect to operate an rf SQUID with substantially higher values of Γ than is the case for the dc SQUID (see Sec. II.C). Although this important fact has been known experimentally for many years, only very recently has the work of Chesca (1998) provided a quantitative explanation. In contrast to previous theories of the rf SQUID in which one regards thermal noise as a perturbation on a noise-free system, Chesca solves the Smoluchowski equation for the situation in which thermal fluctuations dominate. Thus both the signal produced by the SQUID and the noise are found in a unified calculation that yields analytical results. For the case $\beta'_L \leq 1$ and $\omega_{rf} \leq R/L$, Chesca finds

$$\varepsilon \approx 3\Gamma^2 \left(1 + \frac{T_k}{T} \frac{1}{\kappa^2 Q} \frac{R/L}{\omega_{rf}} \right) \frac{\exp(L/L'_{th})}{L/L'_{th}} \frac{k_B T L'_{th}}{R}. \quad (2.21)$$

Here, $L'_{th} = (\Phi_0/2\pi)^2 / k_B T$ and T_k is the effective noise temperature of the tank circuit, including any contribution from the preamplifier. If one assumes $L/L'_{th} = \beta'_L \Gamma \ll 1$ and that $\kappa^2 Q$ can be made sufficiently large that $(T_k/T)(R/\omega_{rf}L)/\kappa^2 Q \ll 1$, Eq. (2.21) can be written in the alternative forms

$$\varepsilon \approx 3k_B T / (\beta'_L)^2 (R/L) \quad (2.22a)$$

$$\approx 3k_B T \Phi_0 / 2\pi \beta'_L I_0 R. \quad (2.22b)$$

Interestingly, Eq. (2.22a) is identical to the result found perturbatively for the rf SQUID for low values of Γ . The value for ε in Eq. (2.22b) is equal to $3/4\pi \beta'_L (1 + \beta'_L)$ times that for the dc SQUID in the limit $\Gamma \beta'_L < 0.2$.

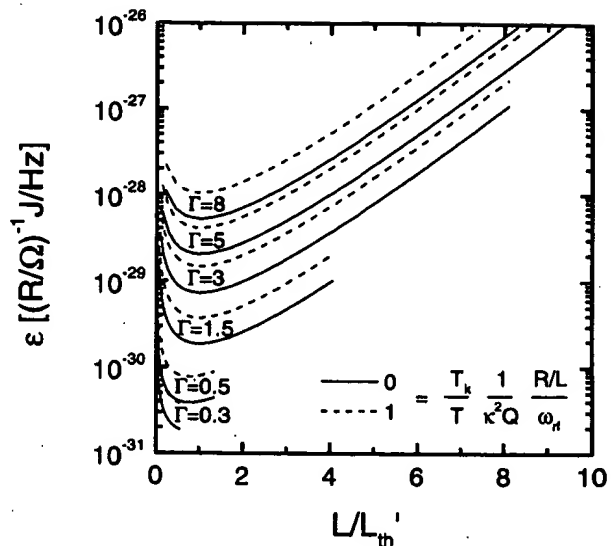


FIG. 8. ε vs L/L'_{th} for nonhysteretic rf SQUID at 77 K (Chesca, 1998).

Equation (2.21) is plotted in Fig. 8 for the two cases $(T_k/T)(1/\kappa^2 Q)(R/\omega_{rf}L) = 0$ and 1, and for six values of Γ . One concludes from these plots that the optimal values are (Chesca, 1998)

$$\beta'_L = 1 \quad \text{if } \Gamma \leq 1, \quad (2.23a)$$

$$\beta'_L = 1/\Gamma \quad \text{if } \Gamma \geq 1. \quad (2.23b)$$

We note that for the lowest value of Γ plotted, 0.3, the curve is cut off at $\beta'_L \Gamma = L/L'_{th} = 0.55$, at which value the noise energy approaches $10^{-31} \text{ JHz}^{-1}$ for $R = 1 \Omega$. For the case $\Gamma \geq 1$, the noise energy is higher and the optimal SQUID inductance is approximately $L'_{th} \approx 100 \text{ pH}$ at 77 K. Again, this value is about two times higher than for the dc SQUID at 77 K. One consequence of this result is that one can expect to use rf SQUIDS with an area about two times higher than dc SQUIDS.

III. THIN FILMS: FABRICATION AND 1/f NOISE

In this section, we discuss issues related to the fabrication of epitaxial thin films for high- T_c SQUIDS and flux-coupling input circuits. Key requirements for the films are high crystalline quality and either elimination or efficient pinning of flux vortices, in order to achieve both good electrical transport properties and low levels of 1/f noise. For some structures, for example, multiturn flux transformers (Sec. VI.C) or multiloop magnetometers (Sec. VI.D), one requires two or more superconducting films separated by an insulating layer. Hence all layers must be of high crystalline quality. To achieve heteroepitaxial growth of such multilayer structures, it is essential that the various films have comparable lattice constants and thermal-expansion coefficients, that they are chemically compatible at the relatively high deposition temperatures, typically 700–800 °C, and that they can be deposited with sufficiently smooth surfaces to al-

low subsequent layers to grow with high structural and electrical integrity and without electrical shorts between them. Moreover, one must be able to pattern the films without introducing a significant deterioration in their properties.

A. Materials

Despite the wide variety of high- T_c compounds, work on SQUIDS has been mostly restricted to YBCO. This is largely because only YBCO films with their c axis normal to the substrate ("c-axis films") have been shown to have sufficiently strong flux pinning at 77 K to ensure both high critical-current densities in the ab plane—several 10^6 A cm^{-2} —and acceptably low levels of $1/f$ noise. Furthermore, because of the worldwide effort that has been focused on YBCO, its physical properties and growth mechanisms are well understood and high-quality thin films can be grown *in situ* by a variety of deposition techniques on a number of substrate materials. As a result, it seems unlikely that YBCO will be supplanted as the superconductor of choice, although $\text{NdBa}_2\text{Cu}_3\text{O}_{7-x}$ is worthy of consideration because of its superior stability.

There are a number of substrates suitable for growing high-quality YBCO films (for a discussion see Scheel *et al.*, 1991; Somekh and Barber, 1992; Braginski, 1993, 1996; Wellstood *et al.*, 1994; Phillips, 1996). To fabricate low-noise SQUIDS, one usually chooses substrates that are closely lattice matched to YBCO and have comparable thermal expansion coefficients, notably (100) SrTiO_3 , LaAlO_3 , and NdGaO_3 , thus allowing the YBCO films to grow with a high degree of crystallographic perfection. In addition, MgO substrates are frequently used since they are relatively inexpensive and allow one to grow YBCO films with acceptable electrical properties.

B. Thin-film deposition

Among the many different techniques used to deposit YBCO *in situ* (for reviews, see Somekh and Barber, 1992; Phillips, 1993; Wellstood *et al.*, 1994), those most commonly applied to SQUID fabrication are pulsed laser deposition and sputtering, although a few groups have successfully used coevaporation. All of these techniques produce smooth YBCO films with excellent electrical properties. Typical YBCO films, 100–300 nm thick, grown on lattice-matched substrates such as SrTiO_3 (STO), have critical current densities at 77 K of $(2-5) \times 10^6 \text{ A cm}^{-2}$. The surface roughness of the best films, usually determined by atomic force microscopy, is below 10 nm and the half-width of the x-ray rocking curve (005 line) is typically 0.1–0.3°. The critical-current densities in such films are two orders of magnitude higher than in high-quality YBCO single crystals, indicating that a high density of defects, which provide strong pinning sites, must be present.

To deposit Ag or Au layers for contact pads, one can use thermal evaporation, electron-beam evaporation,

sputtering, or ion-beam-assisted deposition, usually with the substrate at room temperature. To achieve a low metal/YBCO contact resistance ($<10^{-6} \Omega \text{ cm}^2$) one should deposit the metal layer either *in situ* or after only a brief exposure to air (Russek *et al.*, 1994, 1996). If the YBCO film is stored in air for any length of time or exposed to photoresist, low-energy Ar-ion-beam cleaning of the surface and/or postannealing in oxygen at 400–500 °C is necessary to achieve a low contact resistance.

C. Patterning

Patterning techniques that are well established in semiconductor and low- T_c superconductor technology are not necessarily applicable to YBCO thin films. One immediate problem is that contact of YBCO with water or water-soluble chemicals degrades the superconducting properties. Second, the use of dry-etching methods in a vacuum can lead to a significant heating of the sample and thus to oxygen loss at the edges. Given these limitations, however, a number of techniques have been used successfully to pattern YBCO films down to submicrometer dimensions without degrading their properties; for reviews, see Braginski (1993) and Wellstood *et al.* (1994).

Conventional photomasking followed by dry etching is the most widely used technique for patterning SQUID devices based on YBCO films or multilayers. However, sometimes special masks are used, especially for step-edge and ramp-edge junctions (Sec. IV) and for patterning submicrometer structures (Barth *et al.*, 1993; Schneider *et al.*, 1993; van der Harg *et al.*, 1995). Among dry-etching methods, the most commonly used is Ar-ion beam milling. To minimize damage to the YBCO, one restricts the beam energies to between 350 and 500 eV, the latter being the most common value, and the beam current density to below 1 mA/cm^2 . To reduce heating of the film, it is also important to cool the sample, either with water or particularly for submicrometer dimensions, preferably with liquid nitrogen. Alff *et al.* (1992) and Schneidewind *et al.* (1995) reported systematic studies of the effects of ion-beam voltage, current density and sample cooling on the dependence of the critical-current density on the linewidth of YBCO films. Generally, for high-quality, c -axis YBCO films, the edges are damaged over a length of much less than $1 \mu\text{m}$ provided the sample is water-cooled and the beam energy and current density do not exceed the values given above.

D. Multilayer processing

All multilayer structures for multiturn flux transformers, integrated magnetometers and multiloop SQUIDS involve a YBCO/insulator/YBCO trilayer. Of course, additional layers might be advantageous, for example, a superconducting ground plane. However, although integrated magnetometers with up to 15 epitaxial layers have been made (Lee *et al.*, 1991), it is difficult to maintain high crystalline quality throughout so many layers

as is required for low levels of $1/f$ noise. Thus we confine our attention to trilayers. The insulator is generally one of the substrate materials listed in Sec. III.A; the most widely used is SrTiO_3 . As an alternative to the various insulating materials, $\text{PrBa}_2\text{Cu}_3\text{O}_{7-x}$ (PBCO) has been used in the fabrication of multiturn flux transformers (Keene *et al.*, 1993; Keene, Goodyear *et al.*, 1994).

An important issue related to the integrity of the insulator is the oxygen content of the lower YBCO film. To ensure proper oxygenation of a single YBCO film it is usually sufficient to vent the deposition chamber with 0.5–1 atm. O_2 and to cool the sample from the deposition temperature to room temperature in about 30 min. The use of this process after the deposition of a high-quality insulating layer on a YBCO film can result in a reduced transition temperature because the insulator inhibits the necessary oxygen diffusion (Humphreys *et al.*, 1991; Ludwig, Koelle *et al.*, 1995; Ockenfuß *et al.*, 1995). To reoxygenate the lower YBCO film fully, one can either increase the annealing time considerably (Ludwig, Koelle *et al.*, 1995) or perform the annealing in an oxygen plasma rather than in molecular O_2 (Yanamoto *et al.*, 1991; Humphreys *et al.*, 1991; Ockenfuß *et al.*, 1995).

In actual multilayer devices, the need to pattern each layer separately, usually with photolithographic processing, greatly complicates matters. Multiturn flux transformers, integrated magnetometers and multiloop SQUIDS all contain the basic elements of a superconducting interconnect technology: *crossovers* and *vias*. In these structures, one has to produce edges over which subsequent layers grow with high crystalline quality; in particular, the growth of YBCO over edges steeper than 45° results in grain boundaries and thus leads to a reduction in critical current (Jia *et al.*, 1991).

Various processes suitable for multilayer magnetometers were developed and have been extensively reviewed (Wellstood *et al.*, 1994; Braginski, 1996). In the process that was used to fabricate most of the low-noise multilayer magnetometers discussed in Secs. VI.C and VI.D, each layer is patterned by Ar-ion beam etching. To obtain the gently sloped edges on the lower layers, essential for the epitaxial growth of subsequent layers, one usually bakes the photoresist after development, yielding to a significant rounding of the edges (David *et al.*, 1994). The subsequent Ar-ion milling at an angle of typically $45\text{--}60^\circ$ produces edges on the patterned film with ramp angles below 20° . Another key issue is the protection of the surface of the lower YBCO film, since photoresist attacks the YBCO surface thus degrading the growth of subsequent layers (Ludwig, Koelle *et al.*, 1995). To protect the YBCO, one commonly deposits an *in situ* SrTiO_3 layer, 20–50 nm thick, over the lower YBCO film, thus preventing its contact with photoresist (Missert *et al.*, 1993). Alternatively, a brief Ar-ion beam etch has been used to clean the surfaces before the deposition of the next layer (Keene, Goodyear *et al.*, 1994; Shen *et al.*, 1995). With these techniques, critical-current densities up to $3 \times 10^6 \text{ A cm}^{-2}$ for crossovers (Ludwig, Koelle *et al.*, 1995) and above $1 \times 10^6 \text{ A cm}^{-2}$

for vias (DiIorio, Yoshizumi, Yang, Maung, Zhang, and Power, 1993; Keene *et al.*, 1993) have been achieved in separate test structures at 77 K.

E. $1/f$ Noise in YBCO films

As we pointed out earlier, the main requirement for YBCO films used in SQUIDS is a low level of the magnetic flux noise generated by the thermally activated motion of flux vortices. To optimize the deposition process one should, in principle, measure the flux noise of each YBCO film. To our knowledge, such noise measurements have been performed only by the Berkeley group. As a simpler alternative, many groups measure the critical-current density j_c as an estimate of the flux pinning, but one must be careful in drawing conclusions about flux noise from measurements of j_c . These measurements are generally performed with strong driving forces applied by currents, and thus provide information on the pinning of the vortex lattice, that is, on the pinning forces. In contrast, flux noise measurements, performed in weak magnetic fields (below 10^{-4} T) reflect the dynamics of weakly interacting vortices in the superconducting sample and probe their pinning energies. For example, Ludwig, Koelle *et al.* (1995) found that *ex situ* YBCO/ SrTiO_3 /YBCO trilayers exhibited relatively high levels of flux noise despite the fact that similar test structures had high critical-current densities in both YBCO films. Furthermore, flux noise measurements on YBCO single crystals irradiated with protons or heavy ions indicated that protons proved to be more effective in reducing the flux noise while both produced comparable increases in critical-current density (Shaw *et al.*, 1996).

To study the flux noise in high- T_c thin films and single crystals, Ferrari *et al.* (1988, 1989, 1994) measured their fluctuating magnetization using a low- T_c , thin film SQUID in the shape of a 1-mm-square washer. The SQUID was operated in a flux-locked loop with a typical flux noise of $2\mu\Phi_0 \text{ Hz}^{-1/2}$ at 1 Hz. The experiment was designed to allow tight inductive coupling between the SQUID, maintained at or near 4.2 K, and the sample, the temperature of which could be raised to above T_c . Subsequently, the availability of high- T_c SQUIDS with low levels of $1/f$ noise allowed the measurement of the flux noise of high- T_c films in liquid nitrogen more straightforwardly by mounting them directly on such a SQUID, patterned into a 0.5-mm-square washer, with a typical flux noise of $15\mu\Phi_0 \text{ Hz}^{-1/2}$ at 1 Hz (Koelle *et al.*, 1993; Ludwig, Koelle *et al.*, 1995; Ludwig, Dantsker, Koelle, Kleiner, Miklich, and Clarke, 1995).

In their early work, Ferrari *et al.* (1988) found that the $1/f$ flux noise of a YBCO thin film decreases dramatically as the crystalline quality of the sample improves. For example, for a polycrystalline YBCO film they found a flux-noise power of $3 \times 10^{-4} \Phi_0^2/\text{Hz}$ at 1 Hz and 40 K, whereas values below $10^{-10} \Phi_0^2/\text{Hz}$ at 1 Hz and 77 K were obtained for high-quality epitaxial YBCO films (Shaw *et al.*, 1996). On the other hand, for YBCO single crystals, the flux-noise power at 1 Hz was more than a factor of 50 higher than the latter value, even after the

incorporation of artificial defects by proton irradiation (Shaw *et al.*, 1996). This result indicates that there must be a high density of effective, intrinsic pinning sites in high-quality (that is, magnetically quiet) epitaxial YBCO films, but unfortunately, little is known about their nature. Thus a film with low $1/f$ flux noise may have pinning sites with high activation energies or short hopping distances, or a combination of both; alternatively, the sample may simply contain fewer vortices. Studies in which various parameters controlling sample quality are systematically and independently varied are very much needed to shed light on these issues. Furthermore, the microstructural quality of patterned film edges may also be crucial, although its impact on $1/f$ noise has yet to be clarified.

The general tendencies observed for single YBCO films also apply to multilayers. Since the upper YBCO film in patterned YBCO/insulator/YBCO trilayers tends to be of poorer quality than a single YBCO film, its flux noise is generally higher. Nevertheless, Ludwig, Koelle *et al.* (1995) and Ludwig, Dantsker, Koelle, Kleiner, Miklich, and Clarke (1995) have demonstrated that a careful optimization of the multilayer fabrication process allows one to fabricate *ex situ* trilayers with low levels of $1/f$ flux noise.

Last, the level of $1/f$ noise in a given film generally increases strongly with the ambient magnetic field in which it is cooled unless its linewidth is made sufficiently narrow. These issues are deferred to Sec. IX.

IV. HIGH- T_c JOSEPHSON JUNCTIONS

The requirements for a successful junction technology include a nonhysteretic I - V characteristic, with properties close to the predictions of the RSJ model, a high I_0R product, controllable and reproducible parameters (I_0, R, C), high yield, high stability under room-temperature storage and thermal cycling, and low $1/f$ noise. These requirements are very well satisfied in low- T_c junctions by the Nb- Al_2O_3 -Nb trilayer technology (Gurvitch *et al.*, 1983). Unfortunately, a comparable high- T_c technology does not yet exist, for the following reasons: First, in contrast to Nb, high- T_c materials require epitaxial growth, imposing severe constraints on the choice of materials and processing techniques. Second, again in contrast to Nb, the superconducting coherence length ξ is both short and highly anisotropic, typically 2 nm in the ab -plane and 0.2 nm in the c -axis direction. As a result, the properties of high- T_c materials are highly susceptible to structural and chemical changes on atomic length scales; in particular, the superconducting order parameter can be strongly suppressed at a superconductor-insulator interface, in turn reducing the I_0R product substantially (Deutscher and Müller, 1987). Thus the superconducting electrodes need to have perfect crystallinity, and a well-defined interface has to be achieved within a single unit cell. Third, the barrier materials are generally oxides close to a metal-insulator transition with a complex crystal structure and a strong sensitivity to defects on an atomic length scale.

As a result, transport across the barrier is highly dependent on microstructural imperfections in the barrier and at its interface with the electrodes. Thus a well-defined barrier with high crystalline quality and homogeneity is required.

In the following we review those types of high- T_c junctions which have been most successfully used in SQUIDS. We divide them into two classes (Gross *et al.*, 1997): junctions with intrinsic interfaces and junctions with extrinsic interfaces. We do not discuss a third class, junctions without interfaces (weakened structures), since these have not been used widely in practical devices.

A. Junctions with intrinsic interfaces

The strong anisotropy of high- T_c superconductors with respect to both crystal structure and transport properties provides the basis for new types of weak links exploiting *intrinsic* interfaces and/or barriers. This new class of Josephson junctions, which has no analog in low- T_c superconductors, involves either the weak coupling in the ab plane between two superconducting grains with different orientations, the so-called grain-boundary junctions (GBJ's), or the intrinsic Josephson effect in the c -axis direction. While the feasibility of intrinsic Josephson junctions (Kleiner *et al.*, 1992; Kleiner and Müller, 1994) for SQUIDS has not been demonstrated, GBJ's were the basis of the first dc SQUIDS fabricated from polycrystalline thin films of YBCO (Koch *et al.*, 1987). Although grain sizes and orientations were uncontrolled, these devices provided the first evidence that high- T_c grain boundaries act as junctions and may be used in SQUIDS. Shortly after, junctions and dc SQUIDS were fabricated across single grain boundaries in epitaxial YBCO films on polycrystalline STO substrates (Tsuei *et al.*, 1989; Hagerhorst *et al.*, 1989). Subsequently, engineered GBJ's were developed, and the most important types are bicrystal, and step-edge GBJ's [Fig. 9(a) and (b)]. Although important historically, biepitaxial GBJ's (Char *et al.*, 1991) are no longer used for SQUIDS, because of their small I_0R products. For reviews on GBJ's see Gross (1994) and Gross *et al.* (1995).

1. Bicrystal grain-boundary junctions

The key to both the development of a useful high- T_c Josephson junction technology and the understanding of transport across grain boundaries was provided by the pioneering work at IBM, Yorktown Heights on bicrystal GBJ's (Chaudhari *et al.*, 1988; Dimos *et al.*, 1988; Manhart *et al.*, 1988; Dimos *et al.*, 1990; Gross *et al.*, 1990a, 1990b, 1991). These junctions are fabricated by the epitaxial growth of a high- T_c thin film on a bicrystal substrate with a predetermined misorientation angle θ [Fig. 9(a)]. In contrast to other GBJ fabrication techniques, this method can be used to obtain arbitrary misorientation angles and geometries, such as [001] and [100] tilt or [100] twist grain boundaries (Dimos *et al.*, 1990), enabling a systematic study of transport across high- T_c grain boundaries. Their straightforward fabrication

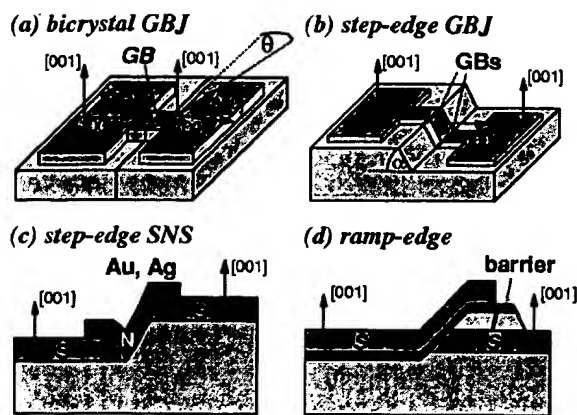


FIG. 9. Types of high- T_c Josephson junctions.

makes these junctions the most reliable and successful currently available, both for SQUIDS and more generally for any application which does not require many junctions at arbitrary positions on the substrate. Any substrate which supports the epitaxial growth of high- T_c films is suitable, including SrTiO_3 (Dimos *et al.*, 1988), YSZ (Ivanov *et al.*, 1991), Si (Chen *et al.*, 1991), NdGaO_3 (Quincey, 1994), MgO (Beck *et al.*, 1995), LaAlO_3 (Chen *et al.*, 1996), and r plane Al_2O_3 (Sapphire) (Vale *et al.*, 1997). Most work on bicrystal junctions has involved YBCO, but other superconductors have been investigated, including $\text{Bi}_2\text{Sr}_2\text{CaCu}_2\text{O}_8$ (Mayer *et al.*, 1993), $\text{Tl}_2\text{Ba}_2\text{CaCu}_2\text{O}_8$ (Kawasaki *et al.*, 1993), $\text{HgBa}_2\text{CaCu}_2\text{O}_6$ (Gupta *et al.*, 1994), and $\text{La}_{1.85}\text{Sr}_{0.15}\text{CuO}_4$ (Beck *et al.*, 1996).

Bicrystal junctions generally exhibit characteristics reasonably close to the RSJ model, provided θ exceeds a critical value, about 10° for YBCO (Dimos *et al.*, 1990; Gross, 1994). The critical-current density j_c for YBCO junctions decreases exponentially with increasing θ (Gross and Mayer, 1991; Ivanov *et al.*, 1991). This behavior is explained in part by the faceting of the grain boundary combined with d -wave pairing symmetry (Hilgenkamp *et al.*, 1996); however, it seems likely that a further contribution arises from an increase of the barrier thickness with increasing θ . For fixed θ , the critical-current density can be changed by more than one order of magnitude by appropriate annealing in oxygen (Kawasaki *et al.*, 1992), implying that the barrier thickness or height depends on oxygen content. Most SQUIDS have been made on 24° or 36° bicrystals, but recently 30° bicrystals have also become commercially available. At 77 K the $I_0R(j_c\rho_n)$ product of such junctions made from c -axis YBCO films on 24° bicrystals is typically 0.1–0.3 mV; comparable values have recently been reported on 30° bicrystals (Minotani, Kawakami *et al.*, 1997; Beyer *et al.*, 1998). The corresponding critical-current density j_c is of the order of 10^4 A/cm^2 at 77 K and the temperature-independent specific resistance-area product ρ_n is about $10^{-8} \Omega \text{ cm}^2$. Although standard deviations in I_0R of around 20% have been reported for junctions on a given bicrystal (Miklich *et al.*, 1993), the

parameters often vary much more widely because of variations in the quality of the bicrystal substrate (McDaniel *et al.*, 1997).

2. Step-edge grain-boundary junctions

The step-edge GBJ, which is also widely used, is based on the fact that an epitaxially grown, c -axis YBCO film changes its orientation at a steep step in the substrate or deposited dielectric [Fig. 9(b)]. This technique, initially realized by Simon *et al.* (1991), was subsequently refined by several groups (Herrmann *et al.*, 1991; Sun, Gallagher, Callegari *et al.*, 1993; Herrmann *et al.*, 1995; Pettiette-Hall *et al.*, 1995; Yi *et al.*, 1996). Common substrate materials are SrTiO_3 and LaAlO_3 . For large step angles ($\alpha > 70^\circ$) the two grain boundaries grow with different orientations, causing the lower junction to have a much lower critical-current density than the upper junction (Jia *et al.*, 1992). Thus, at least for currents not too far above I_0 , the junction properties are determined solely by the lower grain boundary.

The substrate steps are aligned along major cubic axes of the substrate, and are usually patterned by standard lithography and Ar-ion milling so that their location can be chosen at will. This advantage over the bicrystal technique enables one to fabricate more complex circuits. Even for SQUIDS which require only one or two junctions, this flexibility in layout can be important, for example, for minimizing parasitic inductances.

It has been proposed that the grain boundaries formed at step edges behave as junctions because of their defect structure (Herrmann *et al.*, 1995), since 90° grain boundaries in planar films do not exhibit such behavior. Thus the properties of step-edge junctions depend strongly on the microstructure of the milled step and on the film-growth conditions, leading to greater spreads in parameters than for bicrystal junctions. The use of carbonlike diamond masks and very low milling rates improve the definition of the steps, and hence their reproducibility (Sun, Gallagher, Callegari *et al.*, 1993; Yi *et al.*, 1996). Dillmann *et al.* (1996) have used annealing processes to trim the parameters of their junctions. For a detailed review of the fabrication of step-edge junctions for SQUIDS, see Braginski (1996).

B. Junctions with extrinsic interfaces

This class of junctions involves a thin, deposited interlayer of insulating or normal material between two superconducting electrodes. Hence extrinsic interfaces are involved, and the control of their properties requires an advanced fabrication technology, usually involving the heteroepitaxial growth of high- T_c and interlayer materials. The transport and noise properties of these junctions are even less well understood than those for GBJ's. Although low-noise SQUIDS based on these junctions have been reported, the absence of reproducible fabrication processes has hindered their widespread use. Figures 9(c) and (d) illustrate two possible configurations:



the step-edge junction with a non-epitaxial noble-metal interlayer, and the ramp-edge junction with an epitaxially grown interlayer.

1. Step-edge SNS junctions

DiIorio *et al.* (1991), DiIorio, Yoshizumi, Yang, Maung, Zang, and Power (1993), and DiIorio *et al.* (1995) introduced the SNS junction illustrated in Fig. 9(c), and systematic studies of their properties have been carried out at NIST (Ono *et al.*, 1991, 1993; Rosenthal *et al.*, 1993; Reintsema *et al.*, 1995) and FZ Jülich (Grove *et al.*, 1996; Bode *et al.*, 1996). In principle, fabrication is simple: one cuts a steep step in the substrate, 50–100 nm high, using photolithography and Ar-ion milling, and deposits a high- T_c film directionally, so that the film does not grow on the step. Without breaking vacuum, one fills the gap by directional deposition of a Au or Ag layer, which makes contact to the a - b planes of the high- T_c films.

Very high I_0R products, up to 1 mV at 77 K, and high normal resistance, above 10 Ω for 4–8 μm widths, have been reported. However, the transport and noise properties are still unsettled issues. The I - V characteristics often exhibit excess current. The normal resistance appears to be determined by the boundary resistance at the SN interfaces, and various models for the transport have been suggested, for example, SINIS (Reintsema *et al.*, 1995) or ScNS (Bode *et al.*, 1996); c denotes point contacts at the SN interfaces. The major problem appears to be the lack of control of the interface properties which determine R and are most likely responsible for the large spreads in I_0 . These difficulties have hindered the widespread application of this type of junction to SQUIDS.

2. Ramp-edge Josephson junctions

These junctions require the fabrication of an epitaxial trilayer with two superconducting electrodes separated by a thin barrier layer. Current transport is along the a - b planes of the c -axis oriented electrode films, taking advantage of the larger coherence length along this direction. One fabricates a ramp-edge junction [Fig. 9(d)] by first depositing a YBCO film and covering it with a thick, insulating film. Next, one patterns a ramp with a shallow angle (typically 10° to 20°) using ion milling or anisotropic wet etching, and finally deposits the barrier material and top electrode *in situ*. The top electrode effectively shields the magnetic-field component normal to the film surface. Hence ramp-edge junctions may offer an important advantage over planar GBJ's for operation in magnetically unshielded environments. Furthermore, ramp-edge junctions may be more robust against aging and thermal cycling compared to GBJ's since the barrier/interfaces are not directly exposed to the environment.

Gao *et al.* (1990, 1992) pioneered ramp-edge junctions with YBCO electrodes and a $\text{PrBa}_2\text{Cu}_3\text{O}_7$ barrier. Subsequently, many other barrier materials such as ruthenates or doped YBCO have been investigated (see, for

example, Gross *et al.*, 1997 and references therein). The key requirement is a lower electrode with a smooth ramp edge of excellent crystalline quality to support the growth of a thin, homogenous barrier. Thus any damage caused by milling the ramp or by its exposure to air has to be healed prior to deposition of the barrier. The need to pattern the ramp with an *ex situ* process can be avoided by patterning the lower electrode with a microshadow mask (Strikovskiy and Engelhardt, 1996).

Ramp-edge junctions with Ca- or Co-doped YBCO barriers show behavior close to proximity effect coupling (Kleinsasser and Delin, 1995; Delin and Kleinsasser, 1996), with low or negligible interface resistance, but with junction resistances too low for SQUID applications. On the other hand, for ruthenate or PBCO barriers the junction resistance is dominated by interface resistance rather than the intrinsic barrier resistivity, and transport is explained via tunneling through localized states in the barrier or interface, which has a high defect density (Dömel *et al.*, 1995; Satoh *et al.*, 1995; Schilling, 1997). Using bromine etching to form the ramp, Faley, Poppe, Jia *et al.* (1995) fabricated a quasiplanar junction with PBC(Ga)O barriers that exhibited negligible interface resistance; hence the resistance of these junctions scaled with barrier thickness. Junctions 5 μm wide and with barriers 20 nm thick exhibited I - V characteristics close to that of the RSJ model with $I_0R \sim 200 \mu\text{V}$ and $R \sim 1 \Omega$ at 77 K, making them good candidates for SQUIDS.

C. Discussion of high- T_c junctions

For most high- T_c junctions, one finds the following common properties:

- (i) They are internally shunted and at 77 K produce I - V characteristics reasonably close to the RSJ model. The most common deviation from the RSJ characteristic is an excess supercurrent. Possible candidates for its origin are a nonsinusoidal current-phase relation (Ilichev *et al.*, 1998), superconducting shorts through the barrier, or Andreev reflection at the barrier interfaces (Alff *et al.*, 1998). At lower temperatures, that is, higher critical currents, the characteristics may become hysteretic, implying that even at 77 K β_c may not be too much below unity.
- (ii) The critical-current density generally increases linearly with decreasing temperature, while, at least for GBJ's, the resistance-area product ρ_n is nearly independent of temperature (Gross, 1994).
- (iii) The I_0R ($j_c\rho_n$) products are smaller than the gap voltage, typically below 300 μV at 77 K. Values of $j_c\rho_n$ up to about 1 mV at 77 K have been reported for some junctions, but always seem to be associated with large excess currents. Grain-boundary junctions (Gross, Chaudhari, Kawasaki *et al.*, 1990; Russek *et al.*, 1990; Hermann *et al.*, 1991) and junctions with artificial barriers show a scaling $j_c\rho_n \propto (j_c)^p$, where $p \approx 0.5$ over seven orders of

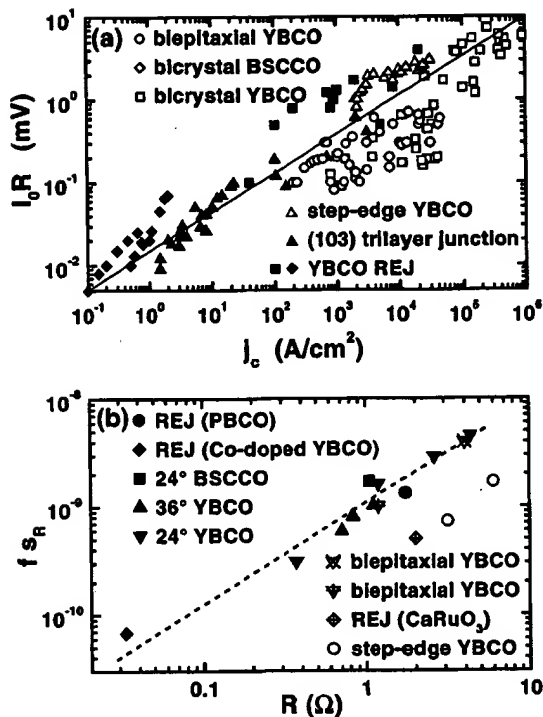


FIG. 10. Scaling behavior of various high- T_c Josephson junctions: (a) I_0R product vs critical current-density j_c at 4.2 K; a line with slope 0.5 has been drawn through the data (Gross *et al.*, 1997); (b) $f s_R$ vs normal resistance R ; the dashed line is a guide to the eye (Marx and Gross, 1997).

magnitude in j_c , as shown in Fig. 10(a) (Gross, 1994; Gross *et al.*, 1997, and references therein).

- (iv) Most junctions exhibit large levels of low-frequency $1/f$ noise arising from fluctuations of the critical current and the junction resistance (Kawasaki *et al.*, 1992; Miklich *et al.*, 1992; Marx, Fath *et al.*, 1995). The normalized spectral densities $s_I \equiv S_{I_0}/I_0^2$ and $s_R \equiv S_R/R^2$ for critical-current and resistance fluctuations are temperature independent and proportional to the junction resistance (Marx and Gross, 1997), as shown in Fig. 10(b). Defining $S_{I_0}/I_0^2 = a^2/f$ one finds typically $a^2 \approx 10^{-8} R/\Omega$, which is about three orders of magnitude larger than for Nb junctions with shunt resistances of a few ohms (Foglietti *et al.*, 1986; Savo *et al.*, 1987). Furthermore, the relation $(s_I/s_R)^{1/2} \approx 1/(1-p)$ observed for GBJ's (Gross, 1994; Marx, Fath *et al.*, 1995) strongly suggests that the low-frequency noise and scaling of I_0R have the same microscopic origin.

The universal scaling of $j_c \rho_n$, s_I , and s_R is an important feature of high- T_c junctions because it may be the key to understanding their transport and noise properties and offers the possibility of adjusting important junction parameters for optimum SQUID performance. The fact that both GBJ's and junctions with artificial barriers have the same scaling suggests a common transport mechanism governed by thin interface layers. However, the details of this mechanism are still controversial.

Since proximity effect coupling cannot explain the observed transport properties for the vast majority of junctions, several models have been proposed that include the effects of a boundary resistance between S and N layers (SNIS, SINIS) (Kupriyanov and Likharev, 1990) or of constrictions (ScNS, SNcNS) (Aminov *et al.*, 1996; Golubov and Kupriyanov, 1996). On the other hand, for grain-boundary junctions it has been proposed that resonant tunneling of quasiparticles via localized states in an insulating barrier acts as an intrinsic normal shunt (Gross and Mayer, 1991). This model, known as the intrinsically shunted junction model, naturally explains the low I_0R product in terms of an intrinsic shunt due to a high density of localized states. The universal scaling of I_0R with j_c suggests that the density of localized states is about the same in all junctions. The trapping and release of charge carriers in localized states lead to fluctuations in the local barrier height which cause I_0 and R to fluctuate with antiphase correlation (Marx, Alff *et al.*, 1995), thus explaining the high level of $1/f$ noise in junctions with a high density of localized states. The same scaling of I_0R with j_c is predicted by a channel model (Moeckly *et al.*, 1993) in which the Josephson current in GBJ's is restricted to narrow superconducting filaments in a weakly conducting medium. However, this model cannot account for the observed phase correlation of I_0 and R fluctuations, since the superconductive and resistive channels are spatially separated.

The scaling behavior described above has important consequences for the optimization of SQUIDS. At $T = 77$ K, j_c is typically 10^4 A/cm² for 24° YBCO grain boundaries, corresponding to $I_0R \approx 100$ μ V. Hence for junctions of width w and thickness $d \approx 200$ nm critical currents of about 20 μ A (w/μ m) are typical. Thus to achieve $\beta_L = 1$ for an inductance $L \approx 50$ pH one requires $w \sim 1$ μ m, close to the minimum linewidth achievable with photolithography. Increasing I_0R with oxygen annealing or reducing the misorientation angle may not be very useful unless one can achieve submicron patterning without significant damage to the edges of the film. We note that for $p = 0.5$, an increase in I_0R by a factor of 3 requires an increase in j_c by an order of magnitude. An alternative to submicron patterning may be thinning of the film in the junction region; however, this approach is not applicable to all types of junctions, may be detrimental to the junction properties, and can contribute a significant kinetic inductance.

Clearly, it is highly desirable to have a lower critical-current density for the same I_0R product, but this would require reduction of the density of localized states which, in turn, would result in an increase of ρ_n for fixed j_c . Even if this goal could be achieved, since $\beta_c \propto j_c \rho_n^2 C_s$ increases with ρ_n^2 for fixed j_c and C_s , such junctions may become hysteretic at 77 K. In contrast, a change in $I_0R \propto j_c^{1/2}$ causes $j_c \rho_n^2$ to be constant and leaves β_c approximately unchanged (neglecting the change in the specific capacitance C_s with effective barrier thickness). Although junctions with high values of ρ_n are occasionally reported in the context of high performance

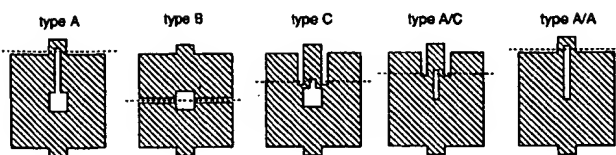


FIG. 11. Five configurations of planar dc SQUID fabricated at Berkeley. Dashed lines indicate the bicrystal boundary along which the junctions are formed. Outer dimension is typically $500 \times 500 \mu\text{m}^2$.

dc SQUIDS (Lee *et al.*, 1995; Glyantsev *et al.*, 1996), detailed data on their transport characteristics have not been presented.

For the optimization of SQUIDS a detailed knowledge of the junction transport mechanism may not be necessary. However, control of the junction parameters is essential, and may only be possible if the transport mechanism is understood. This, in turn, may require the fabrication of junctions with well-defined interfaces and barriers. Such a technology is not yet at hand: spreads in I_0 and R are typically $\pm 20\%$ on chip and usually much higher from chip to chip. Although these large spreads may be unacceptable for applications which require many junctions, they have not prevented the fabrication of low noise SQUIDS. Nevertheless, to allow a more systematic study of SQUID performance and to clarify discrepancies between experimental results and theory for high- T_c dc SQUIDS (Sec. V.C), a more reproducible technology is highly desirable. To complicate the issue, integrated SQUID magnetometers may require the incorporation of high-quality junctions into low-noise thin-film multilayers. The successful integration of a controllable, high-yield junction technology with a low-noise multilayer technology has still to be demonstrated.

V. dc SQUIDS

A. Practical devices

Early high- T_c dc SQUIDS were generally fabricated in the geometry of a square washer, following the most widely used configuration of low- T_c SQUIDS (Ketchen, 1981; Jaycox and Ketchen, 1981). Figure 11 shows a selection made at Berkeley. In these devices, it was implicitly assumed that ultimately the SQUIDS would be inductively coupled to flux transformers with planar, spiral input coils as is common practice with low- T_c magnetometers. Subsequently, various other magnetometer configurations emerged, in addition to the multiturn flux transformer (Sec. VI.C), and for reasons of minimizing the $1/f$ noise in ambient magnetic fields (Sec. IX.A) it is desirable to make SQUIDS with rather narrow linewidths. Thus a wide variety of SQUID configurations have been investigated, and we do not attempt to review them here; rather we shall describe some of the more useful types in Sec. VI in the context of magnetometers. Most SQUIDS are still made with either bicrystal or

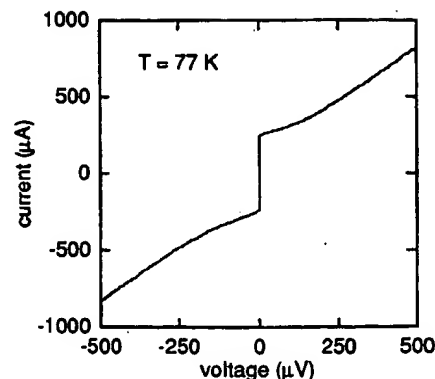


FIG. 12. I - V characteristics of bicrystal, type B dc SQUID at 77 K; $L = 41 \text{ pH}$, $I_0 = 120 \mu\text{A}$, $R = 1.28 \Omega$.

step-edge grain-boundary junctions, and these have yielded the highest performance to date.

With few exceptions, the SQUID is immersed directly in liquid nitrogen. To attenuate external magnetic-field fluctuations, above all the ubiquitous 50 or 60 Hz fields and their harmonics, one may surround either the dewar with a mu-metal shield or the SQUID with a high- T_c shield. Mu-metal shields have the advantage of reducing both the ambient static field and time-varying field substantially, while high- T_c shields generally offer greater attenuation of time-varying fields, but do not reduce the ambient field if they are cooled in it. Thus a combination of both types of shields is often desirable in evaluating the intrinsic noise of SQUIDS. It is also imperative to exclude radio-frequency interference, most commonly by running the measurement in a screened room.

Figure 12 shows a representative I - V characteristic for a YBCO SQUID, grown on a STO bicrystal, operated at 77 K. In Fig. 13 we have plotted the voltage V across the SQUID vs the applied flux Φ for a series of bias currents. As the current is increased, the amplitude of the oscillations increases smoothly to a maximum and then decreases. The SQUID is normally operated at the bias current that gives the maximum value of V_Φ .

B. Readout schemes

In virtually all applications, SQUIDS are operated in a flux-locked loop in which the voltage change across the

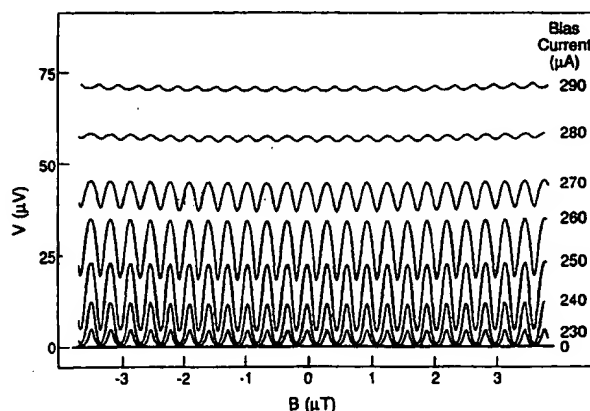


FIG. 13. V vs Φ for dc SQUID of Fig. 12 for seven values of bias current.

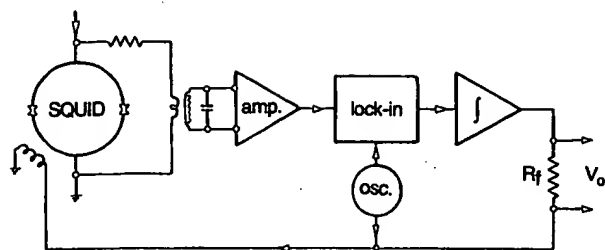


FIG. 14. Flux-locked loop for dc SQUID.

SQUID induced by an applied flux is amplified and fed back as an opposing flux. This feedback circuit linearizes the response of the SQUID, provides a straightforward means of measuring the intrinsic noise of the SQUID, and enables one to track inputs equivalent to many flux quanta. The input stage of the electronic circuitry is designed to add negligibly to the intrinsic noise of the SQUID. Drung (1996) has given a detailed review of a variety of schemes; here we review briefly the two most commonly used.

1. Flux modulation

In the widely used flux modulation scheme (Forgacs and Warnick, 1967), shown in Fig. 14, one applies a sinusoidal or square-wave flux modulation to the SQUID with a peak-to-peak amplitude of $\Phi_0/2$ and a frequency f_m of typically 100 kHz. The resulting alternating voltage across the SQUID is coupled to a room-temperature preamplifier via either a cooled LC series-resonant circuit (Clarke *et al.*, 1976) or a cooled transformer (Ketchen *et al.*, 1978). The voltage gain of either coupling circuit is usually chosen to transform the dynamic resistance of the SQUID at its operating point to the value required to optimize the noise temperature of the preamplifier. Since this noise temperature is typically a few kelvin, the preamplifier contributes negligible noise to a device operating at 77 K. After amplification, the signal is lock-in detected at the frequency f_m . If the quasistatic flux is $n\Phi_0$ (n is an integer), the V - Φ curve is symmetric about this local minimum and the voltage contains components only at the frequency $2f_m$. Thus the output of the lock-in detector is zero. On the other hand, if the flux is shifted away slightly from the local minimum, the voltage across the SQUID contains a component at frequency f_m and there will be an output from the lock-in detector. After integration (cf. Fig. 14), this signal is fed back as a current through a feedback resistor R_f to a coil inductively coupled to the SQUID; usually the same coil is used for both flux modulation and feedback. The flux fed back opposes the applied flux to keep the flux in the SQUID constant; the voltage developed across R_f is proportional to the applied flux. One can measure the intrinsic flux noise of the SQUID by connecting the output voltage to a spectrum analyzer in the absence of any input signal.

Ideally, the bandwidth for an optimized flux-locked loop extends to one half the modulation frequency. For unshielded applications in which the SQUID is exposed

to the magnetic noise of the environment, a more important figure of merit is often the slew rate, that is, the maximum rate of change of flux that the system is able to track without losing lock. For an ideal single-pole integrator, the slew rate is $2\pi f_1 \Phi_0/4$, where f_1 is the frequency at which the open-loop gain of the feedback loop falls to unity (Drung, 1996). A considerable improvement in the slew rate at low frequencies can be achieved by means of a two-pole integrator (Giffard, 1980; Wellstood *et al.*, 1984). Using a high- T_c SQUID with a 500-kHz flux modulation and a single-pole filter, Dantsker *et al.* (1994) obtained a slew rate of $10^5 \Phi_0 \text{ s}^{-1}$ at 900 Hz. Recently, Koch *et al.* (1996) described a flux-locked loop with a modulation frequency of 16 MHz, using a resonant matching circuit with a superconducting, thin-film transformer to match the SQUID to the amplifier. The system had a closed-loop bandwidth exceeding 2.5 MHz and a slew rate greater than $10^6 \Phi_0 \text{ s}^{-1}$ at frequencies up to 1 MHz. Subsequently, Penny *et al.* (1997) used a transmission-line transformer feeding a matched transmission line to couple the SQUID to the amplifier. With a low- T_c SQUID they achieved a bandwidth of 5 MHz, a slew rate of $1.9 \times 10^6 \Phi_0 \text{ s}^{-1}$ at 200 Hz, and a flux noise of $5.5 \mu\Phi_0 \text{ Hz}^{-1/2}$. The performance with high- T_c SQUIDS has not yet been reported.

A further issue of particular importance when the outputs of SQUIDS are subtracted to form electronic gradiometers (Sec. VIII.A) is the linearity of the flux-locked loop. To investigate the nonlinearity, Nichols *et al.* (1996) measured the harmonic generation using a high- T_c SQUID with 130-kHz flux modulation and a single-pole integrator. For input signals at frequencies up to 248 Hz and rms amplitudes up to $20 \Phi_0$, 2nd, 3rd, and 4th harmonics were each 115 dB below the fundamental. At higher frequencies the harmonic content began to increase because of the reduction in the open-loop gain. It was also shown that the amplitudes of the even harmonics depended critically on the amplitude of the 130-kHz flux modulation, becoming zero when the peak-to-peak value was precisely $\Phi_0/2$.

The slew rate and linearity that have been achieved are likely to be adequate for most applications in which the magnetometer is static. For situations in which the magnetometer is moved in the earth's magnetic field—for example, in towed systems—the demands are substantially higher, and the performance may or may not be adequate.

As will be shown later (Sec. V.D), fluctuations in the critical current and resistance of the junctions are a major source of $1/f$ noise in dc SQUIDS. Fortunately, their contributions can be greatly reduced by a number of schemes (Koch *et al.*, 1983; Foglietti *et al.*, 1986; Dössel *et al.*, 1991), which have been successfully applied to high- T_c SQUIDS (Koch *et al.*, 1992; Miklich *et al.*, 1993; Grundler, Eckart *et al.*, 1993). At the operating point of SQUIDS, the critical-current noise dominates the resistance noise and contributes $1/f$ noise in two ways. Fluctuations at frequencies $\ll f_m$ that are in phase at the two junctions give rise to a voltage noise across the SQUID that is eliminated by flux modulation at frequency f_m .

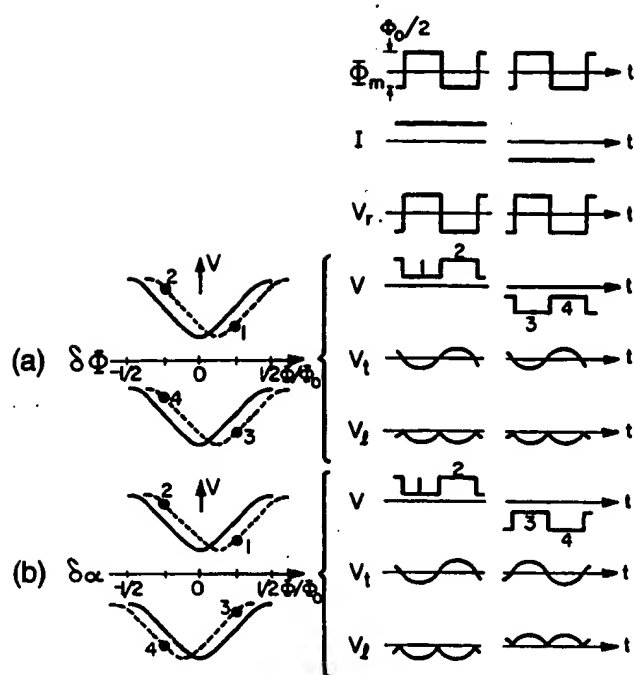


FIG. 15. Principle of bias-reversal scheme to reduce $1/f$ noise due to out-of-phase critical-current fluctuations. The left-hand column shows the V - Φ curves (solid lines), and the dashed lines indicate the effect of (a) an external flux change $\delta\Phi$ and (b) a flux change $\delta\alpha$ generated by out-of-phase critical-current fluctuations. The right-hand column shows, as a function of time t , (top to bottom) the flux modulation Φ_m , the bias current I , and the reference voltage V_r used to lock-in detect the signal from the SQUID; the next three rows are for an external flux change $\delta\Phi$, and show the voltage V across the SQUID, the voltage V_1 across the secondary of the tuned transformer and the output V_2 of the lock-in detector; the last three rows show the same voltages for an out-of-phase critical-current fluctuation (Koch *et al.*, 1983).

Fluctuations that are out-of-phase at the two junctions are equivalent to a flux noise that is not reduced by this scheme. Instead, one makes use of the fact that the apparent shift of the V - Φ characteristic along the flux axis changes polarity if one reverses the polarity of the bias current whereas the flux due to an input signal (or "flux noise") does not.

As an example of one of the bias-reversal schemes, we briefly describe that developed by Koch *et al.* (1983); the principle is illustrated in Fig. 15 and its implementation in Fig. 16. The SQUID is flux-modulated with a 100-kHz square wave of peak-to-peak amplitude $\Phi_m = \Phi_0/2$. Synchronously with the modulation, the bias current I through the SQUID is reversed, for example, at a frequency $f_r = 3.125$ kHz. The resistance bridge shown in Fig. 16 minimizes the 3.125 kHz switching transients across the transformer. Simultaneously with the bias reversal, a flux $\Phi_0/2$ is applied to the SQUID. In Figs. 15(a) and (b) we see that the bias reversal changes the sign of the voltage across the SQUID while the flux shift ensures that the sign of the flux-to-voltage transfer function remains the same. The transformer coupling the SQUID to the preamplifier is often tuned at the modulation frequency with a Q of about 3, so that any 100-kHz signals at the secondary are approximately sinusoidal.

We assume that the SQUID is operated in the usual flux-locked loop, with the output from the lock-in detector integrated and fed back to the SQUID (Fig. 16). Thus the 100-kHz signal across the SQUID consists of just the error signal. Suppose now that we apply a small external flux $\delta\Phi$ to the SQUID at a frequency well below f_r . The V - Φ curves are shifted as in Figs. 15(a), and the 100-kHz flux modulation switches the SQUID between the points 1 and 2 for positive bias and 3 and 4 for negative bias. As a function of time, the voltage V across

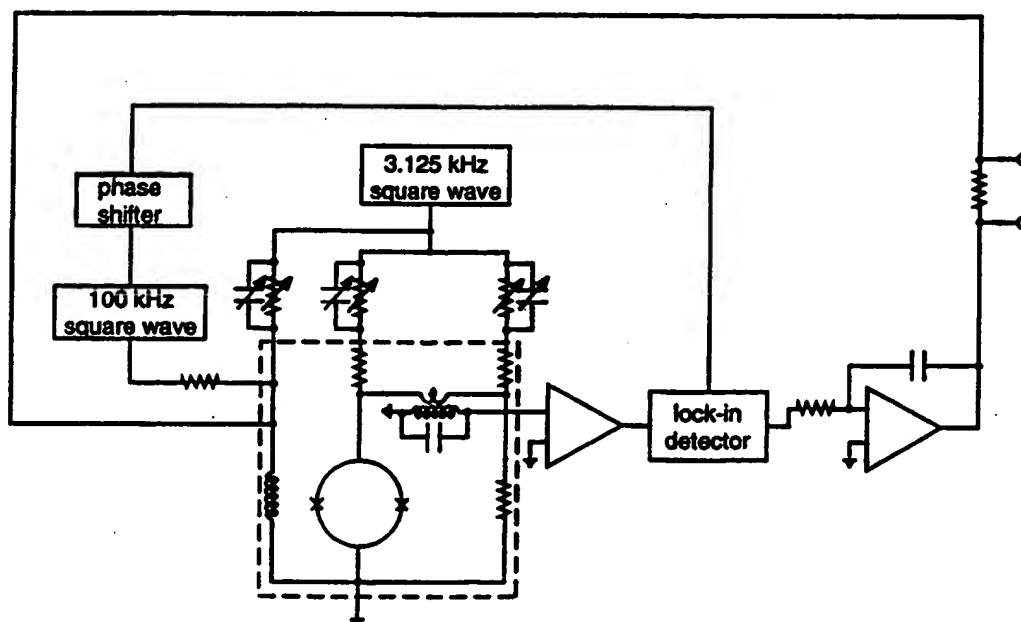


FIG. 16. Schematic for flux-locked loop with bias current reversal. Cryogenic components are enclosed in the dashed box (Koch *et al.*, 1983).

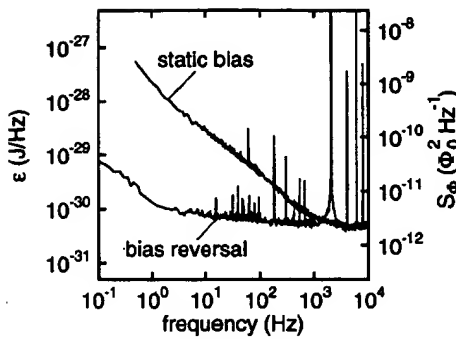


FIG. 17. Spectral density of flux noise of representative high- T_c dc SQUID with flux modulation and bias current reversal.

the SQUID is as shown in Fig. 15, and the signal across the tuned transformer V_t is at the fundamental frequency. When this signal is mixed with the reference voltage V_r , the output from the lock-in detector V_L will consist of a series of negative-going peaks for both polarities of the bias current. The average of this output produces a negative signal proportional to $\partial\Phi$ which is then used to cancel the flux applied to the SQUID. Thus, in the presence of bias reversal and flux shift, the SQUID responds to an applied flux in the usual way.

We consider now the effects of $1/f$ noise on the critical currents. The in-phase mode is eliminated by the 100-kHz flux modulation. Suppose, instead, we have an out-of-phase critical-current fluctuation at a frequency below f_r . Because the flux generated by this fluctuation *changes sign* when the bias current is reversed, the V - Φ curves are displaced in opposite directions. As a result, the voltage across the SQUID undergoes a phase change of π when the bias current is reversed, as shown in Fig. 15. Consequently, the voltage at the output of the lock-in due to the out-of-phase critical-current fluctuation changes sign each time the bias current is reversed, and the time average of the signal over periods much longer than $1/f_r$ is zero. Thus the $1/f$ noise due to both in-phase and out-of-phase critical-current fluctuations is eliminated by this scheme.

Figure 17 shows the spectral density of the flux noise of a representative SQUID operated with flux modulation and with and without bias reversal. Without bias reversal, $1/f$ noise is evident for frequencies below about 2 kHz. The application of bias reversal reduces the level of $1/f$ noise dramatically, by two orders of magnitude at 1 Hz, demonstrating that the $1/f$ noise indeed arose from critical-current fluctuations.

2. Direct readout

A "direct readout" scheme eliminates the need for a coupling network between the SQUID and the amplifier, and enables one to use particularly simple electronics for the flux-locked loop (Drung, 1994). In addition, it allows one to achieve bandwidths around 10 MHz relatively easily (Drung, 1996). The output of the current-biased SQUID is connected directly to one terminal of a low-noise, bipolar amplifier; an offset bias voltage is applied to the other terminal. After amplification, the sig-

nal is integrated and fed back via a resistor to a coil coupled to the SQUID. Since the preamplifier noise, typically $1 \text{ nV Hz}^{-1/2}$, usually dominates the SQUID noise, typically $0.1 \text{ nV Hz}^{-1/2}$ for low- T_c SQUIDS, it must be reduced to a tolerable level by increasing the transfer function. In the additional positive feedback (APF) scheme (Drung *et al.*, 1990) this increase is achieved by shunting the SQUID with an inductor L_a , with a mutual inductance M_a to the SQUID, in series with a resistor R_a . When the SQUID is current biased, a change in the voltage across the SQUID due to an applied flux generates a current through the shunting network and a flux in the SQUID. Thus the V - Φ characteristic becomes asymmetric, and the transfer function is enhanced by a factor $1/(1 - G_a)$ in the region of positive feedback; here

$$G_a = [M_a + (\partial\Phi/\partial I)_V] V_\Phi / R_a \quad (5.1)$$

is the APF gain. The maximum slew rate is concomitantly reduced by a factor $(1 - G_a)$. Thus for wideband systems G_a should be just high enough to make the effect of the preamplifier voltage noise negligible compared to the intrinsic SQUID noise. For a low- T_c SQUID and an effective APF gain of 0.57, a flux-locked bandwidth of 5 MHz was achieved with a white flux noise of $3.4 \mu\Phi_0 \text{ Hz}^{-1/2}$, corresponding to a magnetic-field noise of $1.6 \text{ fT Hz}^{-1/2}$. We note that the flux-to-current transfer coefficient of the SQUID at constant voltage, $(\partial\Phi/\partial I)_V$, is not affected by APF, so that the current noise of the amplifier may become important. If necessary, this contribution can be reduced by bias-current feedback (Drung and Koch, 1993).

To remove $1/f$ noise due to critical-current fluctuations, as for the flux-modulation scheme, one has to reverse the bias current (Drung, 1995); at the same time the bias voltage is reversed and a flux shift is applied to maintain the same polarity of the flux-to-voltage transfer function. Using this bias-reversal scheme, Ludwig *et al.* (1997) recently reported a modified, directly coupled flux-locked loop for high- T_c SQUIDS. Using a preamplifier with a voltage noise of $0.44 \text{ nV Hz}^{-1/2}$, their high- T_c SQUIDS could be operated without APF with a total rms white noise typically 20% higher than the intrinsic rms noise of the SQUID. For an optimum bias-reversal frequency of around 100 kHz, it was demonstrated that $1/f$ noise due to critical-current fluctuations can effectively be suppressed without increasing the white-noise level (Drung, Ludwig *et al.*, 1996; Drung, Dantsker *et al.*, 1996; Ludwig *et al.*, 1997). In addition, a maximum bandwidth of about 1 MHz and slew rates close to $10^6 \Phi_0/\text{s}$ were achieved.

C. White noise

In this section, we present data on the white noise measured by a number of groups: Biomagnetic Technologies, Inc., San Diego, Philips, Hamburg, University

of California, Berkeley, University of Hamburg, University of Jena, and University of Twente. The SQUIDS were made with either grain-boundary or SNS ramp-edge junctions. For the devices discussed, L ranged from 10 to 210 pH, and $I_0 R$ from below 10 μV to 300 μV . Although values of $I_0 R$ of 300 μV or larger are desirable, such values are generally achieved only with high values of I_0 . As a result, β_L is often well above unity, and sometimes greater than 10. Values of β_L near unity were achieved only for $I_0 R$ below 200 μV . One should bear in mind that some of the estimated values of L are likely to be rather uncertain, because of both the intricate geometries of the SQUID loops and the possible contributions of kinetic inductance (Töpfer and Uhlmann, 1994; Hildebrandt and Uhlmann, 1995).

We now compare the measured results with the theoretical predictions of Sec. II.C. Similar comparisons have been made by Enpuku (1993) and Enpuku *et al.* (1993, 1994), Enpuku, Tokita *et al.* (1995), Keene *et al.* (1995), and Koch (1997). To give an overview of SQUIDS with widely varying parameters, it is convenient to present the results in terms of the dimensionless parameters Γ , β_L , and $\Gamma\beta_L$. For the devices discussed, Γ ranges from 0.004 to 1.8, β_L ranges from 0.12 to 65, and $\Gamma\beta_L$ ranges from 0.03 to 0.65; the majority of the values of $\Gamma\beta_L$ are above the desirable upper limit of 0.15.

We begin by recalling from Sec. II that $v_\phi(\beta_L; \Gamma\beta_L) = f(\beta_L)g(\Gamma\beta_L)$, with $f(\beta_L) = v_\phi(\beta_L; \Gamma\beta_L = \frac{1}{80})$ and $g(\Gamma\beta_L) = v_\phi(\beta_L; \Gamma\beta_L) / v_\phi(\beta_L; \Gamma\beta_L = \frac{1}{80})$. We find $v_\phi(\beta_L, \Gamma\beta_L)$ and $v_\phi(\beta_L, \Gamma\beta_L = \frac{1}{80})$ from Eqs. (2.5) and (2.6), respectively. In Figs. 18(a) and (b) the solid lines represent $v_\phi/f(\beta_L)$ and $v_\phi/g(\Gamma\beta_L)$ as functions of $\Gamma\beta_L$ and β_L , respectively. To compare the data with these predictions, we calculate the experimental values of $v_\phi/f(\beta_L)$ and $v_\phi/g(\Gamma\beta_L)$ and plot them as points in Fig. 18. The data show the same general trend as the theory, but relatively few points fall on or close to the predicted curves. Most of the data lie well below the predicted values, sometimes by as much as an order of magnitude. We note that not all authors measure the maximum value of V_ϕ directly, for example, by applying a small oscillating flux, but instead measure the peak-to-peak voltage swing ΔV and assume $V_\phi \approx \pi \Delta V / \Phi_0$. This estimate assumes that the voltage is sinusoidal in Φ , which is at best only an approximation.

We turn now to the dimensionless flux noise $s_\phi = S_\phi(2\pi I_0 R / \Phi_0) = s_v / v_\phi^2$. In the simulations, we saw that s_ϕ can be factorized as $s_\phi(\beta_L; \Gamma\beta_L) \approx f_\phi(\beta_L)g_\phi(\Gamma\beta_L)$, where we defined $f_\phi(\beta_L) = s_\phi(\beta_L; \Gamma\beta_L = \frac{1}{80})$ and $g_\phi(\Gamma\beta_L) = s_\phi(\beta_L; \Gamma\beta_L) / s_\phi(\beta_L; \Gamma\beta_L = \frac{1}{80})$. In Figs. 19(a) and (b) we plot s_ϕ/f_ϕ vs $\Gamma\beta_L$ and s_ϕ/g_ϕ vs β_L , respectively, together with the theoretical curves. In both cases the reduced noise power is as much as two orders of magnitude too high. One can explain this discrepancy only partly by the reduced value of the transfer function, which enters as v_ϕ^{-2} .

From Figs. 18 and 19 we see that the discrepancy between theory and experiment is roughly the same for all values of $\Gamma\beta_L$ and β_L . We also investigated whether

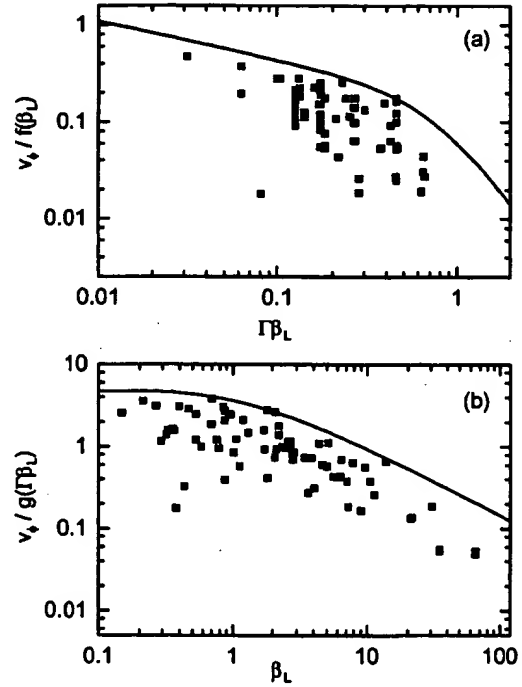


FIG. 18. Transfer function of dc SQUID: (a) Measured transfer function v_ϕ , normalized to the theoretical value $f(\beta_L)$, vs $\Gamma\beta_L$ for a wide selection of SQUIDS (solid squares); solid line corresponds to Eq. (2.5). (b) Measured transfer function normalized to the theoretical value $g(\Gamma\beta_L)$ vs β_L ; solid line corresponds to Eq. (2.6).

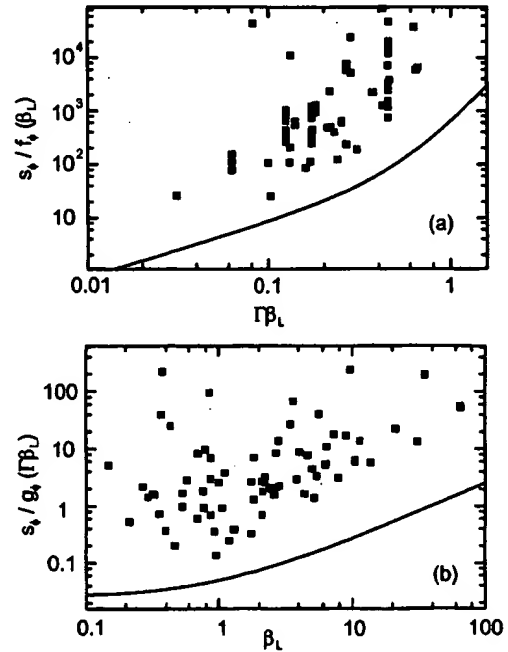


FIG. 19. Flux noise of dc SQUID: (a) Measured flux noise power, normalized to the theoretical value $f_\phi(\beta_L)$, vs $\Gamma\beta_L$ for the same SQUIDS as in Fig. 18 (solid squares); solid line corresponds to Eq. (2.8). (b) Measured flux noise power, normalized to the theoretical value $g_\phi(\Gamma\beta_L)$ vs β_L ; solid line corresponds to Eq. (2.9).

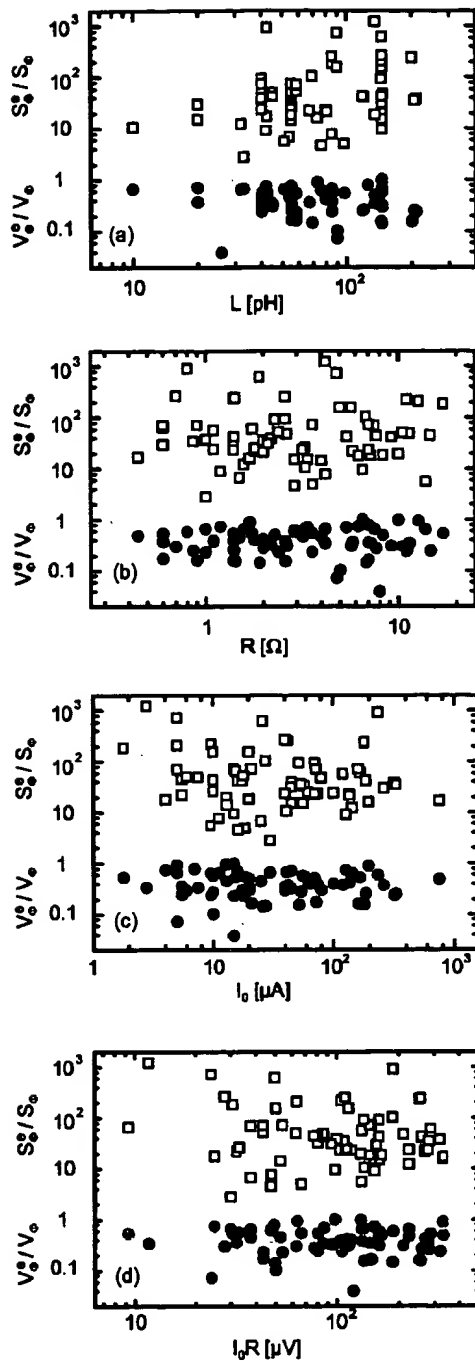


FIG. 20. For a wide selection of dc SQUIDS: ratio of measured and calculated transfer functions V_{ϕ}^e/V_{ϕ} (solid circles) and ratio of measured and calculated flux noise powers S_{ϕ}^e/S_{ϕ} (open squares) as a function of (a) SQUID inductance, (b) junction resistance, (c) junction critical current, and (d) $I_0 R$.

systematic trends occur as functions of the absolute values of L , R , I_0 , or $I_0 R$ by plotting V_{ϕ}^e/V_{ϕ} (solid circles) and S_{ϕ}^e/S_{ϕ} (open squares) versus these parameters in Fig. 20. The plots clearly show that there are no systematic trends throughout the ranges of parameters. However, for some devices V_{ϕ}^e/V_{ϕ} approaches unity; a similar result has been found by Koch (1997). Generally, the scatter in S_{ϕ}^e/S_{ϕ} is much greater than in V_{ϕ}^e/V_{ϕ} . We also calculated S_{ϕ} by using the measured value V_{ϕ}^e in-

stead of using its predicted value. The scatter was reduced, but no systematic trends became apparent.

What are the possible reasons for the high values of white noise that are almost universally observed? One explanation is that some measurements may have been taken with improperly set bias conditions; however, this is an unlikely explanation for most of the data. Second, experience with low- T_c SQUIDS suggests that environmental noise and noise from the readout electronics are improbable explanations. A third possibility is that the SQUID inductances are significantly underestimated, for example, because of a higher than anticipated kinetic inductance. Enpuku, Tokita *et al.* (1995) show that actual inductance values, 1.4 to 2 times higher than the estimated values, would explain much of the discrepancy; however, for some 40 pH devices, the actual value would have to be as much as 4 times higher, which is unreasonable. For example, Lee *et al.* (1995) estimated that the kinetic inductance for their devices was about 15% of the geometric inductance. Thus this explanation seems somewhat unlikely. A fourth explanation (Foglietti *et al.*, 1995) is that the junctions have a current-phase relation that is far from sinusoidal and that excess critical currents would lead one to overestimate the value of $I_0 R$ obtained from the I - V characteristics. Since $I_0 R$ enters v_{ϕ} and s_{ϕ} as a normalization factor, the high value would lead one to overestimate v_{ϕ} in the theory, and underestimate s_{ϕ} . A fifth explanation for the observed discrepancies between theory and experiment could be the presence of resonances. While the model in Sec. II ignores parasitic effects, the large dielectric constant of the commonly used SrTiO_3 substrates results in a substantial spurious capacitance. Transmission-line resonances (Enpuku *et al.*, 1996), as well as capacitive feedback effects (Enpuku *et al.*, 1997), have been demonstrated to influence the SQUID performance significantly. These possibilities cannot be entirely ruled out since the published noise data for dc SQUIDS are rarely accompanied by detailed measurements of the I - V characteristics. However, the reasonably good fit of a least some I - V characteristics to the RSJ model (for example, Gross and Chaudhari, 1992), the dependence of the amplitude of Shapiro steps on microwave power, and the reasonably good quality diffraction patterns of the critical current in a magnetic field suggest that they are not strong candidates. Finally, an effective bath temperature of roughly 2 T could explain the results (Enpuku, 1993). A twofold increase in temperature would double the value of $\Gamma\beta_L$ and reduce L_{th} to 160 pH. Thus one would have to shift the data in Figs. 18(a) and 19(a) to the right by a factor of 2 to account for the higher noise. This higher temperature could arise from some nonequilibrium process in the junction, for example, random telegraph signals from flux motion at characteristic frequencies well above the measurement bandwidth. The resulting Lorentzian power spectra would be white below the hopping frequencies. To our knowledge, there is no experimental evidence to support this notion, but it would be worth-

while to extend the measurements to much higher frequencies to see whether or not the noise decreased.

Finally, we note that, although they are significantly above theoretical predictions, impressive levels of noise have been achieved at 77 K, for example, $1.4 \mu\Phi_0 \text{ Hz}^{-1/2}$ with $L=13 \text{ pH}$ (Kawasaki *et al.*, 1991) and $2.2 \mu\Phi_0 \text{ Hz}^{-1/2}$ with $L=51 \text{ pH}$ (Cantor *et al.*, 1995); the corresponding noise energies were about $3 \times 10^{-31} \text{ JHz}^{-1}$ and $2 \times 10^{-31} \text{ JHz}^{-1}$, respectively.

D. Flicker (1/f) noise

For many applications, for example biomagnetism (Sec. X.A) and magnetotellurics (Sec. X.D), one requires the low level of noise to extend down to frequencies of 1 Hz or lower; if that were the case, high- T_c SQUIDS would be adequate for most purposes. Unfortunately, low-frequency $1/f$ noise, which is observed in low- T_c SQUIDS but is generally not a serious issue, is a severe problem in high- T_c SQUIDS and a great deal of effort has been expended in attempting to understand its origins and reduce its magnitude. Early high- T_c dc SQUIDS made from polycrystalline YBCO films (Koch *et al.*, 1989) exhibited large levels of $1/f$ noise, which increased the noise energy at 1 Hz to above $10^{-26} \text{ JHz}^{-1}$. Since that time, there have been dramatic reductions in the level of $1/f$ noise, and the $1/f$ corner frequency f_c (the frequency at which the extrapolated values of the white noise and $1/f$ noise intersect) has been reduced from $\sim 1 \text{ kHz}$ to $\sim 1 \text{ Hz}$.

Work on low- T_c dc SQUIDS (Koch *et al.*, 1983) showed that there are generally two separate sources of $1/f$ noise. One arises from the motion of vortices in the body of the SQUID: even when the SQUID is cooled in zero field, some fraction of the vortices formed at T_c remain pinned at defects. The vortex hopping rate increases exponentially as the pinning energy is reduced, so that the microstructure of the film and the related pinning energies play an important role in determining the low-frequency noise (Ferrari *et al.*, 1994). As we have seen in Sec. III, the microstructural quality of films is particularly crucial. When the SQUID is cooled in a nonzero magnetic field, in general the additional vortices so formed create high noise levels (Sec. IX.A). Unfortunately, one cannot relate the magnitude of the $1/f$ noise to any other measurable physical quantity, so that a direct noise measurement is the only means of characterizing the quality of a given film. It is important to note that $1/f$ noise due to vortex motion cannot be reduced by any bias reversal scheme.

The second source of $1/f$ noise is fluctuations in the critical current of the junctions which, as we saw in Sec. IV.C, can attain high levels. These fluctuations contribute in two independent ways: an "in-phase" mode, in which the critical currents of the two junctions fluctuate in phase to produce a voltage across the SQUID, and an "out-of-phase" mode in which the two fluctuating critical currents produce a current around the SQUID loop. Resistance fluctuations also contribute $1/f$ noise. However, at the low voltages where SQUIDS are operated

critical-current fluctuations dominate, and we shall not address resistance fluctuations further.

The first measurements of flux noise in high- T_c dc SQUIDS made from epitaxial YBCO films and with well-defined grain-boundary junctions were made by Gross *et al.* (1990a, 1990b). Measuring the voltage noise directly with a low- T_c SQUID preamplifier, they found similar levels of $1/f$ noise for both their SQUIDS and, after they had cut the loop, for the individual junctions. Furthermore, at temperatures well below T_c the $1/f$ voltage noise of the SQUIDS was constant, independent of V_Φ , providing strong evidence that in-phase critical-current fluctuations dominated the SQUID noise below 1 kHz. At temperatures just below T_c , however, they found that the $1/f$ noise power scaled with V_Φ^2 , and attributed this to the rapid increase in the flux noise near T_c observed by Ferrari *et al.* (1989). Subsequently, Koch *et al.* (1992) measured the $1/f$ noise in bicrystal grain-boundary SQUIDS using flux modulation alone and also flux modulation combined with bias reversal. At 77 K, they found that bias reversal reduced the $1/f$ noise power by up to two orders of magnitude, demonstrating that critical-current fluctuations dominate the $1/f$ noise observed in SQUIDS with high-quality thin films, and that one needs to reduce both the in-phase and out-of-phase components.

In practice, the reduction of $1/f$ noise with bias reversal is optimized empirically, but nonetheless, there are predictions for the magnitudes of the in-phase and out-of-phase contributions (Koch *et al.*, 1983; Foglietti *et al.*, 1986). The in-phase mode produces a voltage noise with a spectral density $S_V \approx (\partial V / \partial I_0)^2 S_{I_0} / 2 \approx (V - IR_d)^2 \times S_{I_0} / 2I_0^2$, and the out-of-phase mode produces a term $S_v \approx L^2 S_{I_0} V_\Phi^2 / 2$. Here, R_d is the dynamic resistance. As mentioned in Sec. IV.C, one can write $s_I = S_{I_0}(f) / I_0^2 \approx a^2 / f$, where a is temperature independent and approximately equal to $10^{-4} (R/\Omega)^{1/2}$ for a wide variety of junctions. From these results, one can derive the approximate expressions

$$S_\Phi^{1/2}(\text{in-phase}) \approx s_I^{1/2} |V - IR_d| / \sqrt{2} V_\Phi \\ \approx (70 \mu\Phi_0 \text{ Hz}^{-1/2}) 10^4 a \zeta v_\Phi^{-1} (f/\text{Hz})^{-1/2}, \quad (5.2a)$$

where $\zeta = |V - IR_d| / I_0 R \sim 1$, and

$$S_\Phi^{1/2}(\text{out-of-phase}) \approx s_I^{1/2} \beta_L \Phi_0 / 2\sqrt{2} \\ \approx (35 \mu\Phi_0 \text{ Hz}^{-1/2}) 10^4 a \beta_L (f/\text{Hz})^{-1/2}. \quad (5.2b)$$

For optimized values of high- T_c dc SQUIDS at 77 K, $\beta_L = 1$, $\Gamma = 0.2$, and $I_0 R = 100 \mu\text{V}$, we estimate a flux noise of about 200 (100) $\mu\Phi_0 \text{ Hz}^{-1/2}$ at 1 Hz for the in-phase (out-of-phase) contribution, substantially above measured levels of white noise. These estimates are in reasonable agreement with experimental observations, and emphasize the need for bias reversal with any high- T_c SQUID used for low-frequency measurements.

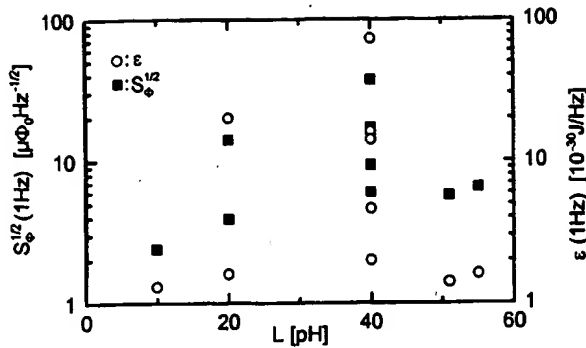


FIG. 21. $S_{\Phi}^{1/2}$ (1 Hz) and ϵ (1 Hz) of dc SQUIDS with various inductances, obtained at 77 K with flux modulation and bias reversal. (Data are from Koelle, Miklich, Ludwig *et al.*, 1993; Koelle, Miklich, Dantsker *et al.*, 1993; Koelle, Dantsker *et al.*, 1993; Miklich *et al.*, 1993; Cantor *et al.*, 1995; Lee *et al.*, 1995; Faley, Poppe, Urban *et al.*, 1995; Friedl *et al.*, 1992 and Grun-dler *et al.*, 1995).

We conclude this discussion with examples of $1/f$ noise in dc SQUIDS cooled in nominally zero magnetic field. In Fig. 21 we plot $S_{\Phi}^{1/2}$ (1 Hz) and ϵ (1 Hz) for ten SQUIDS, with L between 10 and 55 pH, obtained with flux modulation and bias reversal. In the best devices, the noise energies approach 10^{-30} JHz $^{-1}$ at 1 Hz, a performance that is very adequate provided the SQUIDS can be coupled to appropriate pickup loops without further increases in the $1/f$ noise. However, as we discuss in Sec. IX.A, the level of $1/f$ noise in SQUIDS cooled in an ambient magnetic field such as that of the earth can be much higher than in zero field unless the linewidths are kept suitably narrow.

VI. dc SQUID MAGNETOMETERS

SQUIDS are mostly used as magnetometers or gradiometers. However, although SQUIDS are exquisitely sensitive to magnetic flux, their small area generally makes them relatively insensitive to magnetic field. An exception is the large square-washer design used for both dc and rf SQUIDS, which we discuss in Secs. VI.A and VII.A, respectively. Apart from these cases, one usually couples an additional superconducting structure to the SQUID to enhance its sensitivity to magnetic field; the magnetic-field noise is $S_B^{1/2}(f) = S_{\Phi}^{1/2}(f)/A_{\text{eff}}$, where A_{eff} is the effective area of the magnetometer. Clearly, one endeavors to make A_{eff} as large as possible without increasing $S_{\Phi}(f)$ so as to produce high sensitivity to magnetic fields.

A. Square-washer designs

In this SQUID configuration (Ketchen 1981; Jaycox and Ketchen, 1981) a square washer with outer length D focuses flux into a square inner hole of length d . The effective area is dD (Ketchen *et al.*, 1985), and the inductance is $L_h = 1.25 \mu_0 d$ for $W = (D - d)/2 > d$ (Jaycox and Ketchen, 1981). In practice, however, the incorporation of the two Josephson junctions into the SQUID

loop modifies these expressions for A_{eff} and L . Five high- T_c dc SQUIDS grown on bicrystal substrates are shown in Fig. 11, and differ in the placement of the junctions intersecting the SQUID loop. In type A the junctions are outside the washer, and are thus far away from the region of strong field compression. The slit of length $l \approx W$ between the SQUID hole and the junctions can cause a significant increase in A_{eff} over the value dD , for example by a factor of 2.5 for $D = 250 \mu\text{m}$ and $d = 25 \mu\text{m}$ (Miklich *et al.*, 1993). More importantly, it increases the inductance by $L_{\text{slit}} \approx (0.3 - 0.4 l/\mu\text{m})\text{pH}$ (Wen, 1969). Thus, if one wishes to limit the total inductance to 40 pH, the maximum washer size is $200 \mu\text{m}$ even if there is no hole ($d = 0$) as in type A/A. In contrast, for types B or C, the inductance is approximately L_h , independent of the washer size D . However, the effective area A_{eff} is significantly less than dD for $D \gg d$, because of the focusing of flux into the slits outside the SQUID loop (Miklich *et al.*, 1993; Tanaka *et al.*, 1994). The latter effect is minimized in type A/C: for example, for $D = 500 \mu\text{m}$ and $L = 40$ pH one finds $A_{\text{eff}} \approx 0.015 \text{ mm}^2$, roughly a factor of two larger than for type B or C with the same values of D and L or for a 40-pH type A/A SQUID (Ludwig, Dantsker, Koelle, Kleiner, Miklich, Nemeth *et al.*, 1995).

A general calculation of the SQUID inductance and effective area requires a numerical treatment, for example solving the London equations for the specific geometry. Several groups have performed such calculations (Chang, 1981; Hosoya *et al.*, 1989; Sheen *et al.*, 1991; Töpfer, 1991; Uhlmann and Töpfer, 1992; Hildebrandt and Uhlmann, 1995). More simply, one can estimate the SQUID inductance by summing the inductance of the hole L_h the inductance of the slit L_{slit} which may be modeled as two coplanar striplines, and the inductance of the junction striplines $L_j = L_{j,g} + L_{j,k}$, which has a geometric and kinetic term. For a homogeneous current distribution the kinetic term is approximately $L_{j,k} \approx \mu_0 (\lambda^2/t) 2l_j/w$, where λ is the London penetration depth, t the film thickness, w the junction width and l_j the length of the junction striplines (Meservey and Tedrow, 1969). The contribution of L_j should be small, typically a few pH, if l_j/w is kept close to unity. This estimate of L should be accurate to within $\pm 10\%$.

For most dc SQUIDS with these geometries, the relatively small effective area implies that $S_B^{1/2}$ is inadequate for most applications. For example, with $A_{\text{eff}} = 0.015 \text{ mm}^2$ and $S_{\Phi}^{1/2} = 10 \mu\Phi_0/\text{Hz}^{1/2}$ one finds $S_B^{1/2} = 1.3 \text{ pT/Hz}^{1/2}$ well above the resolution of $10\text{--}100 \text{ fT/Hz}^{1/2}$ typically required. However, larger washers (Koelle, Miklich, Ludwig *et al.*, 1993; Tanaka *et al.*, 1994) have achieved a magnetic-field noise of about $150 \text{ fT/Hz}^{1/2}$ at 1 kHz and $500 \text{ fT/Hz}^{1/2}$ at 1 Hz with SQUID inductances of $40\text{--}100$ pH and washers of $5\text{--}11 \text{ mm}$. Comparable performance has been achieved with flux-focusing plates of similar size coupled to washer SQUIDS $2 \times 2 \text{ mm}^2$ in size (Tanaka *et al.*, 1994; Itozaki *et al.*, 1996). The $1/f$ noise in these devices tends to be high, and in some cases the motion of vortices trapped in the washer limits the effectiveness of bias reversal in

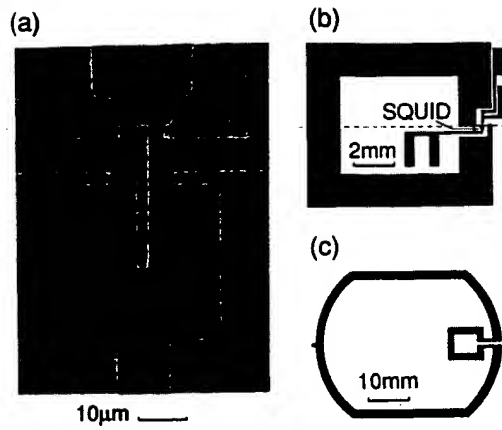


FIG. 22. Directly coupled magnetometer: (a) Photograph of 20 pH dc SQUID connected to the pickup loop shown in (b). Dashed line indicates grain boundary. (c) Configuration of single-layer YBCO flux transformer (Koelle, Miklich, Dantsker *et al.*, 1993).

reducing it (Koelle, Miklich, Ludwig *et al.*, 1993). Because of this limited performance, various alternative approaches for increasing the effective area have been pursued. There are two broad classes. The first is based on multilayer designs such as the flux transformer-coupled SQUID (Ketchen, 1981; Jaycox and Ketchen, 1981) (Sec. VI.C) or the fractional-turn SQUID (Zimmerman, 1971) (Sec. VI.D), which were successfully used for low- T_c magnetometers. However, the need for lower SQUID inductances and hence smaller SQUIDS for operation at 77 K has made optimum coupling of signal into the SQUID more challenging. Furthermore, multilayer high- T_c devices are more susceptible to excess $1/f$ noise and its reduction has been a major issue during the past years (Sec. III). As a result, single-layer designs have been developed which typically have less efficient coupling but benefit from straightforward fabrication, and lower levels of $1/f$ noise.

B. Directly coupled magnetometer

The directly coupled magnetometer (Matsuda *et al.*, 1991; Koelle, Miklich, Ludwig *et al.*, 1993) shown in Figs. 22(a) and (b) consists of a large pickup loop of inductance L_p and area A_p directly connected to the SQUID body of inductance $L \ll L_p$. A magnetic field B applied to the pickup loop induces a screening current $J = BA_p/L_p$, which in turn links a flux $(L - L_j)J$ to the SQUID. Here L_j is the parasitic inductance of the strip-lines incorporating the junctions, to which the current does not couple. The effective area is

$$A_{\text{eff}} = (L - L_j)A_p/L_p \pm A_s, \quad (6.1)$$

where $A_s \ll A_{\text{eff}}$ is the effective area of the bare SQUID. The sign of A_s depends on the relative senses of the SQUID and the pickup loop. Koelle, Miklich, Ludwig *et al.* (1993) investigated devices grown on STO bicrystals. In their best device, a 20 pH SQUID with $I_0 = 45 \mu\text{A}$ and $R = 3.4 \Omega$ coupled to a 47 mm^2 pickup loop,

they achieved a flux noise of $93 \text{ fT Hz}^{-1/2}$ at frequencies down to 1 Hz using bias reversal.

Subsequently, improvements in performance were achieved by reducing the large mismatch between L_p and L (Cantor *et al.*, 1995; Lee *et al.*, 1995). One can increase the ratio A_p/L_p by using a pickup loop with a large linewidth, $(d_1 - d_2)/2$, where d_1 and d_2 are the outer and inner dimensions. In the limit $(d_1 - d_2) > 2d_2$ in which $A_p = d_1 d_2$ and $L_p = 1.25 \mu_0 d_2$, from Eq. (6.1) we find $A_{\text{eff}} = 4d_1(L - L_j)/5\mu_0$; we have neglected A_s . Given the dependence of $S_\Phi(f)$ on L , I_0 , and R discussed in Sec. II.C, one can then optimize $S_B(f)$.

Using Eq. (6.1) for A_{eff} , together with Eqs. (2.8) and (2.9) over the ranges $0.01 < \Gamma\beta_L < 1$ and $0.4 < \beta_L < 5.6$, one finds

$$\begin{aligned} \frac{S_B^{1/2}}{(\text{fT Hz}^{-1/2})} &= \frac{262 \text{ pH}}{L_{\text{th}}} \frac{1}{(d_1/\text{mm})(L - L_j)/L_j} \\ &\times \left\{ \frac{1 + \beta_L}{I_0 R / \text{mV}} \left[\frac{80L}{L_{\text{th}}} + \left(1 + \frac{4L}{L_{\text{th}}} \right)^{4.1} - 1 \right] \right\}^{1/2}. \end{aligned} \quad (6.2)$$

Clearly, $S_B^{1/2}$ scales with $1/d_1$. For a given value of L_j one can find a minimum in $S_B^{1/2}$ as a function of L/L_{th} , which depends on $I_0 R$ and β_L . As mentioned in Sec. II.C, the noise can be optimized in different ways: one way is to keep $I_0 R$ constant and to vary I_0 by changing the junction area A_j . However, this is difficult to achieve for practical reasons, since large $I_0 R$ products are associated with high critical-current densities and hence the smallest values of I_0 are determined by the smallest linewidth that can be patterned. Alternatively, according to the scaling relation $I_0 R \propto j_c^{1/2}$ found for many high- T_c junctions, one may keep $I_0 R^2$ constant with fixed A_j and vary I_0 , for example, by changing the oxygen content in grain-boundary junctions. In this case $(1 + \beta_L)/(I_0 R) \propto (1 + \beta_L)/\beta_L^{1/2}$, which has a minimum at $\beta_L = 1$. The result of this optimization procedure is shown in Fig. 23 where we plot $S_B^{1/2}$ vs L/L_{th} for the stated values of $I_0 R$, L_{th} , L_j , d_1 , and A_j and for six values of β_L ranging from 0.4 to 5.0. There is a shallow minimum at $L/L_{\text{th}} \approx 0.3$, corresponding to $L \approx 100 \text{ pH}$ at 77 K. The dependence on β_L is weak, although $\beta_L = 1$ is optimum: the minimum magnetic-field noise varies from 11 to 13 $\text{fT Hz}^{-1/2}$ over the range of β_L plotted. Notice that the optimum value of L/L_{th} , about 0.3, is rather higher than that for the lowest noise energy found in Sec. II.C. The reason is that the coupling efficiency between L_p and L increases more rapidly in this range than V_Φ decreases. In an earlier analysis based on the work of Enpuku, Tokita *et al.* (1995), Cantor (1996) found a shallow minimum in $S_B^{1/2}$ vs L corresponding to $S_B^{1/2} \approx 32 \text{ fT Hz}^{-1/2}$ for $\beta_L = 1$, $d_1 = 9.3 \text{ mm}$, $I_0 R = 100 \mu\text{V}$, and $L_j = 8.4 \text{ pH}$; $S_B^{1/2}$ remained below $40 \text{ fT Hz}^{-1/2}$ for $30 \text{ pH} < L - L_j < 170 \text{ pH}$. This result differs somewhat from the prediction of Eq. (6.2) because Enpuku *et al.* find a faster reduction in V_Φ for $L/L_{\text{th}} \geq 0.4$ (Fig. 2).

The performance of directly coupled magnetometers with near optimum parameters can be appreciably bet-

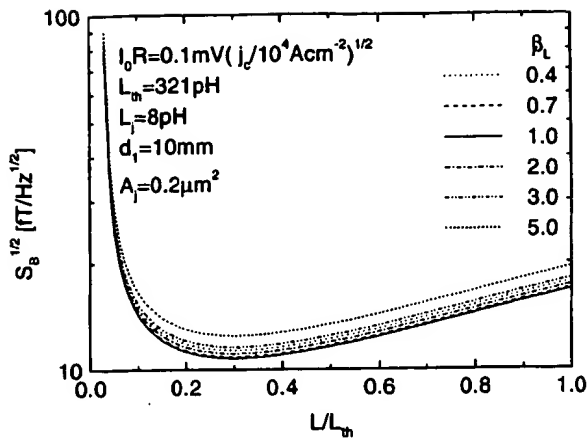


FIG. 23. Calculated rms magnetic-field resolution $S_B^{1/2}$ at 77 K vs normalized SQUID inductance L/L_{th} for directly coupled magnetometer in which the pick-up loop has an outer dimension $d_1 = 10$ mm. The curves were calculated for six values of β_L and fixed junction cross-section $A_j = 0.2 \mu\text{m}^2$ by varying j_c and hence $(I_0 R)^2$.

ter than that of the earlier devices. For $d_1 = 9.3$ mm, $d_2 = 3$ mm, and $L = 50$ pH, Lee *et al.* (1995) and Cantor (1996) achieved best results of about $40 \text{ fT Hz}^{-1/2}$ at 1 kHz and $60 \text{ fT Hz}^{-1/2}$ at 1 Hz (with bias reversal). Using a $19 \times 19 \text{ mm}^2$ pickup loop on a $20 \times 20 \text{ mm}^2$ bicrystal, the same group achieved $14 \text{ fT Hz}^{-1/2}$ at 1 kHz and $26 \text{ fT Hz}^{-1/2}$ at 1 Hz (Fig. 24) (Cantor *et al.*, 1995). In similar work, Glyantsev *et al.* (1996) reported a noise level as low as $20 \text{ fT Hz}^{-1/2}$ at 1 kHz for a 150 pH SQUID coupled to a pickup loop with an outer diameter of 8 mm. However, they did not use bias reversal, and the noise was well above $100 \text{ fT Hz}^{-1/2}$ at 1 Hz. Recently, using an STO bicrystal with a 30° misorientation angle and a pickup loop with $d_1 = 9$ mm and $d_2 = 3$ mm, Beyer *et al.* (1998) obtained $23 \text{ fT Hz}^{-1/2}$ at 1 kHz and $67 \text{ fT Hz}^{-1/2}$ at 1 Hz. These values were achieved with bias reversal in the PTB magnetically shielded room; the

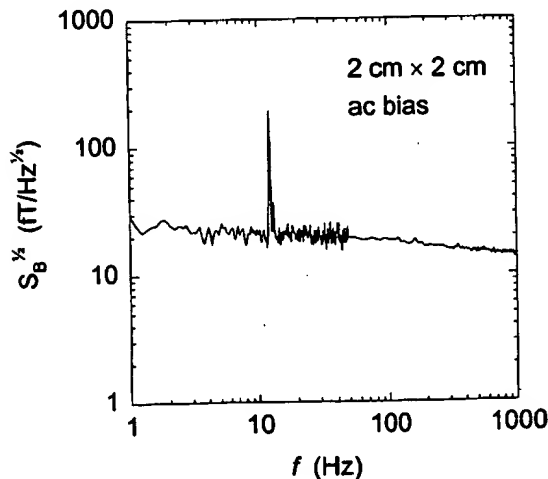


FIG. 24. Magnetic-field noise in a directly coupled magnetometer with bicrystal junctions and a $19 \times 19 \text{ mm}^2$ pickup loop. The estimated inductance is 51 pH (Cantor *et al.*, 1995).

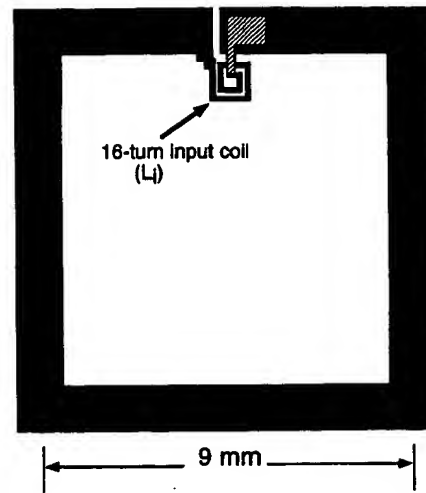


FIG. 25. Schematic layout of multilayer flux transformer (not to scale). Multiturn input coil (only two turns are shown) is either coupled to the SQUID in a flip-chip arrangement or deposited directly on top of it.

noise at low frequencies was dominated by environmental noise.

To complete this section, we note that the effective area of the directly coupled magnetometer can be further increased by coupling it in a flip-chip arrangement to a single-layer flux transformer [Fig. 22(c)] on a separate substrate (Koelle, Miklich, Dantsker *et al.*, 1993). The small loop of the transformer (which is inductively coupled to the magnetometer pickup loop) has inductance L_{ti} and area A_{ti} and is in series with the large loop of inductance L_{tp} and area A_{tp} . The effective area is

$$A_{\text{eff}} \approx \frac{L - L_j}{L_p} \left(A_p + \frac{A_{tp} \alpha_t (L_p L_{ti})^{1/2}}{L_{ti} + L_{tp}} \right), \quad (6.3)$$

where α_t is the coupling coefficient between L_{ti} and L_p . For the devices shown in Fig. 22, the transformer yielded a gain of 3.4 and the magnetic-field noise improved to $31 \text{ fT Hz}^{-1/2}$ at 1 kHz and $39 \text{ fT Hz}^{-1/2}$ at 1 Hz.

C. Flux transformer with multiturn input coil

The effective area of a SQUID may be efficiently enhanced by coupling it to a superconducting flux transformer with a multiturn input coil (Fig. 25). The transformer is a closed superconducting circuit consisting of a large-area pickup loop and a much smaller, multiturn input coil to couple flux into the SQUID. A magnetic field applied to the pickup loop induces a supercurrent that conserves the total magnetic flux and induces flux into the SQUID. The total effective area of the magnetometer is given by

$$A_{\text{eff}} = A_p M_i / (L_i + L_p) \pm A_s, \quad (6.4)$$

where A_s is the effective area of the bare SQUID (including flux focusing, see Sec. VI.A), A_p and L_p are the area and inductance of the pickup loop, $M_i = \alpha(L L_i)^{1/2}$ is the mutual inductance between the SQUID inductance L and the input-coil inductance L_i , and α is the

coupling coefficient. The sign of A_s depends on the sense of the winding of the coil relative to the pickup loop. Assuming that α does not depend on L_i and L and making certain approximations (Martinis and Clarke, 1985), one finds the effective area is maximum when $L_i = L_p$:

$$A_{\text{eff}} = \alpha A_p (L/L_p)^{1/2}/2; \quad (6.5)$$

we have neglected A_s . In contrast to the directly coupled magnetometer (Sec. VI.B), the flux transfer into the SQUID can be optimized for a given value of L_p by varying the number of turns n on the input coil until $L_i = L_p$. For low- T_c SQUIDS integrated with multiturn input coils, the relations between M_i , L_i , L , and n (Ketchen, 1981) for the tightly coupled limit are usually in good agreement with experimental data (Jaycox and Ketchen, 1981). For high- T_c magnetometers on the other hand, there are only a few experimental studies on the coupling between the input coil and the SQUID (David et al., 1995; Ludwig, Dantsker, Koelle, Kleiner, Miklich, Nemeth et al., 1995; Kugai et al., 1996), and the situation is less well understood. Ludwig, Dantsker, Koelle, Kleiner, Miklich, Nemeth et al. (1995) found that although α depends strongly on the SQUID design, being higher for type A/A and A/C than for type B and C devices (Fig. 11), it can be greater than 0.5 even for flip-chip magnetometers. Coupling the same transformer to different SQUID types, these authors showed that A_{eff} is proportional to A_s , that is, the magnetic-field gain is constant. According to Eq. (6.5), A_{eff} increases with increasing SQUID inductance L , but larger values of L do not necessarily produce lower magnetic-field noise. Using Eq. (6.5) one finds $S_B = 8(S_\Phi/2L)L_p/\alpha^2 A_p^2$, so that minimizing S_B with respect to L is equivalent to minimizing the noise energy $\varepsilon = S_\Phi/2L$. From Fig. 5 we know that for 77 K and $\beta_L = 1$, the (effective) SQUID inductance should not exceed 40–50 pH, although one should bear in mind that Eq. (6.5) is valid only so long as α is independent of L and L_i . We note also that the flux transformer reduces the effective SQUID inductance to $L[1 - \alpha^2 L_i/(L_i + L_p)]$ (Zimmerman, 1971). However, this correction is small for $L_i = L_p$ and $\alpha \leq 0.5$.

1. Flip-chip magnetometers

The advantage of the flip-chip configuration over the integrated magnetometer is that problems related to the junction process can be separated from those related to the interconnect technology. One forms a flip-chip magnetometer by clamping the SQUID and the flux transformer chips together with either photoresist or a thin mylar sheet between them. The input coil and pickup loop of the transformer are usually patterned in one YBCO layer, and the crossover between the innermost turn of the coil and the pickup loop in the other. The first YBCO flux transformer with a multiturn input coil operating at 77 K was made by Wellstood et al. (1990) using shadow masks. The first multilayer flip-chip magnetometers were reported almost simultaneously by groups at Berkeley (Miklich et al., 1991; Wellstood et al.,

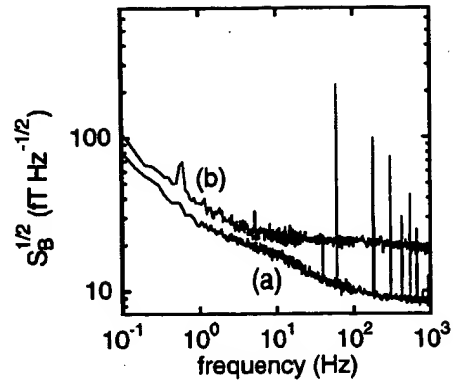


FIG. 26. Magnetic-field noise of (a) flip-chip magnetometer with a $9 \times 9 \text{ mm}^2$ pickup loop and 16-turn input coil (Dantsker et al., 1995), (b) the $\frac{1}{16}$ -turn, 7-mm-diameter SQUID shown in Fig. 28 (Ludwig, Dantsker, Kleiner et al., 1995).

1992) and IBM (Oh et al., 1991). Since this early work, many groups have described the fabrication of multiturn flux transformers (Freltoft et al., 1993; Hilgenkamp et al., 1993) and the operation of flip-chip magnetometers at 77 K (Grundler, David et al., 1993; Miklich et al., 1993; Roas et al., 1993; Keene, Goodyear et al., 1994; Keene et al., 1995; Dantsker et al., 1995; Fife et al., 1995; Ludwig, Koelle et al., 1995; Scharnweber et al., 1995; Schilling et al., 1995; Kugai et al., 1996).

The lowest magnetic-field noise was achieved by Dantsker et al. (1995), who used an 81 mm^2 pickup loop and a 16-turn input coil coupled to a $500 \text{ }\mu\text{m}$ washer SQUID (type A/A in Fig. 11) with bicrystal junctions: $8.5 \text{ fT Hz}^{-1/2}$ at 1 kHz and $27 \text{ fT Hz}^{-1/2}$ at 1 Hz (Fig. 26). This performance depended critically on both the technology for fabricating multilayer structures with low levels of low-frequency flux noise and the use of a SQUID with a low flux noise. The uncoupled SQUID had a peak-to-peak modulation voltage $V_{pp} = 55 \text{ }\mu\text{V}$ and a white flux noise of $7.3 \text{ }\mu\Phi_0 \text{ Hz}^{-1/2}$. The flux transformer was aligned so that the crossover covered about 90% of the length of the SQUID slit, reducing the SQUID inductance from 70 to about 30 pH, close to the optimum. As a result, V_{pp} increased to $108 \text{ }\mu\text{V}$, and the flux noise decreased to $4.9 \text{ }\mu\Phi_0 \text{ Hz}^{-1/2}$.

During the progressive reduction in $1/f$ magnetic-field noise from that in the first flip-chip magnetometer (Miklich et al., 1991), $1.7 \text{ pT Hz}^{-1/2}$ at 1 Hz, to that reported by Dantsker et al. (1995), it was important to understand the sources of excess flux noise in these multilayer structures. According to the model of Ferrari et al. (1991) and Wellstood et al. (1991), there are two distinct mechanisms by which this noise is coupled into the SQUID. First, the SQUID senses directly the magnetic flux produced by a vortex moving in the YBCO films of the flux transformer ("direct noise"). Second, a vortex moving perpendicularly to a YBCO line induces a screening current in the transformer to conserve the total magnetic flux, coupling flux into the SQUID ("indirect noise"). Together with flux-noise measurements on various components of transformers, the model has been used to analyze sources of excess flux noise (Lud-

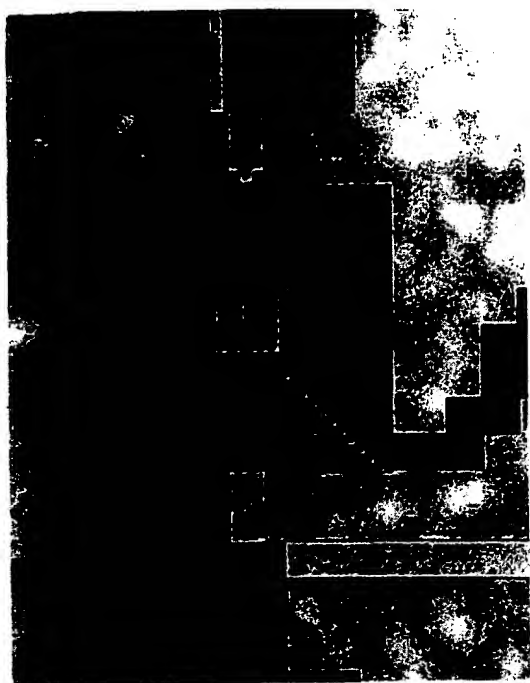


FIG. 27. Photograph of 12-turn input coil and SQUID of an integrated magnetometer with 500- μm SQUID washer located in lower YBCO layer. Bicrystal junctions are outside the washer.

wig, Koelle *et al.*, 1995; Ludwig, Dantsker, Koelle, Kleiner, Miklich, and Clarke, 1995), but it does not account for the degraded quality of YBCO films at the edges of crossovers and vias. To study the spatial distribution of critical-current densities and thus locate potential noise sources, several groups have successfully used such techniques as low-temperature scanning electron microscopy (Husemann *et al.*, 1993; Hollin *et al.*, 1994; Gerber *et al.*, 1996), low-temperature laser scanning microscopy (Sivakov *et al.*, 1994), magnet-optical imaging (Govorkov *et al.*, 1997) and scanning micro-Raman spectroscopy (Dieckmann *et al.*, 1996).

2. Integrated magnetometers

In an attempt to improve the inductive coupling between the SQUID and the input coil, several groups have integrated them on the same chip, thus reducing the spacing to the thickness of the insulating layer. Early monolithic SQUID magnetometers involving three YBCO layers and operating at 77 K (Lee *et al.*, 1991; DiIorio, Yoshizumi, Yang, Maung, and Power, 1993) exhibited large levels of low-frequency flux noise. As a result, attention turned to a simplified design requiring only two superconducting layers (Kromann *et al.*, 1993; Hilgenkamp *et al.*, 1994; David *et al.*, 1995; DiIorio *et al.*, 1995; Ludwig, Dantsker, Koelle, Kleiner, Miklich, Nemeth *et al.*, 1995; Shen *et al.*, 1995). In all cases, the insulator was SrTiO_3 . The SQUID washer is used as either a crossunder or crossover for the flux transformer, obviating the need for an extra superconducting layer. The input coil and SQUID of such a magnetometer are

shown in Fig. 27. The lowest magnetic-field noise was reported by Drung, Ludwig *et al.* (1996) using a magnetometer with 36° SrTiO_3 bicrystal junctions fabricated at NKT (Shen *et al.*, 1995), namely $9.7 \text{ fT Hz}^{-1/2}$ at 1 kHz and $53 \text{ fT Hz}^{-1/2}$ at 1 Hz. Whereas the effective area $A_{\text{eff}} = 1.72 \text{ mm}^2$ for the $8.3 \times 8.6 \text{ mm}^2$ pickup loop is comparable to that measured by others for their integrated devices, the SQUID parameters $R = 9 \text{ } \Omega$ and $I_0 = 5.7 \text{ } \mu\text{A}$ for an inductance of about 130 pH are close to optimum.

Despite this impressive performance, integrated magnetometers do have some disadvantages. One problem, reported by several groups, is that the V - Φ curves are often distorted by microwave resonances (Hilgenkamp *et al.*, 1994; Ludwig, Dantsker, Koelle, Kleiner, Miklich, Nemeth *et al.*, 1995; Drung, Ludwig *et al.*, 1996). Such resonances have not been reported for flip-chip magnetometers. These resonances in the input-coil-washer structure are well known from low- T_c devices to degrade the SQUID performance (Ryhänen *et al.*, 1989). Enpuku *et al.* (1997) and Minotani, Enpuku *et al.* (1997) recently reported the calculation of distorted V - Φ characteristics in good agreement with the data measured on high- T_c devices under the assumption that there is a parasitic capacitance between the input coil and the SQUID washer. Hilgenkamp *et al.* (1995) eliminated the resonances by means of a resistor between the SQUID and the input coil that shunted this parasitic capacitance. Another drawback is that the yield of high-performance integrated devices is well below that of flip-chip, multilayer devices. Finally, there is no compelling evidence that the coupling coefficient of integrated magnetometers is significantly higher than that for flip-chip devices (Ludwig, Dantsker, Koelle, Kleiner, Miklich, Nemeth *et al.*, 1995).

D. Multiloop magnetometer

An alternative multilayer approach to achieving large effective areas is the multiloop magnetometer or fractional-turn SQUID, originally proposed and demonstrated by Zimmerman (1971) with a machined niobium device. The essential idea is to connect N loops in parallel, thus reducing the total inductance to a level acceptable for a SQUID, while keeping the effective area large. Drung *et al.* (1990, 1991) developed sensitive multiloop SQUID magnetometers, based on their niobium thin-film technology; with eight parallel loops and a diameter of 7.2 mm these devices have a typical noise of $1.5 \text{ fT Hz}^{-1/2}$ down to a few Hz at 4.2 K. These devices have been used successfully for multichannel biomagnetic studies (Koch, Cantor *et al.*, 1991; Drung and Koch, 1993).

In the thin-film multiloop magnetometer, shown schematically in Fig. 28(a), N loops (for clarity, only four are drawn) are connected in parallel with the connection made at the center via coplanar lines. The two junctions connect the upper and lower superconducting films of the central trilayer. Compared with a flux-transformer-coupled magnetometer, the multiloop magnetometer

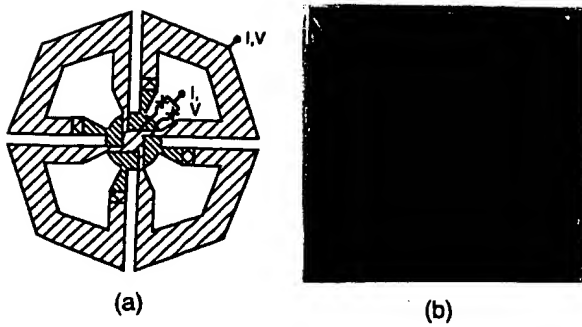


FIG. 28. Multiloop magnetometer: (a) Schematic layout of $\frac{1}{4}$ -turn SQUID magnetometer. Cross-shaded regions indicate vias between upper and lower superconducting films. (b) Photograph of $\frac{1}{4}$ -turn YBCO SQUID with outer diameter of 7 mm. Junctions are located close to the center (Ludwig, Dantsker, Kleiner *et al.*, 1995).

has the advantage that the current induced in each of the N loops when it is rotated in the earth's magnetic field is much smaller than that induced in a single loop of the same area. Furthermore, the device contains no closed superconducting loops, so that the maximum induced supercurrent is limited to the critical current of the junctions.

A comprehensive theory for thin-film multiloop SQUIDS and their performance at 77 K has been given by Drung *et al.* (1995). The effective area A_{eff} and inductance L_{eff} are given by

$$A_{\text{eff}} = A_p / N - A_s \quad (6.6)$$

and

$$L_{\text{eff}} = L_p / N^2 + L_s / N + L_j. \quad (6.7)$$

Here, A_p and L_p are the area and inductance of the large, outer loop, A_s and L_s are the average area and inductance of one spoke of the cartwheel, and L_j is the parasitic inductance of the connections from the pickup loops to the junctions. Calculation of the magnetic-field noise and transfer function as a function of N , based on the simulations of Enpuku *et al.* (1993) for $V_\Phi(L)$ and $S_\Phi^{1/2}$, shows that the optimum value of N for a minimum magnetic-field noise increases strongly with the overall size. For a diameter of 7 mm, the optimum number of loops is 15 to 20, considerably more than typically used in the low- T_c case. Using these calculations, Drung *et al.* (1995) designed a high- T_c multiloop SQUID with 16 parallel loops and an outer diameter of 7 mm. They estimated $L_{\text{eff}} = 145$ pH, which is at the upper limit of acceptability for 77 K operation (Sec. II.C), and $A_{\text{eff}} = 1.77 \text{ mm}^2$.

In the first practical realization of this magnetometer, Ludwig, Dantsker, Kleiner *et al.* (1995) used their YBCO-SrTiO₃-YBCO multilayer technology and bicrystal junctions to make the magnetometer shown in Fig. 28(b). Most of the area of the pickup loops is patterned in the upper YBCO film, and each loop makes contact to the lower YBCO layer in the center (cross-shaded region). The two 24° bicrystal junctions are located in the lower YBCO film and also make contact to the up-

per and lower YBCO films in the central trilayer region. A voltage modulation as high as $20 \mu\text{V}$ was observed despite the relatively high inductance, and resulted from the nearly ideal junction parameters, $I_0 = 13 \mu\text{A}$ and $R = 10 \Omega$. The effective area of 1.89 mm^2 was close to the predicted value. Using a flux-locked loop with 100 kHz flux modulation and bias reversal, the authors measured a magnetic-field noise of $18 \text{ fT Hz}^{-1/2}$ at 1 kHz and $37 \text{ fT Hz}^{-1/2}$ at 1 Hz (Fig. 26). Similar multiloop magnetometers based on the same design were subsequently made, using step-edge junctions (David *et al.*, 1996; Drung, Dantsker *et al.*, 1996) or PBCO ramp junctions (Reimer, Schilling *et al.*, 1995; Reimer, Ludwig *et al.*, 1995).

Two other high- T_c magnetometers involving multiloops differ from the design discussed above. Fife *et al.* (1995) coupled eight multiloop pickup coils with an outer diameter of 8.5 mm directly to a low-inductance washer SQUID with bicrystal junctions. The noise at 60 K with bias reversal was $100 \text{ fT Hz}^{-1/2}$ above 3 Hz. Scharnweber and Schilling (1996, 1997) recently reported an integrated magnetometer in which a flux transformer with a multiturn input coil and a multiloop pickup coil is inductively coupled to a low-inductance washer SQUID. For their best magnetometer, with four parallel loops 8.5 mm in diameter, at 77 K they measured a magnetic field noise of $44 \text{ fT Hz}^{-1/2}$ at 1 kHz with a static bias current and $100 \text{ fT Hz}^{-1/2}$ at 1 Hz with bias reversal.

E. Comparison of magnetometers

Given the plethora of magnetometer designs, which should one choose for a particular application? Of course, integrated, multilayer magnetometers—the multiturn flux transformer grown on a square washer SQUID or the fractional-turn SQUID—are very appealing and offer the highest sensitivity for a given area, at least in the white noise. Unfortunately, the currently low yield of junctions with acceptable values of I_0 and R means that the yield of integrated magnetometers with high performance is correspondingly low. Consequently, on a commercial basis their price is correspondingly high, probably too high for most real-world applications. Thus one should examine the alternatives, namely single-layer and flip-chip, multilayer magnetometers.

The directly coupled magnetometer is appealing in its simplicity, requiring only a single layer in a bicrystal or step-edge junction technology. Noise levels below $30 \text{ fT Hz}^{-1/2}$ have been achieved on $10 \times 10 \text{ mm}^2$ bicrystals and below $20 \text{ fT Hz}^{-1/2}$ on $20 \times 20 \text{ mm}^2$ bicrystals; however, the larger bicrystals are currently very expensive. Fortunately, provided one can avoid an increase in the low-frequency noise in the presence of the earth's magnetic field (Sec. IX), the performance of the magnetometers on the smaller chip is adequate for geophysics, and probably also for magnetocardiology. Nonetheless, despite the simplicity of fabricating these single-layer devices, one has to accept the fact that the chip-to-chip variability in the junction parameters currently ensures

that the yield of high-performance magnetometers is less than 100%. Even though substrates can be repolished and reused two or three times, the cost of manufacturing a single magnetometer with low noise is likely to remain higher than desirable.

An alternative philosophy is to fabricate (say) ten square-washer SQUIDS on a $10 \times 10 \text{ mm}^2$ chip, select the best and dice the chip accordingly. Experience suggests that one should obtain several SQUIDS with low noise with this procedure. One then couples each of these selected devices to a multiturn flux transformer in a flip-chip arrangement. Thus one separates the fabrication of the single-layer SQUIDS from the multilayer process for the flux transformer. As a further step towards lowering the cost of flux transformers dramatically, one should develop processes for depositing them in quantity on two-inch or preferably four-inch wafers using coevaporation (Berberich *et al.*, 1994; Matijasevic *et al.*, 1997). If one could develop such large-scale processing for flux transformers, for the currently available junction technologies this approach would appear to be the most economical, and could be used for all applications.

VII. rf SQUIDS

Although there has been substantially more effort to develop high- T_c dc SQUIDS, progress with rf SQUIDS has been excellent. Several groups have investigated rf SQUIDS (for example, Zani *et al.*, 1991; Tinchev and Hinken, 1992; Tinchev, 1997) but since the most concentrated effort has been made at FZ, Jülich, we shall largely focus on their work. We note that the main body of this work preceded the theory of Chesca (1998), and that a great deal of progress was made on largely empirical grounds. Furthermore, it is difficult to measure the critical current of the junction precisely without opening the loop, so that in at least some of the devices reported it is not clear whether β_L' was greater or less than unity. It is possible that some of them were operated in a "mixed mode" in which the signal was produced by variations in both inductance and dissipation. For these reasons, it is often impracticable to compare the experimental results with theoretical predictions.

A. rf SQUIDS with lumped resonant circuits

The first rf SQUID magnetometers with high sensitivity (Zhang, Mück, Herrmann *et al.*, 1992; Zhang, Mück *et al.*, 1993) consisted of large YBCO square washers with step-edge, grain-boundary junctions [Fig. 29(a)], grown on $10 \times 10 \text{ mm}^2$ SrTiO_3 substrates. The junctions were generally formed along the inner edge of the square washer to avoid the large parasitic inductance of the long slit. The SQUID was inductively coupled to the inductor of an LC tank circuit, which was resonant at 20 MHz in the early experiments. Subsequently, these authors increased the resonance frequency to about 150 MHz to increase the flux-to-voltage transfer coefficient and to reduce the level of white noise (see Sec. II). In addition to the rf excitation, the SQUID was flux modu-

lated in the usual way and operated in a flux-locked loop. The SQUIDS could be operated in both the hysteretic and nonhysteretic modes. For example, Zhang, Mück, Herrmann *et al.* (1992) reported a transfer function greater than $40 \mu\text{V}/\Phi_0$ for SQUIDS in either mode, operated at 150 MHz.

Zhang, Mück *et al.* (1993) varied both the outer and inner dimensions (d_1 and d_2) of the square washer to find the optimum magnetic-field sensitivity. The effective area $d_1 d_2$ increases with both d_1 and d_2 , while the inductance L scales with d_2 . Since $S_\Phi^{1/2}$ increases with L for both hysteretic and nonhysteretic modes, although with a different functional dependence, one expects to find a minimum. The optimum value, $170 \text{ fT Hz}^{-1/2}$, occurred for $d_2 \approx 150 \mu\text{m}$, and corresponded to a flux noise of $7 \times 10^{-5} \Phi_0 \text{ Hz}^{-1/2}$; the noise was white at frequencies down to 1 Hz. For larger inner dimensions the flux noise increased more rapidly than the effective area. At the time, this performance was the best obtained for a high- T_c magnetometer at 77 K.

There are several points to note about this result. First, the estimated inductance of this rf SQUID, about 240 pH, is larger than that of any useful dc SQUID. As a result, the effective area is substantially higher than for dc SQUIDS. In fact, the flux noise and noise energy of this rf SQUID are unremarkable by the standards of dc SQUIDS: it is the large effective area that produces the relatively low magnetic-field noise. The lack of $1/f$ noise is notable, and occurs for two reasons. In the first instance, as will be discussed in Sec. VII.C, the combination of rf and low-frequency flux modulation eliminates $1/f$ noise due to fluctuations in critical current. Of course, this scheme cannot reduce flux noise due to the motion of vortices in the square washer. Second, the relatively high level of white flux noise is now a virtue in that the $1/f$ knee is moved to a correspondingly low frequency.

Zhang, Mück *et al.* (1993) improved the performance of this device by coupling it to a flux concentrator, made of bulk YBCO, 43 mm in diameter. This magnetometer exhibited a white noise of $60 \text{ fT Hz}^{-1/2}$ at frequencies down to about 5 Hz; the additional $1/f$ noise was due to flux noise in the concentrator. Subsequently, Zhang *et al.* (1994) fabricated single-layer rf SQUIDS with several directly coupled pickup loops, improving the noise to $120 \text{ fT Hz}^{-1/2}$. They also fabricated a device in which the SQUID, in the form of a slit, was coupled to a $9 \times 9 \text{ mm}^2$ pickup loop, and achieved $90 \text{ fT Hz}^{-1/2}$ down to about 4 Hz. They achieved their best performance, however, by coupling a $8 \times 8 \text{ mm}^2$ square washer SQUID with a $200 \times 200 \mu\text{m}$ hole to a single-layer flux transformer [inset, Fig. 30(a)] in a flip-chip arrangement. With a pickup loop of $40 \times 40 \text{ mm}^2$ they achieved a magnetic-field noise of $24 \text{ fT Hz}^{-1/2}$ at frequencies down to 0.5 Hz [Fig. 30(a)].

More recently, Ockenfuß *et al.* (1997) made a systematic study of thin-film, single-layer flux transformers. The flux transformers were deposited on either 1" or 2" diameter substrates. Each transformer in turn was

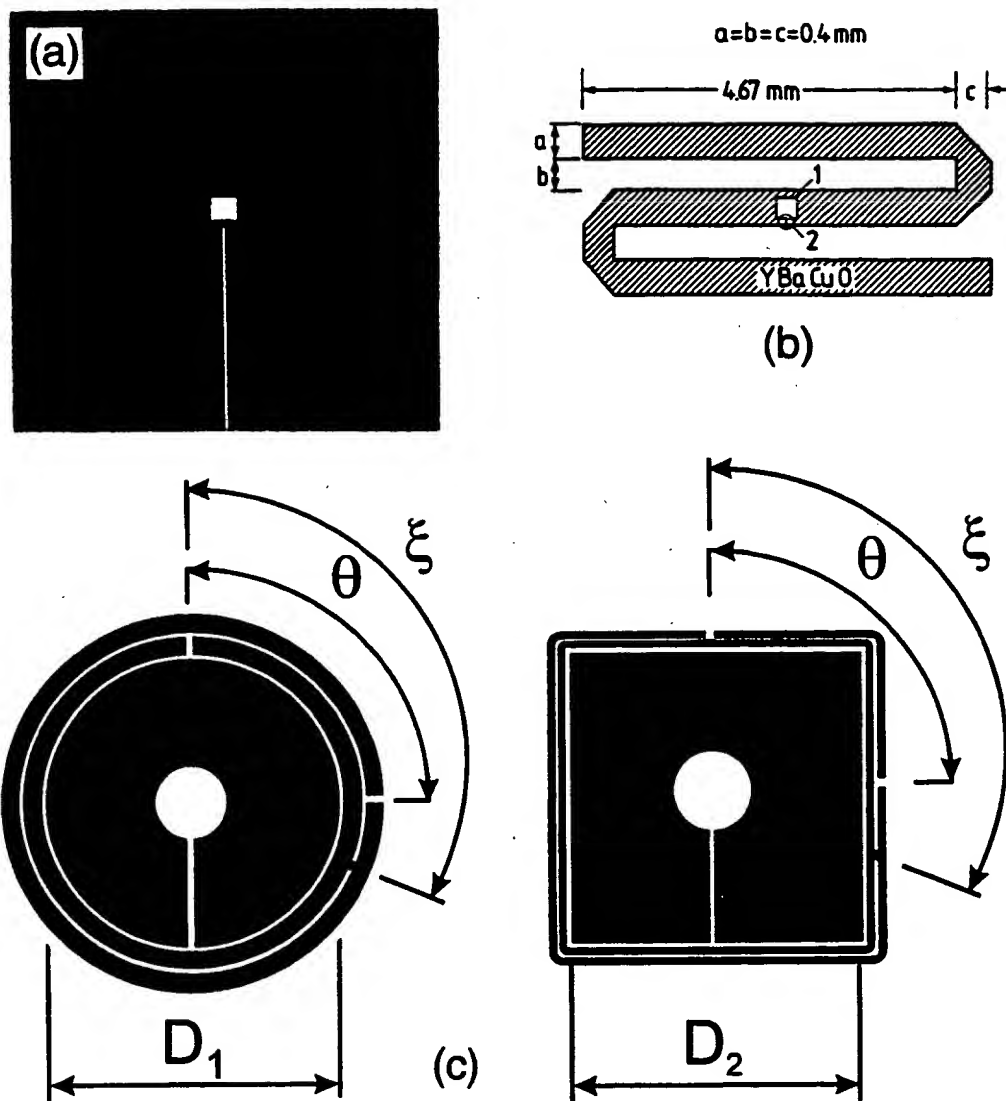


FIG. 29. Selection of rf SQUIDS from FZ, Jülich: (a) $6 \times 6\text{ mm}^2$ square-washer SQUID (Zhang, Mück, Hermann, *et al.*, 1993), (b) S-shaped microstrip SQUID (Zhang, Mück, Bode *et al.*, 1992), (c) coplanar microwave resonators (Zhang, Wolters *et al.*, 1997).

coupled in a flip-chip arrangement to an rf SQUID with a $200 \times 200\text{ }\mu\text{m}^2$ hole in an $8 \times 8\text{ mm}^2$ washer, operated at 200 MHz. The authors systematically reduced the width w_p of the pickup loop and measured the effective area and gain of the magnetometer. The maximum effective areas of 2.93 mm^2 and 4.94 mm^2 for the 1" and 2" transformers, respectively, were achieved for the maximum values of w_p , 8.2 and 19.0 mm; the corresponding magnetic field gains were 2.71 and 4.57. The magnetic-field noise above 10 Hz for these two cases was $52\text{ fT Hz}^{-1/2}$ and $30\text{ fT Hz}^{-1/2}$.

As a final remark, we note that all of the rf SQUIDS described above were at least somewhat undercoupled, that is, $\kappa^2 Q < 1$, so that the performance was less than optimum. Very recently, He *et al.* (1998) used a scheme in which they inductively coupled the lumped LC-resonant circuit to a coil that is connected to the $50\text{ }\Omega$ transmission line supplying the rf signal. This approach, which was demonstrated at frequencies from 221 to 950 MHz, increases $\kappa^2 Q$ and reduces the flux noise compared with that obtained with conventional tank circuits.

B. rf SQUIDS with distributed element resonators

The devices described above involve lumped tank circuits consisting of a wire-wound coil and a capacitor. The flux noise achieved represents the limit of what can be achieved at 150–200 MHz. As is evident from Eq. (2.15), further reductions in noise require high-frequency operation, but it then becomes difficult to achieve the required high values of Q with lumped circuits. As a result, devices operating at higher frequencies have involved various kinds of microwave resonators (Daly *et al.*, 1991; Zhang, Mück, Bode *et al.*, 1992, Zhang *et al.*, 1995, Zhang, Soltner, Wolters *et al.*, 1997, Zhang, Zander *et al.*, 1997, Zhang, Wolters *et al.*, 1997; Hein *et al.*, 1995). Zhang, Mück, Bode *et al.* (1992) described an S-shaped microstrip resonator with the $100 \times 100\text{ }\mu\text{m}^2$ SQUID loop in its central region [Fig. 29(b)]; subsequently, the loop was reduced to $100 \times 100\text{ }\mu\text{m}^2$ (Mück, 1993), with the longer side parallel to the edge of the resonator. The microstrip was formed by placing the

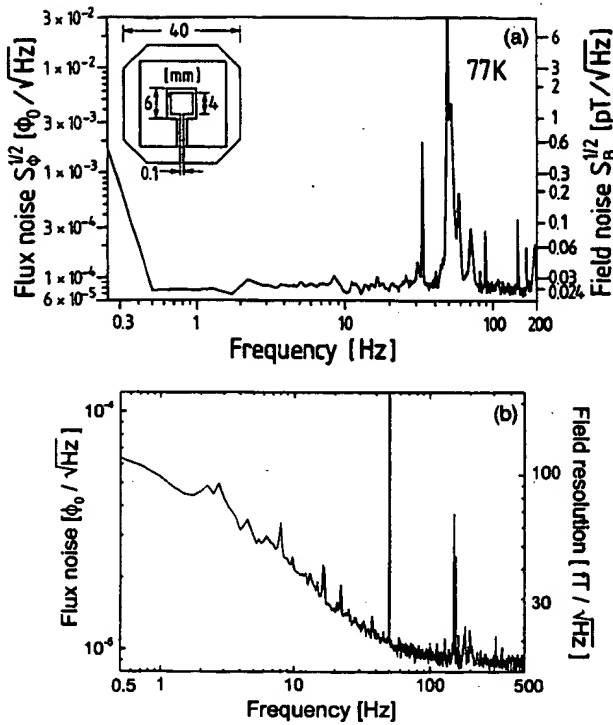


FIG. 30. Noise of rf SQUID magnetometers: (a) Magnetic flux and magnetic-field noise of 150-MHz SQUID with single-layer flux transformer with the configuration shown in the inset (Zhang *et al.*, 1994). (b) Magnetic-field noise of microwave resonator SQUID with 13-mm flux concentrator shown in Fig. 29(c) (Zhang, Wolters *et al.*, 1997).

0.5-mm-thick LaAlO_3 substrate on a copper ground-plane, and coupled to the room-temperature electronics via a $50\ \Omega$ coaxial cable. At 3 GHz, the best of these devices yielded a flux noise of $1.6 \times 10^{-5}\ \Phi_0\ \text{Hz}^{-1/2}$, corresponding to a noise energy of about $6 \times 10^{-30}\ \text{JHz}^{-1}$. However, the small effective area of the SQUID resulted in a relatively high magnetic-field noise, about $1\ \text{pT}\ \text{Hz}^{-1/2}$.

Subsequently, Zhang and coworkers improved the magnetic-field sensitivity of microwave SQUIDS operating at about 1 GHz. In their first design, Zhang *et al.* (1995) used a stack of $10 \times 10 \times 1\ \text{mm}^3$ SrTiO_3 substrates, stacked face-to-face, as a dielectric resonator. The stack was placed above a $4 \times 4\ \text{mm}^2$ washer SQUID with a $60 \times 60\ \mu\text{m}^2$ inner hole. The stack was driven at resonance via a capacitively coupled line and the output voltage was also coupled out capacitively via a second line. With a frequency of 0.911 GHz and under optimum conditions, the flux noise was $10^{-5}\ \Phi_0\ \text{Hz}^{-1/2}$ and the magnetic-field noise was $105\ \text{fT}\ \text{Hz}^{-1/2}$; the latter noise was improved to $30\ \text{fT}\ \text{Hz}^{-1/2}$ by means of a single-layer flux transformer with a 22 mm pickup loop.

In a later design, Zhang, Soltner, Wolters *et al.* (1997) used an integrated resonator in which the circular rf SQUID was surrounded by a line, patterned in the same YBCO film, containing a gap that provided the capacitance necessary for the resonant circuit. The signal from the resonator was coupled out either capacitively or inductively; inductive coupling has the advantage that the

coil can also be used for both flux modulation and flux feedback. At frequencies from 0.511 to 1.1 GHz typical values of Q were around 5000, so that the requirement $\kappa^2 Q \geq 1$ was readily achievable. In the latest version of this device, Zhang, Zander *et al.* (1997) and Zang, Wolters *et al.* (1997) used the coplanar resonator designs shown in Fig. 29(c). Two coplanar lines surround the flux concentrator, which is coupled to the rf SQUID washer (2.5 or 3.5 mm in diameter) in a flip-chip configuration. The relative position of the gaps in the coplanar lines and the location of a short between them allows one to adjust the resonance frequency. For a SQUID with a $10 \times 500\ \mu\text{m}^2$ inner hole ($L \approx 260\ \text{pH}$) coupled to a resonator with a 13-mm-diameter flux concentrator, Zhang, Wolters *et al.* (1997) obtained a white flux noise of $8.5 \times 10^{-6}\ \Phi_0\ \text{Hz}^{-1/2}$, corresponding to a noise energy of $6 \times 10^{-31}\ \text{JHz}^{-1}$ and a magnetic-field noise of $16\ \text{fT}\ \text{Hz}^{-1/2}$ [Fig. 30(b)]. The noise at 1 Hz, however, was substantially higher, about $100\ \text{fT}\ \text{Hz}^{-1/2}$, and most likely arose from the motion of vortices in the resonator. This configuration is particularly appealing in its simplicity, enabling one to design the device with appropriate parameters very straightforwardly and offering simple fabrication with a minimum of additional cryogenic components.

In a further step towards higher sensitivity, very recently Zhang *et al.* (1998) described a new design in which a multiturn flux transformer is integrated with the coplanar resonator. The pickup loop is connected to two coils, a multiturn coil to couple in low-frequency signals and a single-turn coil to couple in rf currents. A two-hole SQUID is coupled to these coils in a flip-chip configuration to form a magnetometer. The separation of rf and low-frequency currents is a key factor that enables the authors to achieve a high quality factor.

C. $1/f$ noise

In the rf SQUIDS described above the onset of $1/f$ noise generally occurs at a relatively low frequency—1 Hz or less—provided one uses a flux-locked loop. This low $1/f$ knee frequency is due in part to the fact that the white flux noise is generally higher than for dc SQUIDS, but the major reason is the action of the readout scheme in eliminating $1/f$ noise arising from critical-current fluctuations (Giffard, 1980; Mück, Heiden, and Clarke 1994). We first describe this effect for hysteretic SQUIDS.

We first consider the effect on $V_T^{(0)}$ [Eq. (2.11)] of a fluctuation δI_0 in I_0 at a frequency much less than $\omega_H/2\pi$. The value of Φ_c is increased to $L(I_0 + \delta I_0)$, so that the transitions from the $k=0$ state to the $+1$ and -1 states occur at the flux values $L(I_0 + \delta I_0)$ and $-L(I_0 + \delta I_0)$, respectively. As a result, $V_T^{(0)}$ is increased to

$$\tilde{V}_T^{(0)} = \omega_H L_T (\Phi_c + L \delta I_0) / M. \quad (7.1)$$

We see that $1/f$ noise in the critical current results in a $1/f$ noise component in the demodulated rf voltage.

However, when the SQUID is flux modulated and operated in a flux-locked loop, the effect of critical-current fluctuations is greatly reduced. Consider the effect of an applied flux $\delta\Phi < \Phi_0/2$ on the characteristics shown in Fig. 6. The asymmetry introduced into the hysteresis loops causes the SQUID to make its transition from the $k=0$ to the $k=+1$ state at a lower rf flux, reducing the voltage across the tank circuit to

$$V_T^{(+\delta)} = \omega_{rf} L_T (\Phi_c - \delta\Phi) / M \quad (0 < \delta\Phi < \Phi_0/2). \quad (7.2)$$

In the region DF of Fig. 6(c), the SQUID traverses only the $k=0 \leftrightarrow k=+1$ hysteresis loop. Similarly, if we now change the flux to $-\delta\Phi$ ($|\delta\Phi| < \Phi_0/2$), the voltage is

$$V_T^{(-\delta)} = \omega_{rf} L_T |(-\Phi_c + \delta\Phi)| / M \quad (-\Phi_0/2 < \delta\Phi < 0). \quad (7.3)$$

The SQUID now traverses only the $k=0 \leftrightarrow k=-1$ hysteresis loop; the modulus sign in Eq. (7.3) reflects the fact that the detection of the peak value of the rf voltage is insensitive to whether the transition occurs on a positive or negative peak of the rf current. Suppose now that I_0 undergoes a slow fluctuation to a new value $I_0 + \delta I_0$. The peak voltage across the tank circuit changes to

$$\tilde{V}_T^{(+\delta)} = \omega_{rf} L_T (\Phi_c + L \delta I_0 - \delta\Phi) / M \quad (0 < \delta\Phi < \Phi_0/2) \quad (7.4)$$

and

$$\tilde{V}_T^{(-\delta)} = \omega_{rf} L_T |-(\Phi_c + L \delta I_0) + \delta\Phi| / M \quad (-\Phi_0/2 < \delta\Phi < 0). \quad (7.5)$$

We see that the effect of a (say) positive fluctuation δI_0 is to increase \tilde{V}_T uniformly for all values of applied flux; correspondingly, the demodulated voltage vs flux curve will be shifted uniformly to a higher voltage. However, when the usual modulating flux at frequency f_m with a peak-to-peak amplitude of $\Phi_0/2$ is applied to the SQUID, the amplitude of the resulting voltage at f_m is unaffected by this shift. Thus, when this signal is mixed down with the same frequency f_m , the resulting quasi-static output voltage is unaffected by fluctuations in the critical current. Any slow fluctuations in the amplitude of the rf driving current are similarly suppressed.

Mück, Heiden, and Clarke (1994) examined the $1/f$ noise in Nb rf SQUIDS operated in the hysteretic mode at 4.2 K. For a SQUID at 3 GHz, operated in a flux-locked loop with conventional flux modulation, they found that the flux noise was white at frequencies down to below 0.5 Hz. However, when they operated the SQUID open loop in the absence of flux modulation, the spectral density of the noise was $1/f$ at frequencies below about 1 kHz, and three orders of magnitude higher at 1 Hz than in the previous measurement. These results show very clearly that the conventional operating mode of the rf SQUID eliminates the effects of critical-current fluctuations.

In the case of nonhysteretic rf SQUIDS ($\beta_L' < 1$), the critical current is small so that the amplitude of the $1/f$ noise fluctuations in the critical current, which scales as

I_0 , is also correspondingly low. This factor contributes to the low level of $1/f$ flux noise observed in these devices (Chesca, 1998). In addition, flux modulation suppresses $1/f$ flux noise due to critical-current fluctuations (Mück, Clarke, and Heiden, 1994). The value of the tank circuit voltage V_T is proportional to I_0 [Eq. (2.19)], but in addition V_Φ also depends on I_0 [Eq. (2.20)]. As a result, a fluctuation in I_0 results in not only a fluctuation in the component of V_T at the same frequency but also in the amplitude of the component at the flux modulation frequency. Since, however, the feedback loop is (ideally) sensitive only to the phase of the flux modulation, these amplitude fluctuations will not contribute to the output of the phase-sensitive detector. Thus critical-current fluctuations are suppressed by modulation and feedback as in the hysteretic mode.

VIII. GRADIOMETERS

In Sec. VI we described magnetometers with a white noise level below $10 \text{ fT Hz}^{-1/2}$, a sensitivity adequate for most practical applications. However, in many of these applications—good examples are magnetocardiography and nondestructive evaluation—one needs to detect weak signals against a background of magnetic noise that is many orders of magnitude higher. In urban environments, the dominant source of noise is the 50 or 60 Hz signals, and a large number of harmonics, from power lines: peak-to-peak amplitudes can range from 20 nT to $1 \mu\text{T}$. Additionally, traffic (trains, subways, cars) can cause even stronger disturbances. For this reason, most sensitive measurements with low- T_c magnetometers—particularly of biomagnetic signals—are currently made in a magnetically shielded room. However, except for enclosures, such as that at the PTB, Berlin, with very high levels of attenuation, most shielded rooms do not reduce the 50 or 60 Hz fields sufficiently, and one requires a gradiometer to discriminate against distant noise sources with small gradients in favor of nearby signal sources. The traditional low- T_c gradiometer is wound from niobium wire: two pickup loops wound in opposition and mounted on a common axis with a baseline (separation) of typically 0.1 m are connected in series with an input coil inductively coupled to a SQUID (Zimmerman and Frederick, 1971). Such a device measures the first-derivative axial gradient $\partial B_z / \partial z$. The addition of a third coil midway between the two loops results in a second-derivative gradiometer measuring $\partial^2 B_z / \partial z^2$. In the case of axial gradiometers, the separation of one pickup loop and the signal source is generally made rather less than the baseline, so that the instrument effectively detects the magnetic field from the source. Thin-film gradiometers have also been made, measuring either an axial gradient (Hoenig et al., 1991) or more usually planar devices measuring an off-diagonal gradient of the form $\partial B_z / \partial x$ (Hämäläinen et al., 1993).

Early wire-wound gradiometers were balanced by adjusting the positions of small, superconducting pellets, sometimes to an accuracy of 1 part in 10^6 . (We define

“balance” as the ratio of the output of the SQUID when a uniform magnetic field is applied to the gradiometer to the output when the same field is applied to one pickup loop.) However, a myriad of interacting, mechanically adjusted components becomes impractical for more than a few channels. Current practice is to use magnetometers and first-derivative gradiometers for the software generation of second or third derivatives (Vrba, 1996).

The lack of suitable wire eliminates the wire-wound, high- T_c gradiometer as an option, and two alternative approaches have been adopted. The first is an electronic gradiometer made by subtracting the signals from separate magnetometers: the gradiometer can be axial or planar, and the baseline can be chosen at will. The second is a planar gradiometer with thin-film pickup loops.

A. Electronic subtraction gradiometers

A high- T_c , axial gradiometer was demonstrated by Tavrin *et al.* (1993a), who mounted two rf SQUIDs one above the other, each with a bulk flux focuser (Zhang, Mück, Herrmann *et al.*, 1992). One sensor was mounted rigidly while the plane inclination of the second, placed 60 mm above, could be adjusted from outside the cryostat to achieve a balance of about 1 part in 10^3 . This system was used to measure magnetocardiograms (MCG) (Sec. X.A) in an unshielded environment, against a 50 Hz background of 1 to 20 nT, although the quality of the cardiograms was limited by $1/f$ noise in the magnetometers, about $1 \text{ pT Hz}^{-1/2}$. Subsequently, Tavrin *et al.* (1994) added a third, vertically stacked sensor to form a second-derivative gradiometer. The lowest sensor was rigidly mounted, while the inclination of the other two, 60 and 120 mm above it, could be adjusted. The three channels, A, B, and C could be added electronically to generate two first-derivatives, $A - B$ and $B - C$, and the second derivative, $A - 2B + C$. The system could be balanced to achieve a common mode rejection ratio of 1 part in 3000 and a gradient rejection of 1 part in 100. The magnetic-field noise referred to SQUID A or C was below $300 \text{ fT Hz}^{-1/2}$. Once balanced, the unit required no readjustment after thermal cycling and after transporting it over long distances in the course of examining some 200 human subjects. A similar electronically formed axial gradiometer was recently reported by Borgmann *et al.* (1997) who used a set of adjustable superconducting plates, similar to those in early low- T_c gradiometers, to achieve the final balance. The authors achieved a balance better than 10^4 for uniform background fields and better than 200 for gradient fields. Electronic gradiometers have also been constructed with the magnetometers in the same plane (David *et al.*, 1997; ter Brake, Janssen *et al.*, 1997).

The balance of an electronic gradiometer is limited by the linearity of the flux-locked magnetometers and by the common mode rejection ratio of the subtraction system. In the presence of high background noise, the dynamic range and slew rate of the magnetometers may be challenged. None of these difficulties arises with superconducting gradiometers, which thus have an inherent

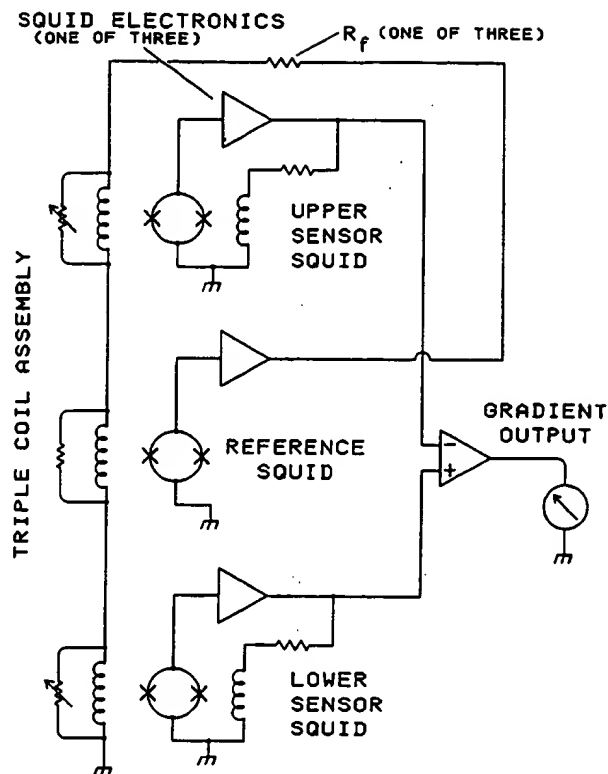


FIG. 31. Configuration of three-SQUID gradiometer (Koch *et al.*, 1993).

advantage over electronic cancellation. However, the three-SQUID gradiometer (TSG) of Koch *et al.* (1993), shown in Fig. 31, also circumvents these problems by using electronic cancellation and subtraction. The center, reference magnetometer operates in a flux-locked loop and applies its output also to a coil coupled to each of the outer magnetometers. Thus the environmental noise at each of the two sensing magnetometers is greatly attenuated, reducing their linearity and slew-rate requirements. The signals from the outer two sensors are then subtracted to form a first-derivative gradiometer. Koch and co-workers demonstrated several versions of the TSG, with baselines of 0.1 to 0.25 m and using both low- T_c and high- T_c SQUIDs. The balance can be adjusted to about 1 part in 4000 by adjusting the feedback currents with room-temperature resistors. A key advantage of this approach is that any noise generated by the central sensor is applied equally to the two outer magnetometers and eliminated in the subtraction. As a result, one can use less sensitive SQUIDs to generate the canceling fields or even a total-field magnetometer, such as a flux gate, which can be used to cancel not only the fluctuating fields but also the static field. However, one difficulty with most flux gates is that their bandwidth is typically limited to 100 Hz, so that they cannot be used to cancel harmonics of the 50 or 60 Hz signal. In their original publication, Koch *et al.* reported a white gradient noise of $6 \text{ pT m}^{-1} \text{ Hz}^{-1/2}$ for SQUIDs with $3 \times 3 \text{ mm}^2$ flux-focusing washers. For a baseline of 0.1 m, this result corresponds to a magnetic-field noise of $600 \text{ fT Hz}^{-1/2}$ referred to one sensor.

B. Gradiometric flux transformers

Electronic subtraction enables one to choose an arbitrary baseline and to adjust the balance externally. Experience with low- T_c devices, however, shows that it is notoriously difficult to operate such systems in the harsh environment of a laboratory or a hospital and to achieve an adequate signal-to-noise ratio for clinical applications. Low- T_c systems intended for unshielded operation invariably have a gradiometric flux transformer to bear the brunt of the large level of background noise; even then, an adequate signal-to-noise ratio in unfavorable situations may not be possible (Vrba, 1996). Thus there are strong incentives to develop high- T_c equivalents, albeit in planar geometries. An early gradiometer fabricated from a YBCO-STO-YBCO multilayer (Eideloth et al., 1991) employed a multiturn input coil coupled to two pickup loops of opposite senses in the same plane. The baseline was about 5 mm. The multiturn coil was coupled to a square-washer SQUID in a flip-chip arrangement. At the time, multilayer technology was still in its infancy and the device exhibited substantial levels of $1/f$ noise. The best reported gradient noise at 10 Hz was $400 \text{ pT m}^{-1} \text{ Hz}^{-1/2}$. A similar flip-chip gradiometer with improved $1/f$ noise was reported later by Keene, Chew et al. (1994). However, both gradiometers exhibited poor balance because of the unbalanced SQUID. The balance was improved by two orders of magnitude to about 1 part in 1000 by means of gradiometrically configured SQUIDS (Keene, Chew et al., 1994; Keene et al., 1995).

An alternative gradiometer configuration (Ketchen et al., 1978) consists of two pickup loops in parallel with a SQUID measuring the current induced along the common line [(Fig. 32(a)). This configuration has the disadvantage that large supercurrents are induced around the perimeter when the device is rotated in an ambient field. Knappe et al. (1992), Zakosarenko et al. (1994), Daalmans et al. (1995), Schultze, Stolz et al. (1997), Schmidl, Wunderlich, Dörner, Specht et al. (1997) and Dörner et al. (1997) have all made single-layer, first-derivative gradiometers of this kind, using dc SQUIDS with either step-edge or bicrystal junctions. The baselines are limited by the size of the substrate to about 5 mm, and the best gradient sensitivities are about $50 \text{ pT m}^{-1} \text{ Hz}^{-1/2}$. All the dc SQUID-based gradiometers described above have the disadvantage that the SQUID itself has a non-zero response to magnetic field, producing an intrinsic imbalance. This problem is circumvented in the rf SQUID-based gradiometer by Zhang, Soltner, Krause et al. (1997), resembling the configuration of Fig. 32(a), with a single, step-edge junction intersecting the central strip. This structure is a re-creation of the Nb "two-hole" rf SQUID (Zimmerman et al., 1970). The device had a baseline of about 5 mm and was balanced to 1 part in 1000. The gradient field noise was about $100 \text{ pT m}^{-1} \text{ Hz}^{-1/2}$ above 10 Hz. One of these gradiometers was used to perform eddy-current measurements of cracks in aluminum in an unshielded environment.

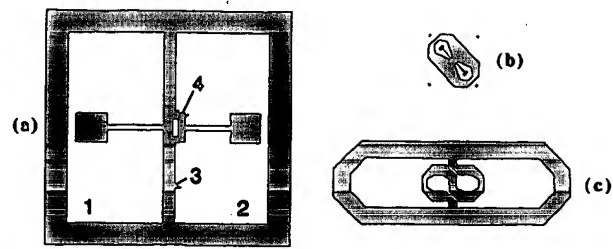


FIG. 32. Gradiometers: (a) Principle of single-layer, planar gradiometer with parallel inductances 1 and 2. A gradient $\partial B_z / \partial x$ induces a current in the central strip 3 that links flux to the SQUID 4 (Daalmans, 1995). (b) First-derivative planar gradiometer on a $10 \times 10 \text{ mm}^2$ chip that is coupled to (c) the gradiometric structure on a two-inch substrate (Faley et al., 1997).

Several attempts have been made to extend the baseline using single-layer gradiometers in a flip-chip arrangement (Daalmans, 1995; Faley et al., 1997). The concept is illustrated in Figs. 32(b) and (c) (Faley et al., 1997), which shows a dc SQUID with quasiplanar PBCO junctions on a $10 \times 10 \text{ mm}^2$ chip that is inductively coupled to a gradiometric flux transformer on a 50 mm substrate. The central strip in the transformer is intended to reduce the inductance and pickup area of the SQUID by screening. The baseline was 20 mm, the balance about 1 part in 1800 and the noise $5 \text{ pT m}^{-1} \text{ Hz}^{-1/2}$ at 1 kHz. A comparable sensitivity was reported by Daalmans (1995).

It should be noted that all the single-layer, thin-film gradiometers lose substantial sensitivity because the inductances of the pickup loops are mismatched to the input coil coupling them to the SQUID. This drawback, together with the relatively short baseline of even the largest devices (20 mm) implies that none of them is practicable for applications such as magnetocardiology. However, as demonstrated already, they may be well-suited to nondestructive evaluation (NDE). To achieve high enough sensitivity and a long enough baseline for magnetocardiology with this approach would require a multiturn input coil fabricated on a substrate at least 50 mm and preferably 100 mm in length. This somewhat daunting prospect has yet to be tackled.

A new approach to single-layer, thin-film gradiometers was recently demonstrated by Dantsker, Froehlich et al. (1997) who fabricated the asymmetric, planar gradiometer shown schematically in Fig. 33(a). The gradiometer consists of a directly coupled SQUID magnetometer with a pickup loop of inductance L_m and area A_m , and a superconducting flux transformer with an input loop of inductance L_i and area A_i connected to a pickup loop of inductance L_p and area A_p . The mutual inductance between the magnetometer and input loop is $M_i = \alpha(L_m L_i)^{1/2}$. With a suitable choice of these parameters, one attains the balance condition

$$\alpha = [A_m / (A_p + A_i)] (L_p + L_i) / (L_i L_m)^{1/2} \quad (8.1)$$

for which the directly coupled magnetometer produces zero response to a uniform magnetic field B_z . On the other hand, a magnetic field δB_z applied only to the

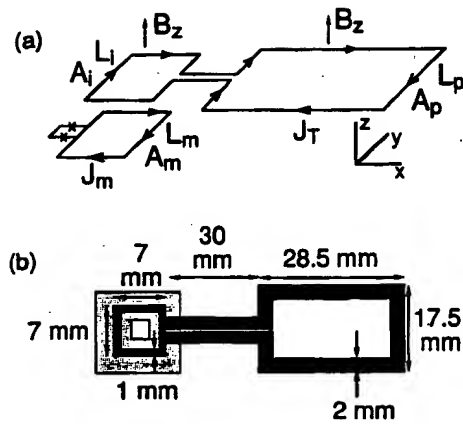


FIG. 33. Configuration of asymmetric, planar gradiometer coupled to a directly coupled magnetometer: (a) schematic, (b) experimental (shaded square represents magnetometer) (Dantsker, Froehlich *et al.*, 1997).

magnetometer and the input loop induces a current $\delta J_m = \eta \delta B_z A_m / L_m$ in the magnetometer loop, where

$$\eta = [L_p / L_i + 1 - \alpha (L_m / L_i)^{1/2} A_i / A_m] / (L_p / L_i + 1 - \alpha^2) \quad (8.2)$$

represents the screening effect of the flux transformer.

The physical configuration of the gradiometer is shown in Fig. 33(b). The single-layer directly coupled magnetometer was patterned in a 150-nm-thick YBCO film laser-deposited on a $10 \times 10 \text{ mm}^2$ SrTiO_3 bicrystal. The outer and inner dimensions of the magnetometer loop are 10 and 2 mm, respectively, yielding an estimated inductance $L_m = 4 \text{ nH}$ and area $A_m = 20 \text{ mm}^2$. The flux transformer was fabricated from a 260-nm-thick YBCO film coevaporated on a 100 mm r -plane sapphire wafer. For these dimensions, balance is predicted to occur for $\alpha = 0.43 \pm 0.04$. The corresponding value $\eta = 0.95$ implies that the flux transformer reduces the intrinsic sensitivity of the magnetometer by only 5%. The baseline—the separation between the midpoints of the two loops—is 48 mm.

The gradiometer was balanced by sliding the flux transformer over the magnetometer, immersed in liquid nitrogen, thereby varying the coupling coefficient α . A balance of about 1 part in 3000 was achieved with respect to magnetic fields perpendicular to the plane of the gradiometer, while the intrinsic balance with respect to in-plane fields was about 1 part in 1400. Operated in an unshielded environment, the gradiometer reduced the 60 Hz peak by a factor of 1600 compared with the bare magnetometer.

This approach to gradiometers has several advantages. The fact that the intrinsic magnetic-field sensitivity of the magnetometer is reduced by only a few percent by the presence of the transformer is particularly appealing for high- T_c devices, for which resolution is at a premium. It should not be necessary to use particularly high quality films, since vortex motion in a flux transformer with a relatively large area and inductance does not contribute significantly to the overall $1/f$ magnetic-field noise (Koelle, Miklich, Dantsker *et al.*, 1993). The

general principle can be extended to other derivatives of the magnetic field: for example, the addition of a second, identical pickup loop on the opposite side of the input loop would produce a gradiometer sensitive to $\partial^2 B_z / \partial x^2$. The high degree of balance and long baseline make this gradiometer eminently suitable for multichannel arrays for biomagnetic measurements. However, it would be impracticable to balance these gradiometers mechanically—a more realistic approach might be to mount the transformer permanently on the magnetometer and to achieve the final balance by laser trimming.

Finally, which of these gradiometers should one use? Currently, the two major applications are biomagnetism and NDE (Secs. X.A and X.B). For NDE, one generally does not require particularly high sensitivity, and a relatively compact, single-layer gradiometer with a baseline of 5–10 mm is likely to be adequate. For biomagnetism, the situation is more complex. Good results have been achieved with electronic subtraction of magnetometers, but limitations of slew rate, linearity and CMRR present difficulties for unshielded operation. Still, this approach is the only one that can measure an axial gradient. For the immediate future, at least, gradiometric flux transformers are limited to planar configurations. Ideally, one would like to fabricate a long-baseline gradiometer with a multiturn, multilayer input coil, with an inductance to match that of the pick-up loops, inductively coupled to the SQUID. In practice, the cost of manufacturing such structures on large substrates—say, four inch—is likely to be prohibitive. The best alternative would seem to be the asymmetric, planar gradiometer, provided it can be balanced adequately without recourse to mechanical adjustment.

IX. SQUID'S IN UNSHIELDED ENVIRONMENTS

Sections VI and VII illustrate the low levels of magnetic flux and field noise achieved with high- T_c SQUIDS and magnetometers. All these results, however, were obtained with the devices cooled and operated inside magnetic shields which attenuate the ambient static and time-varying fields by large factors. In this section, we discuss the operation of high- T_c SQUIDS in the ambient environment, without magnetic shielding, as is essential for some applications. For example, it is obviously impractical to shield an airplane wing undergoing nondestructive evaluation. In the case of geophysical applications, one measures fluctuating magnetic fields generated either naturally or by man-made sources, and has no option other than to operate the magnetometer unshielded. In biomagnetic measurements, magnetically-shielded rooms large enough to enclose a patient and multiple SQUID sensors are commercially available and have been widely used with low- T_c SQUIDS, but their price—as high as \$0.5 M—adds substantially to the overall cost of the system. This is particularly true for systems with a relatively small number of channels, for example, for magnetocardiography, and the elimination of the MSR would do much to make such techniques more financially accessible.

A SQUID exposed to the ambient environment is adversely affected by a variety of sources. These can be categorized into sources that are extrinsic—arising directly from the environment—and sources that are intrinsic to the SQUID. Examples of environmental noise sources are nearby power lines (typical amplitudes are 20 nT–1 μ T at 50 or 60 Hz), computer displays (40 to 80 Hz), lasers, elevators, and automobiles. These extrinsic noise sources and their harmonics and intermodulation products obscure the signal of interest such as a magnetocardiogram, and their reduction requires gradiometers (Sec. VIII) or active cancellation. One possible intrinsic effect is the reduction of the critical current, resulting in a decrease in the transfer function and an increase in the white noise. For example, Miklich *et al.* (1994) found that the critical current of their 3- μ m-wide bicrystal junctions decreased by 15% when they were cooled in a 100 μ T field. However, this problem can be largely eliminated by reducing the width of the junctions: Dantsker, Tanaka, and Clarke (1997) found an insignificant reduction in the critical current of 1- μ m-wide junctions cooled in 130 μ T. We note that ramp-edge junctions are intrinsically shielded and also suffer a negligible critical current reduction in comparable fields (Faley, Poppe, Urban *et al.*, 1995).

A. 1/f noise

The low-frequency flux noise power of most high- T_c SQUIDS increases when they are cooled in the earth's field, by as much as a factor of 50. This increase is caused by the thermally activated hopping of weakly pinned vortices which penetrate the YBCO film during cooling. Ferrari *et al.* (1994) used a low- T_c dc SQUID to measure the noise in YBCO films cooled in static fields B_0 and found that at low frequencies $S_\Phi(f)$ scaled as $1/f$ for cooling fields above a few μ T. Furthermore, $S_\Phi(f)$ scaled linearly with B_0 [Fig. 34(a)], as expected for the uncorrelated hopping of vortices since $S_\Phi(f)$ is expected to be proportional to the number of vortices and hence to B_0 . Miklich *et al.* (1994) found similar increases for a dc SQUID [Fig. 34(b)] and a directly coupled magnetometer, although $S_\Phi(f)$ did not always scale linearly with B_0 . Other authors (Faley, Poppe, Urban *et al.*, 1995; Tanaka *et al.*, 1995; Glyantsev *et al.*, 1996) confirmed these findings, in SQUIDS, and Keene *et al.* (1996) found that the low-frequency noise of their planar gradiometers increased substantially for cooling fields above 15 μ T. The flux noise for the SQUID in Fig. 34(b) at $B_0 = 50 \mu$ T is about $200 \mu\Phi_0/\text{Hz}^{1/2}$ at 1 Hz. Even coupled to the best flux transformer described in Sec. VI.C, this excess noise would limit the magnetic-field resolution to about $400 \text{ fT}/\text{Hz}^{1/2}$, an order of magnitude greater than that of the most sensitive sensors in zero field. Recently, however, Schmidt *et al.* (1996) showed that the flux noise in one of their directly coupled magnetometers, about $10 \mu\Phi_0/\text{Hz}^{1/2}$ at 1 Hz, was nearly independent of magnetic field up to 100 μ T, but gave no details of the fabrication process or geometry.

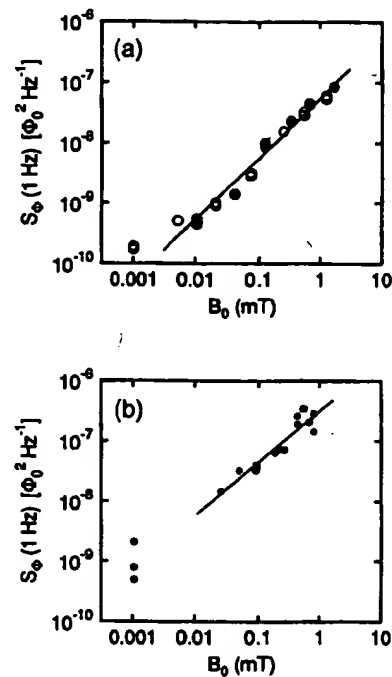


FIG. 34. Flux noise S_Φ (1 Hz) vs cooling field B_0 : (a) for a YBCO film at 77 K, measured with a low- T_c SQUID. Filled and open circles indicate reversed direction of B_0 , line is least-squares fit. (b) for YBCO dc SQUID with bicrystal junctions and 250- μ m washer, measured with bias reversal (Miklich *et al.*, 1994).

Reduction of the excess $1/f$ noise in SQUIDS operated in unshielded environments is clearly essential. One must eliminate either the motion or the presence of flux vortices, and we now examine the approaches that have been investigated.

To reduce the motion of a given density of vortices, one has to create strong pinning sites. Shaw *et al.* (1996) showed that proton or heavy-ion irradiation of single crystals of YBCO not only increased the critical-current density but also reduced the $1/f$ noise substantially. However, the critical-current densities were still substantially lower and the $1/f$ noise in ambient fields still substantially higher than the values in thin films. Furthermore, heavy-ion irradiation at doses up to the level at which T_c starts to degrade does not increase the critical current of thin films that already have high critical-current densities (Barbour *et al.*, 1992), implying that pinning in these films as grown is already close to optimum. Thus it seems unlikely that this approach will materially reduce the level of $1/f$ noise in thin YBCO films cooled in an ambient magnetic field.

One method of eliminating the excess $1/f$ noise is to cancel the static field that causes it. For medical applications, some groups, for example Aarnink *et al.* (1995), have used a three-axis flux-gate magnetometer as a reference sensor that controls the current through three orthogonal sets of cancellation coils surrounding the dewar. This technique can reduce the ambient field to about 1%, but the flux-gate magnetometers themselves generate excess noise. This noise can be reduced if one

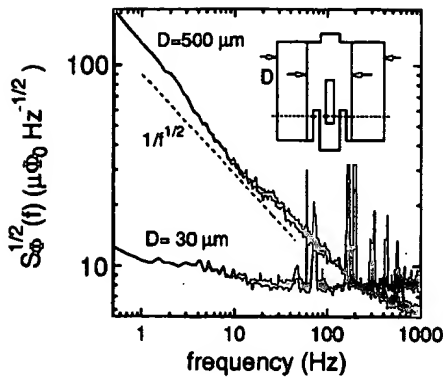


FIG. 35. $S_{\Phi}^{1/2}(f)$ for dc SQUID shown in the inset cooled in a field of $24 \mu\text{T}$. Upper trace is for device with outer dimension $D=500 \mu\text{m}$, lower trace is after repatterning to a width $D=30 \mu\text{m}$ (dotted lines). Inset not to scale. Dashed line indicates grain boundary (Dantsker et al., 1996).

uses SQUID gradiometers. A simpler and perhaps more practical version of this method is the three-SQUID gradiometer (Koch et al., 1993, see Sec. VIII.A) with the reference SQUID replaced with a flux-gate magnetometer. Of course, none of these methods is appropriate for geophysical measurements in which one is interested in fluctuations in the ambient magnetic field.

The most practical method of eliminating the excess $1/f$ noise is to design the superconducting components of the magnetometer so that flux vortices do not enter. For a film of width w cooled in a perpendicular field B_0 , Clem (1996) has shown that it is energetically unfavorable for flux to penetrate provided $w \leq (\pi\Phi_0/4B_0)^{1/2}$. Dantsker et al. (1996) studied the $1/f$ noise produced by SQUIDS with various film widths as a function of the magnetic field in which they were cooled. The upper trace of Fig. 35 is the flux noise $S_{\Phi}^{1/2}(f)$ of a square-washer bicrystal SQUID with outer dimensions of $500 \mu\text{m}$ and a slit $100 \mu\text{m}$ long and $4 \mu\text{m}$ wide, cooled in $24 \mu\text{T}$. The observed $1/f$ spectrum is typical for such devices. The SQUID was subsequently repatterned to reduce the outer dimension to $30 \mu\text{m}$ and the linewidth to $13 \mu\text{m}$, as indicated by dotted lines in the inset. The lower trace shows that the low-frequency noise is dramatically lower, by two orders of magnitude in power at 1 Hz . Similar measurements on SQUIDS with linewidths ranging from 4 to $13 \mu\text{m}$ showed that the flux noise at 1 Hz , typically $8\text{--}20 \mu\Phi_0 \text{ Hz}^{-1/2}$, was independent of the cooling field up to a threshold B_T , above which the noise increased rapidly, indicating that vortices begin to penetrate the film. Although B_T increased with decreasing linewidth, the increase was slower than Clem's model predicts. For example, in the first batch of devices B_T was about $33 \mu\text{T}$ for $w=4 \mu\text{m}$, a field about three times less than the predicted value $\pi\Phi_0/4w^2 \approx 100 \mu\text{T}$. It was suggested that poor-quality edges, which offer low-energy sites where vortices tend to nucleate, were the most likely cause of the lower threshold. However, subsequent work (see below) showed that threshold fields of over $100 \mu\text{T}$ could be achieved with more carefully patterned edges. We note that edges should be vertical

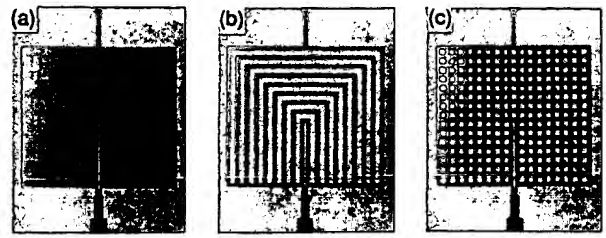


FIG. 36. Photographs of (a) a solid, thin-film dc SQUID, (b) a SQUID with eight slots and (c) with 248 holes. The outer dimensions of each device are $186 \mu\text{m} \times 204 \mu\text{m}$ (Dantsker, Tanaka, and Clarke, 1997).

to give the highest threshold field, a requirement that is the antithesis of the smoothly beveled edges needed for multilayer structures.

We now discuss the implications of this result to directly coupled magnetometers in which we use a SQUID with a narrow linewidth. We show that the pickup loop is expected to add negligible $1/f$ noise even though its linewidth is often several millimeters wide and thus the film is penetrated by vortices even in low cooling fields. The motion of the vortices generates screening currents which couple an indirect flux noise $S_{\Phi}^{\text{in}}(f)$ to the SQUID. For a square pickup loop of outer and inner dimension d_1 and d_2 and inductance L_p , this indirect noise is given by (Dantsker et al., 1996)

$$S_{\Phi}^{\text{in}}(f) \approx S_{\Phi}^U(f) \alpha_d^2 (L/L_p)^2 (d_1 + d_2)/(d_1 - d_2). \quad (9.1)$$

Here, $S_{\Phi}^U(f)$ is the spectral density of the flux noise of an unpatterned YBCO film measured by a SQUID placed directly over it, typically $10^{-9} \Phi_0^2/\text{Hz}$ at 1 Hz for high-quality films cooled in $B_0=50 \mu\text{T}$ (Ferrari et al., 1994). Taking the typical values $L \approx 20 \text{ pH}$, $\alpha_d \approx 1$ and $L_p \approx 5 \text{ nH}$ for a magnetometer pickup loop with $d_1 \approx 10 \text{ mm}$ and $d_2 \approx 2 \text{ mm}$, we find $S_{\Phi}^{\text{in}}(1 \text{ Hz}) \approx 10^{-14} \Phi_0^2/\text{Hz}$. This value is several orders of magnitude below the flux noise of the SQUID (for example, Fig. 35). The best directly coupled magnetometers on a $10 \times 10 \text{ mm}^2$ substrate have a noise of about $50 \text{ fT Hz}^{-1/2}$ (Lee et al. 1995; Beyer et al., 1998), and with appropriate SQUID design it should be possible to achieve this result in the earth's field at frequencies down to (say) 1 Hz . This would be adequate for most geophysical applications.

We turn next to a discussion of multilayer devices. In the case of the multiloop magnetometer (Sec. VI.D), at least in principle, it should be possible to reduce all the linewidths to (say) $4 \mu\text{m}$, so that the $1/f$ noise should not increase in ambient fields up to about $100 \mu\text{T}$. For a square-washer SQUID coupled to a multiturn flux transformer, however, it is clearly out of the question to reduce the outer dimensions of the SQUID. Dantsker, Tanaka, and Clarke (1997) tackled this problem using SQUIDS with the configurations shown in Figs. 36(b) and (c). Once again, the key is to maintain narrow linewidths. In the first design [Fig. 36(b)] the SQUID washer is interpenetrated by eight slots, each $8 \mu\text{m}$ wide, separating nine YBCO strips, each $4 \mu\text{m}$ wide. In the second design [Fig. 36(c)] 248 holes, each $8 \times 8 \mu\text{m}$, di-

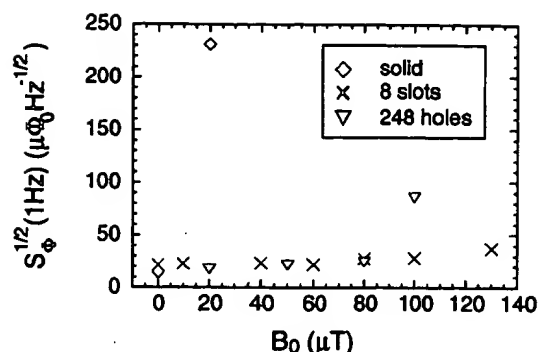


FIG. 37. $S_\phi^{1/2}$ (1 Hz) vs cooling field B_0 for the three SQUIDS shown in Fig. 36 (Dantsker, Tanaka, and Clarke, 1997).

vide the washer into a grid of 4- μm -wide lines. Figure 37 compares $S_\phi^{1/2}$ (1 Hz) for three devices made on a single chip in the configurations of Fig. 36, cooled in static magnetic fields B_0 . The noise of the solid SQUID increases rapidly with B_0 , much like the device in Fig. 34(b). The SQUID with slots, on the other hand, shows no significant increase in the noise for fields up to at least 100 μT . At 130 μT the noise has increased somewhat, suggesting that vortex entry occurred just below this field. For the device with 248 holes $S_\phi^{1/2}$ (1 Hz) also shows no increase for cooling fields up to at least 80 μT . Furthermore, measurements of the mutual inductance M_i between each of the SQUIDS in Fig. 36 and a seven-turn input coil revealed that the presence of slots or holes reduces M_i by no more than 14%. Since the flux noise generated by the pickup loop is expected to be unimportant, these results suggest that it should be possible to operate magnetometers with multiturn input coils in the earth's magnetic field with no increase in 1/f noise.

However, it should be stressed that when a device is moved in an ambient magnetic field, the induced supercurrents are very likely to generate vortices and increase the noise. For example, Keene *et al.* (1996) rotated a planar gradiometer in static fields as high as 70 μT and measured a monotonic increase in the 1/f noise as they turned the device through 90°; furthermore they observed large random telegraph signals (RTS) over some narrow angular ranges. Thus, after any such devices are moved in a static field, it is likely to be necessary to raise their temperature briefly above T_c to release the induced currents.

Earlier, Koch *et al.* (1995) had investigated the effect of cooling a directly coupled magnetometer inside a magnetic shield which they subsequently removed, exposing the device to an ambient field. They showed that the current generated in the pickup loop by the field caused vortices to enter the material. Exposure to a field of 50 μT , for example, caused a substantial increase in the level of 1/f noise. We note that, according to our discussion concerning Eq. (9.1), the density of vortices generated by these currents must far exceed the density produced by the ambient field itself. If this were not the case, the 1/f noise contribution of the loop would be negligible. Koch *et al.* (1995) demonstrated that this flux

entry and ensuing 1/f noise could be prevented by means of a "flux dam"—a weak link in the pickup loop that limits the circulating current to its critical current. With the flux dam in place, exposing the magnetometer to 50 μT after a zero-field cool resulted in a considerably smaller increase in the 1/f noise. More recently, Miliken, Brown, and Koch (1997) reported a directly coupled magnetometer containing a flux dam in which the noise of several hundred $\text{fT Hz}^{-1/2}$ at 1 Hz did not increase significantly when the device was exposed to fields as high as 34 μT following a zero-field cool. Thus for magnetometers that are subject to being moved, the lowest levels of 1/f noise are likely to be achieved with a combination of narrow linewidths and a flux dam.

B. Hysteresis

Magnetic hysteresis in a SQUID-based instrument manifests itself as a shift of the voltage-flux characteristics along the flux axis after the magnetic field is cycled. This effect is undesirable if one wishes to keep track of the absolute value of the magnetic field or to measure gradients in large fluctuating background fields. Magnetic hysteresis is observed for low- T_c and high- T_c SQUIDS and is related to vortex entry and pinning near the edges of thin films (Koch *et al.*, 1989; Sun *et al.*, 1992; Sun, Gallagher, and Koch, 1993; Sun *et al.*, 1994; Clem *et al.*, 1993; Purpura *et al.*, 1993; Keene *et al.*, 1996). The degree of hysteresis is expressed by the hysteresis parameter $h = \delta\Phi/\Delta\Phi$, where $\delta\Phi$ is the flux error caused by sweeping the applied flux between $\pm\Delta\Phi$. For integrated thin-film low- T_c gradiometers operated at 4.2 K in the ambient magnetic field, a magnetic hysteresis as low as 10^{-9} – 10^{-11} (Koch, Ketchen *et al.*, 1991) has been measured. Initial studies on high- T_c dc SQUIDS based on polycrystalline films showed high levels of nonlinear hysteresis (Foglietti *et al.*, 1989; Koch *et al.*, 1989). For grain-boundary dc SQUIDS involving epitaxial YBCO films on bicrystals, Gross and Chaudhari (1992) reported $h < 10^{-6}$ at 77 K for $\Delta\Phi \leq \Phi_0$.

Sun and co-workers made systematic studies of the hysteresis in low- T_c and high- T_c dc SQUIDS using cycling fields ranging from 10 μT to 1 mT peak to peak. In each case they found both time-independent and time-dependent hysteresis. The time-independent hysteresis appeared above a threshold field of a few hundred microtesla. The threshold field had a similar temperature dependence to the critical-current density of the thin films, suggesting a relation between this hysteresis and flux pinning. Sun *et al.* (1994) developed a quantitative model involving the Lorentz force on vortices due to screening currents, the surface barrier to flux entry, and the pinning force of defects in the superconducting film. Within this model they showed that the observed threshold field corresponds to the value at which the Lorentz force equals the sum of the surface barrier and the pinning force. Since the screening currents and hence the Lorentz force on a vortex are maximum at the edges of the film and decay into film, the vortices are swept into the film until the Lorentz force becomes smaller than

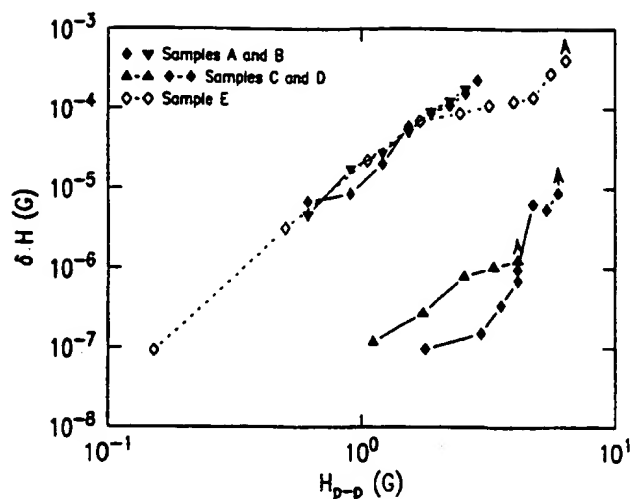


FIG. 38. Hysteresis of YBCO dc SQUIDS with a 240- μm square washer. Lower traces are for devices prepared with higher edge quality and show a significant reduction in hysteresis (Sun *et al.*, 1994).

the pinning force. The distance over which the vortices penetrate into the washer and the ensuing degree of hysteresis are predicted to depend crucially on the local pinning force near the film edges, in agreement with the dramatic reduction of the hysteresis achieved by improving the quality of the film edges (Sun, Gallagher, Callagari *et al.*, 1993). This improvement is illustrated in Fig. 38. Clearly, to obtain small hysteresis one requires a high average critical-current density in the films. However, the hysteresis is dominated by the local properties close to the edges: for example, a single grain boundary cutting across the edge of a SQUID washer increased the hysteresis by several orders of magnitude (Sun *et al.*, 1994). Keene *et al.* (1996) made similar measurements of hysteresis in a gradiometric, high- T_c SQUID coupled to a gradiometric flux transformer with multiturn input coils. For cycling fields up to 70 μT , the hysteresis parameter averaged 3×10^{-6} . When the measurements were repeated on the SQUID without the flux transformer, the hysteresis was little changed for cycling fields below 40 μT but increased dramatically for higher fields. The authors attribute this behavior to the pinning of the radial motion of vortices in the SQUID by the input coils. It is particularly important to note that high edge-pinning forces are a key to producing low levels of both $1/f$ noise and hysteresis, and imply steep film edges. This requirement is, unfortunately, not compatible with the need for gently sloping edges on all but the last film of a multilayer structure.

C. rf interference

Environmental rf fields may have a major effect on SQUIDS. In their simulations, Koch *et al.* (1994) coupled rf signals to dc SQUIDS as both a flux and a bias current, via the input and output circuitry of the SQUID. They showed that rf interference distorts the V - Φ characteristic by both reducing its amplitude and

creating an asymmetry about the $\Phi_0/2$ point. The first effect increases the white noise of the SQUID but, when conventional flux modulation is used, does not create a shift in the output of the flux-locked loop. The second effect can lead to a large increase in the level of low-frequency noise; however Koch and co-workers showed that this problem can largely be eliminated by using bias current reversal.

One can often effectively eliminate rf interference by means of appropriate shielding. However, this may not be possible in certain situations, notably for systems that are required to move in the earth's field; such motion induces eddy currents in the shield. In these situations, the combined use of flux modulation and bias reversal greatly reduces the effects of rf interference. Koch *et al.* (1994) emphasize that the rf coupling is reduced by making the superconducting structure small so as to decrease their antenna gain and, especially, by making the input and output circuits and the SQUID itself as balanced as possible. A high degree of balance prevents common mode rf fields, which have no effect on the SQUID, from creating differential signals that couple to the current and flux biases.

D. Temperature fluctuations

The effects of temperature fluctuations or drifts on the output of a high- T_c SQUID have been largely ignored until recently. However, these effects can be substantial (Milliken, Koch *et al.*, 1997; ter Brake *et al.*, 1997). Such fluctuations can be induced, for example, by changes in the ambient pressure above the liquid nitrogen bath. A change in temperature modifies the penetration depth and hence the effective sensing area of a SQUID, producing a flux change in the presence of an ambient magnetic field. For typical devices in the earth's magnetic field, the change in flux can be as high as $0.5 \Phi_0/\text{K}$. To achieve a noise level of (say) $10 \mu\Phi_0 \text{ Hz}^{-1/2}$ with this temperature coefficient would require a temperature stability of a few tens of $\mu\text{K Hz}^{-1/2}$ at frequencies above 1 Hz. The effect of temperature fluctuations can be reduced by appropriate design of the SQUID and flux transformer, stabilizing the ambient pressure, providing a long thermal time constant between the bath and the device, and reducing the ambient field. These are complicated issues that require further attention.

X. APPLICATIONS

The first practical measurement with a high- T_c SQUID was probably the use of a bulk rf SQUID by Likhachev *et al.* (1990) to detect the magnetocardiogram of a human subject. Since then, as the sensitivity of SQUIDS has progressively improved, the range of applications has grown rapidly. Currently, there is most interest in magnetocardiography and, to a lesser extent, magnetoencephalography, nondestructive evaluation (NDE), and SQUID "microscopes." Geophysical instrumentation is receiving growing attention and appears to

have an important future. We shall review each of these topics in turn. Of the various other applications, we mention just two. One is the SQUID picovoltmeter, in which the voltage to be measured is coupled in series with a resistor and a multturn, single-layer film that is inductively coupled to a directly coupled magnetometer (Miklich *et al.*, 1995; Faley *et al.*, 1997). The other is the spinner magnetometer, in which a geophysical sample is rotated, typically at 10 rev/sec, just below the bottom of a dewar containing a high- T_c SQUID (Tincev, 1997). The resulting oscillating magnetic field enables one to determine the static magnetization of the sample.

A. Biomagnetism

Biomagnetism refers quite generally to the measurement of magnetic fields produced by any living organism but, apart from experiments on magnetotactic bacteria mentioned in Sec. X.C, it appears that high- T_c magnetometers have been used only to detect signals from the human body. These fields range from several tens of picotesla from the human heart down to a few tens of femtotesla from the spinal cord (Wikswa, 1995). The majority of the commercial low- T_c SQUIDs ever made are employed in multichannel systems for magnetoencephalography (MEG)—measurements of signals from the human brain. This application demands a magnetic-field resolution of a few $\text{fT Hz}^{-1/2}$ at frequencies down to about 1 Hz. As discussed in Sec. VI, the best high- T_c SQUID magnetometers have a white noise below $10 \text{ fT Hz}^{-1/2}$, but at 1 Hz the noise is about a factor of 3 higher. Thus high- T_c magnetometers are not yet quite good enough for clinical MEG, although there have been several demonstrations of neuromagnetic measurements (Zhang, Tavrín *et al.*, 1993; DiIorio *et al.*, 1995; Curio *et al.*, 1996; Drung, Ludwig *et al.*, 1996). On the other hand, the requirements for magnetocardiography (MCG)—measurements of signals from the human heart—are somewhat more relaxed, and as a result most biomagnetic measurements with high- T_c SQUIDs have focused on this application.

Although the peak signal amplitudes in MCG are several tens of picotesla, there is fine structure of clinical interest with a mean amplitude of about 2 pT (David *et al.*, 1997). The base-to-peak amplitude of a biomagnetic signal to be identified in a single measurement in a bandwidth Δf is given by $B_p = c_R S_B^{1/2} (\Delta f)^{1/2}$. The crest factor c_R is determined by the probability that an observed magnetic field is signal rather than noise, and a value of about 4 is used under the assumption that the noise is white throughout the measurement bandwidth (Ott, 1988). Thus for the typical values $\Delta f = 200 \text{ Hz}$ and $B_p = 2 \text{ pT}$, the sensor should have a noise below $35 \text{ fT Hz}^{-1/2}$. Although magnetocardiograms measurements have been obtained by a number of groups to illustrate the performance of their magnetometers, only a few such recordings, obtained in a well-shielded environment, are of sufficient quality to yield diagnostically useful information. The best data were obtained in the magnetically shielded room of the PTB in Berlin with

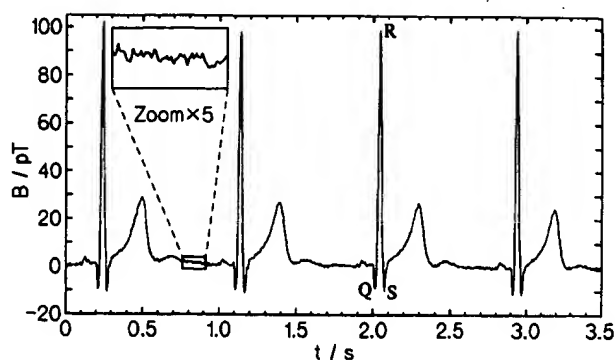


FIG. 39. Real-time trace of magnetocardiogram recorded with NKT integrated magnetometer in magnetically shielded room at PTB in Berlin. The measurement was performed in a bandwidth of 0.016–200 Hz without power line filter. Inset illustrates very low peak-to-peak noise (Drung, Ludwig *et al.*, 1996).

several kinds of multilayer magnetometers (Drung, Ludwig *et al.*, 1996; Drung, Dantsker *et al.*, 1996). The highest signal-to-noise ratio was obtained with an integrated magnetometer involving a multturn input coil, fabricated at NKT, which had a noise of $10 \text{ fT Hz}^{-1/2}$ at 1 kHz and $53 \text{ fT Hz}^{-1/2}$ at 1 Hz (Drung, Ludwig *et al.*, 1996). An unfiltered, real-time MCG measurement with this device is illustrated in Fig. 39. The measurement bandwidth was 200 Hz, resulting in a base-to-peak noise amplitude of 0.75 pT and a signal-to-noise ratio of 130 for the peak value. The latter value is considered acceptable for MCG with low- T_c systems. The sensitivity of this particular high- T_c magnetometer was adequate to detect wide-band MEG signals produced by both the central and peripheral nervous systems, with amplitudes of 100 fT or less (Curio *et al.*, 1996; Drung, Ludwig *et al.*, 1996).

Subsequently, Burghoff *et al.* (1996) used a high- T_c rf SQUID magnetometer in the Berlin shielded room to record the MCG of both a healthy subject and a subject with arrhythmia. The noise of the sensor was $35\text{--}40 \text{ fT Hz}^{-1/2}$ at 200 Hz. To assess the performance of the high- T_c magnetometer, the PTB 37-channel, low- T_c system (Koch, Cantor *et al.*, 1991) was used as a reference. Although the rms noise of the high- T_c sensor was a factor of 4 higher than the low- T_c sensors, one half of this disadvantage was regained from the shorter distance between the high- T_c magnetometer and the thorax. The ability to place high- T_c SQUIDs closer to the signal source clearly relaxes their sensitivity requirement somewhat compared with their low- T_c counterparts. A further potential advantage of liquid nitrogen-cooled sensors is that the cryogenic package can be made quite compact. Schilling *et al.* (1996) measured a MCG with a cryostat containing only 0.1 liter of liquid nitrogen.

The systems we have just described have only a single channel. However, most applications require a multichannel system to enable one to map fields from the heart at different locations. The most elaborate high- T_c systems have been built at the Superconducting Sensor Laboratory in Japan: 4 channels (Tanaka *et al.*, 1994), 16 channels (Itozaki *et al.*, 1994), and 32 channels (Itozaki

et al., 1996). Their sensors were 5-mm-washer dc SQUIDS with a noise of $70\text{--}250 \text{ fT Hz}^{-1/2}$ at 1 kHz and $300\text{--}800 \text{ fT Hz}^{-1/2}$ at 1 Hz; to protect them from moisture, the SQUIDS were sealed in an epoxy resin package. The 32 SQUIDS were in a flat 6×6 array, with each corner location unoccupied, with 40 mm separation. Magnetocardiogram recordings were obtained in a small magnetic shield, with inner dimensions $0.8 \times 0.8 \times 2 \text{ m}^3$. Although the noise specifications did not fulfill the requirements listed earlier, Itozaki and co-workers were able to obtain magnetocardiographic isofield contour maps of the *R*, *S*, and *T* waves.

To our knowledge, the only multichannel system using multilayer technology is the four-channel system of DiIorio *et al.* (1995), who used integrated, multiturn magnetometers. The noise levels were $70 \text{ fT Hz}^{-1/2}$ at 1 kHz and $280 \text{ fT Hz}^{-1/2}$ at 1 Hz. These authors obtained both MCG's and MEG's in a magnetically shielded room.

All the systems described so far involved magnetometers, and can thus be used only in a magnetically shielded room, which, as pointed out in Sec. IX, is expensive. If one hopes to see SQUIDS in widespread use, one is required not only to replace liquid ^4He with liquid N_2 but also to eliminate the need for expensive shielding. This requirement has driven extensive development of gradiometers: since the separation of the sensor and the source is only a few tens of millimeters, even high-order gradiometers behave as magnetometers for the signal source, provided the baseline is sufficiently long (Vrba, 1996).

Tavrin *et al.* (1994) and Borgmann *et al.* (1997) used second-order electronic gradiometers to record good-quality MCG's in unshielded environments. However, the bandwidth was only 0–30 Hz, which is insufficient for some of the high-frequency information of clinical interest. Weidl *et al.* (1997) used a single-layer, planar gradiometer with a 4-mm baseline to record MCG's in an unshielded environment with a bandwidth of 250 Hz. The *R* peak was just resolved in a real-time trace. The authors demonstrated that the signal-to-noise ratio could be significantly improved by averaging, by using notch filters, and by triggering the recording with the peak of the electrocardiogram (Seidel *et al.*, 1997).

Progress towards the development of multichannel systems for unshielded operation has been reported by Woeltgens *et al.* (1997), David *et al.* (1997), ter Brake, Janssen *et al.* (1997), and ter Brake, Karunanithi *et al.* (1997). David *et al.* fabricated a nine-channel system based on directly coupled dc SQUID magnetometers, each of which was enclosed in a fiberglass module to protect it from moisture. Each module contained a resistive heater so that the SQUID could be driven into the normal state to release trapped magnetic flux. To reduce the environmental noise David *et al.* (1997) used a copper coil around the dewar as a reference magnetometer that fed compensating currents into a coil surrounding the planar magnetometer array. They also used digital subtraction to form first-derivative gradiometers. The combination of these techniques reduced the

noise at 30 Hz from about $30 \text{ pT Hz}^{-1/2}$ to about $1 \text{ pT Hz}^{-1/2}$ for each channel, an order of magnitude above the intrinsic noise of the sensors. This performance made it possible to obtain contour maps after 80 averages, with the aid of a template matching technique. Compensating the component of the earth's static magnetic field perpendicular to the plane of the magnetometers did not reduce the noise any further. The excess noise was believed to arise from gradients in the environmental noise or the motion of vortices in the YBCO films. The latter effect could presumably be eliminated by reducing the linewidths of the superconducting films sufficiently (Sec. IX.A).

Ter Brake, Janssen *et al.* (1997), and ter Brake, Karunanithi *et al.* (1997) made a similar seven-channel system, also encapsulating their directly coupled magnetometers to exclude moisture. They used groups of three neighboring magnetometers in the planar array to form electronic first- and second-order gradiometers. Noise rejection was limited to about 2% by lack of planarity and by variations in the transfer functions of the individual SQUIDS, which resulted in varying gains and phase shifts in the flux-locked loops.

The five-channel system of Woeltgens *et al.* (1997) makes use of the TSG (Koch *et al.*, 1993). Three magnetometers were stacked in the *z* direction to form the TSG, and two more magnetometers were used to cancel residual *x* and *y* components of the noise. In addition, the outputs from a three-axis flux-gate magnetometer were coupled to three sets of external coils to provide active noise cancellation. The lowest noise achieved was about $400 \text{ fT Hz}^{-1/2}$ at 1 Hz (Koch, 1997).

We have seen that single-channel, multilayer magnetometers operating in a magnetically shielded environment have sufficient resolution to obtain clinically meaningful MCG's. Packages to protect the sensors and to enable excess flux to be expelled have been developed. However, no multichannel system has yet been demonstrated that even approaches the performance of the best single-channel devices, suggesting that such high- T_c sensors are not yet routinely available. With regard to unshielded systems, a good deal of progress has been made, but substantially more will have to be made before the noise levels approach that of high- T_c directly coupled magnetometers, about $100 \text{ fT Hz}^{-1/2}$, let alone the much lower noise levels of low- T_c systems. One might hope some of the recent progress reported in Secs. VIII and IX will lead to lower noise in unshielded systems in the near future.

B. Nondestructive evaluation

Nondestructive evaluation (NDE) is the noninvasive identification of structural or material flaws in a specimen. Examples are the imaging of surface and subsurface cracks or pits due to corrosion or fatigue in aging aircraft and reinforcing rods in concrete structures (Wiksw, 1995). While there is a variety of acoustic, thermal, and electromagnetic techniques currently used in NDE, these methods are often not entirely adequate for de-

tecting flaws at an early enough stage, usually because of a lack of spatial or depth resolution.

An important application of high- T_c SQUIDS in NDE is to replace induction coils in eddy-current imaging, a widely used method for the detection of subsurface damage in metallic structures such as aircraft (Wiksw, 1995). In this technique, one applies an alternating magnetic field produced by a drive coil and lock-in detects the fields generated by the induced eddy currents in the structure. The eddy currents are diverted by structural flaws resulting in distortions of the magnetic field. Since the eddy currents flow over a skin depth, which is inversely proportional to the square root of the frequency, deep defects require correspondingly low frequencies. Thus the flat frequency response of SQUIDS is a distinct advantage over the response of coils which falls off with decreasing frequency. Furthermore, high- T_c SQUIDS are distinctly preferable to low- T_c SQUIDS because their associated dewars or cryocoolers can be lighter and more compact. The insertion of SQUIDS into the NDE market is largely contingent on one's ability to retain high sensitivity in a mobile unit capable of operating in the magnetically unfriendly environment of an aircraft maintenance hangar or a factory.

Demonstrations of eddy-current NDE using high- T_c SQUIDS have been reported by a number of groups, especially during the past two years. Both dc and rf SQUIDS have been used in a variety of magnetometer and gradiometer configurations. The drive coil is mounted on the cryostat and typically has a double- D configuration to minimize the excitation field at the SQUID, which is mounted at the point where the field changes sign. For most realistic applications, one scans the SQUID and drive coil over the sample.

In one such system Tavrín *et al.* (1995) used an electronic SQUID gradiometer consisting of two high- T_c SQUIDS in a dewar of liquid nitrogen suspended over a sample that was scanned linearly at about 7 mm/s in an unshielded laboratory environment. The authors successfully imaged a series of slots cut into a copper plate as well as a 6-mm hole in a 1-mm-thick sheet of aluminum situated beneath two additional sheets of the same material. In a similar unshielded system Carr *et al.* (1977) used an electronic gradiometer consisting of two dc SQUIDS that was scanned above three 3-mm-thick layers of aircraft-grade aluminum held together by rivets and containing simulated defects 2–4 mm long radiating from the rivet centers in all three layers. Excitation fields were applied at two discrete frequencies and the resulting signals were lock-in detected and subtracted in an appropriate manner to distinguish the defects in the deeper layer from those in the surface layer.

In a step towards practical development of this technology, Hohmann *et al.* (1997) reported NDE measurements of structures in an unshielded environment using dc and rf SQUID-based magnetometers and monolithic gradiometers cooled by a commercial Joule-Thomson cryocooler. Either the sample or the sensor was scanned on a mobile x - y stage; the latter mode was aimed at

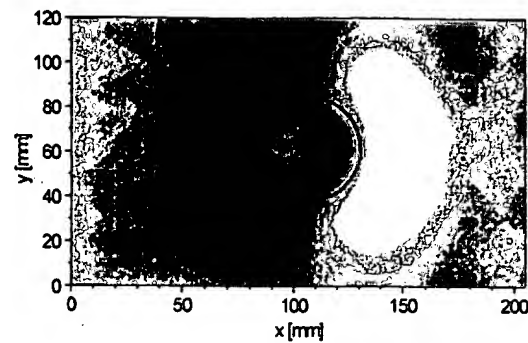


FIG. 40. Eddy-current image of a corrosion pit in an aluminum sheet ($1.5 \times 200 \times 400$ mm) situated beneath four aluminum sheets of equal size (Hohmann *et al.*, 1997).

investigating the possibility of a mobile SQUID system. Among the flaws analyzed were a corrosion pit and a simulated fatigue crack in an aluminum sheet; both were hidden underneath four intact 1.5-mm-thick aluminum plates. Figure 40 shows the image of a corrosion pit detected at a drive frequency of 20 Hz with the cryocooler in motion.

Kreutzbruck, Tröll *et al.* (1997), Mück *et al.* (1997), and Kreutzbruck *et al.* (1998) developed two NDE systems, one with the sensors cooled by liquid nitrogen and the other with them cooled by a miniature Stirling refrigerator, which chills neon gas to about 50 K. Each system contained up to four rf SQUIDS operated at 3 GHz, with a noise of about $1 \text{ pT Hz}^{-1/2}$ above 1 Hz and a high slew rate and dynamic range to allow unshielded operation. This group reported an impressive demonstration of one of their systems in an aircraft hangar to detect flaws in felloes that were rotated close to the dewar at 6–20 rpm. The felloe consists of a hollow steel cylinder containing six ferromagnetic steel bars, at 60° intervals, for heat dissipation, and three venting holes, 10 mm in diameter, at 120° intervals. Thus, in searching for cracks in the felloe, it is necessary to distinguish their signature from the signals produced by the bars and holes. Figure 41 shows the amplitude and phase of the magnetic field detected by the SQUID as the felloe is rotated through 360° . A 4-mm-long crack is easily distinguished from the periodic signals from the bars and holes. The authors developed an algorithm that combines the amplitude and phase data to make the periodic signals vanish, leaving a prominent signal from the crack [Fig. 41(c)]. Similar work has been reported by Krause *et al.* (1997), who tested aircraft wheels with a mobile SQUID system in the Lufthansa maintenance facility at Frankfurt airport. Although still at the prototype stage, these techniques have considerable promise as an NDE tool for the aircraft industry.

Historically, much of the early research on NDE with low- T_c SQUIDS was concerned with the detection of magnetic fields generated by specimens containing magnetized components (Donaldson *et al.*, 1990; Banchet *et al.*, 1995), and several groups are now using high- T_c devices for this approach. Schmidl, Wunderlich, Dörner, Specht, Linzen *et al.* (1997) and Kasai *et al.*

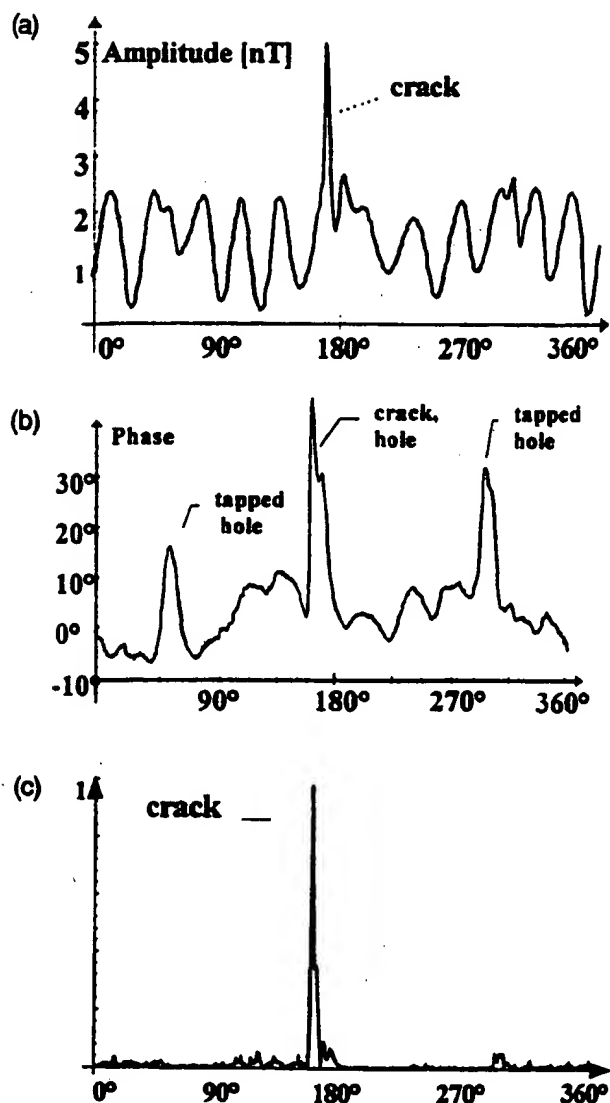


FIG. 41. Crack detection in an aircraft felloe: (a) Amplitude and (b) phase of gradiometer signal produced by eddy currents during one rotation of the felloe. The crack is indicated. The periodic signal is due to ferromagnetic steel bars located in the felloe at 60° intervals and three tapped holes at 120° intervals. (c) Result of algorithm to suppress signals from the steel bars and holes. (Mück et al., 1997).

(1997) used a planar dc SQUID gradiometer and a magnetometer, respectively, to scan samples of steel to explore the correlation between mechanical stress and magnetic-field distribution. The latter group imaged the magnetic field contours resulting from different degrees of residual stress in the material. This method is a unique probe of the mechanical or thermal stress to which a sample has been subjected. We have recently become aware of work by Tavrín et al. (1999), under contract with a manufacturer of turbine engines. These authors detect ferrous inclusions in the disks of turbine engine rotors using a high- T_c , second-order electronic SQUID gradiometer in an unshielded environment. This work represents an important step beyond "proof-of-concept" in introducing high- T_c SQUIDS into the NDE market. In a very different application Nagaishi et al.

(1997) used a high- T_c dc SQUID magnetometer to detect fine magnetic particles in a rapidly moving copper wire. In their arrangement, the nitrogen-cooled SQUID was surrounded by a magnetic shield and the wire was pulled through holes in the shield about 15 mm below the SQUID at speeds of 10 to 500 m/min. Iron particles as small as $50\text{ }\mu\text{m}$ in diameter were detected. The goal of this technique is to locate impurities that make the wire brittle, causing it to break.

Although some of the measurements we have just described are at the prototype stage, there have been impressive demonstrations on aircraft components. Fortunately, these techniques do not require the highest sensitivity, since the Nyquist noise generated by the sample can be on the order of $1\text{ pT Hz}^{-1/2}$. This noise level is much lower than that of coils conventionally used for eddy current NDE. Thus, although some development remains, the future of NDE based on high- T_c SQUIDS is very promising indeed.

C. Scanning SQUID microscopy

Magnetic microscopes based on low- T_c dc SQUIDS have been used to image static magnetic fields with a combination of high field and spatial resolution (for example, Mathai et al., 1993; Vu and Van Harlingen, 1993; Tsuei et al., 1994). This development led, shortly afterwards, to the development of high- T_c SQUID microscopes (Black et al., 1993; Black, 1995; Lee et al., 1996, 1997), in which the sample may be at either 77 K or at room temperature. Most often, the sample is scanned over the SQUID in a two-dimensional raster to produce an image. The scanning stage, made from nonmagnetic composite material, is driven by threaded rods turned by stepper motors. The frequency at which the image is obtained ranges from near zero, where one simply measures the static magnetic field produced by the sample, to beyond 1 GHz.

Figure 42 shows a microscope in which the sample is maintained at room temperature. The SQUID is mounted in vacuum at the upper end of a sapphire rod, the lower end of which is cooled by liquid nitrogen. Superinsulation surrounding the rod ensures that the temperature gradient along it is negligible. The SQUID is separated from room temperature and atmospheric pressure by a window, which may be either a $75\text{-}\mu\text{m}$ -thick sapphire disk or a $3\text{-}\mu\text{m}$ -thick Si_3N_4 window fabricated on a Si chip. In the first case, the SQUID-to-sample separation is typically $150\text{ }\mu\text{m}$, whereas in the latter, the separation can be as low as $15\text{ }\mu\text{m}$. The entire system is surrounded by a mu-metal shield to exclude spurious magnetic field fluctuations, and the SQUID is operated in a flux-locked loop.

A novel application of the microscope, in which the sample is held fixed, is the detection of the motion of magnetotactic bacteria (Lee et al., 1997). Each bacterium contains a series of magnetite particles giving it a magnetic moment of about $5 \times 10^{-16}\text{ A cm}^2$. As an example of such measurements, Fig. 43 shows the spectral density of the magnetic-field fluctuations produced by an

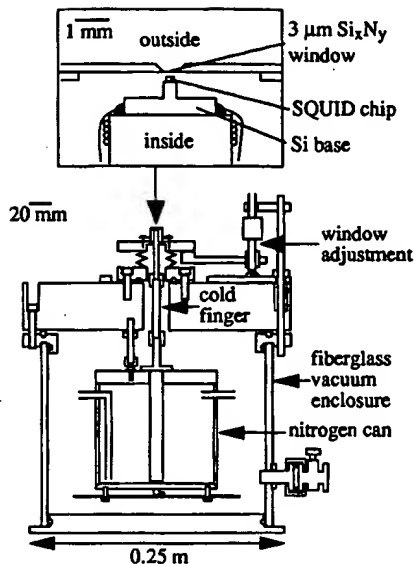


FIG. 42. Sectional side view of scanning SQUID microscope, without X - Y scanner (Chemla et al., 1997).

ensemble of dead bacteria in water. The bacteria undergo Brownian rotation, producing a Lorentzian power spectrum of the form $1/[1+(\omega\tau_0)^2]$, where $\tau_0 = \alpha_r/k_B T$ is the characteristic rotation time of the bacteria and α_r is the rotational damping coefficient. The fitted value of τ_0 , 15.9 s, is in good accord with predictions assuming a bacterial diameter of $1\text{ }\mu\text{m}$ and a length of $4\text{ }\mu\text{m}$. Measurements underway include the dynamics of living bacteria (Chemla et al., 1997), the effects of an applied magnetic field, and the migration of bacteria through porous media.

We turn now to higher-frequency operation. In the frequency range from 1 kHz to 1 MHz, Black et al. (1994) operated the SQUID open loop and used a drive coil to apply a sinusoidal magnetic field to induce eddy currents in the sample and modulate the flux in the SQUID. The magnetic response of the sample is determined by measuring the amplitude and phase of the output from the SQUID: the out-of-phase component corresponds to the eddy current in the sample. This approach resembles the eddy current technique described in Sec. X.B, but enables one to operate at substantially higher frequencies.

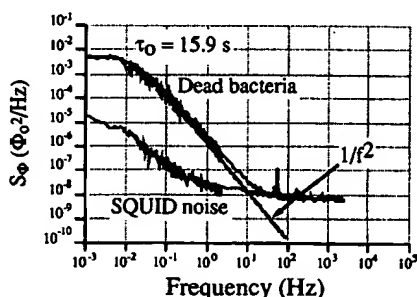


FIG. 43. Spectral density of dead magnetotactic bacteria with fitted Lorentzian (solid line). Lower power spectrum represents the SQUID noise (Lee et al., 1997).

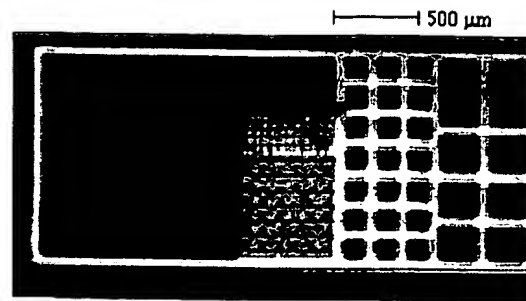


FIG. 44. Image of patterned thin film of Cu scanned over SQUID with 9 GHz Josephson frequency (Black et al., 1995).

Black et al. (1995b, 1995) extended the imaging frequency from 1 MHz to 1 GHz by applying a rf field to the sample, which, in turn, couples an rf flux Φ_{rf} into the SQUID. The rf flux smooths out the V - Φ curve of the SQUID, reducing the modulation depth. Thus, when the SQUID is also flux-modulated at a low frequency, $f_m = 25\text{ kHz}$, one can show that the modulation depth is given by

$$V(\Phi_{rf}) = V_0 J_0(2\pi\Phi_{rf}/\Phi_0), \quad (10.1)$$

where V_0 is the value with no rf field and J_0 is the zero-order Bessel function of the first kind. Equation (10.1) can be inverted to find Φ_{rf} provided it is sufficiently small. This technique was used to image a wire in the shape of a meander pattern.

For frequencies higher than 1 GHz, one can use the SQUID itself as the source of the field excitation (Black et al., 1995a, 1995). The oscillating magnetic fields at the Josephson frequency corresponding to the bias voltage induce eddy currents in the nearby sample which couple fields back into the SQUID. The essential effect is to reduce the inductance of the SQUID, thereby increasing the voltage modulation depth measured at low frequencies. Thus by monitoring the modulation depth as the sample is scanned over the SQUID one can obtain images at microwave frequencies. Figure 44 shows an image of a 500-nm-thick Cu film that had been patterned into a series of grids of various sizes. The SQUID was $40\text{ }\mu\text{m}$ from the grid, and the Josephson frequency was about 9 GHz. The brightest regions correspond to an increase in modulation depth of about 2%.

In concluding this section, we note that the best scanning SQUID microscopes with cold samples have a spatial resolution of perhaps $5\text{ }\mu\text{m}$, while those with room-temperature samples have a resolution that is more like $30\text{--}50\text{ }\mu\text{m}$. A recent innovation (Pitzius et al., 1997), however, has dramatically improved the spatial resolution for cold samples, albeit at the price of magnetic-field sensitivity. These authors use a soft magnetic tip to focus the flux from the sample into the SQUID, and were able to achieve a spatial resolution of the order of $0.1\text{ }\mu\text{m}$. A similar principle has been used by Tavrín and Siegel (1997) to examine room-temperature samples.

D. Geophysics

A particularly appealing application of high- T_c SQUID magnetometers is in geophysical surveying



(Clarke, 1983), for example, magnetotellurics, controlled-source electromagnetics, and cross-borehole sounding. In magnetotellurics, one measures simultaneously the fluctuating horizontal components of the electric and magnetic fields at the earth's surface; these fluctuating fields originate in the magnetosphere and ionosphere. From these frequency-dependent fields one calculates the impedance tensor of the ground and hence estimates the spatial variation of the resistivity of the ground. Frequencies of interest are typically 10^{-3} – 10^2 Hz, and the corresponding skin depths, assuming a resistivity of $10 \Omega\text{m}$, are 50 km to 150 m. To eliminate the effects of local noise sources, one cross-correlates the fluctuating fields with those measured with a remote reference magnetometer 5–10 km away. Applications of magnetotellurics include surveying for oil and gas, and locating subsurface fault lines. In controlled-source electromagnetics, one uses a transmitter to supply large current or magnetic pulses to the ground, and determines the magnetic response. The naturally occurring fluctuating fields are now a source of noise, and a remote magnetometer is used to cancel them. In cross-borehole sounding, a receiver in one borehole is used to detect magnetic pulses from a transmitter in a second borehole. From the real and imaginary parts of the received signal one deduces the susceptibility of the ground between the two boreholes, and models the porosity.

Currently, these magnetic measurements are made with induction coils. In fact, in the late 1970s and early 1980s, low- T_c SQUID magnetometers were used very successfully in magnetotellurics (Clarke *et al.*, 1983) and exploited commercially. However, the inconvenience of using liquid helium, particularly in remote areas of the world, coupled with the drop in the price of oil which severely curtailed oil prospecting, led to the abandonment of cryogenic sensors. The advent of liquid nitrogen-cooled magnetometers, on the other hand, has renewed interest in this application. Below about 1 Hz, the spectral density of the noise in coils increases as $1/f^3$, whereas that of SQUIDs increases as $1/f$, giving the latter magnetometer a substantial advantage at low frequencies. Furthermore, coils for use below 1 Hz can be as long as 1.5 m, and the deployment of three such coils orthogonally, buried in the ground for stability, is a tedious undertaking. Thus a three-axis high- T_c magnetometer in a compact dewar with a long hold time becomes very competitive.

Dantsker *et al.* (1994) constructed a three-axis magnetometer based on directly coupled magnetometers, and showed that it had sufficient slew rate for use in the field. Wang *et al.* (1997) reported preliminary experiments using a high- T_c magnetometer for magnetotellurics and transient electromagnetics. Matzander *et al.* (1997) deployed a system with a white noise of $200 \text{ fT Hz}^{-1/2}$ and a $1/f$ knee of 10 Hz, and used it successfully to demonstrate controlled-source electromagnetic measurements. A system for shallow borehole sounding is under development (Drung *et al.*, 1997; Radic *et al.*, 1997).

What sensitivity does one require, for example, for magnetotellurics? A white noise of 20 – $30 \text{ fT Hz}^{-1/2}$ and a $1/f$ knee of 1 Hz would be competitive; needless to say, these noise levels must be attained with the magnetometer operating in the earth's magnetic field, so that elimination of low-frequency noise due to vortex motion is imperative (Sec. IX.A). The fabrication of such a system is eased by the fact that there are no tight space constraints, and one could almost certainly use single-layer components, for example, a dc or rf SQUID coupled to a large-area flux transformer in a flip-chip arrangement.

XI. CONCLUDING REMARKS

The performance of high- T_c dc and rf SQUIDs and of magnetometers based upon them has progressed to the point where, in principle, it is adequate for many practical applications. One notable exception is magnetoencephalography, where the magnetic-field noise of a few $\text{fT Hz}^{-1/2}$ at frequencies down to below 1 Hz routinely achieved with low- T_c devices is still somewhat beyond the reach of their high- T_c counterparts. What, then, are the major issues remaining in the fabrication and operation of the high- T_c devices and what are the most likely uses of them in the next few years?

Many groups can routinely deposit high-quality thin films of YBCO with low levels of $1/f$ flux noise in zero magnetic field. Very few, however, have anything like the same capability to deposit a YBCO-STO-YBCO structure, with each layer patterned to form a flux transformer, with guaranteed electrical integrity let alone low levels of $1/f$ noise. The multilayer magnetometers with the lowest white magnetic-field noise all exhibit $1/f$ noise at 1 Hz, even when cooled in zero magnetic field. Since unpatterned trilayers can be made with negligible excess noise, the noise in patterned structures is presumably associated with edges. It is likely—but not assured—that sufficiently careful engineering of these edges, perhaps accompanied by more transmission electron microscopy, will reduce the flux noise power at 1 Hz by the required order of magnitude. With regard to junctions, despite enormous progress with artificial barriers, the workhorse for SQUIDs remains the grain-boundary junction. Even bicrystal grain-boundary junctions are not entirely routine: although one often can produce, say, a dozen SQUIDs on a bicrystal that all exhibit quantum interference, not all of them have optimum characteristics and correspondingly low noise. The degree of irreproducibility represents the variability in the bicrystal substrates, and it is not obvious that a great deal of improvement can be made. Thus the field still awaits the invention of a new junction technology that offers both high yield and high $I_0 R$ product. For the moment, at least from an economic standpoint, the best philosophy is probably to fabricate relatively large numbers of SQUIDs, select the best, and couple them to a suitable input circuit in a flip-chip arrangement.

Most research has been focused on dc SQUIDs, probably because their performance at 4.2 K has been much superior to rf SQUIDs. However, the advantage

of the dc SQUID over the rf SQUID at 77 K is much narrower, in part because one can use a somewhat larger inductance for the latter so that the effective area and intrinsic magnetic-field sensitivity are higher. To date, magnetometers based on dc SQUIDS have achieved lower noise than those of comparable size based on rf SQUIDS, particularly at low frequencies. However, this advantage has been due largely to the use of multilayer flux transformers coupled to dc SQUIDS, and may not persist now that such transformers are being used with rf SQUIDS. On the other hand, the fact that the white noise in dc SQUIDS is generally higher than predicted remains an important issue. If this problem is eventually resolved, for example, by the introduction of a more "perfect" type of junction, the performance of dc SQUIDS may well improve substantially. Furthermore, the possibility of significant crosstalk between rf SQUIDS in a multichannel system may prove to be a significant challenge. Thus the question of whether to choose dc or rf SQUIDS is still open, and may ultimately depend on the application at hand.

We have emphasized issues of operating SQUIDS in an unshielded environment. The fact that the $1/f$ noise can increase dramatically when a high- T_c SQUID is cooled in the earth's field is peculiar to high- T_c superconductors: because they are operated at much lower temperatures and have much higher flux-pinning energies, low- T_c SQUIDS do not suffer from this drawback. Hopefully, the introduction of narrow linewidths has solved the problem for high- T_c devices cooled in a static field, although this has yet to be demonstrated for a SQUID coupled to a multilayer, multiturn flux transformer. The use of a "flux dam" offers the possibility of maintaining low $1/f$ noise even after the ambient field is changed. In common with low- T_c SQUIDS, for most applications the operation of high- T_c SQUIDS without shielding generally raises the issue of ambient magnetic-field noise. The solution—the gradiometer—is the same for both techniques. However, 4.2 K systems have an inexpensive "low tech" approach based on niobium wire that is not available to 77 K systems. In high- T_c systems, the current options are to subtract the outputs of two or more magnetometers or to make planar, thin-film gradiometers. The former approach requires no new thin-film components and can be easily implemented with diagonal or off-diagonal first- or second-order gradients, arbitrarily long baselines, and in ingenious configurations such as the three-SQUID gradiometer. The thin-film gradiometers have the advantage of substantial rejection of uniform magnetic-field noise—say, by three orders of magnitude—by a passive, linear, noise-free device. It is straightforward to make gradiometers with short-baselines—a few millimeters—that are very adequate for nondestructive evaluation. On the other hand, a baseline of, say, 50 mm is more of a challenge. Single-layer, symmetric flux transformers have been used successfully but lose sensitivity because the inductance of their large-area pickup loops cannot be matched to the much lower inductance of the SQUID. The solution, of course, is to use multiturn input coils, but the cost of

making multilayer structures on large substrates is likely to be prohibitive. An alternative solution is the asymmetric gradiometer which requires only a single-layer flux transformer and does not significantly reduce the intrinsic sensitivity of the magnetometer to which it is coupled. The choice of gradiometers is another area that remains to be resolved.

Turning briefly to applications of high- T_c SQUIDS, we have seen impressive demonstrations of both MEG and MCG. However, as already noted, the sensitivity of high- T_c sensors is marginal for the former systems and while these systems are confined to relatively few centers and to a magnetically shielded room, the cost and higher boil-off rate of liquid ^4He are not overriding issues. On the other hand, one might hope that MCG will become a more widespread modality over the next few years, for example, in the assessment of damage to heart muscle following a cardiac infarction, for the diagnosis of heart arrhythmia and for locating the source of certain kinds of arrhythmia. Here, the benefits of liquid nitrogen as a cryogen—or indeed of a cryocooler in the longer term—combined with unshielded operation are highly desirable. Although clinical trials on large numbers of patients have yet to be performed, MCG currently appears to be the largest potential application of high- T_c SQUIDS. Whether or not this field materializes depends not only on the development of suitable, low-noise gradiometers for unshielded operations but also on the availability of funding for suitable trials.

A second application, nondestructive evaluation (NDE), is the one where the most "real world" progress has been made, for example, for the evaluation of aircraft components. Techniques involving both eddy currents and remanent magnetization have been successfully implemented. This is an area in which the ultimate sensitivity of SQUIDS is not required—generally $1 \text{ pT Hz}^{-1/2}$ is more than sufficient—and in which short-baseline gradiometers are adequate. The ability of the SQUID to operate in a static field and over a very wide range of frequencies gives an advantage over flux-gate magnetometers, and the fact that the sensitivity is maintained at arbitrarily low frequencies offers a distinct advantage over coils. This area seems poised for rapid growth.

Novel "SQUID microscopes" can be used in either a scanning or a static mode. The potential of these microscopes for biology is intriguing. One novel example is in immunoassay (Kötitz *et al.*, 1997). Here, one labels an antibody with a tiny magnetic particle and exposes it to an appropriate antigen in the solid phase. The binding of the antibody with the antigen is detected by means of the remanent magnetization imparted to the immobilized particle. Another potential use of the microscope is to detect low-frequency nuclear magnetic resonance (NMR) and nuclear quadrupole resonance of room-temperature samples, for example, NMR of hyperpolarized ^{129}Xe (TonThat *et al.*, 1997).

The use of high- T_c SQUIDS in geophysics is "straightforward" now that low levels of $1/f$ noise can be realized in the earth's magnetic field. One should not

underestimate the sensitivity of commercially available coils in these applications, but since the space constraints on a three-axis magnetometer are not severe, one should be able to achieve $10 \text{ fT Hz}^{-1/2}$ at 1 Hz, with a $1/f^{1/2}$ increase at lower frequencies, using a single-layer flux transformer. Such a system, packaged with suitably rugged dewar and electronics, would be very competitive for low-frequency applications at the earth's surface. In the longer term, the use of SQUID magnetometers for cross-borehole sounding would offer a distinct advantage over coils.

What will it take to foster this wide range of applications? Currently, most of these techniques continue to be practiced by people who are experts in SQUIDS and, indeed, who have made the devices themselves. Clearly, this situation must change if high- T_c SQUIDS are to be widely deployed. This change will require not only more user-friendly packaging but also lower pricing. Lower costs imply larger-scale manufacturing, and it is to be hoped that one or more companies will soon see fit to adopt the necessary processing technologies. However, one should recognize that the total system price is often dominated by the cost of the cryogenics, be it liquid nitrogen or a cryocooler. This additional expense must be justified in terms of improved performance compared with competing technologies if SQUID-based instruments are to be widely adopted.

Note added in proof. Chesca (1998b, 1999) developed an analytic theory for dc SQUIDS operating in the presence of large thermal fluctuations, similar to his approach for rf SQUIDS. This work is based on solving the two-dimensional Fokker-Planck equation, which is equivalent to the coupled Langevin equations. Chesca finds analytical solutions for the dc SQUID in the limit $\beta_L < 1/\pi$. The noise energy ε scales as $\varepsilon \propto \Gamma^4$, for fixed L , and the optimum SQUID inductance is found to be $L = L_{th}/\pi$ ($\approx 10 \text{ pH}$ at $T = 77 \text{ K}$) for $\Gamma > 1$.

In a systematic study of the transfer function and thermal noise of YBCO dc SQUIDS, Barthel *et al.* (1999) compare both numerical simulations and Chesca's analytical approach with experimental results obtained for a wide range of noise parameters up to $\Gamma = 5$. Several predictions of the analytical theory could be verified experimentally, and a good qualitative agreement with both theories is observed. Furthermore, the numerical simulations performed in the limit of large thermal fluctuations show excellent agreement with the analytic theory.

Zhang *et al.* (1999) demonstrated a design of a planar multiturn flux transformer integrated with a superconducting labyrinth resonator serving as the planar tank circuit for a YBCO thin film rf SQUID magnetometer. When coupled to a 210 pH double-hole washer SQUID in flip-chip configuration the magnetometer showed a white magnetic field noise as low as $11.5 \text{ fT Hz}^{-1/2}$ (above $f \approx 3 \text{ kHz}$). However, the noise at 10 Hz was more than one order of magnitude above the white noise level, presumably due to $1/f$ noise from poor film quality.

Kittel *et al.* (1998) have fabricated and tested a planar, thin-film, second-derivative gradiometer. The flux trans-

former consisted of two identical pickup loops placed one on each side of a smaller loop that was inductively coupled to a directly coupled magnetometer; this configuration can be envisioned as a second pickup loop coupled to the left-hand side of the smaller loop in Fig. 33(b). The overall length of the flux transformer was 80 mm, and the baselines for the first- and second-derivatives were 62 mm and 31 mm, respectively. By mechanically adjusting the separation between the magnetometer and the flux transformer, the authors achieved a typical rejection of uniform magnetic fields of 50 ppm. The residual first-order gradient response was at most 1.4% relative to the second-order gradient response.

Fleet *et al.* (1999) have described a high T_c scanning SQUID microscope for detecting flaws in computer chips. The room-temperature sample could be brought to within $30 \text{ }\mu\text{m}$ of the SQUID, which was cooled by a cryocooler. A 3 kHz current was passed through the circuit, which was on the far side of the chip from the SQUID, and the magnetic field images obtained by the SQUID were inverted to generate two-dimensional current density distributions. This technique enabled the authors to achieve a spatial resolution of $75 \text{ }\mu\text{m}$, substantially less than the SQUID-circuit separation of $340 \text{ }\mu\text{m}$. A short-circuit on the chip was located.

ACKNOWLEDGMENTS

In preparing this review we have benefitted from help from many people. We gratefully acknowledge discussions with L. Alff, K. Barthel, R. Cantor, B. Chesca, R. Dittmann, O. Dössel, D. Drung, R. Gross, R. H. Koch, H.-J. Krause, A. Marx, M. Mück, and M. Siegel. We are indebted to A. I. Braginski, B. Chesca, and R. Gross, each of whom read one section and made constructive comments. The following authors supplied us with figures: R. Cantor, B. Chesca, G. M. Daalmans, D. Drung, M. I. Faley, R. Gross, R. Hohmann, H.-J. Krause, R. H. Koch, A. Marx, M. Mück, T. Nagaishi, J. Z. Sun, Y. Tavrín, F. C. Wellstood, and Y. Zhang. B. Salisbury prepared the entire manuscript. This work was partly supported by the Director, Office of Energy Research, Office of Basic Energy Sciences, Materials Sciences Division of the U.S. Department of Energy under Contract No. DE-AC03-76SF00098.

REFERENCES

- Aarnink, W. A. M., P. J. van den Bosch, T.-M. Roelofs, M. Verbiesen, H. J. Holland, H. J. M. ter Brake, and H. Rogalla, 1995, *IEEE Trans. Appl. Supercond.* **5**, 2470.
- Alff, L., G. M. Fischer, R. Gross, F. Kober, A. Beck, K. D. Husemann, T. Nissel, F. Schmidl, and C. Burckhardt, 1992, *Physica C* **200**, 277.
- Alff, L. S., S. Kleefisch, U. Schoop, M. Zittartz, T. Kemen, T. Bauch, A. Marx, and R. Gross, 1998, *Eur. Phys. J. B* **5**, 423.
- Ambegaokar, V., and B. I. Halperin, 1969, *Phys. Rev. Lett.* **22**, 1364.
- Aminov, B. A., A. A. Golubov, and M. Y. Kupriyanov, 1996, *Phys. Rev. B* **53**, 365.

- Banchet, J., J. Jouglar, P.-L. Vuillermoz, P. Waltz, and H. Weinstock, 1995, *IEEE Trans. Appl. Supercond.* **5**, 2486.
- Barbour, J. C., E. L. Venturini, D. S. Ginley, and J. F. Kwak, 1992, *Nucl. Instrum. Methods Phys. Res. B* **65**, 531.
- Barone, A., and G. Paterno, 1982, *Physics and Applications of the Josephson Effect* (Wiley, New York).
- Barth, R., B. Spangenberg, C. Jäckel, H. G. Roskos, H. Kurz, and B. Holzapfel, 1993, *Appl. Phys. Lett.* **63**, 1149.
- Barthel, K., D. Koelle, B. Chesca, A. I. Braginski, A. Marx, R. Gross, and R. Kleiner, 1999, *Appl. Phys. Lett.* (in press).
- Beck, A., O. M. Froehlich, D. Koelle, R. Gross, H. Sato, and M. Naito, 1996, *Appl. Phys. Lett.* **68**, 3341.
- Beck, A., A. Stenzel, O. M. Froehlich, R. Gerber, R. Gerdemann, L. Alff, B. Mayer, R. Gross, A. Marx, J. C. Villegier, and H. Moriceau, 1995, *IEEE Trans. Appl. Supercond.* **5**, 2192.
- Bednorz, J. G., and K. A. Müller, 1986, *Z. Phys. B* **64**, 189.
- Berberich, P., B. Utz, W. Prusseit, and H. Kinder, 1994, *Physica C* **219**, 497.
- Beyer, J., D. Drung, F. Ludwig, T. Minotani, and K. Enpuku, 1998, *Appl. Phys. Lett.* **72**, 203.
- Black, R. C., 1995, Ph.D. thesis, University of Maryland.
- Black, R. C., A. Mathai, F. C. Wellstood, E. Dantsker, A. H. Miklich, D. T. Nemeth, J. J. Kingston, and J. Clarke, 1993, *Appl. Phys. Lett.* **62**, 2128.
- Black, R. C., F. C. Wellstood, E. Dantsker, A. H. Miklich, J. J. Kingston, D. T. Nemeth, and J. Clarke, 1994, *Appl. Phys. Lett.* **64**, 1.
- Black, R. C., F. C. Wellstood, E. Dantsker, A. H. Miklich, D. Koelle, F. Ludwig, and J. Clarke, 1995, *IEEE Trans. Appl. Supercond.* **5**, 2137.
- Black, R. C., F. C. Wellstood, E. Dantsker, A. H. Miklich, D. T. Nemeth, D. Koelle, F. Ludwig, and J. Clarke, 1995a, *Appl. Phys. Lett.* **66**, 99.
- Black, R. C., F. C. Wellstood, E. Dantsker, A. H. Miklich, D. T. Nemeth, D. Koelle, F. Ludwig, and J. Clarke, 1995b, *Appl. Phys. Lett.* **66**, 1267.
- Bode, M., M. Grove, M. Siegel, and A. I. Braginski, 1996, *J. Appl. Phys.* **80**, 6378.
- Borgmann, J., P. David, G. Ockenfuß, R. Otto, J. Schubert, W. Zander, and A. I. Braginski, 1997, *Rev. Sci. Instrum.* **68**, 2730.
- Braginski, A. I., 1993, in *The New Superconducting Electronics*, NATO ASI series, edited by H. Weinstock and R. W. Ralston (Kluwer Academic, Dordrecht), p. 89.
- Braginski, A. I., 1996, in *SQUID Sensors: Fundamentals, Fabrication and Applications*, NATO ASI Series, edited by H. Weinstock (Kluwer Academic, Dordrecht), p. 235.
- Bruines, J. J. P., V. J. de Waal, and J. E. Mooji, 1982, *J. Low Temp. Phys.* **46**, 383.
- Burghoff, M., L. Trahms, Y. Zhang, H. Bousack, and J. Borgmann, 1996, *J. Clin. Eng.* **21**, 62.
- Cantor, R., 1996, in *SQUID Sensors: Fundamentals, Fabrication and Applications*, NATO ASI Series, edited by H. Weinstock (Kluwer Academic, Dordrecht), p. 179.
- Cantor, R., L. P. Lee, M. Teepe, V. Vinetskiy, and J. Longo, 1995, *IEEE Trans. Appl. Supercond.* **5**, 2927.
- Carr, C., D. McA. McKirdy, E. J. Romans, and G. B. Donaldson, 1997, *IEEE Trans. Appl. Supercond.* **7**, 3275.
- Chang, W. H., 1981, *IEEE Trans. Magn.* **MAG-17**, 764.
- Char, K., M. S. Colclough, L. P. Lee, and G. Zaharchuk, 1991, *Appl. Phys. Lett.* **59**, 2177.
- Chaudhari, P., J. Mannhart, D. Dimos, C. C. Tsuei, C. C. Chi, M. M. Opreysko, and M. Scheuermann, 1988, *Phys. Rev. Lett.* **60**, 1653.
- Chemla, Y. R., T. S. Lee, J. Clarke, M. Adamkiewicz, and B. Buchanan, 1997, in *Extended Abstracts of the 6th International Superconductive Electronics Conference (ISEC'97)*, Berlin, edited by H. Koch and S. Knappe (Physikalisch-Technische Bundesanstalt, Braunschweig), Vol. 1, p. 140.
- Chen, J., T. Yamashita, H. Suzuki, K. Nakajima, H. Kurosawa, Y. Mutoh, Y. Hirotsu, H. Myoren, and Y. Osaka, 1991, *Jpn. J. Appl. Phys., Part 1* **30**, 1964.
- Chen, Y. F., Z. G. Ivanov, E. A. Stepantsov, A. Ya. Tzalenchuk, S. Zarembinski, T. Claeson, and L.-G. Johansson, 1996, *J. Appl. Phys.* **79**, 9221.
- Chesca, B., 1998a, *J. Low Temp. Phys.* **110**, 963.
- Chesca, B., 1998b, *J. Low Temp. Phys.* **112**, 165.
- Chesca, B., 1999, *IEEE Trans. Appl. Supercond.* (in press).
- Clarke, J., 1983, *IEEE Trans. Magn.* **MAG-19**, 288.
- Clarke, J., 1996, in *SQUID Sensors: Fundamentals, Fabrication and Applications*, NATO ASI Series, edited by H. Weinstock (Kluwer Academic, Dordrecht), p. 1.
- Clarke, J., T. D. Gamble, W. M. Goubau, R. H. Koch, and R. F. Miracky, 1983, *Geophys. Pros.* **31**, 149.
- Clarke, J., W. M. Goubau, and M. B. Ketchen, 1976, *J. Low Temp. Phys.* **25**, 99.
- Clem, J., 1996, unpublished.
- Clem, T. R., J. W. Purpura, R. F. Wiegert, and W. L. Goodman, 1993, *IEEE Trans. Appl. Supercond.* **3**, 1848.
- Colclough, M. S., C. E. Gough, M. Keene, C. M. Muirhead, N. Thomas, J. S. Abell, and S. Sutton, 1987, *Nature (London)* **328**, 47.
- Curio, G., D. Drung, H. Koch, W. Müller, U. Steinhoff, L. Trahms, Y. Q. Shen, P. Vase, and T. Freltoft, 1996, *Neurosci. Lett.* **206**, 204.
- Daalmans, G. M., 1995, *Appl. Supercond.* **3**, 399.
- Daalmans, G. M., L. Bär, M. Kühnl, D. Uhl, M. Selent, and J. Ramos, 1995, *IEEE Trans. Appl. Supercond.* **5**, 3109.
- Daly, K. P., J. Burch, S. Coons, and R. Hu, 1991, *IEEE Trans. Magn.* **MAG-27**, 3066.
- Danilov, V. V., K. K. Likharev, and O. V. Snigirev, 1980, in *SQUID'80, Superconducting Quantum Interference Devices and their Applications*, edited by H. D. Hahlbohm and H. Lübbig (Walter de Gruyter, Berlin), p. 473.
- Dantsker, E., O. Froehlich, S. Tanaka, K. Kouznetsov, J. Clarke, Z. Lu, V. Matijasevic, and K. Char, 1997, *Appl. Phys. Lett.* **71**, 1712.
- Dantsker, E., D. Koelle, A. H. Miklich, D. T. Nemeth, F. Ludwig, J. Clarke, J. T. Longo, and V. Vinetskiy, 1994, *Rev. Sci. Instrum.* **65**, 3809.
- Dantsker, E., F. Ludwig, R. Kleiner, J. Clarke, M. Teepe, L. P. Lee, N. McN. Alford, and T. Button, 1995, *Appl. Phys. Lett.* **67**, 725.
- Dantsker, E., S. Tanaka, and J. Clarke, 1997, *Appl. Phys. Lett.* **70**, 2037.
- Dantsker, E., S. Tanaka, P.-Å. Nilsson, R. Kleiner, and J. Clarke, 1996, *Appl. Phys. Lett.* **69**, 4099.
- David, B., O. Dössel, V. Doormann, R. Eckart, W. Hoppe, J. Krüger, H. Laudan, and G. Rabe, 1997, *IEEE Trans. Appl. Supercond.* **7**, 3267.
- David, B., D. Grundler, R. Eckart, K. Fanghänel, J. P. Krumme, V. Doormann, and O. Dössel, 1994, *Supercond. Sci. Technol.* **7**, 287.

- David, B., D. Grundler, S. Krey, V. Doormann, R. Eckart, J. P. Krumme, G. Rabe, and O. Dössel, 1996, *Supercond. Sci. Technol.* **9**, A96.
- David, B., D. Grundler, J.-P. Krumme, and O. Dössel, 1995, *IEEE Trans. Appl. Supercond.* **5**, 2935.
- Delin, K. A., and A. W. Kleinsasser, 1996, *Supercond. Sci. Technol.* **9**, 227.
- Deutscher, G., and K. A. Müller, 1987, *Phys. Rev. Lett.* **59**, 1745.
- de Waal, V. J., P. Schrijner, and R. Llubra, 1984, *J. Low Temp. Phys.* **54**, 215.
- Dieckmann, N., A. Bock, and U. Merkt, 1996, *Appl. Phys. Lett.* **68**, 3626.
- DiIorio, M. S., K.-Y. Yang, and S. Yoshizumi, 1995, *Appl. Phys. Lett.* **67**, 1926.
- DiIorio, M. S., S. Yoshizumi, K.-Y. Yang, M. Maung, and B. Power, 1993, in *Advances in Superconductivity V*, edited by Y. Bando and H. Yamauchi (Springer, Tokyo), p. 1161.
- DiIorio, M. S., S. Yoshizumi, K.-Y. Yang, M. Maung, J. Zhang, and B. Power, 1993, *IEEE Trans. Appl. Supercond.* **3**, 2011.
- DiIorio, M. S., S. Yoshizumi, K.-Y. Yang, J. Zhang, and M. Maung, 1991, *Appl. Phys. Lett.* **58**, 2552.
- Dillmann, F., V. N. Glyantsev, and M. Siegel, 1996, *Appl. Phys. Lett.* **69**, 1948.
- Dimos, D., P. Chaudhari, and J. Mannhart, 1990, *Phys. Rev. B* **41**, 4038.
- Dimos, D., P. Chaudhari, J. Mannhart, and F. K. LeGoues, 1988, *Phys. Rev. Lett.* **61**, 219.
- Dömel, R., C. Horstmann, M. Siegel, A. I. Braginski, and M. Y. Kupriyanov, 1995, *Appl. Phys. Lett.* **67**, 1775.
- Donaldson, G., S. Evanson, M. Otaka, K. Hasegawa, T. Shimizu, and K. Takaku, 1990, *Br. J. Non-Destr. Test.* **32**, 238.
- Dörrer, L., S. Wunderlich, F. Schmidl, H. Schneidewind, U. Hübner, and P. Seidel, 1997, *Appl. Supercond.* (in press).
- Dössel, O., B. David, M. Fuchs, W. H. Kullmann, and K.-M. Lüdeke, 1991, *IEEE Trans. Magn.* **MAG-27**, 2797.
- Drung, D., 1994, *IEEE Trans. Appl. Supercond.* **4**, 121.
- Drung, D., 1995, *Appl. Phys. Lett.* **67**, 1474.
- Drung, D., 1996, in *SQUID Sensors: Fundamentals, Fabrication and Applications*, NATO ASI Series, edited by H. Weinstock (Kluwer Academic, Dordrecht), p. 63.
- Drung, D., R. Cantor, M. Peters, T. Ryhänen, and H. Koch, 1991, *IEEE Trans. Magn.* **MAG-27**, 3001.
- Drung, D., R. Cantor, M. Peters, H.-J. Scheer, and H. Koch, 1990, *Appl. Phys. Lett.* **57**, 406.
- Drung, D., E. Dantsker, F. Ludwig, H. Koch, R. Kleiner, J. Clarke, S. Krey, D. Reimer, B. David, and O. Doessel, 1996, *Appl. Phys. Lett.* **68**, 1856.
- Drung, D., S. Knappe, and H. Koch, 1995, *J. Appl. Phys.* **77**, 4088.
- Drung, D. and H. Koch, 1993, *IEEE Trans. Appl. Supercond.* **3**, 2594.
- Drung, D., F. Ludwig, W. Müller, U. Steinhoff, L. Trahms, Y. Q. Shen, M. B. Jensen, P. Vase, T. Holst, T. Freltoft, and G. Curio, 1996, *Appl. Phys. Lett.* **68**, 1421.
- Drung, D., T. Radic, H. Matz, H. Koch, S. Knappe, S. Menkel, and H. Burkhardt, 1997, *IEEE Trans. Appl. Supercond.* **7**, 3283.
- Ehnholm, G. J., 1977, *J. Low Temp. Phys.* **29**, 1.
- Eidelloth, W., B. Oh, R. P. Robertazzi, W. J. Gallagher, and R. H. Koch, 1991, *Appl. Phys. Lett.* **59**, 3473.
- Enpuku, K., 1993, *Jpn. J. Appl. Phys., Part 2* **32**, L1407.
- Enpuku, K., H. Doi, G. Tokita, and T. Maruo, 1995, *IEEE Trans. Appl. Supercond.* **5**, 2762.
- Enpuku, K., T. Maruo, and T. Minotani, 1996, *J. Appl. Phys.* **80**, 1207.
- Enpuku, K., T. Maruo, and T. Minotani, 1997, *IEEE Trans. Appl. Supercond.* **7**, 3355.
- Enpuku, K., T. Muta, K. Yoshida, and F. Irie, 1985, *J. Appl. Phys.* **58**, 1916.
- Enpuku, K., Y. Shimomura, and T. Kisu, 1993, *J. Appl. Phys.* **73**, 7929.
- Enpuku, K., K. Sueoka, K. Yoshida, and F. Irie, 1985, *J. Appl. Phys.* **57**, 1691.
- Enpuku, K., G. Tokita, and T. Maruo, 1994, *J. Appl. Phys.* **76**, 8180.
- Enpuku, K., G. Tokita, T. Maruo, and T. Minotani, 1995, *J. Appl. Phys.* **78**, 3498.
- Erné, S. N., H.-D. Hahlbohm, and H. Lübbig, 1976, *J. Appl. Phys.* **47**, 5440.
- Falco, C. M. and W. H. Parker, 1975, *J. Appl. Phys.* **46**, 3238.
- Faley, M. I., U. Poppe, C. L. Jia, U. Dähne, Yu. Goncharov, N. Klein, K. Urban, V. N. Glyantsev, G. Kunkel, and M. Siegel, 1995, *IEEE Trans. Appl. Supercond.* **5**, 2091.
- Faley, M. I., U. Poppe, K. Urban, H. Hilgenkamp, H. Hennes, W. Aarnink, J. Flokstra, and H. Rogalla, 1995, *Appl. Phys. Lett.* **67**, 2087.
- Faley, M. I., U. Poppe, K. Urban, H.-J. Krause, H. Soltner, R. Hohmann, D. Lomparski, R. Kutzner, R. Wördenweber, H. Bousack, A. I. Braginski, V. Y. Slobodchikov, A. V. Gapeilyuk, V. V. Khanin, and Y. V. Maslennikov, 1997, *IEEE Trans. Appl. Supercond.* **7**, 3702.
- Ferrari, M. J., M. Johnson, F. C. Wellstood, J. Clarke, A. Inam, X. D. Wu, L. Nazar, and T. Venkatesan, 1989, *Nature (London)* **341**, 723.
- Ferrari, M. J., M. Johnson, F. C. Wellstood, J. Clarke, P. A. Rosenthal, R. H. Hammond, and M. R. Beasley, 1988, *Appl. Phys. Lett.* **53**, 695.
- Ferrari, M. J., M. Johnson, F. C. Wellstood, J. J. Kingston, T. J. Shaw, and J. Clarke, 1994, *J. Low Temp. Phys.* **94**, 15.
- Ferrari, M. J., J. J. Kingston, F. C. Wellstood, and J. Clarke, 1991, *Appl. Phys. Lett.* **58**, 1106.
- Fife, A. A., G. Anderson, V. Angus, C. Backhouse, K. Betts, M. B. Burbank, R. A. Cragg, K. Ferguson, F. Habib, P. R. Kubik, J. Nomura, M. Smith, P. Spear, W. Westera, Hu Zhou, S. Govorkov, B. Heinrich, J. C. Irwin, and W. B. Xing, 1995, *IEEE Trans. Appl. Supercond.* **5**, 3113.
- Fleet, E. H., S. Chatrathorn, F. C. Wellstood, S. M. Green, and L. A. Knauss, 1999, *IEEE Trans. Appl. Supercond.* (in press).
- Foglietti, V., W. J. Gallagher, M. B. Ketchen, A. W. Kleinsasser, R. H. Koch, S. I. Raider, and R. L. Sandstrom, 1986, *Appl. Phys. Lett.* **49**, 1393.
- Foglietti, V., R. H. Koch, W. J. Gallagher, B. Oh, B. Bumble, and W. Y. Lee, 1989, *Appl. Phys. Lett.* **54**, 2259.
- Foglietti, V., R. H. Koch, J. Z. Sun, R. B. Laibowitz, and W. J. Gallagher, 1995, *J. Appl. Phys.* **77**, 378.
- Forgacs, R. L., and A. F. Warnick, 1967, *Rev. Sci. Instrum.* **38**, 214.
- Freltoft, T., Y. Q. Shen, and P. Vase, 1993, *IEEE Trans. Appl. Supercond.* **3**, 2937.
- Friedl, G., M. Vildić, B. Roas, D. Uhl, F. Bömmel, M. Römheld, B. Hillenbrand, B. Stritzker, and G. M. Daalmans, 1992, *Appl. Phys. Lett.* **60**, 3048.

- Gao, J., W. A. M. Aarnink, G. J. Gerritsma, and H. Rogalla, 1990, *Physica C* **171**, 126.
- Gao, J., Y. Boguslavskij, B. B. G. Klopman, D. Terpstra, D. Wijbrans, G. J. Gerritsma, and H. Rogalla, 1992, *J. Appl. Phys.* **72**, 525.
- Gerber, R., D. Koelle, R. Gross, R. P. Huebener, F. Ludwig, E. Dantsker, R. Kleiner, and J. Clarke, 1996, *Appl. Phys. Lett.* **68**, 1555.
- Giffard, R. P., 1980, in *Superconducting Quantum Interference Devices and Their Applications*, edited by H. D. Hahlbohm and H. Lübbig (de Gruyter, Berlin), p. 445.
- Giffard, R. P., J. C. Gallop, and B. N. Petley, 1976, *Prog. Quantum Electron.* **4**, 301.
- Glyantsev, V. N., Y. Tavrín, W. Zander, J. Schubert, and M. Siegel, 1996, *Supercond. Sci. Technol.* **9**, A105.
- Golubov, A. A., and M. Y. Kupriyanov, 1996, *Physica C* **259**, 27.
- Govorkov, S., A. A. Fife, G. Anderson, V. Haid, Hu Zhou, B. Heinrich, and J. Chrzanowski, 1997, *IEEE Trans. Appl. Supercond.* **7**, 3235.
- Gross, R., in *Interfaces in High- T_c Superconducting Systems*, edited by S. L. Shinde and D. A. Rudman (Springer, New York), p. 176.
- Gross, R., L. Alff, A. Beck, O. M. Froehlich, R. Gerber, R. Gerdemann, A. Marx, B. Mayer, and D. Koelle, 1995, in *Proceedings of the 2nd Workshop on HTS Applications and New Materials*, edited by D. H. Blank (University of Twente, The Netherlands), p. 8.
- Gross, R., L. Alff, A. Beck, O. M. Froehlich, D. Koelle, and A. Marx, 1997, *IEEE Trans. Appl. Supercond.* **7**, 2929.
- Gross, R., and P. Chaudhari, 1992, in *Principles and Applications of Superconducting Quantum Interference Devices*, edited by A. Barone (World Scientific, Singapore), p. 419.
- Gross, R., P. Chaudhari, D. Dimos, A. Gupta, and G. Koren, 1990, *Phys. Rev. Lett.* **64**, 228.
- Gross, R., P. Chaudhari, M. Kawasaki, and A. Gupta, 1990, *Phys. Rev. B* **42**, 10735.
- Gross, R., P. Chaudhari, M. Kawasaki, and A. Gupta, 1991, *IEEE Trans. Magn.* **MAG-27**, 3227.
- Gross, R., P. Chaudhari, M. Kawasaki, M. B. Ketchen, and A. Gupta, 1990a, *Appl. Phys. Lett.* **57**, 727.
- Gross, R., P. Chaudhari, M. Kawasaki, M. B. Ketchen, and A. Gupta, 1990b, *Physica C* **170**, 315.
- Gross, R., and B. Mayer, 1991, *Physica C* **180**, 235.
- Grove, M., R. Dittmann, M. Bode, M. Siegel, and A. I. Braginski, 1996, *Appl. Phys. Lett.* **69**, 696.
- Grundler, D., B. David, R. Eckart, and O. Dössel, 1993, *Appl. Phys. Lett.* **63**, 2700.
- Grundler, D., B. David, and O. Dössel, 1995, in *Proceedings of the Second European Conference on Applied Superconductivity (EUCAS'95)*, Institute of Physics Conference Series No. **148**, Edinburgh, edited by D. Dew-Hughes (Institute of Physics, Bristol/Philadelphia), p. 1625.
- Grundler, D., R. Eckart, B. David, and O. Dössel, 1993, *Appl. Phys. Lett.* **62**, 2134.
- Gupta, A., J. Z. Sun, and C. C. Tsuei, 1994, *Science* **265**, 1075.
- Gurvitch, M., M. A. Washington, and H. A. Huggins, 1983, *Appl. Phys. Lett.* **42**, 472.
- Hagerhorst, J. M., J. D. Mannhart, M. M. Oprysko, M. R. Scheuermann, and C. C. Tsuei, 1989, *Laser and Particle-Beam Modification of Chemical Processes on Surfaces*, edited by A. W. Johnson, G. L. Loper and T. W. Sigmon, *Mat. Res. Soc. Symp. Proc.* Vol. **129**, 347.
- Hämäläinen, M., R. Hari, R. J. Ilmoniemi, J. Knuutila, and O. V. Lounasmaa, 1993, *Rev. Mod. Phys.* **65**, 413.
- Hansma, P. K., 1973, *J. Appl. Phys.* **44**, 4191.
- He, D. F., X. H. Zeng, H.-J. Krause, H. Soltner, F. Rüders, and Y. Zhang, 1998, *Appl. Phys. Lett.* **72**, 696.
- Hein, M. A., S. Schmöe, M. Strupp, H. Piel, Y. Zhang, and A. I. Braginski, 1995, *IEEE Trans. Appl. Supercond.* **5**, 2501.
- Herrmann, K., Y. Zhang, M. Mück, J. Schubert, and A. I. Braginski, 1991, *Supercond. Sci. Technol.* **4**, 583.
- Herrmann, K., G. Kunkel, M. Siegel, J. Schubert, W. Zander, A. I. Braginski, C. L. Jia, B. Kabius, and K. Urban, 1995, *J. Appl. Phys.* **78**, 1131.
- Hildebrandt, G., and F. H. Uhlmann, 1995, *IEEE Trans. Appl. Supercond.* **5**, 2766.
- Hilgenkamp, J. W. M., G. C. S. Brons, J. G. Soldevilla, R. P. J. Ijsselsteijn, J. Flokstra, and H. Rogalla, 1994, *Appl. Phys. Lett.* **64**, 3497.
- Hilgenkamp, J. W. M., R. P. J. Ijsselsteijn, A. J. H. M. Rijnders, P. A. C. Tavares, J. Flokstra, and H. Rogalla, 1993, *J. Alloys Compd.* **195**, 707.
- Hilgenkamp, H., J. Mannhart, and B. Mayer, 1996, *Phys. Rev. B* **53**, 14586.
- Hilgenkamp, J. W. M., F. J. G. Roesthuis, S. Hoogeveen, L. D. Vargas Llona, J. Flokstra, and H. Rogalla, 1995, in *Proceedings of the 2nd Workshop on HTS Applications and New Materials*, edited by D. H. A. Blank (Enschede, The Netherlands), p. 117.
- Hoenig, H. E., G. M. Daalmans, L. Bär, F. Bömmel, A. Paulus, D. Uhl, H. J. Weisse, S. Schneider, H. Seifert, H. Reichenberger, and K. Abram-Fuchs, 1991, *IEEE Trans. Magn.* **MAG-27**, 2777.
- Hohmann, R., H.-J. Krause, H. Soltner, Y. Zhang, C. A. Copetti, H. Bousack, and A. I. Braginski, 1997, *IEEE Trans. Appl. Supercond.* **7**, 2860.
- Hollenhorst, H. N., and R. P. Giffard, 1980, *J. Appl. Phys.* **51**, 1719.
- Hollin, C. A., J. S. Abell, S. W. Goodyear, N. G. Chew, and R. G. Humphreys, 1994, *Appl. Phys. Lett.* **64**, 918.
- Hosoya, M., E. Goto, N. Shimizu, and Y. Harada, 1989, *IEEE Trans. Magn.* **MAG-25**, 1111.
- Humphreys, R. G., J. S. Satchell, N. G. Chew, J. A. Edwards, S. W. Goodyear, and M. N. Keene, 1991, *Mater. Sci. Eng.* **B** **10**, 293.
- Husemann, K.-D., R. Gross, R. P. Huebener, and B. Roas, 1993, *Appl. Phys. Lett.* **62**, 2871.
- Il'ichev, E., V. Zakosarenko, V. Schultze, H.-G. Meyer, H. E. Hoenig, V. N. Glyantsev, and A. Golubov, 1998, *Appl. Phys. Lett.* **72**, 731.
- Itozaki, H., S. Tanaka, T. Nagaishi, and H. Kado, 1994, *IEICE Trans. Electron.* **E77-C**, 1185.
- Itozaki, H., S. Tanaka, H. Toyoda, T. Hirano, Y. Haruta, M. Nomura, T. Saijou, and H. Kado, 1996, *Supercond. Sci. Technol.* **9**, A38.
- Ivanov, Z. G., P. Å. Nilsson, D. Winkler, J. A. Alarco, T. Claesson, E. A. Stepantsov, and A. Ya. Tzalenchuk, 1991, *Appl. Phys. Lett.* **59**, 3030.
- Jackel, L. D., and R. A. Buhrman, 1975, *J. Low Temp. Phys.* **19**, 201.
- Jaklevic, R. C., J. Lambe, A. H. Silver, and J. E. Mercereau, 1964, *Phys. Rev. Lett.* **12**, 159.
- Jaycox, J. M., and M. B. Ketchen, 1981, *IEEE Trans. Magn.* **17**, 400.

- Jia, C. L., B. Kabius, K. Urban, K. Herrmann, G. J. Cui, J. Schubert, W. Zander, A. I. Braginski, and C. Heiden, 1991, *Physica C* **175**, 545.
- Jia, C. L., B. Kabius, K. Urban, K. Herrmann, J. Schubert, W. Zander, and A. I. Braginski, 1992, *Physica C* **196**, 211.
- Josephson, B. D., 1962, *Phys. Lett.* **1**, 251.
- Josephson, B. D., 1965, *Adv. Phys.* **14**, 419.
- Kang, D.-J., W. E. Booij, M. G. Blamire, and E. J. Tarte, 1997, in *Extended Abstracts of the 6th International Superconductive Electronics Conference (ISEC'97)*, Berlin, edited by H. Koch and S. Knappe (Physikalisch-Technische Bundesanstalt, Braunschweig), Vol. 3, p. 40.
- Kasai, N., N. Ishikawa, H. Yamakawa, K. Chinone, S. Nakayama, and A. Odawara, 1997, *IEEE Trans. Appl. Supercond.* **7**, 2315.
- Kawasaki, M., P. Chaudhari, and A. Gupta, 1992, *Phys. Rev. Lett.* **68**, 1065.
- Kawasaki, M., P. Chaudhari, T. H. Newman, and A. Gupta, 1991, *Appl. Phys. Lett.* **58**, 2555.
- Kawasaki, M., E. Sarnelli, P. Chaudhari, A. Gupta, A. Kussmaul, J. Lacey, and W. Lee, 1993, *Appl. Phys. Lett.* **62**, 417.
- Keene, M. N., N. G. Chew, S. W. Goodyear, J. A. Edwards, R. G. Humphreys, K. Lander, and J. S. Satchell, 1994, *Physica C* **230**, 110.
- Keene, M. N., N. J. Exon, R. G. Humphreys, and N. G. Chew, 1996, *J. Appl. Phys.* **79**, 8783.
- Keene, M. N., S. W. Goodyear, N. G. Chew, R. G. Humphreys, J. S. Satchell, J. A. Edwards, and K. Lander, 1994, *Appl. Phys. Lett.* **64**, 366.
- Keene, M. N., S. W. Goodyear, J. S. Satchell, J. A. Edwards, N. G. Chew, and R. G. Humphreys, 1993, *IEEE Trans. Appl. Supercond.* **3**, 2430.
- Keene, M. N., J. S. Satchell, S. W. Goodyear, R. G. Humphreys, J. A. Edwards, N. G. Chew, and K. Lander, 1995, *IEEE Trans. Appl. Supercond.* **5**, 2923.
- Ketchen, M. B., 1981, *IEEE Trans. Magn.* **17**, 387.
- Ketchen, M. B., W. J. Gallagher, A. W. Kleinsasser, S. Murphy, and J. R. Clem, 1985, in *SQUID'85, Superconducting Quantum Interference Devices and their Applications*, edited by H. D. Hahlbohm and H. Lübbig (Walter de Gruyter, Berlin), p. 865.
- Ketchen, M. B., W. M. Goubau, J. Clarke, and G. B. Donaldson, 1978, *Appl. Phys.* **49**, 4111.
- Kittel A., K. A. Kouznetsov, R. McDermott, B. Oh, and John Clarke, 1998, *Appl. Phys. Lett.* **73**, 2197.
- Kleiner, R., 1996, unpublished.
- Kleiner, R., and P. Müller, 1994, *Phys. Rev. B* **49**, 1327.
- Kleiner, R., F. Steinmeyer, G. Kunkel, and P. Müller, 1992, *Phys. Rev. Lett.* **68**, 2394.
- Kleinsasser, A. W., and K. A. Delin, 1995, *Appl. Phys. Lett.* **66**, 102.
- Knappe, S., D. Drung, T. Schurig, H. Koch, M. Klinger, and J. Hinken, 1992, *Cryogenics* **32**, 881.
- Koch, H., R. Cantor, D. Drung, S. N. Erne, K. P. Matthies, M. Peters, T. Ryhänen, H. J. Scheer, and H. D. Hahlbohm, 1991, *IEEE Trans. Magn.* **MAG-27**, 2793.
- Koch, R. H. 1994, unpublished.
- Koch, R. H. 1997, private communication.
- Koch, R. H., J. Clarke, W. M. Goubau, J. M. Martinis, C. M. Pegrum, and D. J. Van Harlingen, 1983, *J. Low Temp. Phys.* **51**, 207.
- Koch, R. H., W. Eidelloth, B. Oh, R. P. Robertazzi, S. A. Andrek, and W. J. Gallagher, 1992, *Appl. Phys. Lett.* **60**, 507.
- Koch, R. H., V. Foglietti, J. R. Rozen, K. G. Stawiasz, M. B. Ketchen, D. K. Lathrop, J. Z. Sun, and W. J. Gallagher, 1994, *Appl. Phys. Lett.* **65**, 100.
- Koch, R. H., W. J. Gallagher, B. Bumble, and W. Y. Lee, 1989, *Appl. Phys. Lett.* **54**, 951.
- Koch, R. H., M. B. Ketchen, W. J. Gallagher, R. L. Sandstrom, A. W. Kleinsasser, D. R. Gambrel, T. H. Field, and H. Matz, 1991, *Appl. Phys. Lett.* **58**, 1786.
- Koch, R. H., J. R. Rozen, J. Z. Sun, and W. J. Gallagher, 1993, *Appl. Phys. Lett.* **63**, 403.
- Koch, R. H., J. R. Rozen, P. Wöltgens, T. Picunko, W. J. Goss, D. Gambrel, D. Lathrop, R. Wiegert, and D. Overway, 1996, *Rev. Sci. Instrum.* **67**, 2968.
- Koch, R. H., J. Z. Sun, V. Foglietti, and W. J. Gallagher, 1995, *Appl. Phys. Lett.* **67**, 709.
- Koch, R. H., C. P. Umbach, G. J. Clark, P. Chaudhari, and R. B. Laibowitz, 1987, *Appl. Phys. Lett.* **51**, 200.
- Koelle, D., E. Dantsker, D. T. Nemeth, F. Ludwig, and J. Clarke, 1993, unpublished.
- Koelle, D., A. H. Miklich, E. Dantsker, F. Ludwig, D. T. Nemeth, J. Clarke, W. Ruby, and K. Char, 1993, *Appl. Phys. Lett.* **63**, 3630.
- Koelle, D., A. H. Miklich, F. Ludwig, E. Dantsker, D. T. Nemeth, and J. Clarke, 1993, *Appl. Phys. Lett.* **63**, 2271.
- Kötitz, R., H. Matz, L. Trahms, H. Koch, W. Weitschies, T. Rheinländer, W. Semmler, and T. Bunte, 1997, *IEEE Trans. Appl. Supercond.* **7**, 3678.
- Krause, H.-J. Y. Zhang, R. Hohmann, M. Grünekle, M. I. Faley, D. Lomparski, M. Maus, H. Bousack, and A. I. Braginski, 1997, in *Proceedings of the Third European Conference on Applied Superconductivity (EUCAS'97)*, Ueldhoven Institute of Physics Conference Series No. 158, edited by H. Rogalla and D. H. A. Blank (Institute of Physics, Philadelphia), p. 775.
- Kreutzbruck, M. v., M. Mück, U. Baby, and C. Heiden, 1998, in *Studies in Applied Electromagnetics and Mechanics* (IOS Press Amsterdam, The Netherlands), Vol. 13, p. 345.
- Kreutzbruck, M. v., J. Tröll, M. Mück, C. Heiden, and Y. Zhang, 1997, *IEEE Trans. Appl. Supercond.* **7**, 3279.
- Kromann, R., J. J. Kingston, A. H. Miklich, L. T. Sagdahl, and J. Clarke, 1993, *Appl. Phys. Lett.* **63**, 559.
- Kugai, H., T. Nagaishi, and H. Itozaki, 1996, in *Advances in Superconductivity VIII*, edited by H. Hayakawa and Y. Enomoto (Springer, Tokyo), p. 1145.
- Kupriyanov, M. Y., and K. K. Likharev, 1990, *Sov. Phys. Usp.* **160**, 49.
- Kurkijärvi, J., 1972, *Phys. Rev. B* **6**, 832.
- Kurkijärvi, J., 1973, *J. Appl. Phys.* **44**, 3729.
- Kuzmin, L. S., K. K. Likharev, V. V. Migulin, E. A. Polunin, and N. A. Simonov, 1985, in *SQUID'85, Superconducting Quantum Interference Devices and their Applications*, edited by H.-D. Hahlbohm and H. Lübbig (Walter de Gruyter, Berlin), p. 1029.
- Lee, L. P., K. Char, M. S. Colclough, and G. Zaharchuk, 1991, *Appl. Phys. Lett.* **59**, 3051.
- Lee, L. P., J. Longo, V. Vinetskiy, and R. Cantor, 1995, *Appl. Phys. Lett.* **66**, 1539.
- Lee, T. S., Y. R. Chemla, E. Dantsker, and J. Clarke, 1997, *IEEE Trans. Appl. Supercond.* **7**, 3147.
- Lee, T. S., E. Dantsker, and J. Clarke, 1996, *Rev. Sci. Instrum.* **67**, 4208.
- Likhachev, A. G., V. N. Polushkin, S. V. Uchaikin, and B. V. Vasiliev, 1990, *Supercond. Sci. Technol.* **3**, 148.

- Likharev, K. K., 1986, *Dynamics of Josephson Junctions and Circuits* (Gordon and Breach, New York).
- Likharev, K. K. and B. T. Ulrich, 1978, *Dynamics of Josephson Junction Circuits: Basic Theory* (Moscow University, Moscow; in Russian).
- Ludwig, F., J. Beyer, D. Drung, S. Bechstein, and Th. Schurig, 1997, *Appl. Supercond.* **5**, 345.
- Ludwig, F., E. Dantsker, R. Kleiner, D. Koelle, J. Clarke, S. Knappe, D. Drung, H. Koch, N. McN. Alford, and T. W. Button, 1995, *Appl. Phys. Lett.* **66**, 1418.
- Ludwig, F., E. Dantsker, D. Koelle, R. Kleiner, A. H. Miklich, and J. Clarke, 1995, *Appl. Supercond.* **3**, 383.
- Ludwig, F., E. Dantsker, D. Koelle, R. Kleiner, A. H. Miklich, D. T. Nemeth, J. Clarke, D. Drung, J. Knappe, and H. Koch, 1995, *IEEE Trans. Appl. Supercond.* **5**, 2919.
- Ludwig, F., E. Dantsker, D. T. Nemeth, D. Koelle, A. H. Miklich, J. Clarke, S. Knappe, H. Koch, and R. E. Thomson, 1994, *Supercond. Sci. Technol.* **7**, 273.
- Ludwig, F., D. Koelle, E. Dantsker, D. T. Nemeth, A. H. Miklich, J. Clarke, and R. E. Thomson, 1995, *Appl. Phys. Lett.* **66**, 373.
- Mannhart, J., P. Chaudhari, D. Dimos, C. C. Tsuei, and T. R. McGuire, 1988, *Phys. Rev. Lett.* **61**, 2476.
- Martinis, J. M., and J. Clarke, 1985, *J. Low Temp. Phys.* **61**, 227.
- Marx, A., L. Alff, and R. Gross, 1995, *Appl. Phys. Lett.* **67**, 1929.
- Marx, A., U. Fath, W. Ludwig, R. Gross, and T. Amrein, 1995, *Phys. Rev. B* **51**, 6735.
- Marx, A., and R. Gross, 1997, *Appl. Phys. Lett.* **70**, 120.
- Mathai, A., D. Song, Y. Gim, and F. C. Wellstood, 1993, *IEEE Trans. Appl. Supercond.* **3**, 2609.
- Matijasevic, V., Z. Lu, T. Kaplan, and C. Huang, 1997, in *Proceedings of the Third European Conference on Applied Superconductivity (EUCAS'97)*, Veldhoven Institute of Physics Conference Series No. 158, p. 189.
- Matsuda, M., Y. Murayama, S. Kiryu, N. Kasai, S. Kashiwaya, M. Koyanagi, and T. Endo, 1991, *IEEE Trans. Magn.* **MAG-27**, 3043.
- Matzander, U., U. Kalberkamp, V. Rath, K.-D. Husemann, G. Panaitow, E. Zimmermann, and Y. Zhang, 1997, in *Extended Abstracts of the 6th International Superconductive Electronics Conference (ISEC'97)*, Berlin, edited by H. Koch and S. Knappe (Physikalisch-Technische Bundesanstalt, Braunschweig), Vol. 3, p. 355.
- Mayer, B., L. Alff, T. Träuble, R. Gross, P. Wagner, and H. Adrian, 1993, *Appl. Phys. Lett.* **63**, 996.
- McCumber, D. E., 1968, *J. Appl. Phys.* **39**, 3113.
- McDaniel, E. B., S. C. Gausephohl, C.-T. Li, M. Lee, J. W. P. Hsu, R. A. Rao, and C. B. Eom, 1997, *Appl. Phys. Lett.* **70**, 1882.
- Mercereau, J. E., 1970, *Rev. Phys. Appl.* **5**, 13.
- Meservey, R., and P. M. Tedrow, 1969, *J. Appl. Phys.* **40**, 2028.
- Miklich, A. H., J. Clarke, M. S. Colclough, and K. Char, 1992, *Appl. Phys. Lett.* **60**, 1899.
- Miklich, A. H., J. J. Kingston, F. C. Wellstood, J. Clarke, M. S. Colclough, K. Char, and G. Zaharchuk, 1991, *Appl. Phys. Lett.* **59**, 988.
- Miklich, A. H., D. Koelle, E. Dantsker, D. T. Nemeth, J. J. Kingston, R. F. Kroman, and J. Clarke, 1993, *IEEE Trans. Appl. Supercond.* **3**, 2434.
- Miklich, A. H., D. Koelle, F. Ludwig, D. T. Nemeth, E. Dantsker, and J. Clarke, 1995, *Appl. Phys. Lett.* **66**, 230.
- Miklich, A. H., D. Koelle, T. J. Shaw, F. Ludwig, D. T. Nemeth, E. Dantsker, and J. Clarke, 1994, *Appl. Phys. Lett.* **64**, 3494.
- Milliken, F. P., S. L. Brown, and R. H. Koch, 1997, *Appl. Phys. Lett.* **71**, 1857.
- Milliken, F. P., R. H. Koch, S. L. Brown, R. A. Altman, W. J. Gallagher, S. G. Haupt, and D. K. Lathrop, 1997, *J. Appl. Phys.* **82**, 6301.
- Minotani, T., K. Enpuku, and Y. Kuroki, 1997, *J. Appl. Phys.* **82**, 457.
- Minotani, T., S. Kawakami, T. Kiss, Y. Kuroki, and K. Enpuku, 1997, *Jpn. J. Appl. Phys., Part 2* **36**, L1092.
- Missert, N., T. E. Harvey, and R. H. Ono, 1993, *Appl. Phys. Lett.* **63**, 1690.
- Moeckley, B. H., D. K. Lathrop, and R. A. Buhrman, 1993, *Phys. Rev. B* **47**, 400.
- Mück, M., 1993, *IEEE Trans. Appl. Supercond.* **3**, 2003.
- Mück, M., J. Clarke, and C. Heiden, 1994, *Proc. SPIE* **2160**, p. 180.
- Mück, M., C. Heiden, and J. Clarke, 1994, *J. Appl. Phys.* **75**, 4588.
- Mück, M., M. v. Kreutzbruck, U. Baby, J. Tröll, and C. Heiden, 1997, *Physica C* **282-287**, 407.
- Nagaishi, T., H. Kugai, H. Toyoda, and H. Itozaki, 1997, *IEEE Trans. Appl. Supercond.* **7**, 2886.
- Nakane, H., Y. Tarutani, T. Nishino, H. Yamada, and U. Kawabe, 1987, *Jpn. J. Appl. Phys., Part 2* **26**, L1925.
- Nichols, D. G., E. Dantsker, R. Kleiner, M. Mück, and J. Clarke, 1996, *J. Appl. Phys.* **80**, 6032.
- Nisenoff, M., 1970, *Rev. Phys. Appl.* **5**, 21.
- Ockenfuß, G. J., J. Borgmann, M. Reese, and R. Wördenweber, 1997, *IEEE Trans. Appl. Supercond.* **7**, 3698.
- Ockenfuß, G. J., R. Wördenweber, T. A. Scherer, R. Unger, and W. Jutzi, 1995, *Physica C* **243**, 24.
- Oh, B. D., R. H. Koch, W. J. Gallagher, R. P. Robertazzi, and W. Eidelloth, 1991, *Appl. Phys. Lett.* **59**, 123.
- Ono, R. H., J. A. Beall, M. W. Cromar, T. E. Harvey, M. E. Johansson, C. D. Reintsema, and D. A. Rudman, 1991, *Appl. Phys. Lett.* **59**, 1126.
- Ono, R. H., L. R. Vale, K. R. Kimminau, J. A. Beall, M. W. Cromar, C. D. Reintsema, T. E. Harvey, P. A. Rosenthal, and D. A. Rudman, 1993, *IEEE Trans. Appl. Supercond.* **3**, 2389.
- Ott, H. W., 1988, *Noise Reduction Techniques in Electronic Systems*, Second Edition (Wiley, New York), p. 233.
- Penny, R. D., D. K. Lathrop, E. E. Magnuson, B. D. Thorson, B. R. Whitecotton, R. H. Koch, and J. R. Rosen, 1997, *IEEE Trans. Appl. Supercond.* **7**, 2323.
- Pettiette-Hall, C. L., J. A. Luine, J. Murduck, J. F. Burch, R. Hu, M. Sergeant, and D. St. John, 1995, *IEEE Trans. Appl. Supercond.* **5**, 2087.
- Phillips, J., 1993, in *The New Superconducting Electronics*, NATO ASI series, edited by H. Weinstock and R. W. Ralston (Kluwer Academic, Dordrecht), p. 59.
- Phillips, J., 1996, *J. Appl. Phys.* **79**, 1829.
- Pitzius, P., V. Dworak, and U. Hartmann, 1997, in *Extended Abstracts of the 6th International Superconductive Electronics Conference (ISEC'97)*, Berlin, edited by H. Koch and S. Knappe (Physikalisch-Technische Bundesanstalt, Braunschweig), Vol. 3, p. 395.
- Purpura, J. W., T. R. Clem, and R. F. Wiegert, 1993, *IEEE Trans. Appl. Supercond.* **3**, 2445.
- Quincey, P. G., 1994, *Appl. Phys. Lett.* **64**, 517.

- Radic, T. D. Drung, S. Knappe, and S. Menkel, 1997, in *Extended Abstracts of the 6th International Superconductive Electronics Conference (ISEC'97)*, Berlin, edited by H. Koch and S. Knappe (Physikalisch-Technische Bundesanstalt, Braunschweig), Vol. 3, p. 352.
- Reimer, D., F. Ludwig, M. Schilling, S. Knappe, and D. Drung, 1995, in *Proceedings of the Second European Conference on Applied Superconductivity (EUCAS'95)*, Edinburgh, edited by D. Dew-Hughes (Institute of Physics, Bristol, Philadelphia) Institute of Physics Conference Series No. 148, p. 1605.
- Reimer, D., M. Schilling, S. Knappe, and D. Drung, 1995, *IEEE Trans. Appl. Supercond.* **5**, 2342.
- Reintsema, C. D., R. H. Ono, G. Barnes, L. Borchardt, T. E. Harvey, G. Kunkel, D. A. Rudman, L. R. Vale, N. Missert, and P. A. Rosenthal, 1995, *IEEE Trans. Appl. Supercond.* **5**, 3405.
- Roas, B., L. Bär, M. Kühnl, G. Daalmans, and F. Bömmel, 1993, in *Proceedings of European Conference on Applied Superconductivity (EUCAS'93)*, edited by H. C. Freyhardt (DGM Informationsgesellschaft, Oberursel), p. 1335.
- Rosenthal, P. A., E. N. Grossman, R. H. Ono, and L. R. Vale, 1993, *Appl. Phys. Lett.* **63**, 1984.
- Russek, S. E., D. K. Lathrop, B. H. Moeckly, R. A. Buhrman, D. H. Shin, and J. Silcox, 1990, *Appl. Phys. Lett.* **57**, 1155.
- Russek, S. E., S. C. Sanders, A. Roshko, and J. W. Ekin, 1994, *Appl. Phys. Lett.* **64**, 3649.
- Russek, S. E., S. C. Sanders, C. C. Clickner, and J. W. Ekin, 1996, *Applied Superconductivity Conference (ASC'96)*, Pittsburgh, PA (unpublished).
- Ryhänen, T., H. Seppä, R. Ilmoniemi, and J. Knuutila, 1989, *J. Low Temp. Phys.* **76**, 287.
- Satoh, T., M. Y. Kupriyanov, J. Tsai, M. Hidaka, and H. Tsuge, 1995, *IEEE Trans. Appl. Supercond.* **5**, 2612.
- Savo, B., F. C. Wellstood, and J. Clarke, 1987, *Appl. Phys. Lett.* **50**, 1757.
- Scharnweber, R., and M. Schilling, 1996, *Appl. Phys. Lett.* **69**, 1303.
- Scharnweber, R., and M. Schilling, 1997, *IEEE Trans. Appl. Supercond.* **7**, 3485.
- Scharnweber, R., K.-O. Subke, and M. Schilling, 1995, in *Proceedings of the Second European Conference on Applied Superconductivity (EUCAS'95)*, Edinburgh, edited by D. Dew-Hughes (Institute of Physics, Bristol/Philadelphia) Institute of Physics Conference Series No. 148, p. 1609.
- Scheel, H. J., M. Berkowski, and B. Chabotes, 1991, *J. Cryst. Growth* **115**, 19.
- Schilling, M., 1997, *IEEE Trans. Appl. Supercond.* **7**, 2960.
- Schilling, M., S. Krey, and R. Scharnweber, 1996, *Appl. Phys. Lett.* **69**, 2751.
- Schilling, M., R. Scharnweber, and S. Völkl, 1995, *IEEE Trans. Appl. Supercond.* **5**, 2346.
- Schmidl, R., S. Wunderlich, L. Dörrer, H. Specht, J. Heinrich, K.-U. Barholz, H. Schneidewind, U. Hübner, and P. Seidel, 1997, in *Proceedings of the Third European Conference on Applied Superconductivity (EUCAS'97)*, Veldhoven, edited by H. Rogalla and D. H. A. Blank (Institute of Physics, Philadelphia), Vol. 158, p. 651.
- Schmidl, R., S. Wunderlich, L. Dörrer, H. Specht, S. Linzen, H. Schneidewind, and P. Seidel, 1997, *IEEE Trans. Appl. Supercond.* **7**, 2756.
- Schmidt, J. M., L. P. Lee, A. Matlashov, M. Teepe, V. Vinetskiy, and R. Cantor, 1996, *Biomag'96*, Santa Fe, New Mexico, Abstracts p. 340.
- Schneider, J., H. Kohlstedt, and R. Wördenweber, 1993, *Appl. Phys. Lett.* **63**, 2426.
- Schneidewind, H., F. Schmidl, S. Linzen, and P. Seidel, 1995, *Physica C* **250**, 191.
- Schultze, V., R. Ijsselsteijn, V. Zakosarenko, F. Thrum, E. Il'ichev, and H. G. Meyer, 1997, in *Extended Abstracts of the 6th International Superconductive Electronics Conference (ISEC'97)*, Berlin, edited by H. Koch and S. Knappe (Physikalisch-Technische Bundesanstalt, Braunschweig), Vol. 3, p. 71.
- Schultze, V., R. Stolz, R. Ijsselsteijn, V. Zakosarenko, L. Fritsch, F. Thrum, E. Il'ichev, and H.-G. Meyer, 1997, *IEEE Trans. Appl. Supercond.* **7**, 3473.
- Seidel, P., R. Weidl, S. Brabetz, F. Schmidl, H. Nowak, and U. Leder, 1997, in *Extended Abstracts of the 6th International Superconductive Electronics Conference (ISEC'97)*, Berlin, edited by H. Koch and S. Knappe (Physikalisch-Technische Bundesanstalt, Braunschweig), Vol. 3, p. 321.
- Shaw, T. J., J. Clarke, R. B. van Dover, L. F. Schneemeyer, and A. E. White, 1996, *Phys. Rev. B* **54**, 15411.
- Sheen, D. M., S. M. Ali, D. E. Oates, R. S. Withers, and J. A. Kong, 1991, *IEEE Trans. Appl. Supercond.* **1**, 108.
- Shen, Y. Q., Z. J. Sun, R. Kromann, T. Holst, P. Vase, and T. Freltoft, 1995, *Appl. Phys. Lett.* **67**, 2081.
- Simon, R., J. B. Bulman, J. F. Burch, S. B. Coons, K. P. Daly, W. D. Dozier, R. Hu, A. E. Lee, J. A. Luine, C. E. Platt, and M. J. Zani, 1991, *IEEE Trans. Magn.* **MAG-27**, 3209.
- Sivakov, A. G., A. P. Zhuravel, O. G. Turutanov, I. M. Dmitrenko, J. W. M. Hilgenkamp, G. C. S. Brons, J. Flokstra, and H. Rogalla, 1994, *Physica C* **232**, 93.
- Somekh, R. E. and Z. H. Barber, 1992, in *Physics and Materials Science of High Temperature Superconductors, II*, edited by R. Kossowsky, B. Raveau, D. Wohlleben, and S. K. Patapi (Kluwer Academic, Dordrecht), p. 443.
- Stewart, W. C., 1968, *Appl. Phys. Lett.* **12**, 277.
- Strikovskiy, M. D., and A. Engelhardt, 1996, *Appl. Phys. Lett.* **69**, 2918.
- Sun, J. Z., W. J. Gallagher, A. C. Callegari, V. Foglietti, and R. H. Koch, 1993, *Appl. Phys. Lett.* **63**, 1561.
- Sun, J. Z., W. J. Gallagher, and R. H. Koch, 1992, *Appl. Phys. Lett.* **61**, 3190.
- Sun, J. Z., W. J. Gallagher, and R. H. Koch, 1993, *IEEE Trans. Appl. Supercond.* **3**, 2022.
- Sun, J. Z., W. J. Gallagher, and R. H. Koch, 1994, *Phys. Rev. B* **50**, 13664.
- Tanaka S., H. Itozaki, and H. Kado, 1995, in *Proceedings of the 7th International Symposium on Superconductivity (ISS '94)*, Advances in Superconductivity VII, edited by K. Yamafuji and T. Morishita (Springer, Tokyo), p. 1117.
- Tanaka, S., H. Itozaki, H. Toyoda, N. Harada, A. Adachi, K. Okajima, and H. Kado, 1994, *Appl. Phys. Lett.* **64**, 514.
- Tavrin, Y., H.-J. Krause, W. Wolf, V. Glyantsev, J. Schubert, W. Zander, and H. Bousack, 1995, *Cryogenics* **36**, 83.
- Tavrin Y., and M. Siegel, 1997, in *Proceedings of the Third European Conference on Applied Superconductivity (EUCAS'97)*, Veldhoven, edited by H. Rogalla and D. H. A. Blank (Institute of Physics, Philadelphia), No. 158, p. 719.
- Tavrin, Y., M. Siegel, and J. Hinken, 1999, *IEEE Trans. Appl. Supercond.* (in press).
- Tavrin, Y., Y. Zhang, M. Mück, A. I. Braginski, and C. Heiden, 1993a, *IEEE Trans. Appl. Supercond.* **3**, 2477.
- Tavrin, Y., Y. Zhang, M. Mück, A. I. Braginski, and C. Heiden, 1993b, *Appl. Phys. Lett.* **62**, 1824.

- Tavrin, Y., Y. Zhang, W. Wolf, and A. I. Braginski, 1994, *Supercond. Sci. Technol.* **7**, 265.
- ter Brake, H. J. M., W. A. M. Aarnink, P. J. van den Bosch, J. W. M. Hilgenkamp, J. Flokstra, and H. Rogalla, 1997, *Supercond. Sci. Technol.* **10**, 512.
- ter Brake, H. J. M., N. Janssen, J. Flokstra, D. Veldhuis, and H. Rogalla, 1997, *IEEE Trans. Appl. Supercond.* **7**, 2545.
- ter Brake, H. J. M., R. Karunanithi, H. J. Holland, J. Flokstra, D. Veldhuis, L. Vargas, J. W. M. Hilgenkamp, W. Jaszczuk, N. Janssen, F. J. G. Roesthuis, and H. Rogalla, 1997, *Meas. Sci. Technol.* **8**, 927.
- Tesche, C. D., and J. Clarke, 1977, *J. Low Temp. Phys.* **29**, 301.
- Tesche, C. D., and J. Clarke, 1979, *J. Low Temp. Phys.* **37**, 397.
- Tinchev, S. S., 1997, in *Microwave Physics and Technique* (Kluwer Academic, Dordrecht), p. 173.
- Tinchev, S. S., and J. H. Hinken, 1992, in *Superconducting Devices and their Applications*, edited by H. Koch and H. Lübbig, Springer Proceedings in Physics, (Springer, Berlin/Heidelberg), Vol. 64, p. 102.
- TonThat, Dinh M., M. Ziegeweid, Y.-Q. Song, E. J. Munson, S. Appelt, A. Pines, and J. Clarke, 1997, *Chem. Phys. Lett.* **272**, 245.
- Töpfer, H., 1991, in *Superconductivity and Cryoelectronics*, edited by W. Krech, P. Seidel, and H. G. Meyer (World Scientific, Singapore), p. 170.
- Töpfer, H., and F. H. Uhlmann, 1994, in *Proceedings of the Seventh International Symposium on Weak Superconductivity*, Smolenice, p. 336.
- Tsuei, C. C., J. R. Kirtley, C. C. Chi, L. S. Yu-Jahnes, A. Gupta, T. Shaw, J. Z. Sun, and M. B. Ketchen, 1994, *Phys. Rev. Lett.* **73**, 593.
- Tsuei, C. C., J. Mannhart, and D. Dimos, 1989, in *Proceedings of the Topical Conference on High T_c Superconducting Thin Films, Devices and Applications*, Atlanta, GA, 1988, edited by G. Mararitondo, R. Joint, and M. Onellion (AIP, New York), p. 194.
- Uhlmann, H., H. Töpfer, F. Verwiebe, and J. Uhlig, 1992, in *Superconducting Devices and their Applications*, edited by H. Koch and H. Lübbig, Springer Proceedings in Physics (Springer, Berlin/Heidelberg), Vol. 64, p. 292.
- Vale, L. R., R. H. Ono, and D. A. Rudman, 1997, *IEEE Trans. Appl. Supercond.* **7**, 3193.
- van der Harg, A. J. M., E. van der Drift, and P. Hadley, 1995, *IEEE Trans. Appl. Supercond.* **5**, 1448.
- Voss, R. F., 1981, *J. Low Temp. Phys.* **42**, 151.
- Vrba, J., 1996, in *SQUID Sensors: Fundamentals, Fabrication and Applications*, NATO ASI Series, edited by H. Weinstock (Kluwer Academic, Dordrecht), p. 117.
- Vu, L. N., and D. J. Van Harlingen, 1993, *IEEE Trans. Appl. Supercond.* **3**, 1918.
- Wang, S. G., L. H. Zhang, C. J. Wang, and Y. D. Dai, 1997, M2S-HTSC-V, *Fifth International Conference, Materials and Mechanisms of Superconductivity, High-Temperature Superconductors*, Beijing, China, p. 31.
- Weidl, R., S. Brabetz, F. Schmidl, F. Klemm, S. Wunderlich, and P. Seidel, 1997, *Supercond. Sci. Technol.* **10**, 95.
- Weinstock H., 1996, Ed., *SQUID Sensors: Fundamentals, Fabrication and Applications* (Kluwer Academic, Dordrecht).
- Wellstood, F., C. Heiden, and J. Clarke, 1984, *Rev. Sci. Instrum.* **55**, 952.
- Wellstood, F. C., J. J. Kingston, and J. Clarke, 1994, *J. Appl. Phys.* **75**, 683.
- Wellstood, F. C., J. J. Kingston, M. J. Ferrari, and J. Clarke, 1990, *Appl. Phys. Lett.* **57**, 1930.
- Wellstood, F. C., J. J. Kingston, M. J. Ferrari, and J. Clarke, 1991, *IEEE Trans. Magn.* **27**, 2569.
- Wellstood, F. C., A. H. Miklich, J. J. Kingston, M. J. Ferrari, J. Clarke, M. S. Colclough, K. Char, and G. Zaharchuk, 1992, in *Superconducting Devices and their Applications*, edited by H. Koch and H. Lübbig, Springer Proceedings in Physics (Springer, Berlin/Heidelberg), Vol. 64, p. 162.
- Wen, C. P., 1969, *IEEE Trans. Microwave Theory Tech.* **MTT-17**, 1087.
- Wikswow, Jr., J. P., 1995, *IEEE Trans. Appl. Supercond.* **5**, 74.
- Woeltgens, P. J. M., R. H. Koch, R. Matthews, S. L. Brown, R. A. Altman, W. J. Gallagher, S. G. Haupt, and D. K. Lathrop, 1996, *Applied Superconductivity Conference (ASC'96)*, Pittsburgh (unpublished).
- Wu, M. K., J. R. Ashburn, C. J. Torng, P. H. Hor, R. L. Meng, L. Gao, N. Z. Huang, Y. Q. Wang, and C. W. Chu, 1987, *Phys. Rev. Lett.* **58**, 908.
- Yanamoto, K., B. M. Lairson, J. C. Bravman, and T. H. Geballe, 1991, *J. Appl. Phys.* **69**, 7189.
- Yi, H. R., M. Gustafsson, D. Winkler, E. Olsson, and T. Claesson, 1996, *J. Appl. Phys.* **79**, 9213.
- Zakosarenko, V., F. Schmidl, H. Schneidewind, L. Dörrer, and P. Seidel, 1994, *Appl. Phys. Lett.* **65**, 779.
- Zani, M. J., J. A. Luine, G. S. Lee, J. M. Murduck, R. Ha, M. J. Levis, R. A. Davidheiser, and L. R. Eaton, 1991, *IEEE Trans. Magn.* **MAG-27**, 2557.
- Zhang, Y., M. Gottschlich, H. Soltner, E. Sodtke, J. Schubert, W. Zander, and A. I. Braginski, 1995, *Appl. Phys. Lett.* **67**, 3183.
- Zhang, Y., U. Krüger, R. Kutzner, R. Wördenweber, J. Schubert, W. Zander, E. Sodtke, and A. I. Braginski, 1994, *Appl. Phys. Lett.* **65**, 3380.
- Zhang, Y., M. Mück, M. Bode, K. Herrmann, J. Schubert, W. Zander, A. I. Braginski, and C. Heiden, 1992, *Appl. Phys. Lett.* **60**, 2303.
- Zhang, Y., M. Mück, K. Herrmann, J. Schubert, W. Zander, A. I. Braginski, and C. Heiden, 1993, *IEEE Trans. Appl. Supercond.* **3**, 2465.
- Zhang, Y., M. Mück, K. Herrmann, W. Zander, J. Schubert, A. I. Braginski, and C. Heiden, 1992, *Appl. Phys. Lett.* **60**, 645.
- Zhang, Y., H. Soltner, H.-J. Krause, E. Sodtke, W. Zander, J. Schubert, M. Grünekle, D. Lomparski, M. Banzer, H. Bousack, and A. I. Braginski, 1997, *IEEE Trans. Appl. Supercond.* **7**, 2866.
- Zhang, Y., H. Soltner, N. Wolters, W. Zander, J. Schubert, M. Banzet, and A. I. Braginski, 1997, *IEEE Trans. Appl. Supercond.* **7**, 2870.
- Zhang, Y., Y. Tavrin, M. Mück, A. I. Braginski, C. Heiden, S. Hampson, C. Pantev, and T. Elbert, 1993, *Brain Topography* **5**, 379.
- Zhang, Y., N. Wolters, X. H. Zeng, J. Schubert, W. Zander, H. Soltner, M. Banzet, F. Rüdgers, and A. I. Braginski, 1997, *Appl. Supercond.* (in press).
- Zhang, Y., W. Zander, J. Schubert, F. Rüdgers, H. Soltner, M. Banzet, N. Wolters, X. H. Zeng, and A. I. Braginski, 1997, *Appl. Phys. Lett.* **71**, 704.
- Zhang, Y., H. R. Yi, J. Schubert, W. Zander, M. Banzet, and A. I. Braginski, 1998, *Appl. Phys. Lett.* **72**, 2029.

- Zhang, Y., H. R. Yi, J. Schubert, W. Zander, H.-J. Krause, H. Bousack, and A. I. Braginski, 1999, IEEE Trans. Appl. Supercond. (in press).
- Zimmerman, J. E., 1971, J. Appl. Phys. **42**, 4483.
- Zimmerman, J. E., J. A. Beall, M. W. Cromar, and R. H. Ono, 1987, Appl. Phys. Lett. **51**, 617.
- Zimmerman, J. E., and N. V. Frederick, 1971, Appl. Phys. Lett. **19**, 16.
- Zimmerman, J. E., P. Thiene, and J. T. Harding, 1970, J. Appl. Phys. **41**, 1572.

**This Page is Inserted by IFW Indexing and Scanning
Operations and is not part of the Official Record**

BEST AVAILABLE IMAGES

Defective images within this document are accurate representations of the original documents submitted by the applicant.

Defects in the images include but are not limited to the items checked:

- ☒ **BLACK BORDERS**
- ☐ **IMAGE CUT OFF AT TOP, BOTTOM OR SIDES**
- ☐ **FADED TEXT OR DRAWING**
- ☐ **BLURRED OR ILLEGIBLE TEXT OR DRAWING**
- ☐ **SKEWED/SLANTED IMAGES**
- ☐ **COLOR OR BLACK AND WHITE PHOTOGRAPHS**
- ☐ **GRAY SCALE DOCUMENTS**
- ☒ **LINES OR MARKS ON ORIGINAL DOCUMENT**
- ☐ **REFERENCE(S) OR EXHIBIT(S) SUBMITTED ARE POOR QUALITY**
- ☐ **OTHER:** _____

IMAGES ARE BEST AVAILABLE COPY.

As rescanning these documents will not correct the image problems checked, please do not report these problems to the IFW Image Problem Mailbox.